

1. REPORT NUMBER  CA10-0939	2. GOVERNMENT ASSOCIATION NUMBER	3. RECIPIENT'S CATALOG NUMBER
4. TITLE AND SUBTITLE Validating the Durability of Corrosion Resistant Mineral Admixture Concrete		5. REPORT DATE  December 2010
7. AUTHOR  Xianming Shi, Yajun Liu, Zhengxian Yang, Michael Berry, Prathish Kumar Rajaraman		6. PERFORMING ORGANIZATION CODE
9. PERFORMING ORGANIZATION NAME AND ADDRESS Corrosion & Sustainable Infrastructure Laboratory Western Transportation Institute P.O. Box 174250 Montana State University Bozeman, MT 59717-4250		8. PERFORMING ORGANIZATION REPORT NO.  SJSU ALM - 116
12. SPONSORING AGENCY AND ADDRESS California Department of Transportation Engineering Service Center 1801 30th Street, MS 9-2/5i Sacramento, California 95816		10. WORK UNIT NUMBER
		11. CONTRACT OR GRANT NUMBER  59A0535
		13. TYPE OF REPORT AND PERIOD COVERED Final Report 6/30/2006 - 6/30/2010
		14. SPONSORING AGENCY CODE

15. SUPPLEMENTARY NOTES  
 Prepared in cooperation with the State of California Department of Transportation.

16. ABSTRACT  
 The objectives of this research are to validate chloride diffusion coefficients of mineral admixture concrete mix designs currently developed by the Caltrans for corrosion mitigation, and to verify the adequacy of existing measures to mitigate corrosion caused by exposure to marine environments and deicing salt applications. To this end, this research includes a comprehensive literature review on relevant topics, a laboratory investigation and a modeling effort. Various laboratory tests were conducted to investigate the compressive strength of and chloride diffusivity in mortar and concrete samples with cement partially replaced by various minerals (class F and class N fly ash, ultra-fine fly ash, silica fume, metakaolin and ground granulated blast-furnace slag), the porosity of mineral concretes, the freeze-thaw resistance of mineral mortars in the presence of deicers, and the effect of mineral admixtures on the chloride binding and chemistry of the pore solution in mortar. The modeling effort explores the important features of ionic transport in concrete and develops a two-dimensional finite-element-method (FEM) model coupled with the stochastic technique. The numerical model is then used to examine the service life of reinforced concrete as a function of mix design (i.e., partial replacement of cement by mineral admixtures), concrete cover depth, surface chloride concentrations, and presence of cracks and coarse aggregates.

17. KEY WORDS Fly ash, silica fume, metakaolin, slag, mineral admixtures, supplementary cementitious materials, rebar corrosion, reinforced concrete, chloride ingress, environmentally friendly concrete, service life prediction	18. DISTRIBUTION STATEMENT No restrictions. This document is available to the public through the National Technical Information Service, Springfield, VA 22161
19. SECURITY CLASSIFICATION (of this report)  Unclassified	20. NUMBER OF PAGES  179
	21. COST OF REPORT CHARGED

## **DISCLAIMER STATEMENT**

This document is disseminated in the interest of information exchange. The contents of this report reflect the views of the authors who are responsible for the facts and accuracy of the data presented herein. The contents do not necessarily reflect the official views or policies of the State of California or the Federal Highway Administration. This publication does not constitute a standard, specification or regulation. This report does not constitute an endorsement by the Department of any product described herein.

For individuals with sensory disabilities, this document is available in Braille, large print, audiocassette, or compact disk. To obtain a copy of this document in one of these alternate formats, please contact: the Division of Research and Innovation, MS-83, California Department of Transportation, P.O. Box 942873, Sacramento, CA 94273-0001.

## **ACKNOWLEDGEMENTS**

The authors acknowledge the financial support provided by the California Department of Transportation as well as the Research & Innovative Technology Administration (RITA) at the U.S. Department of Transportation for this project. The authors are indebted to the Caltrans Research Manager Peter S. Lee and the technical panel consisting of Rob Reis, Doug Parks, Rudy Lopez, and Charlie Sparkman, for their continued support throughout this project. We owe our thanks to Doran Glauz and Larry McCrum at Caltrans for discussions related to the handling and preparation of the coarse and fine aggregates prior to the batching operations. We appreciate the following professionals who provided assistance to this research: Richard Sullivan (Caltrans), Richard Halverson (Headwaters Resources), Steve Beck (Western Pozzolan Co.), Jim Anderson (BASF/MB Admixtures), Ken McPhalen (Advanced Cement Technologies), Kevin Foody (Boral Material Technologies), Greg Juell (Lehigh Southwest Cement Co.), and Jeff Wiest (Ashgrove Montana City Plant). We also thank Dr. Brett Gunnink of the MSU Civil Engineering Department for coordinating the use of Bulk Materials Laboratory, Concrete Wet Curing Room and other facilities. Finally, we owe our thanks to the following individuals at the Western Transportation Institute for providing help in various stages of the laboratory investigation: Marijean M. Peterson, Doug Cross, Dr. Tuan Anh Nguyen, Levi Ewan, Andrea Beth Leonard, Matthew Mooney, and Eric Schon.

# VALIDATING THE DURABILITY OF CORROSION RESISTANT MINERAL ADMIXTURE CONCRETE

## **Final Report**

Prepared for the



by

Xianming Shi, Ph.D., P.E. (Principal Investigator)

Yajun Liu, Ph.D.

Zhengxian Yang, M.Sc.

Michael Berry, Ph.D.

Prathish Kumar Rajaraman

*Corrosion & Sustainable Infrastructure Laboratory*

*Western Transportation Institute*

*Montana State University, Bozeman, MT 59717*



December 30, 2010

# Table of Contents

<b>ACKNOWLEDGEMENTS</b> .....	<b>II</b>
<b>LIST OF FIGURES</b> .....	<b>VI</b>
<b>LIST OF TABLES</b> .....	<b>VII</b>
<b>ABBREVIATIONS AND ACRONYMS</b> .....	<b>VIII</b>
<b>EXECUTIVE SUMMARY</b> .....	<b>1</b>
<b>CHAPTER 1. INTRODUCTION</b> .....	<b>6</b>
<b>1.1. PROBLEM STATEMENT</b> .....	<b>6</b>
<b>1.2. BACKGROUND</b> .....	<b>7</b>
1.2.1. <i>Chloride-Induced Corrosion of Steel Rebar in Concrete</i> .....	7
1.2.2. <i>Role of Mineral Admixtures in Concrete Durability</i> .....	9
1.2.3. <i>Measuring the Chloride Ingress into Concrete</i> .....	14
<b>1.3. CHALLENGES IN ASSESSING CONCRETE DURABILITY FROM ITS         CHLORIDE DIFFUSIVITY</b> .....	<b>17</b>
1.3.1. <i>Chloride Threshold</i> .....	17
1.3.2. <i>Chloride Binding</i> .....	19
<b>1.4. CHLORIDE TRANSPORT IN CONCRETE AND SERVICE LIFE OF         REINFORCED CONCRETE – A MODELING PERSPECTIVE</b> .....	<b>20</b>
<b>1.5. A PHENOMENOLOGICAL MODEL FOR THE CHLORIDE THRESHOLD OF         PITTING CORROSION OF STEEL IN SIMULATED CONCRETE PORE         SOLUTIONS</b> .....	<b>20</b>
<b>1.6. MODELING CATHODIC PREVENTION FOR UNCONVENTIONAL CONCRETE         IN SALT-LADEN ENVIRONMENT</b> .....	<b>20</b>
<b>1.7. STUDY OBJECTIVES</b> .....	<b>21</b>
<b>1.8. HOW THIS REPORT IS ORGANIZED</b> .....	<b>21</b>
<b>1.9. REFERENCES</b> .....	<b>21</b>
<b>CHAPTER 2. LABORATORY INVESTIGATION</b> .....	<b>31</b>
<b>2.1. EXPERIMENTAL</b> .....	<b>31</b>

2.1.1. <i>Sample Preparation</i> .....	31
2.1.2. <i>Mechanical Testing</i> .....	35
2.1.3. <i>Electro-migration and Natural Diffusion</i> .....	35
2.1.4. <i>Electrochemical Impedance Spectroscopy (EIS) Measurements</i> .....	39
2.1.5 <i>Chloride Binding Capacity and Pore Solution Chemistry of Mortar Samples</i> 40	
2.1.6 <i>Porosity Measurements of Concrete Samples</i> .....	40
2.1.7 <i>Freeze-thaw Resistance of Mortar Samples</i> .....	41
<b>2.2. RESULTS AND DISCUSSION</b> .....	<b>42</b>
2.2.1 <i>Mechanical Properties of Mortar and Concrete Samples and Correlation with Chloride Diffusivity</i> .....	42
2.2.2 <i>Electro-migration Data and Correlation with Porosity</i> .....	48
2.2.3. <i>EIS Data of Concrete and Correlation with Chloride Diffusivity</i> .....	52
2.2.4. <i>Chloride Binding of Mortar and Influence of Mineral Admixtures</i> .....	54
2.2.6. <i>Freeze-thaw Resistance of Mortar in the Presence of Chlorides</i> .....	57
<b>2.3. CONCLUSIONS</b> .....	<b>58</b>
<b>2.4. REFERENCES</b> .....	<b>59</b>
 CHAPTER 3. STOCHASTIC MODELING OF SERVICE LIFE OF REINFORCED CONCRETE IN CHLORIDE-LADEN ENVIRONMENTS .....	 <b>60</b>
<b>3.1. INTRODUCTION</b> .....	<b>60</b>
<b>3.2. METHODOLOGY</b> .....	<b>61</b>
3.2.1. <i>Model for Multi-Species Transport (Method A)</i> .....	62
3.2.2. <i>Model for Single-Species Transport (Method B)</i> .....	63
3.2.3. <i>Input Parameters</i> .....	64
<b>3.3. RESULTS AND DISCUSSION</b> .....	<b>67</b>
3.3.1. <i>Effect of Mix Design on Service Life</i> .....	67
3.3.2. <i>Effect of Surface Chloride Concentration on Service Life</i> .....	68
3.3.3. <i>Effect of Cracking Level on Service Life</i> .....	70
3.3.4. <i>Effect of Coarse Aggregates on Service Life</i> .....	72
3.3.5. <i>Effect of Concrete Cover Depth on Service Life</i> .....	74
<b>3.4. CONCLUDING REMARKS</b> .....	<b>75</b>
<b>3.5. REFERENCES</b> .....	<b>76</b>
 CHAPTER 4. CONCLUSIONS AND RECOMMENDATIONS FOR IMPLEMENTATION ....	 <b>79</b>
<b>4.1. CONCLUSIONS</b> .....	<b>79</b>
<b>4.2. RECOMMENDATIONS FOR IMPLEMENTATION</b> .....	<b>83</b>

## List of Figures

FIGURE 1-1 A typical corrosion cell in a salt-contaminated reinforced concrete.....	8
FIGURE 2-1 Schematic illustration (a) and photo (b) of the experimental setup for the electro-migration test (Note: for the natural diffusion samples, there is no external electric field applied). .....	36
FIGURE 2-2 Photos of the migration tests: (a) electro-migration and (b) natural diffusion. ....	37
FIGURE 2-3 Temporal evolution of chloride concentration in the destination compartment, with data obtained from the electro-migration test of 3% NaCl through a Portland cement mortar specimen. ....	38
FIGURE 2-4 The equivalent circuit used for fitting the EIS data of mortar and concrete	39
FIGURE 2-5 Relationship between compressive strength and chloride diffusion coefficients: (a) mortar samples and (b) concrete samples. ....	46
FIGURE 2-6 Relationship between: (a) chloride diffusivity in mortar and that in non-air-entrained concrete; (b) transformed strength of mortar and 90-day compressive strength of concrete. ....	47
FIGURE 2-7 Temporal evolution of: (a) chloride concentration in destination compartment; and (b) electric current density during the ACMT of concrete samples. ....	50
FIGURE 2-8 Correlation between: (a) porosity and chloride diffusion coefficient for concrete samples; (b) cumulative electrical charge and chloride diffusion coefficient. ....	51
FIGURE 2-9 Correlation between the measured $Q_{\text{cement}}$ (a) and $R_{\text{cement}}$ (b) against chloride diffusion coefficients. ....	53
FIGURE 2-10 Chloride binding isotherms for four kinds of mortar samples. ....	55
FIGURE 2-11 Chloride binding percentage with respect to mix designs of different mortar samples. ....	56
FIGURE 2-12 Weight loss of concrete specimens after freeze-thaw tests in the presence of various chlorides.....	58
FIGURE 3-13 Surface chloride concentration distribution according to the normal distribution: (a) 2 kg/m <sup>3</sup> ; (b) 4 kg/m <sup>3</sup> ; (c) 6 kg/m <sup>3</sup> and (d) 8 kg/m <sup>3</sup> .....	65
FIGURE 3-14 Chloride diffusion coefficient distribution according to the gamma distribution. ....	66
FIGURE 3-15 Chloride corrosion initiation concentration distribution according to the triangular distribution.....	66
FIGURE 3-16 Concrete cover depth distribution according to the normal distribution..	66
FIGURE 3-17 Predicted service life for concrete structures with surface chloride concentrations being (a) 2 kg/m <sup>3</sup> , (b) 4 kg/m <sup>3</sup> , (c) 6 kg/m <sup>3</sup> and (d) 8 kg/m <sup>3</sup> .	69
FIGURE 3-18 Crack configurations with various densities for service life prediction: (a) 50 m <sup>-1</sup> ; (b) 80 m <sup>-1</sup> ; (c) 145 m <sup>-1</sup> and (d) 207 m <sup>-1</sup> . ....	71
FIGURE 3-19 Effect of crack densities on service life prediction: (a) 50 m <sup>-1</sup> ; (b) 80 m <sup>-1</sup> ; (c) 145 m <sup>-1</sup> and (d) 207 m <sup>-1</sup> . ....	72
FIGURE 3-20 Effect of aggregate fraction on chloride-induced corrosion (a) mix design 2, (b) mix design 4, (c) mix design 8 and (d) mix design 11.....	74

FIGURE 3-21 Variation of service life with respect to concrete cover depth. (a) mix design 2, (b) mix design 4 and (c) mix design 8. .... 75

## List of Tables

TABLE 1-1 Summary of Chloride Penetration Test Methods [89].....	15
TABLE 2-2 Preliminary design of experiments to study the influence of concrete mix design parameters on the chloride penetration resistance and durability of concrete, including type and amount of mineral replacement and entrained air content.....	33
TABLE 2-3 Mix design parameters and the properties of concrete samples containing various types and amounts of mineral admixtures.....	34
TABLE 2-4 Mechanical properties, EIS data and chloride diffusivity of mortar samples containing various types and amounts of mineral admixtures.....	39
TABLE 2-5 The properties of mortar samples and concrete containing various types and amounts of mineral admixtures.....	40
TABLE 2-6 Chloride binding parameters measured from the mortar samples containing various mineral admixtures.....	56
TABLE 2-7 Pore solution chemistry in mortar samples containing various types and amounts of mineral admixtures.....	57
TABLE 3-8 Predicted service life for various mix designs, with a surface chloride concentration of $6 \text{ kg/m}^3$ and concrete cover of 50 mm .....	68

## Abbreviations and Acronyms

AASHTO	American Association of State Highway and Transportation Officials
ACMT	accelerated chloride migration test
AgCl	silver chloride
ANN	artificial neural network
ASR	alkali-silica reaction
ASTM	American Society of Testing and Materials
BDS	Bridge Design Specifications
BP	back-propagation
°C	degrees Celsius
C <sub>3</sub> A	tricalcium aluminate
C <sub>4</sub> AF	Friedel's salt, 3CaO•Al <sub>2</sub> O <sub>3</sub> •CaCl <sub>2</sub> •10H <sub>2</sub> O
CaCl <sub>2</sub>	calcium chloride
Caltrans	California Department of Transportation
Ca(OH) <sub>2</sub>	calcium hydroxide
<i>Cl</i> <sub>th</sub>	chloride threshold
CP	cathodic protection
CPre	cathodic prevention
C-S-H	calcium silicate hydrate
<i>D</i> <sub>app</sub>	apparent diffusion coefficient
<i>D</i> <sub>eff</sub>	effective diffusion coefficient
<i>D</i> <sub>ns</sub>	non-steady-state diffusion coefficient
<i>D</i> <sub>s</sub>	steady-state diffusion coefficient
DO	dissolved oxygen
DOT	Department of Transportation
<i>E</i> <sub>corr</sub>	corrosion potential
EDTA	ethylenediaminetetraacetic acid
EDX	energy dispersive x-ray spectroscopy
EFCs	environmentally friendly concretes
EIS	electrochemical impedance spectroscopy
FA	fly ash
FDM	Finite Difference Method
FEM	Finite Element Method
°F	degrees Fahrenheit
FESEM	field emission scanning electron microscopy
FHWA	Federal Highway Administration
GGBFS	ground granulated blast-furnace slag
HCl	hydrochloric acid

IC/ICP	Chromatography-Inductively Coupled Plasma
ITZ	interfacial transition zone
LOI	loss on ignition
MgCl <sub>2</sub>	magnesium chloride
MK	metakaolin
NACE	National Association of Corrosion Engineers
NaCl	sodium chloride
NCHRP	National Center for Highway Research Program
OCP	open circuit potential
OH <sup>-</sup>	hydroxyl
PCC	Portland cement concrete
PDEs	partial differential equations
RCPT	rapid chloride permeability test
RMT	rapid migration test
SCC	self-compacting concrete
SCE	saturated calomel electrode
SCMs	supplementary cementitious materials
SF	silica fume
SHRP	Strategic Highway Research Program
SMSE	sum of mean square error
SSD	surface-saturated-dry
$T_i$	time-to-corrosion (initiation time)
TMS	transformed mortar strength
UFFA	ultra-fine fly ash
$w/c$	water-to-cement ratio
$w/cm$	water-to-cementitious-materials ratio
WTI	Western Transportation Institute



## EXECUTIVE SUMMARY

Prior to this work, Caltrans saw the need for research to validate the corrosion mitigation design assumptions in order to better define the strategies used to design concrete structures with adequate corrosion mitigation measures and thus a “maintenance-free” service life. Additional research was also considered necessary to establish standard, reliable, and rapid test methods for determining chloride diffusion coefficients and chloride thresholds.

In this work, various laboratory tests were conducted to investigate the properties of mortar and concrete samples with cement partially replaced by various minerals (class F and class N fly ash [FA], ultra-fine fly ash [UFFA], silica fume [SF], metakaolin [MK] and ground granulated blast-furnace slag [GGBFS]). The key findings are provided as follows. These include: the compressive strength, Young's modulus, and modulus of toughness of mortar samples at 1-d, 7-d and 28-d; the compressive strength and porosity of concrete samples at 90-d; the chloride diffusivity and EIS measurements of hardened mortar and concrete samples; the natural diffusion of chloride into select concrete samples; the freeze-thaw resistance of mortars in the presence of chloride deicers; and the effect of mineral admixtures on the chloride binding and chemistry of the pore solution in mortar.

The accelerated chloride migration test of hardened concrete specimens found them to feature unusually low chloride diffusivity ( $D_s$  values in the order of  $10^{-13}$  m<sup>2</sup>/s vs. the commonly reported  $10^{-12}$  m<sup>2</sup>/s), corresponding to very high compressive strength. The research findings imply that these high-quality concrete samples tested likely had little or no interfacial transitional zone (ITZ) in them. The chloride diffusivity in high-strength concretes was largely determined by the use of coarse aggregates whereas the effect of mineral admixtures was relatively small.

Some detailed findings from the laboratory investigation are provided as follows.

1. The partial replacement of cement by 20% class F FA and 5% SF, by 20% class F FA and 5% MK, or by 25% class F FA alone greatly reduced the 1-day compressive strength of mortar samples, whereas the partial replacement of cement by 10% MK, 10% SF, 10% UFFA, 50% GGBFS, or 25% class N FA improved the 1-day strength to various degrees.
2. The combined addition of class F and MK dramatically reduced the 7-day compressive strength of mortar samples, followed by the use of GGBFS or SF, whereas the addition of most other minerals (except MK) also decreased the 7-day strength to various degrees.
3. The combined addition of class F and MK increased the 28-day compressive strength of mortar samples, whereas the addition of most other minerals (except GGBFS) decreased the 28-day strength to various degrees.
4. All the SCMs dramatically reduced the 1-day Young's modulus of mortar samples, but they showed mixed effect on the 7-day and 28-day Young's modulus. All the SCMs dramatically reduced the 7-day and 28-day modulus of toughness, but they showed mixed effect on the 1-day modulus of toughness. The reduction in the moduli of concrete is beneficial as it renders the concrete less prone to shrinkage cracking, which in turn, reduces the risk of rapid chloride ingress.
5. According to the EIS measurements after the ACMT using 90-day old mortar samples, all the SCMs dramatically increased the electrical resistivity of the mortar samples in the electrolyte while most SCMs (except GGBFS) decreased the electrical capacitance of the mortar to various degrees.

6. The effect of partially replacing cement with SCMs on the steady-state diffusion coefficient ( $D_s$ ) obtained from the ACMT was evaluated using 90-day old mortar samples. The results indicate that the use of 20% class F FA and 5% SF as cement replacement significantly increased the chloride diffusivity in mortar and the use of 10% MK or 50% GGBFS significantly decreased it, whereas other SCMs decreased the  $D_s$  to various degrees. Note that the  $D_s$  values were all very low (in the order of  $10^{-13}$  m<sup>2</sup>/s), and the chloride diffusivity differences between these highly impermeable concrete samples could be related to the workability and construction practices of the fresh concrete mixes.
7. There is no clear trend related to the effect of SCMs on the 90-day compressive strength of concrete or the chloride diffusivity in the 360-day concrete samples. Nonetheless, the chloride diffusivity is much lower in the concrete mixes than in their corresponding mortar mixes, with the  $D_s$  values in the order of  $10^{-13}$  m<sup>2</sup>/s in concrete and of  $10^{-11}$  m<sup>2</sup>/s in mortar. This highlights the important role of coarse aggregates in slowing down the chloride ingress into concrete.
8. All the mortar mixes had a 28-day compressive strength above 4,000 psi (27.6 MPa) whereas the non-air-entrained concrete mixes at 90 days on average featured twice as high a compressive strength. Such extremely high strength values suggest that the hardened concrete had outstanding microstructure, which is consistent with their extremely low  $D_s$  values indicative of chloride diffusivity. The compressive strength of air-entrained concrete was consistently lower than that of their non-air-entrained counterpart, yet the differences in their chloride diffusivity were not as appreciable.
9. The natural diffusion results indirectly confirmed the order of magnitude of  $D_s$  values of concrete specimens obtained from the ACMT.
10. Generally speaking, the lower  $D_s$  values corresponded to the higher compressive strength values, as both indicate high quality of the mortar or concrete. The lower  $D_s$  values in mortar corresponded to the lower  $D_s$  values in the non-air-entrained concrete, indicating that chloride diffusion in the mortar phase contributed to the overall chloride diffusion in the concrete.
11. There is a strong proportional correlation between the transformed mortar strength and the concrete strength, suggesting that the mortar phase is an integral component of the heterogeneous concrete matrix and greatly contributes to its compressive strength.
12. The chloride diffusivity generally increases with the volume of permeable voids in concrete.
13. The cumulative charge generally increases with chloride diffusion coefficients.
14. The electrical resistivity of concrete generally decreased after the electro-migration test whereas its electrical capacitance generally increased.
15. Mix design 9 (20% class F FA + 5% MK) and mix design 11 (10% SF) had the lowest binding capacity, whereas mix designs 1 (100% cement), 7 (10% UFFA) and 9 (50% GGBFS) had generally high chloride binding capacity relative to other mixes.
16. The pH data suggest that all the mineral admixtures reduced the alkalinity of the pore solution in the mortar samples, regardless of their type and amount.
17. The weight loss of mortar specimens was the greatest in the presence of diluted NaCl solution, followed by the diluted CaCl<sub>2</sub>, and then by the diluted MgCl<sub>2</sub> solution, whereas the mortar deterioration in the de-ionized water was negligible. In the presence of diluted NaCl solution, the mix designs, the mix designs 13 (10% MK), 15 (10% UFFA) and

particularly 17 (50% GGBFS) showed less weight loss relative to the control, whereas other SCMs exacerbated the freeze-thaw damage with the mix designs 5 (25% class N FA) and particularly 7 (20% class F FA + 5% SF) being the worst. In the presence of diluted  $\text{CaCl}_2$  and  $\text{MgCl}_2$  solutions, the effect of mineral admixtures on the freeze-thaw resistance of mortar followed a trend similar to that seen in the presence of diluted  $\text{NaCl}$  solution, yet with the mix designs 5 (25% class N FA) and 7 (20% class F FA + 5% SF) being the worst respectively. In summary, the partial replacement of cement by 50% GGBFS is most beneficial for the freeze-thaw resistance of mortar, followed by the 10% UFFA or 10% MK replacement; whereas the use of ordinary fly ash and silica fume seems to undermine the freeze-thaw resistance of mortar in the presence of various diluted chloride solutions.

A two-dimensional finite-element-method (FEM) model, coupled with the stochastic technique, was developed to study the service life of reinforced concrete as a function of various influential factors. The FEM model stochastically sampled its inputs. Specifically, the surface chloride concentrations and concrete cover depth follow the normal distribution, whereas the diffusion coefficients and the chloride threshold follow the gamma distribution and the triangular distribution respectively. The nonlinear partial differential equations (PDEs) to characterize the spatial and temporal evolution of ionic species were numerically solved. The key findings are provided as follows.

1. All concrete mixes investigated had a 50%-probability service life of 114 years or longer (with a surface chloride concentration of  $6 \text{ kg/m}^3$  and concrete cover of 50 mm), which highlights the great potential of reinforced concrete as a construction material when the concrete is made using the best practices of construction and curing and is free of cracking. The modeling also suggest that when the concrete is made using the best practices, partially replacing cement with class F FA, SF, MK, or GGBFS tends to decrease the service life of reinforced concrete or at least show little benefits to its service life. This trend contradicts what have been generally reported in published literature, and is likely attributable to the fact that the Portland cement concrete (PCC) made without any mineral admixtures (mixes 1 and 2) featured unusually low chloride diffusion coefficients in the order of  $10^{-13} \text{ m}^2/\text{s}$ . Finally, for all these high-quality concrete mixes, the effects of air entrainment on the chloride diffusivity in concrete and the service life of reinforced concrete were not dramatic and do not show a clear trend.
2. Based on the modeling results, chloride inward-diffusion with the lowest surface chloride concentration is the most sluggish process. With the surface chloride concentration increasing, the service life decreases significantly.
3. The service life of reinforced concrete decreases as the cracking level of the concrete increases. When the crack density is over  $200 \text{ m}^{-2}$ , the service life shows no significant dependence on further increase on crack density, which is attributable to the forming of continuous net-like configuration in the concrete domain.
4. Assuming negligible diffusion of chloride ions in coarse aggregates and absence of interfacial transition zone (ITZ), the chloride diffusion rate in concrete was found to be quite different from its corresponding homogeneous medium. The overall flux decreases as the volume fraction of aggregates increases.
5. For all the mineral concrete mixes investigated, as the concrete cover depth increases, the time to corrosion initiation of rebar in concrete is predicted to increase exponentially, highlighting the importance of cover depth in extending the service life of reinforced concrete exposed to external chlorides. According to the model calculations, it would

take more than 100 years for the chloride ions in an aggressive environment (with surface chloride content of  $8 \text{ kg/m}^3$ ) to reach the threshold level at a depth of 60 mm. It should be cautioned that the chloride diffusivity data used for the model were measured using specimens cored from the center of a large concrete sample. In field construction, the top layer of the concrete cover is likely to have much higher chloride diffusivity than the interior of the concrete, in light of the possible defects derived from bleeding and water evaporation etc. at the top layer. Furthermore, the field construction is unlikely to achieve the same level of detailed quality assurance as implemented in the laboratory study and cracking cannot be fully eliminated for the service life prediction considerations. In this context, a thicker-than-predicted concrete cover is needed for the target service life of concrete structures in the field environment and the importance of good construction and curing practices can not be overemphasized.

6. The technique developed in this work (e.g., multi-species transport model) was found to be very effective in predicting chloride migration and generating statistical conclusions about the service life of reinforced concrete, which allows the civil engineers to estimate the rate of chloride ingress and associated deterioration risk of reinforced concrete. Future improvements could be made to the model so that it takes into account the time-dependency of transport properties of concrete, the corrosion propagation, the chloride penetration mechanisms other than diffusion (e.g., wicking), the structure geometry, the environmental humidity and temperature fluctuations and the decay of structures under coupled physical, chemical, and mechanical deterioration processes etc.

### ***Recommendations for Implementation***

1. The accelerated chloride migration test (ACMT) used in this work should be considered by the Caltrans corrosion technology branch for implementation. When testing the concrete with unusually low chloride diffusivity ( $D_s$  values in the order of  $10^{-13} \text{ m}^2/\text{s}$ ), the test could last up to 2 months using a 30-V applied voltage and a 25-mm thick disc specimen. Nonetheless, for most concrete mixes prepared in the field construction, the chloride diffusivity is expected to be much higher and the test typically would last no more than 2 weeks. An unusually high compressive strength can serve as a warning sign that the concrete may be highly impermeable. In general, the ACMT is anticipated to help Caltrans and other departments of transportation (DOTs) to make the transition from prescriptive specifications of concrete mixes to more performance-based specifications, which then would allow more innovation and flexibility in the materials selection of concrete and likely facilitate the paradigm shift from conventional PCC to EFCs.
2. If coupled the ACMT with the model developed in this work or the simplistic Life-365 software, this would provide a rapid, reliable method for determining the amount of concrete cover needed, based on the amount of chlorides present in the service environment and the required design life. With further improvements on the service life model, it could also be used for life cycle costing and for the timing of repair or rehabilitation strategies.
3. Caltrans should consider additional research phases for this work, such as the development and field evaluation of various types of high performance corrosion-resistant concretes. The research findings from such work should be shared with the DOT Design Engineers, as it may lead to improvements to the current Bridge Design Specifications in mitigating chloride-induced corrosion and deterioration.

4. The research findings imply that the chloride diffusivity in high-strength concretes largely determined by the use of coarse aggregates instead of the mineral admixtures. As such, the role of coarse aggregates in concrete durability should be further explored. The existing ASTM standard on the proportioning of aggregates may be further optimized for conventional and unconventional concrete mixes, in light of their important role in dramatically slowing down chloride ingress. Similarly, how the preparation of aggregates affects the durability of concrete merit further investigation, as it may benefit the internal curing of concrete and minimize its early-age cracking.
5. The processes and procedures used in the new construction should be closely supervised under a systematic quality assurance program, in order to achieve the great potential of reinforced concrete as a construction material and to manage corrosion risks pro-actively. The importance of good construction and curing practices can not be overemphasized, as they greatly reduce the risk of rebar corrosion in concrete.
6. Continued research is needed to explore the effect of partially replacing cement with mineral admixtures on the durability of concrete. The results from this study imply that for concrete with ordinary quality, the mineral admixtures may have great potential in increasing its electric resistivity, enhancing its chloride binding (e.g., the use of 10% UFFA or 50% GGBFS), reducing its chloride diffusivity (e.g., the use of 10% MK or 50% GGBFS), and improving its resistance to freeze-thaw in the presence of diluted deicers (e.g., the use of 50% GGBFS, 10% UFFA, or 10% MK). The use of fly ash and slag etc. may translate to cost savings and reduced energy use, greenhouse gas emissions and landfill waste, without sacrificing quality and long-term performance of the concrete.

## CHAPTER 1. INTRODUCTION

### 1.1. Problem Statement

Concrete is the most widely used man-made building material in the world, owing to its versatility and relatively low cost. Concrete has also become the material of choice for the construction of structures exposed to extreme conditions [1]. Furthermore, sustainability has become an increasingly important characteristic for concrete infrastructure, as the production of Portland cement (the most common binder in concrete) is an energy-intensive process that accounts for a significant portion of global carbon dioxide emissions and other greenhouse gases [2,3]. As such, even slight improvements in the design, production, construction, maintenance, and materials performance of concrete can have enormous social, economic and environmental impacts.

In this context, there are a variety of approaches to enhance the sustainability of concrete and reduce its environmental footprint. One attractive approach is to enhance the durability of concrete infrastructure, since durability is a key cornerstone for sustainability. According to the ASCE 2009 *Report Card for America's Infrastructure*, \$2.2 trillion needs to be invested over five years to 'bring the nation's infrastructure to a good condition' [4], which highlights the urgent need for research devoted to longer-lasting and "maintenance-free" concrete materials.

There is general agreement that the most effective improvement in concrete durability can be achieved at the design and materials selection stage of a project by using adequate concrete cover and high-quality concrete. Usually, an increase in the thickness of the concrete cover leads to beneficial effects, because it increases the barrier to the various aggressive species moving towards the reinforcement and increases the time for corrosion to initiate. In reality, however, the cover thickness cannot exceed certain limits, for mechanical and practical reasons [5]. The Florida Department of Transportation (DOT) adheres to the following specifications for concrete bridge substructures within the 0-12 foot elevation range relative to mean high tide: 1) adequate cover (4 inches for cast-in-place members and 3 inches for prestressed components), and 2) low water-to-cementitious material ( $w/c$ ) ratio concrete with pozzolanic (fly ash or silica fume) or corrosion inhibiting admixtures [12]. In light of advances in concrete technology and requirements of the AASHTO Load and Resistance Factor Design (LRFD) for a 75-year design life, the California Department of Transportation (Caltrans) made significant changes to its Bridge Design Specifications (BDS) Article 8.22 in 2000 and adopted the approach of using the chloride diffusivity through concrete to determine the concrete cover requirements for structures subjected to chloride-bearing environments. The current BDS Article 8.22 provides guidance to the Design Engineer in determining the required cement type, minimum required concrete cover, etc. for corrosion protection of various bridge members [6]. For instance, for bridge members exposed to corrosive soil or water (containing more than 500 ppm of chlorides), the maximum  $w/c$  ratio shall not exceed 0.40. Mineral admixtures conforming to ASTM Designation C 618 Type F or N (e.g., fly ash) are required for all exposure conditions, except for 'non-corrosive'

exposure conditions. For such bridge members as precast piles and pile extensions exposed to corrosive conditions, mineral admixtures conforming to ASTM Designation C 1240 (e.g., silica fume) may be required. The minimum concrete cover required for bridge members ranges from 1 to 5 inches, dependent on the bridge member type and exposure condition [6].

Recent years have seen increasing interest in environmentally-friendly concretes (EFCs), which utilize industrial byproducts or waste materials and thus benefit the environment. Among them, mineral admixtures such as fly ash, silica fume, and slag – have been used to partially replace cement in concrete while shown to enhance concrete durability and improve resistance to chloride diffusion. They are also known as supplementary cementitious materials, or SCMs. Like other state DOTs, Caltrans has developed concrete mixes for corrosion mitigation of structures with the aid of such SCMs. However, the work to date has been based on diffusion coefficient data for low permeability, mineral admixture concretes selected from available literature, which may not represent the materials and exposure conditions seen in California. *Additional research is thus needed to validate the corrosion mitigation design assumptions by Caltrans* in order to better define the strategies used to design concrete structures with adequate corrosion mitigation measures and thus a “maintenance-free” service life.

Furthermore, a significant amount of variability exists in determining chloride diffusion coefficients as an indicator of concrete durability. First, values of chloride diffusion coefficient usually vary from  $10^{-13}$  m<sup>2</sup>/s to  $10^{-10}$  m<sup>2</sup>/s in relation to the concrete properties and the exposure conditions. In particular, these values depend on the concrete pore structure and on all the factors that determine it, such as: mix design parameters (w/c ratio, type and proportion of mineral admixtures and cement, compaction, curing, etc.) and presence of cracks. The chloride diffusion coefficient is also a function of chloride exposure condition (submerged, splash, atmosphere, etc.) and the length of exposure, partly due to hydration of slowly reacting cement constituents such as blast furnace slag or fly ash [5]. When the chloride diffusion coefficient is used to evaluate the risk for reinforcement corrosion and to forecast the service life of concrete structures, chloride threshold is a very important parameter, the value of which is still a subject of controversy. In reality, the determination of chloride diffusion coefficient and chloride threshold is often affected by the method of chloride analysis. Second, existing chloride permeability tests are either very time-consuming for high-quality concrete mixes or too biased to provide reliable chloride diffusion coefficients. *Additional research is thus needed to establish standard, reliable, and rapid test methods for determining chloride diffusion coefficients and chloride thresholds.* Such methods are anticipated to help Caltrans and other DOTs to make the transition from prescriptive specifications of concrete mixes to more performance-based specifications, which then would allow more innovation and flexibility in the materials selection of concrete and likely facilitate the paradigm shift from conventional Portland cement concrete (PCC) to EFCs.

## **1.2. Background**

### *1.2.1. Chloride-Induced Corrosion of Steel Rebar in Concrete*

Concrete normally provides both chemical and physical protection for the steel reinforcement embedded in concrete. The cement hydration leads to the highly alkaline (pH 13 or higher) pore solution of concrete, which promotes the formation of an oxide/hydroxide film at the steel surface, a passive film of about 10 nanometers thick [7]. This protective film effectively insulates the steel and electrolytes so that the corrosion rate is negligible. In addition, the concrete cover prevents or at least retards the ingress of aggressive substances. While the chloride ion ( $\text{Cl}^-$ ) has only a small influence on pore water pH, concentrations as low as 0.6 kilograms per cubic meter ( $\text{kg/m}^3$  by weight of concrete) have been projected to compromise steel passivity [7]. Furthermore, the protection of steel by concrete is compromised by the gradual ingress of atmospheric carbon dioxide into the concrete, a process known as *carbonation*, which reduces the pore solution pH of carbonated concrete to the range of 8 to 9. The corrosion due to carbonation progresses at a much lower rate than that due to chloride ingress [8]. Concrete exposure to acids, sulfates and freeze-thaw cycles may also compromise the protection of steel rebar.

Chloride ingress is one of the major forms of environmental attack to reinforced concrete [9], which leads to corrosion of the reinforcing steel and a subsequent reduction in the strength, serviceability, and aesthetics of the structure. For reinforced concrete structures such as highway bridges, the chloride-induced corrosion of rebar has been a major problem with serious economic and safety implications. Chloride, often originated from marine environments or deicing applications, can initiate rebar corrosion once its concentration at the embedded rebar depth reaches a certain threshold. The local disruption of the passive film initiates corrosion cells between the active corrosion zones (anode) and the surrounding areas that are still passive (cathode) [7,10], as shown in Figure 1-1.

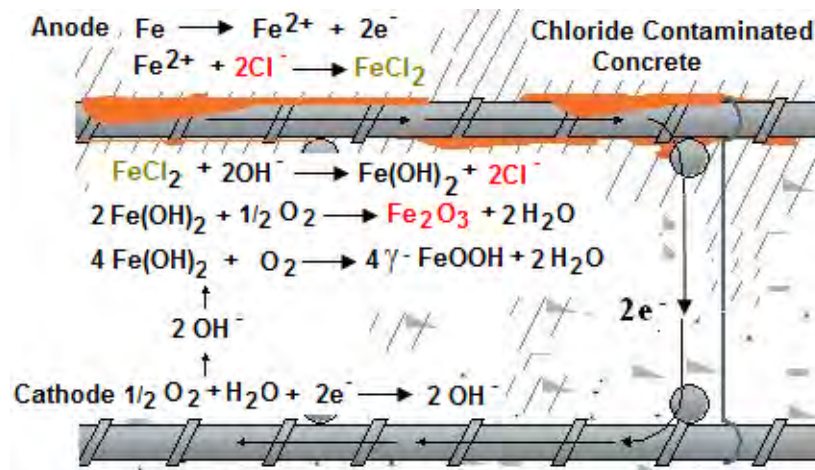


FIGURE 1-1 A typical corrosion cell in a salt-contaminated reinforced concrete

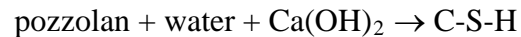
For stable pit growth to be sustained, the relative concentrations of aggressive  $\text{Cl}^-$  and inhibitive  $\text{OH}^-$  should be above a certain ratio, otherwise re-passivation will occur [11]. The accumulation of corrosion products (oxides/hydroxides) in the concrete pore space

near the rebar then builds up hoop stresses around steel and results in cracking or spalling of the concrete, which in turn facilitates the ingress of moisture, oxygen, and chlorides to the embedded rebar and accelerates the corrosion of steel [12].

Corrosive agents, liquid or gaseous, may penetrate the concrete through capillary absorption, hydrostatic pressure, or diffusion. The ingress of gases, water or ions in aqueous solutions into concrete takes place through pore spaces in the cement paste matrix and paste-aggregate interfaces or microcracks. For the durability of concrete, permeability is believed to be the most important characteristic [13], which is related to its microstructural properties, such as the size, distribution, and interconnection of pores and microcracks [14]. For reinforced concrete structures exposed to salt-laden environments, the chloride permeability of concrete has been recognized as a critical intrinsic property of the concrete [15].

### *1.2.2. Role of Mineral Admixtures in Concrete Durability*

Mineral admixtures, generally pozzolanic materials, are mainly glassy siliceous materials that may contain aluminous compounds [5]. The reaction of such materials with Portlandite (i.e., calcium hydroxide) and water generates hydration products similar to those of Portland cement, i.e., calcium silicate hydrates (C-S-H), a rigid gel composed of extremely small particles with a layer structure:



This reaction can also be generally represented as:



whereas the actual stoichiometry of the reaction may vary as a function of the Ca/Si ratio, available water molecules, etc., resulting in various C-S-H that may deviate from the general formula ( $\text{CaH}_2\text{SiO}_4 \cdot 2 \text{H}_2\text{O}$ ).

The use of mineral admixtures such as fly ash, silica fume, slag and metakaolin has been shown to enhance concrete durability [16-18], by increasing chloride binding [19], decreasing chloride permeability [18, 20], elevating threshold chloride content [21], and/or improving the distribution of pore size and shape of concrete matrix [22]. Since some of these materials are cheaper than Portland cement, there is also an economic advantage to wider use. Dhir and Jones [24] used the low-lime fly ash to develop concrete mixes with improved chloride resistance, by improving the pore structure and binding capacity of the concrete. They found that ternary blends (cement and fly ash blended with silica fume or metakaolin) showed the highest chloride resistance. Hossain et al. [25] found that the incorporation of ultra-fine fly ash (UFFA) improved the strength and chloride penetration resistance of concrete, and the incorporation of silica fume had even more pronounced benefits. They also found that the silica fume addition led to low slump and high early-age shrinkage whereas the UFFA addition mitigated these two issues. As such, a ternary blend (with cement, silica fume and UFFA) was developed to feature high early-age strength, improved durability, low slump and low free shrinkage.

Thomas et al. [26] investigated the synergy between silica fume and fly ash, as silica fume compensates for the low early-strength pertinent to fly ash addition while fly ash compensates for the workability issues pertinent to silica fume addition. The combinations of low dosage (3% to 6%) of silica fume and moderate dosage (20% to 30%) of fly ash (despite its high lime content) were found very effective in reducing expansion due to alkali-silica reaction (ASR) and in mitigating sulfate attack. The ternary blends showed significant improvements in reducing chloride penetration and such reduction in diffusivity continued to increase with age. Thomas and Bamforth [20] modeled the chloride diffusion in concrete using data from long-term field and laboratory studies and showed that the incorporation of fly ash and slag may have little influence on the early-age chloride resistance but dramatic benefits after a few years of exposure. Mangat et al. [27] investigated the partial replacement of cement by pulverised fuel ash, slag, and microsilica and showed microsilica to be the most effective in enhancing the corrosion resistance of rebar in concrete. The microsilica addition was found to greatly increase the pore volume in cement paste yet greatly decrease the chloride penetration. Güneysi et al. [28] investigated the rebar corrosion in concrete made of blended cements which contained various proportions of Portland cement clinker, blast furnace slag, natural pozzolans, and limestone powder. Relative to the plain cement concrete, the specimens with blended cements showed superior corrosion performance and generally longer time to corrosion cracking, which correlated very well with the splitting tensile strength data.

There is existing research demonstrating the use of mineral admixtures to improve other aspects of concrete durability, such as effectively mitigating the ASR-induced damage in concrete [29-32]. Papadakis [33] found that replacing aggregates with SCMs (silica fume, low- and high-lime fly ashes) improves the resistance of concrete to carbonation whereas replacing cement with SCMs increases the carbonation depth. In both cases, however, the incorporation of SCMs significantly lowered the total chloride content in concrete at all depths other than the very external surface layer. Mineral admixtures may slow the rate of strength gain in concrete, but do not adversely affect the long-term concrete strength [34] or even improve its strength properties [27, 35, 36]. Concrete mixes with high-volume fly ash or high-volume fly ash and ground slag demonstrate good workability, high compressive strength, and excellent durability (negligible carbonation and very low chloride penetration) [37].

Fly ash (FA) is a byproduct of coal combustion in the generation of electricity, i.e., a finely segregated residue captured from the flue gas at coal-fired power plants. Most FA particles are spherical and amorphous, ranging in size between 10 and 100 microns. With increasing energy costs and heightened concerns about the impact of concrete construction and maintenance activities on the environment, there has been an attendant increase in interest and research activity on the use of FA and other recycled materials in concrete, including those targeting ASR prevention [38-40]. The effectiveness of FA in mitigating mortar bar expansion induced by potassium-acetate-based deicer solution was found to depend on the lime content of FA and its dosage level [41].

The use of FA as a supplemental binder in concrete is common: 15 of the 72 million tons of fly ash produced in the U.S. in 2006 were used for this purpose [42] and many states have allowed the use of performance-specified (ASTM C 1157) cements that contain FA. The efficacy of a particular FA in this regard however is difficult to predict and no single index value or combination of values is an infallible predictor of its performance in concrete [43]. Following the provisions of ASTM C 618, fly ashes can be divided into two primary classes, F and C, based on their chemical composition resulting from the type of the coal burned. Normally Class F FA is produced from anthracite or bituminous coals, whereas Class C FA is produced from lignite or sub-bituminous coals [44]. ASTM C 618 also specifies another class, N, typically for natural pozzolans. This classification system, based on the silica, alumina, and iron oxide content of the ash (as shown in Appendix E1), only indirectly indicates how the ash will behave as an ingredient in concrete. Additional characteristics of importance include the calcium oxide content, fineness, crystalline structure, and loss on ignition (LOI, an indicator of carbon content) of the ash.

There are numerous studies on the effect of FA addition on the durability of concrete. Hedegaard and Hansen [45] argued that replacing cement with FA is likely degrade the water-tightness of concrete, as they found that 1 kg of cement would have to be replaced by 3 kg of FA in order to maintain the same level of water permeability of hardened concrete (at 28 days and 56 days). Wong et al. [46] tested notched mortar specimens and concluded that a 15% cement replacement by class F FA enhanced the bond strength of mortar-aggregate interface and fracture toughness. At high replacement levels (45% and 55%) the FA addition reduced the interfacial bond strength and fracture toughness at 28 days but such reductions were recovered at 90 days. The FA replacement at all levels was found to increase the interfacial fracture energy. Gebler and Klieger [47] found that the use of certain fly ashes degraded the freeze-thaw resistance of air-entrained concrete when cured at low temperature and showed no significant influence for other conditions. The incorporation of FA in concrete generally reduced the resistance of air-entrained concrete to deicing scaling and showed little benefit on its resistance to chloride penetration.

In general, FA addition in concrete is considered an effective measure to mitigate chloride-induced corrosion of rebar in concrete. For instance, using FA blended cement is known to reduce chloride permeability and improve sulfate resistance of concrete [48]. Dhir et al. [49] used the equilibrium method and found that the chloride binding capacity of cement paste increased with the increase in FA replacement level up to 50% and then declined at 67%. In the case of admixed chloride, the increase in chloride binding due to the replacement of FA was also found [50-53]. An increase in chloride binding may be mainly ascribed to the high alumina content in FA [24, 51], which results in the formation of more Friedel's salt [54]. The increase in chloride binding could also be ascribed to the production of more gel during hydration, which results in better physical adsorption of chloride [55]. Other researchers [50, 51, 54] also found that partial replacement of cement with FA has a positive effect on the chloride binding when the cement paste was exposed to a chloride environment. However, Nagataki et al. [56] found that the 30% replacement of cement with FA reduced the chloride binding capacity

of cementitious material in the case of external chlorides. Ampadu et al. [57] found the partial replacement of cement by FA only showed significant benefits in reducing the chloride diffusivity in cement paste at later ages of curing and a 40% replacement level was the best. Thomas [58] reported that chloride threshold decreased with increasing of FA content in marine exposure. These threshold values obtained were 0.7%, 0.65%, 0.5% and 0.2% acid soluble chloride (by mass of cementitious material) for concrete with 0, 15%, 30% and 50% FA, respectively. Despite of these lower threshold values, FA concrete was found to provide better corrosion protection to steel rebar due to of its higher resistance to chloride penetration. Oh et al. [59] also reported lower chloride threshold values with increasing addition of FA, whereas Schiessl and Breit [60] and Alonso et al. [61] reported higher or similar threshold values respectively when replacing cement with FA. For a concrete mix with water-to-cementitious-materials ( $w/cm$ ) ratio of 0.37, the addition of FA (35% cement replacement) and silica fume (27% cement replacement) reduced the chloride diffusion coefficient from  $3.48 \times 10^{-12} \text{ m}^2/\text{s}$  to  $7.35 \times 10^{-13} \text{ m}^2/\text{s}$  and  $1.01 \times 10^{-12} \text{ m}^2/\text{s}$ , but also reduced the pore water pH from 13.84 to 13.39 and 13.47, respectively [12]. Other researchers [62, 63] also reported the reduction of pH in the pore solution as a result of FA addition. The reduction of pore water pH may explain the research finding that the chloride threshold decreased with increasing FA content in concrete, whereas the improved resistance to chloride diffusion may explain the enhanced protection of embedded steel by the FA admixed concrete [23]. Saraswathy and Wong [64] investigated the effect of admixing activated FA on the corrosion resistance of concrete and found that the FA addition significantly improved the corrosion performance of concrete up to a critical moderate replacement level (20% to 30%) and the chemical activation of FA worked the best.

Ultra-fine fly ash (UFFA) is a relatively new pozzolanic admixture and there are a limited number of studies on the effect of its addition on the durability of concrete. It is processed from ordinary FA to obtain finer particles (as shown in Appendix E5). UFFA has been shown to feature higher pozzolanic activity than ordinary fly ashes, to greatly reduce the water demand and air content of concrete, and to produce concrete of higher strength and lower porosity [65, 66]. Hossain et al. [67] found that the restrained mortars containing UFFA or ordinary class F fly ash had lower residual stress levels, less free shrinkage, increased cracking age, and decreased creep effect, relative to the control. The UFFA addition led to more pronounced delay in the age of cracking and in the reduction in creep effect, relative to the ordinary fly ash. Subramaniam et al. [68] observed “a significant reduction in the autogenous shrinkage and an increase in the age of restrained shrinkage cracking” in the concrete admixed with UFFA, relative to the control and the concrete admixed with silica fume. An “increase in the age of restrained shrinkage cracking and a significant increase in the compressive strength” were reported with increasing UFFA addition or decreasing  $w/cm$  ratio.

Silica fume (SF) is typically a byproduct of manufacturing silicon and ferrosilicon alloys, i.e., a finely segregated residue captured from the oxidized vapor on top of the electric arc furnaces. Most SF particles are amorphous and ultra-fine in size, averaging from 0.1 to 0.5 microns, or approximately one hundredth the size of the average cement particle. Owing to its extreme fineness, large surface area and high silica content, SF is a

chemically reactive pozzolan and its use in cementitious systems has been specified by ASTM C 1240 (as shown in Appendix E3). Partial replacement of cement by SF up to 10% did not reduce the workability of fresh concrete, but slump loss with time was observed to increase with replacement level at low  $w/cm$  ratios [69]. As such, the SF addition is often accompanied by the use of a superplasticizer, i.e., high-range water reducer. Cong et al. [70] reported the partial replacement of cement by SF coupled with the superplasticizer addition to increase the compressive strength of concrete, which was largely attributed to the improved strength of its cement paste.

SF is known to considerably reduce the permeability of concrete by refining its microstructure via both chemical and physical pathways, and thus greatly reduce the risk of rebar corrosion in concrete. Selvaraj et al. [71] recently reviewed the influence of silica fume on the factors relevant to the corrosion of reinforcement in concrete, including chloride diffusion, carbonation, oxygen diffusion, pore solution pH, and electrical resistivity of concrete. The partial replacement of cement by silica fume has been reported to reduce the alkalinity of the pore solution and the chloride binding capacity of hardened cement paste [72]. The reduction in pore solution pH is mainly due to the pozzolanic reaction between silicon dioxide and the Portlandite [73]. The reduction in chloride binding capacity by silica fume addition has been reported by other researchers [51, 72, 74], as silica fume reduces the amount of aluminate phases in concrete that are able to chemically bind chlorides and produces C-S-H that seem to have lower chloride sorption than C-S-H generated from cement hydration [74]. These mechanisms can lead to dramatic increase in the  $Cl^-/OH^-$  ratio in the pore solution and may be responsible for the reduction in the chloride threshold value of steel in concrete [21, 75]. Dotto et al. [76] observed that the silica fume addition led to significant improvements in the corrosion performance of the concrete as well as in the compressive strength of concrete, whereas Page and Havdahl [77] observed slightly higher corrosion rates of steel in cement paste containing silica fume.

Ground granulated blast-furnace slag (GGBFS) is a byproduct of making iron and steel, i.e., a fine powder grounded from the glassy, granular material that forms when molten iron blast furnace slag is air quenched with water or steam. GGBFS features a fineness similar to cement particles and contains very limited amount of crystals. GGBFS is highly cementitious in nature and its use in mortar and concrete has been specified by ASTM C 989. Partial replacement of cement by GGBFS up to 80% was observed to reduce the compressive strength of concrete during the first 28 days while the later-age strength increased with the slag replacement up to 60% [78]. Partial replacement of cement by GGBFS up to 80% has demonstrated to improve the corrosion performance of concrete and the 50% replacement level in concrete imparted the best corrosion resistance, which featured the corrosion initiation time of steel rebar 3.2 to 3.8 times as long as the control (depending on the tricalcium aluminate [ $C_3A$ ] content in cement) [79]. The effect of GGBFS addition on the sulfate resistance of concrete was more complex, depending on the replacement level and the cement composition [79]. GGBFS was found to considerably improve the pore structure of concrete, increase its chloride binding capacity (by forming more Friedel's salt), and reduce its chloride diffusivity [80, 81]. While the slag addition improves both chemical and physical binding of chloride [51, 79,

83], it decreases the pH of the pore solution [81]. The effect of partial cement replacement by slag on the chloride threshold value is still controversial, as Gouda and Halaka [82] reported lower threshold values for slag concrete whereas Schiessl and Breit [60] and Oh et al. [59] reported higher or similar threshold values respectively when replacing cement with slag. Cheng et al. [81] investigated the corrosion behavior of reinforced concrete prismatic beams subjected to sustained loadings (37% and 75% of the ultimate load) and 3.5% NaCl solution and found the slag concrete to exhibit lower corrosion rate for a given reduction percentage in flexural rigidity (relative to the control). The partial replacement of cement by GGBFS reduced the electrical charge passing through the concrete (during the rapid chloride penetration test) and the water permeability of concrete. This was the result of GGBFS reacting with water and Portlandite to form extra C-S-H gel and more refined microstructure. A study of slag concrete after 25 years of exposure in a marine tidal zone [84] confirmed the beneficial role of slag in dramatically reducing the chloride ion penetration, especially at relatively high replacement levels (45% to 65%) and low  $w/cm$  ratio (0.40).

Metakaolin (MK) is a material obtained by calcining clay mineral kaolinite between 500-800°C in an externally fired rotary kiln so that it loses water through dehydroxilation (i.e., removal of chemically bonded hydroxyl ions). MK generally has particle size finer than cement but not as fine as silica fume and features a two-dimensional order in crystal structure (as shown in Appendix E4). MK is a highly reactive aluminosilicate pozzolan and its use in cementitious systems has been specified by ASTM C 618. The partial replacement of cement by MK up to 20% was observed to greatly reduce the water absorption of concrete by capillary action but slightly increase the water absorption of concrete by total immersion [85]. The MK addition was found to increase early-age (1-3 days) flexural strength of concrete by as much as 60%; and the finer MK (with surface area 25.4 vs. 11.1 m<sup>2</sup>/g) showed higher reactivity and led to greater strength especially for compressive strength of concrete with low  $w/cm$  ratio (0.40). The MKs were found to consume Portlandite via their pozzolanic reactivity and produce more refined pore structure in concrete [86]. The sulfate resistance of both non-air-entrained and air-entrained concrete was found to increase with the MK replacement level (from 5% to 10% and 15%), by measuring expansion of concrete prisms and compressive strength reduction of concrete tubes [87]. The replacement of cement or sand by MK (10% or 20% by weight of cement) can greatly reduce the chloride permeability, gas permeability and sorptivity of concrete, by decreasing the mean pore size and improving uniformity of the pore size distribution [88]. Both steady- and non-steady-state chloride diffusion tests showed that the MK addition in Portland cement mortar tends to enhance the resistance to chloride transport through both the hydrated cement matrix and the paste-aggregate interfacial transition zone [89]. The MK addition was also found to compensate for the low early-age compressive strength of concrete containing GGBFS [78].

### *1.2.3. Measuring the Chloride Ingress into Concrete*

The chloride ingress into concrete and other cementitious materials is a complex phenomenon involving multiple mechanisms. As such, a wide array of tests have been developed and used to evaluate the resistance of chloride ion penetration into concrete. In 1997, Stanish et al. [90] conducted a literature review to synthesis the state of the art pertinent to testing the chloride penetration resistance of concrete (Table 1-1). And since then, there have been new advances in improving the test methods.

TABLE 1-1 Summary of Chloride Penetration Test Methods [90]

Test Method		Considers Chloride Ion Movement	At a Constant Temperature	Unaffected by Conductors in the Concrete	Approximate Duration of Test Procedure
Long Term	AASHTO T259 (salt ponding)	Yes	Yes	Yes	90 Day after curing and conditioning
	Bulk Diffusion (Nordtest)	Yes	Yes	Yes	40 - 120 Days after curing and conditioning
Short Term	RCPT (T277)	No	No	No	6 hours
	Electrical Migration	Yes	Yes	No	Depends on Voltage and Concrete
	Rapid Migration (CTH)	Yes	Yes	No	8 hours
	Resistivity	No	Yes	No	30 Minutes
	Pressure Penetration	Yes	Yes	Yes	Depends on Pressure and Concrete (but potentially long)
Other	Soptivity – Lab	No	Yes	Yes	1 week incl. Conditioning
	Soptivity-Field	No	Yes	Yes	30 minutes
	Propan-2-ol Counter-diffusion	No	Yes	Yes	14 days with thin paste samples
	Gas Diffusion	No	Yes	Yes	2-3 hrs.

There are two types of natural penetration experiments generally used to measure the chloride diffusion coefficients of concrete. One is the steady-state diffusion tests, such as the *Diffusion Cell Test* in which a concrete specimen is used to separate a chloride solution from a chloride-free solution and periodical measurements of the chloride ion content are conducted until a steady state condition is achieved. The other is from non-steady state tests that involve the ponding or immersion of concrete specimen for a specific duration before measuring the chloride penetration depth or profile, such as the *Salt Ponding Test* [14]. The diffusion coefficients obtained are known as effective ( $D_{eff}$ ) and steady-state ( $D_s$ ), or apparent ( $D_{app}$ ) and non-steady-state ( $D_{ns}$ ) diffusion coefficient, respectively [91, 92]. The ponding test has been standardized as AASHTO T 259 and ASTM C 1543, involving the laborious analysis of chloride content at various depths of the sample after 90 days of ponding, which apparently is not sufficient time for high-quality concrete to produce meaningful chloride concentration profile.

Natural penetration tests (based on ASTM standards) are very time-consuming, especially for measuring the chloride diffusivity in high-quality concrete mixes. The diffusion tests often take a minimum of 1 to 3 years of exposure in simulated weathering conditions before any service life modeling can be conducted [93]. One way to accelerate the ingress of chloride into concrete is to apply a pressure. There is little research on this method, which exposes one face of the concrete to the chloride solution under pressure and drives the chlorides into the concrete under both convection and diffusion [94]. Recently, there has been an increasing demand for rapid, reliable methods for testing the chloride ion penetration resistance in a particular type of concrete and for testing the corrosion risk of rebar in a particular environment.

In the last decades, electric field migration tests have become very popular as they can greatly accelerate the chloride ingress into concrete. *Rapid Migration Test (RMT)* is a method to measure the electrical migration of chloride from one compartment with a chloride solution to the other that is chloride-free [95]. The average depth of chloride penetration is obtained by spraying a colorimetric indicator on the sample, and the value is then divided by the product of the applied voltage and migration time to rate the concrete permeability. Castellote et al. [92] developed a method to derive both  $D_{ns}$  and  $D_s$  from the migration test by monitoring the conductivity of the solution in the anodic compartment (destination solution that was initially distilled water). In our opinion, however, this method may produce misleading results when used to test high-quality concrete over a long time period, since the anolyte conductivity is very sensitive to chemical changes induced by the electrochemical reactions at the anode and the leachates from the test specimen.

*Rapid Chloride Permeability Test (RCPT)* is a method that records the amount of charge passed through a concrete sample in order to evaluate its permeability [96]. By introducing the concept of ion mobility, the similarity between diffusion and migration enables the determination of an ion diffusion coefficient from the migration tests. For PCC and mortar with no or little minerals admixed, it has been shown that the total charge passed is strongly correlated with the integral chloride content of ponding test [97] and with the chloride diffusion coefficient obtained from an accelerated chloride migration test [98, 99]. The RCPT has been standardized as AASHTO T 277 and ASTM C 1202, involving the classification of chloride permeability of concrete based on the charge in the first 6 hours, which again is not sufficient time to differentiate high-quality concrete mixes. Furthermore, the electrical charge passed in the test is related to all ions in the pore solution, not just chloride ions [90]. In addition, RCPT is not suitable for evaluating the chloride permeability of concrete with supplementary cementing materials [15, 100, 101], since the results may be significantly biased due to the change in the chemical composition of the pore solution [91, 102].

*Accelerated Chloride Migration Test (ACMT)* can be considered a modified version of RMT and RCPT, which periodically measures the accumulative chloride ion concentration in the destination compartment either by the potentiometric titration method [103] or using a chloride sensor [98, 99]. The test lasts until significant chloride

ion concentration is detected in the destination compartment, which could be hours, days, or weeks depending on the thickness and quality of the test specimen and the applied voltage. Cho and Chiang [103] investigated the chloride diffusivity in concrete specimens with various  $w/c$  ratio (0.35 to 0.65) and slag content (0% to 70%). They found good and very poor correlation between the charge passed and the non-steady-state diffusion coefficient ( $D_{ns}$ ) obtained from the ponding test, for concrete with and without slag respectively. For both types of concrete, there was a linear correlation between the steady-state diffusion coefficient ( $D_s$ ) obtained from the ACMT and the  $D_{ns}$  obtained from the ponding test, suggesting the ACMT to be a reliable accelerated test method. If the applied voltage is too high (e.g., 60 V), the Joule effect may lead to a higher value of electrical charge passed during RCPT or a higher  $D_s$  value during ACMT, i.e., the temperature increase of the test solutions [96], which can be mitigated by significantly increasing the volume of test solutions (e.g., from 250 mL to 4.5 L) [103]. Furthermore, the geometric shape of the test cell and the resistivity of the concrete specimen could affect the test results [104, 105]. Vivas et al. [106] investigated the chloride diffusivity in 19 concrete mixes prepared with materials typically used in construction in the state of Florida. They found that the RMT test (NordTest NTBuild 492) results had similar or better correlation with the 364-day bulk diffusion test (NordTest NTBuild 443) than those from the RCPT (ASTM C 1202) or the surface resistivity test (FM 5-578) and were less affected by the presence of SCMs in concrete.

### **1.3. Challenges in Assessing Concrete Durability from Its Chloride Diffusivity**

The length of the corrosion propagation stage in concrete is usually found to be relatively short, typically a few years. As a result, much of the emphasis on achieving concrete durability of 75 years or longer is put on achieving a long corrosion initiation stage [107], which is a function of the chloride transport properties of concrete (usually the diffusion coefficient), the surface chloride content dictated by the environment, the concrete cover thickness, and the chloride threshold concentration determining the onset of active corrosion. Note that Pettersson [108] argued that the propagation period could be as long as 50 years or more for high performance concrete featuring high electric resistivity and very limited oxygen availability.

Both the chloride ingress into concrete and the subsequent corrosion initiation of rebar in concrete are complex processes, which are influenced by numerous factors. Therefore, challenges are inherent in assessing concrete durability from its chloride diffusivity, mainly pertinent to the determination of chloride threshold and the quantification of chloride binding effect.

#### *1.3.1. Chloride Threshold*

Chloride threshold of rebar in concrete,  $Cl_{th}$ , can be defined as the content of chloride at the depth of the rebar that is necessary to sustain localized breakdown of its passive film and hence initiate its active corrosion [109]. The time it takes for chloride ions from external sources (marine environments or deicing salt applications) to reach  $Cl_{th}$  at the rebar depth is defined as time-to-corrosion,  $T_i$ . The  $Cl_{th}$  is an important parameter in

modeling and predicting the  $T_i$  and subsequently in assessing the service life of reinforced concrete in chloride-laden environments [81, 110].

The  $Cl_{th}$  data in published literature scatter over a wide range of values [111-113]. One possible reason is that the chloride threshold has different definitions and measurement methods [114-116]. The chloride-to-hydroxyl ionic concentration ratio ( $[Cl^-]/[OH^-]$ ) has been traditionally considered to be a more reliable indicator than the chloride concentration (often expressed as total chloride content by the weight of cement or concrete or free chloride concentration in concrete pore solution), considering that the competition between aggressive  $Cl^-$  and inhibitive  $OH^-$  governs the pitting and repassivation of steel. Research in aqueous solutions has indicated that for chloride-contaminated concrete the pitting corrosion occurs only above a critical  $[Cl^-]/[OH^-]$  ratio [115]. Through a probability simulation model, the threshold  $[Cl^-]/[OH^-]$  for corrosion of bare steel rods in high pH solutions was once predicted to be 0.66 in the presence of oxygen bubbles attached to the steel and 1.4 in the case of air. Such result agreed favorably with experimental data. In the same model, it was concluded that the threshold ratio should be about 1.4 for typical reinforced concrete and in excess of 3 for high-quality concrete with minimal air voids [10]. A number of studies [61, 117-120] exposed reinforcing steel bars to simulated concrete pore solutions and revealed that the threshold  $[Cl^-]/[OH^-]$  ratio increased with increasing pH. The threshold  $Cl/OH$  ratio in mortars has reported higher results (1.17-3.98) than that found in synthetic pore solution (0.25-0.8) [112]. Recently, Ann and Song [115] argued that the ratio of total chloride content to acid neutralization capacity,  $[Cl^-]/[H^+]$ , best presents the chloride threshold level since it takes into account “all potentially important inhibitive (cement hydration products) and aggressive (total chloride) factors”. The different methods used to assess the chloride content or its profile in concrete contributed to the variability in reported  $Cl_{th}$  values. Traditionally, the coring method is commonly used, which involves acquisition of one or more cores from sound concrete between reinforcements at the time of active corrosion initiation. The cores are sliced and analyzed for their chloride content, and the chloride content in the slice near the rebar depth is defined as  $Cl_{th}$ . Recently, both experimental [131] and modeling [125, 130, 132, 133] studies unraveled that chloride content at the top of the rebar trace was higher than that at the same depth away from the rebar, owing to the relatively low content of coarse aggregates in the vicinity of the rebar [128] and the rebar serving as a physical barrier to chloride migration. Thus, it is more reasonable to express  $Cl_{th}$  with the chloride content on the top of rebar trace than that acquired from the core sample.

The lack of universally accepted chloride threshold value is also attributable to the numerous factors that affect steel corrosion in concrete, such as: the pH of concrete pore solution, the electrochemical potential of the steel, and the physical condition of the steel/concrete interface. The pH of concrete pore solution mainly depends on the type of cement and additions and the carbonation level of concrete [121-124]. The potential of the steel is not only related to the steel type and surface condition (e.g., roughness) but also the oxygen availability at the steel surface; the latter is affected by the moisture content of concrete [61, 119, 125]. The physical condition of the steel/concrete interface (especially entrapped air void content) was found to be more dominant in the  $Cl_{th}$  than

chloride binding or buffering capacity of cement matrix or binders [115]. Voids that can be normally found in real structures due to incomplete compaction may weaken the layer of cement hydration products deposited at the steel/concrete interface and thus may favor local acidification required for sustained propagation of pits. The presence of air voids, as well as crevices and microcracks, may decrease the chloride threshold [126-129]. In addition, the presence of sulfate ions, the temperature and the concrete mix proportions and quality may affect the chloride threshold [113, 114, 120, 129]. Li and Sagüés [120] listed a wide array of internal and external factors defining the  $Cl_{th}$ , such as: the composition, surface condition, and configuration of rebar; the concrete chemistry (type and amount of cement and admixtures, type and porosity of aggregates,  $w/c$  ratio, degree of hydration, etc.); the type and source of chloride; and the service environment (humidity, temperature, cracking of concrete, etc.). Angst et al. [114] summarized the state of the art in the  $Cl_{th}$  research in a recent review.

Furthermore, it has been argued that the  $Cl_{th}$  (and  $T_i$ ) should be treated as a distributed parameter represented by a probability function, in light of the statistical nature of the processes involved (e.g., chloride ingress and pitting initiation) and the inherent heterogeneities of the concrete matrix [120, 128, 129]. Li and Sagüés [120] suggested the incorporation of a  $Cl_{th}$  variability term in the service life prediction procedures and durability models. Hartt and Nam [121] reported a range of values for  $Cl_{th}$  and  $T_i$  with seemingly identical slabs and the same exposure condition, as variability was introduced by micro-structural factors such as the size and distribution of entrapped air voids, and the arrangement of aggregates which can significantly affect the tortuosity of chloride ingress path. Currently, there is limited research on the probabilistic nature of how mix design and other factors impact corrosion initiation (as indicated by  $Cl_{th}$  and  $T_i$ ) [121, 125, 130].

### 1.3.2. Chloride Binding

In concrete, chlorides can exist either in the pore solution, chemically bound with concrete  $C_3A$  (tricalcium aluminate) or  $C_4AF$  phases (e.g., Friedel's salt,  $3CaO \bullet Al_2O_3 \bullet CaCl_2 \bullet 10H_2O$ ), or physically held to the surface of hydration products (e.g., adsorption on C-S-H) [134-136]. Chloride binding removes chloride ions from the pore solution, and slows down the rate of penetration [137]. With water-soluble and acid-soluble chlorides referred to as free and total chlorides respectively, the total chloride diffusivity was found to be near three times the free chloride diffusivity [19]. In a Florida DOT study, the relationship between bound and free chlorides was found to follow the Langmuir adsorption isotherm [12]. While previous studies [36, 138] suggest that only free chloride ions in the pore solution are responsible for initiating corrosion of the steel, Glass et al. [111, 139, 140] indicated that bound chlorides may also present a significant risk to steel. One possible reason is that a large part of bound chlorides are released as soon as the pH drops to values below 12 [5].

Chloride binding further complicates the determination of the threshold  $[Cl^-]/[OH^-]$  to initiate corrosion of steel in concrete [141], and the chloride binding and pH of pore solution are two inter-related parameters. It has been observed that the pH of NaCl-

containing alkaline solution increases as the chloride binding increases [135]. Reducing the pH in concrete may destabilize the chloroaluminate and thus reduce the percent of bound chloride [5, 115], and carbonation of concrete can reduce the chloride binding capacity [116, 142] and facilitate the chloride intrusion [143]. Chloride binding evidently decreases with increasing OH<sup>-</sup> above pH 12.6 and a decrease in pH can thus result in decreasing [Cl<sup>-</sup>]/[OH<sup>-</sup>] [144].

The chloride binding capacity is affected by numerous factors, such as the C<sub>3</sub>A and alkali contents of cement [145], use of mineral admixtures [19, 49-56, 71, 73, 78, 79], cation of the chloride salt [146], temperature, and degree of hydration [137].

#### **1.4. Chloride Transport in Concrete and Service Life of Reinforced Concrete – A Modeling Perspective**

This work started with a comprehensive literature review on topics relevant to this study. As detailed in Appendix A, the information on existing research was synthesized pertaining to the computational models to simulate the transport of species in aqueous solution, water-unsaturated and water-saturated cementitious materials, and the service life modeling of reinforced concrete in chloride-laden environments.

#### **1.5. A Phenomenological Model for the Chloride Threshold of Pitting Corrosion of Steel in Simulated Concrete Pore Solutions**

As detailed in Appendix B, a systematic study was also conducted to provide quantitative understanding of the fundamental factors that influence the chloride threshold of pitting corrosion of steel in concrete, by conducting a set of laboratory tests to assess the corrosion potential ( $E_{\text{corr}}$ ) and pitting potential ( $E_{\text{pit}}$ ) of steel coupons in simulated concrete pore solutions. With the aid of artificial neural network (ANN), the laboratory data were then used to establish a phenomenological model correlating the influential factors (total chloride concentration, chloride binding, solution pH, and dissolved oxygen concentration) with the pitting risk (characterized by  $E_{\text{corr}} - E_{\text{pit}}$ ). Three-dimensional response surfaces were then constructed to illustrate such predicted correlations and to shed light on the complex interactions between various influential factors. The results indicate that the threshold [Cl<sup>-</sup>]/[OH<sup>-</sup>] of steel rebar in simulated concrete pore solutions is a function of dissolved oxygen concentration, pH and chloride binding, instead of a unique value. The limitations and practical implications of the research findings were also discussed.

#### **1.6. Modeling Cathodic Prevention for Unconventional Concrete in Salt-laden Environment**

As detailed in Appendix C, numerical studies were conducted to provide a modeling perspective relevant to the use of cathodic protection (CPre) for SCMs-containing concrete in salt-laden environment. Based on the experimentally obtained concrete resistivity and chloride diffusion coefficient data, the Nernst-Planck equations were used to investigate the influence of applied voltage (magnitude, direction, and interruption),

surface chloride concentration, and concrete mix design on the effectiveness of cathodic prevention and the distribution of ionic species in protected concrete. The modeling results revealed that the direction of applied electric voltage has significant effect on the distributions of electrical potential and hydroxyl ions in the reinforced concrete, confirming the benefits of cathodic prevention in significantly increasing hydroxyl concentration near rebar and in slowing down the ingress of chloride into concrete. The performance of intermittent CPre was found to be constrained by the variations in concrete resistance from the anode to the cathode. The model was also useful in illustrating the temporal and spatial evolutions on rebar surface in terms of oxygen, hydroxyl and chloride concentrations on and electrical potential of top rebar as well as such evolutions in concrete domain in terms of concrete resistivity and current density for each mix design. The results shed light on the fundamental processes defining the performance of CPre for new unconventional concrete in salt-laden environment.

### **1.7. Study Objectives**

The objectives of this research are to validate chloride diffusion coefficients of mineral admixture concrete mix designs currently developed by the Caltrans for corrosion mitigation, and to verify the adequacy of existing measures to mitigate corrosion caused by exposure to marine environments and deicing salt applications. To this end, this research includes a comprehensive literature review on relevant topics, a laboratory investigation and a modeling effort. The laboratory investigation examines the compressive strength of and chloride diffusivity in mortar and concrete samples with cement partially replaced by various minerals (class F and class N FA, UFFA, SF, MK and GGBFS), the porosity of mineral concretes, the freeze-thaw resistance of mineral mortars in the presence of deicers, the effect of SCMs on the chloride binding and chemistry of the pore solution in mortar, as well as the pitting risk of steel rebar in simulated pore solutions with various chloride concentration, chloride binding, pH and dissolved oxygen concentration. The modeling effort explores the important features of ionic transport in concrete and develops a two-dimensional finite-element-method (FEM) model coupled with the stochastic technique. The numerical model is then used to examine the service life of reinforced concrete as a function of mix design (i.e., partial replacement of cement by mineral admixtures), concrete cover depth, surface chloride concentrations, and presence of cracks and coarse aggregates.

### **1.8. How This Report Is Organized**

The following chapter will present the methodology, results and discussion pertinent to the laboratory investigation of mortar and concrete samples. Chapter 3 presents the methodology, results and discussion pertinent to the modeling effort. Finally, Chapter 4 summarizes the key findings from both the laboratory and modeling components of this work, followed by suggestions and recommendations for implementation by the Caltrans. Appendices conclude this report.

### **1.9. References**

- [1] Lomborg, B. The skeptical environmentalist: measuring the real state of the world. Cambridge University Press, Cambridge, United Kingdom, pp. 512–540. 2001.
- [2] Mehta P. K. Reducing the Environmental Impact of Concrete. *Concr Int.* 2001; (10): 61-66.
- [3] Van Dam T.J., and Smartz, B.W. Use of Performance Specified (ASTM C1157) Cements in Colorado Transportation Projects: Case Studies, in: *TRB 89<sup>th</sup> Annual Meeting Compendium of Papers DVD*, Transportation Research Board, Washington D.C. 2010.
- [4] ASCE. “Report Card for America’s Infrastructure”, American Society of Civil Engineers, <http://www.infrastructurereportcard.org/>, last accessed on June 1, 2010.
- [5] Bertolini L, Elsener B, Pedferri P, Polder R. Corrosion of steel in concrete: Prevention, diagnosis, repair. Wiley-VCH, Verlag GmbH & Co. KgaA, Weinheim. 2004.
- [6] California Department of Transportation. Bridge Design Specifications, Section 9 – Reinforced Concrete. 2003.
- [7] Hartt W.H., G.P. Rodney, L. Virginie, and D.K. Lysogorski (2004). A Critical Literature Review of High-Performance Corrosion Reinforcements in Concrete Bridge Applications. FHWA-HRT-04-093.
- [8] Basheer L., J. Kropp, and D.J. Cleland. *Constr Buldg Mater* 2001; 15: 93.
- [9] Samples, L. and J. Ramirez, Methods of Corrosion Protection and Durability of Concrete Bridge Decks Reinforced with Epoxy-Coated Bars, Phase I. FHWA/IN/JTRP-98/15. Purdue University, IN. 1999.
- [10] Hausmann D.A. A Probability Model of Steel Corrosion in Concrete, *Mater Perform* 1998; 37(10): 64-68.
- [11] Page C.L., N.R. Short, and W.R. Holden, *Cem Concr Res* 1986; 16: 79.
- [12] Hartt, W., S. Charvin, and S. Lee, Influence of Permeability Reducing and Corrosion Inhibiting Admixtures in Concrete upon Initiation of Salt Induced Embedded Metal Corrosion, prepared for the Florida Department of Transportation. 1999.
- [13] Baykal M. (2000). Implementation of Durability Models for Portland Cement Concrete into Performance-Based Specifications. Austin, TX: The University of Texas at Austin.
- [14] Savas B.Z. (1999). Effects of microstructure on durability of concrete. Raleigh, NC: North Carolina State University.
- [15] Wee T., A. Suryavanshi, and S. Tin. Evaluation of Rapid Chloride Permeability Test (RCPT) Results for Concrete Containing Mineral Admixture, *ACI Mater J* 2000; 97(2): 221-232.
- [16] Toutanji, H. A.; Delatte, D. (2001), Supplementary Materials to Enhance Bridge Deck Durability, Prepared for University Transportation Center for Alabama.
- [17] Gruber K.A., T. Ramlochan, A. Boddy, R.D. Hooton, and M.D.A. Thomas. Increasing Concrete Durability with High-reactivity Metakaolin, *Cem Concr Comp* 2001; 23(6): 479-484.
- [18] Choi, Y.-S.; Kim, J.-G.; Lee, K.-M. Corrosion Behavior of Steel Bar Embedded in Fly Ash Concrete, *Corros Sci* 2006; 48(7): 1733-1745.

- [19] Lu, X.; Li, C.; Zhang, H. Relationship between the Free and Total Chloride Diffusivity in Concrete, *Cem Concr Res* 2002; 32(2): 323-326.
- [20] Thomas, M.D.A.; Bamforth, P. B. Modelling Chloride Diffusion in Concrete: Effect of Fly Ash and Slag, *Cem Concr Res* 1999, 29(4): 487-495.
- [21] Manera, M.; Vennessland, Ø.; Bertolini, L. 008), Chloride Threshold for Rebar Corrosion in Concrete with Addition of Silica Fume, *Corros Sci* 2008; 50(2): 554-560.
- [22] Yang, C. C.; Cho, S. W. An Electrochemical Method for Accelerated Chloride Migration Test of Diffusion Coefficient in Cement-based Materials, *Mater Phys Chem* 2003; 81(1): 116-125.
- [23] Thomas M. *Cem Concr Res* 1996; 26: 515.
- [24] Dhir R.K., and M. R. Jones. Development of Chloride-Resisting Concrete Using Fly Ash, *Fuel* 1999; 78(2): 137-142.
- [25] Hossain A.B., S. Shrestha, and J. Summers. Properties of Concrete Incorporating Ultrafine Fly Ash and Silica Fume, *Transp Res Rec* 2009; 2113: 41-46.
- [26] Thomas M.D.A., M.H. Shehata, S.G. Shashiprakash, D.S. Hopkins, and K. Cail. Use of Ternary Cementitious Systems Containing Silica Fume and Fly Ash in Concrete, *Cem Concr Res* 1999; 29: 1207-1214.
- [27] Mangat P.S., J.M. Khatib and B.T. Molloy. Microstructure, Chloride Diffusion and Reinforcement Corrosion in Blended Cement Paste and Concrete. *Cement and Concrete Composites* 1994; 16(2): 73-81.
- [28] Güneyisi E., T. Özturan, and M. Gesolu. Performance of Plain and Blended Cement Concretes against Corrosion Cracking, in: M.S. Konsta-Gdoutos (Ed.), *Measuring, Monitoring and Modeling Concrete Properties*, 189-198, 2006, Springer. Netherlands.
- [29] Xu G.J.Z., D.F. Watt, and P.P. Hudec. Effectiveness of Mineral Admixtures in Reducing ASR Expansion. *Cem Concr Res* 1995; 25(6): 1225-1236.
- [30] Malvar, L. J., Cline, G. D., Burke, D. F., Rollings, R., Sherman, T. W., and Greene, J. L. Alkali-Silica Reaction Mitigation: State of the Art and Recommendations, *ACI Mater J* 2002; 99: 480-489.
- [31] Taha, B., and Nounu, G. Using Lithium Nitrate and Pozzolanic Glass Powder in Concrete as ASR Suppressors, *Cem Concr Compos* 2008; 30: 497-505.
- [32] Shehata, M.H., and Thomas, M.D.A. The Role of Alkali Content of Portland Cement on the Expansion of Concrete Prisms Containing Reactive Aggregates and Supplementary Cementing Materials, *Cem Concr Res* 2010; 40(4): 569-574.
- [33] Papadakis V.G. Effect of Supplementary Cementing Materials on Concrete Resistance Against Carbonation and Chloride Ingress. *Cem Concr Res* 2000; 30(2): 291-299.
- [34] Caltrans (2002). Memo to Designers 1-5: Protection of Reinforcement against Corrosion Due to Chlorides, Acids and Sulfates.
- [35] Mehta P.K. Pozzolanic and Cementitious By-products in Concrete - Another Look, in: V.M. Malhotra (Ed.), *Proceedings of the Third CANMENT/ACI International Conference*, American Concrete Institute, Michigan, ACI SP 114, vol. 1, 1989, pp. 1-43.
- [36] Mehta P.K. Role of Pozzolanic and Cementitious Material in Sustainable Development of Concrete Industry, in: V.M. Malhotra (Ed.), *Proceedings of the*

- Sixth CANMET/ACI/JCI, International Conference on Fly Ash, Silica Fume and Natural Pozzolans in Concrete, American Concrete Institute, Michigan, ACI SP-178, vol. 1, 1998, pp. 1-20.
- [37] Collepardi, S.; Corinaldesi, V.; Moriconi, G.; Bonora, G.; Collepardi, M. (2000), Durability of High-Performance Concretes with Pozzolanitic and Composite Cements. ACI Special Report SP 192-10, American Concrete Institute.
- [38] Malvar, L.J., and Lenke, L.R. (2006). "Efficiency of Fly Ash in Mitigating Alkali Silica Reaction Based on Chemical Composition", *ACI Mater J*, Vol.103, No.5 pp.319-326.
- [39] Lenke, L.R., and Malvar, L.J. (2009). "Alkali Silica Reaction Criteria for Accelerated Mortar Bar Tests Based on Field Performance Data", in: *Proc. World of Coal Ash*, KY May 4-7, 2009.
- [40] Malvar, L.J. (2010). "ASR Prevention in DOD", in: *TRB 89<sup>th</sup> Annual Meeting Compendium of Papers DVD*, Transportation Research Board, Washington D.C.
- [41] Rangaraju P.R., and J. Desai. Effectiveness of Fly Ash and Slag in Mitigating Alkali-Silica Reaction Induced by Deicing Chemicals, *J Mat In Civ Engrg* 2009; 21: 19-31.
- [42] ACAA (2007). American Coal Ash Association, <http://www.aaa-usa.org/>.
- [43] Joshi, R.C., and Lohtia, R.P. Fly Ash in Concrete: Production, Properties and Uses. (Advances in concrete technology; v.2). Gordon and Breach Science Publishers, Amsterdam, Netherlands, 1997.
- [44] Scheetz B.E., and J. Olanrewaju. Determination of the rate of formation of hydroceramic waste forms made with INEEL calcined wastes. Final report prepared for the Department of Energy. 2001.
- [45] Hedegaard B.E., and T.C. Hansen. Water Permeability of Fly Ash Concretes. *Mater Struct* 1992; 25: 381-387.
- [46] Wong Y.L., L. Lam, C.S. Poon, and F.P. Zhou. Properties of Fly Ash-Modified Cement Mortar-Aggregate Interfaces. *Cem Concr Res* 1999; 29: 1905-1913.
- [47] Gebler S. H., and P. Klieger. Effect of Fly Ash on the Durability of Air-entrained Concrete, in: Proceedings of the 2<sup>nd</sup> International Conference on the Use of Fly Ash, Silica Fume, Slag, and Other Mineral By-Products in Concrete, April 21-25, 1986, Madrid, Spain. ACI publication SP-91.
- [48] Saraswathy V., and H.-W. Song. Corrosion Performance of Fly Ash Blended Cement Concrete: A State-of-Art Review, *Corros Rev* 2006; 24(1-2): 87-122.
- [49] Dhir R.K., M.A.K. El-Mohr, and T.D. Dyer. Developing Chloride Resisting Concrete Using PFA. *Cem Concr Res* 1997; 27(11):1633-1639.
- [50] Byfors K. Chloride Binding in Cement Paste, *Nordic Concr Res* 1986; 5: 27-38.
- [51] Arya C., N.R. Buenfeld, and J.B. Newman. Factors Influencing Chloride Binding in Concrete, *Cem Concr Res* 1990; 20(2):291-300.
- [52] Arya C., and Y. Xu. Effect of Cement Type on Chloride Binding and Corrosion of Steel in Concrete, *Cem Concr Res* 1995; 25(4):893-902.
- [53] Holden W.R., C.L. Page, and N.R. Short. Corrosion of Reinforcement in Concrete Construction, in: : A.P. Crane (Ed.), Chichester: Ellis Horwood Ltd.; 1983. pp. 143-50.

- [54] Wiens U., and P. Schiessl. Chloride Binding of Cement Paste Containing Fly Ash, in: H. Justnes (Ed.), Proceedings of the 10<sup>th</sup> ICCC, Goteborg, Sweden; 1997. pp. 4–10.
- [55] Kayyali O.A., and M.N. Haque. The  $Cl^-: OH^-$  Ratio in Chloride-Contaminated Concrete – A Most Important Criterion, *Mag Concr Res* 1995; 47: 235–242.
- [56] Nagataki S., N. Otsuki, T.H. Wee, and K. Nakashita. Condensation of Chloride Ion in Hardened Cement Matrix Materials and on Embedded Steel Bars, *ACI Mater J* 1993; 90(4): 323-332.
- [57] Ampadu K.O., K. Torii, and M. Kawamura. Beneficial Effect of Fly Ash on Chloride Diffusivity of Hardened Cement Paste, *Cem Concr Res* 1999; 29(4): 585-590.
- [58] Thomas, M., ‘Chloride Threshold in Marine Concrete’, *Cem. Concr. Res.* **26**(4), 1996, 513-519.
- [59] Oh, B. H., Yang, S. Y., and Shin, Y. S., ‘Experimental Investigation of the Threshold Chloride Concentration for Corrosion Initiation in Reinforced Concrete Structures’, *Mag. Concr. Res.* **55**, 2003, 117-124.
- [60] Schiessl, P., and Breit, W., ‘Local Repair Measures at Concrete Structures Damaged by Reinforcement Corrosion – Aspects of Durability’, in *Proceedings of the 4<sup>th</sup> International Symposium on Corrosion of Reinforcement in Concrete Construction*, The Royal Society of Chemistry, Cambridge, 1996, pp. 525-534.
- [61] Alonso, C., Castellote, M., and Andrade, C., ‘Chloride Threshold Dependence of Pitting Potential of Reinforcements’, *Electrochim. Acta* **47**, 2002, 3469-3481.
- [62] Diamond, S., ‘Two Danish Flyashes on Alkali Contents of Pore Solutions of Cement-Flyash Pastes’, *Cem. Concr. Res.* **11**, 1981, 383–394.
- [63] Kawamura, M., Kayyali, O. A., and Haque, M. N., ‘Effect of Flyash on Pore Solution Composition in Calcium and Sodium Chloride-Bearing Mortars’, *Cem. Concr. Res.* **18**, 1988, 763–773.
- [64] Saraswathy, V., and Song, H.-W., ‘Effectiveness of Fly Ash Activation on the Corrosion Performance of Steel Embedded in Concrete’, *Mag. Concr. Res.* **59**(9), 2007, 651-661.
- [65] Obla, K. H., Hill, R. L., Thomas, M. D. A., Shashiprakash, S. G., and Perebatova, O., ‘Properties of Concrete Containing Ultra-Fine Fly Ash’, *ACI Mater. J.* **100**(5), 2003, 1-8.
- [66] Jeon, S., Nam, J.-H., An, J.-H., and Kwon, S.-A., ‘Physical Properties of Rapid-Setting Concrete Using Ultra Fine Fly Ash’, in *Proceedings of Selected Papers from the 2009 GeoHunan International Conference, New Technologies in Construction and Rehabilitation of Portland Cement Concrete Pavement and Bridge Deck Pavement*, GSP 196.
- [67] Hossain, A. B., Fonseka, A., and Bullock, H., ‘Early Age Stress Development, Relaxation, and Cracking in Restrained Low W/B Ultrafine Fly Ash Mortars’, *J. Adv. Concr. Tech.* **6**, 2008, 261-271.
- [68] Subramaniam, K. V., Gromotka, R., Shah, S. P., Obla, K., and Hill, R., ‘Influence of Ultrafine Fly Ash on the Early Age Response and the Shrinkage Cracking Potential of Concrete’, *J. Mater. Civ. Engrg.* **17**(1), 2005, 45-53.

- [69] Duval, R., and Kadri, E. H., 'Influence of Silica Fume on the Workability and the Compressive Strength of High-Performance Concretes', *Cem. Concr. Res.* **28**(4), 1998, 533-547.
- [70] Cong, X., Gong, S., Darwin, D., and McCabe, S. L., 'Role of Silica Fume in Compressive Strength of Cement Paste, Mortar, and Concrete', *Mater. J.* **89**(4), 1989, 375-387.
- [71] Selvaraj, R., Muralidharan, S., and Srinivasan, S., 'The Influence of Silica Fume on the Factors Affecting the Corrosion of Reinforcement in Concrete - a Review', *Struct. Concr. J. FIB* **4**(1), 2003, 19-24.
- [72] Page, C. L., and Vennesland, Ø., 'Pore Solution Composition and Chloride Binding Capacity of Silica-Fume Cement Pastes', *Mater. Struct.* **16**(1), 1983, 19-25.
- [73] Byfors, K., 'Influence of Silica Fume and Flyash on Chloride Diffusion and pH Values in Cement Paste', *Cem. Concr. Res.* **17**, 1987, 115-130.
- [74] Larsen, C. K., Chloride Binding in Concrete, Doctoral Thesis, Report No. 1998: 101, Norwegian University of Science and Technology, NTNU, 1998.
- [75] Pettersson, K., 'Chloride Threshold Value and the Corrosion Rate in Reinforced Concrete', in *Proc. of the Nordic Seminar*, Lund, 1995, pp. 257-266.
- [76] Dotto, J. M. R., de Abreu, A. G., Dal Molin, D. C. C., and Müller, I. L., 'Influence of Silica Fume Addition on Concretes Physical Properties and on Corrosion Behaviour of Reinforcement Bars', *Cem. Concr. Compos.* **26**(1), 2004, 31-39.
- [77] Page, C. L., and Havdahl, J., 'Electrochemical Monitoring of Corrosion of Steel in Microsilica Cement Pastes', *Mater. Struct.* **18**, 1985, 41-47.
- [78] Khatib, J. M., and Hibbert, J. J., 'Selected Engineering Properties of Concrete Incorporating Slag and Metakaolin', *Constr. Bldg. Mater.* **19**(6), 2005, 460-472.
- [79] Al-Gahtani, A. S., Rasheeduzzafar, and Al-Saadoun, S. S., 'Rebar Corrosion and Sulfate Resistance of Blast-Furnace Slag Cement', *J. Mater. Civ. Engrg.* **6**(2), 1993, 223-233.
- [80] Luo, R., Cai, Y., Wang, C., and Huang, X., 'Study of Chloride Binding and Diffusion in GGBS Concrete', *Cem. Concr. Res.* **33**(1), 2003, 1-7.
- [81] Cheng, A., Huang, R., Wu, J.-K., and Chen, C.-H., 'Influence of GGBS on Durability and Corrosion Behavior of Reinforced Concrete', *Mater. Chem. Phys.* **93**, 2005, 404-411.
- [82] Gouda, V. K., 'Corrosion and Corrosion Inhibition of Reinforced Steel. I. Immersed in Alkaline Solutions', *Br. Corros. J.* **5**, 1970, 198-203.
- [83] Dhir, R. K., El-Mohr, M. A. K., and Dyer, T. D., 'Chloride Binding in GGBS Concrete', *Cem. Concr. Res.* **26**(12), 2000, 1767-1773.
- [84] Thomas, M. D. A., Scott, A., Bremner, T., Bilodeau, A., and Day, D., 'Performance of Slag Concrete in Marine Environment', *ACI Mater. J.* **105**(6), 2008, 628-638.
- [85] Khatib, J. M., and Clay, R. M., 'Absorption Characteristics of Metakaolin Concrete', *Cem. Concr. Res.* **34**(1), 2004, 19-29.
- [86] Justice, J. M., and Kurtis, K. E., 'Influence of Metakaolin Surface Area on Properties of Cement-Based Materials', *J. Mater. Civ. Engrg.* **19**(9), 2007, 762-771.

- [87] Al-Akhras, N. M., 'Durability of Metakaolin Concrete to Sulfate Attack', *Cem. Concr. Res.* **36**(9), 2006, 1727-1734.
- [88] Badogiannis, E., and Tsivilis, S., 'Exploitation of Poor Greek Kaolins: Durability of Metakaolin Concrete', *Cem. Concr. Compos.* **31**(2), 2009, 128-133.
- [89] Asbridge, A. H., Chadbourn, G. A., and Page, C. L., 'Effects of Metakaolin and the Interfacial Transition Zone on the Diffusion of Chloride Ions through Cement Mortars', *Cem. Concr. Res.* **31**(11), 2001, 1567-1572.
- [90] Stanish, K. D., Hooton, R. D., and Thomas, M. D. A., *Testing the Chloride Penetration Resistance of Concrete: A Literature Review*, Toronto, ON: Canada, University of Toronto, Toronto, ON, Canada, 1997.
- [91] Andrade, C., Castellote, M., Alonso, C., and González, C., 'Non-Steady-State Chloride Diffusion Coefficients Obtained from Migration and Natural Diffusion Tests. Part I: Comparison between Several Methods of Calculation', *Mater. Struct.* **33**(1), 2000, 21-28.
- [92] Castellote, M., Andrade, C., and Alonso, C., 'Measurement of the Steady and Non-Steady-State Chloride Diffusion Coefficients in a Migration Test by Means of Monitoring the Conductivity in the Anolyte Chamber. Comparison with Natural Diffusion Tests', *Cem. Concr. Res.* **31**(10), 2001, 1411-1420.
- [93] Husain, A., Al-Bahar, S., Salam, S. A., and Al-Shamali, O., 'Accelerated AC Impedance Testing for Prequalification of Marine Construction Materials', *Desalination* **165**, 2004, 377-384.
- [94] Shi, X., Liu, Y., Mooney, M., Berry, M., Hubbard, B., Fay, L., and Leonard, A. B. *Effect of Chloride-based Deicers on Reinforced Concrete Structures*. Final report prepared for the Washington State Department of Transportation. July 2010.
- [95] Stanish, K., Hooton, R. D., and Thomas, M. D. A., 'A Novel Method for Describing Chloride Ion Transport Due to an Electrical Gradient in Concrete: Part 1. Theoretical Description', *Cem. Concr. Res.* **34**(1), 2004, 43-49.
- [96] Ahmed, M. S., Kayali, O., and Anderson, W., 'Evaluation of Binary and Ternary Blends of Pozzolanic Materials Using the Rapid Chloride Permeability Test', *J. Mat. in Civ. Engrg.* **21**(9), 2009, 446-453.
- [97] Whiting, D., 'Rapid Measurement of the Chloride Permeability of Concrete', *Public Roads* **45**(3), 1981, 101-112.
- [98] Yang, Z., Shi, X., Creighton, A. T., and Peterson, M. M., 'Effect of Styrene-Butadiene Rubber Latex on the Chloride Permeability and Microstructure of Portland Cement Mortars', *Constr. Bldg. Mater.* **23**(6), 2009, 2283-2290.
- [99] He, X., and Shi, X., 'Chloride Permeability and Microstructure of Portland Cement Mortars Incorporating Nanomaterials', *Transp. Res. Rec.: J. Transp. Res. Brd.* **2070**, 2008, 13-21.
- [100] Shi, C., Stegemann, J. A., and Caldwell, R. J., 'Effect of Supplementary Cementing Materials on the Specific Conductivity of Pore Solution and Its Implications on the Rapid Chloride Permeability Test (AASHTO T277 and ASTM C1202) Results', *ACI Mater. J.* **95**(4), 1998, 389-394.
- [101] Feldman, R., Prudencio, L. R., and Chan, G., 'Rapid Chloride Permeability Test on Blend Cement and Other Concretes: Correlations between Charge, Initial Current and Conductivity', *Constr. Bldg. Mater.* **13**, 1999, 149-154.

- [102] Wee, T. H., Suryavanshi, A. K., and Tin, S. S., 'Evaluation of Rapid Chloride Permeability Test (RCPT) Results for Concrete Containing Mineral Admixtures', *ACI Mater. J.* **97**(2), 2000, 221-232.
- [103] Cho, S. W., and Chiang, S. C., 'Using the Chloride Migration Rate to Predict the Chloride Penetration Resistance of Concrete', in M. S. Konsta-Gdoutos (ed), *Measuring, Monitoring and Modeling Concrete Properties*, Springer, Netherlands, 2006, pp. 575-581.
- [104] Ghosh P., and Tikalsky, P. J., 'Determination of Diffusion Coefficients and Corrosion Initiation Time for Ternary Cementitious Mixtures', in *TRB 90<sup>th</sup> Annual Meeting Compendium of Papers DVD*, Transportation Research Board, Washington D.C., 2011.
- [105] Diaz, B., Freire, L., N6voa, X. R., Puga, B., and Vivier, V., 'Resistivity of Cementitious Materials Measured in Diaphragm Migration Cells: The Effect of the Experimental Set-up', *Cem. Concr. Res.* **40**(10), 2010, 1465-1470.
- [106] Vivas, E., Boyd, A., and Hamilton III, H. R., *Permeability of Concrete – Comparison of Conductivity and Diffusion Methods*, final report prepared for the Florida Department of Transportation, June 2007.
- [107] Weyers, R.E., 'Corrosion Service Life Model', in W. P. Silva-Araya, O. T. de Rincon, and L. P. O'Neill (eds), *Repair and Rehabilitation of Reinforced Concrete Structures: The State of the Art*, American Society of Civil Engineers, Reston, VA, 1998, p. 105.
- [108] Pettersson, K., 'Service Life of Concrete Structure Including the Propagation Time', in *Concrete under severe conditions 2: environment and loading: Proceedings of the 2nd International Conference on Concrete Under Severe Conditions*, CONSEC'98, Tromsø, Norway, June 21-24, 1998. pp.489-498.
- [109] Schiessl, P., and Raupach, M., 'Influence of Concrete Composition and Microclimate on the Critical Chloride Content in Concrete', in C. L. Page, K. W. J. Treadaway, and P. B. Bamforth (eds), *Corrosion of Reinforcement in Concrete*, Elsevier Applied Science, London, UK, 1990, pp. 49–58.
- [110] Stratfull, R. F., 'The Corrosion of Steel in a Reinforced Concrete Bridge', *Corros.* **13**(3), 1956, 173-178.
- [111] Glass, G. K., and Buenfeld, N. R., 'The Presentation of the Chloride Threshold Level for Corrosion of Steel in Concrete', *Corros. Sci.* **39**(5), 1997, 1001-1013.
- [112] Alonso, C., Andrade, C., Castellote, M., and Castro, P., 'Chloride Threshold Values to Depassivate Reinforcing Bars Embedded in A Standardized OPC Mortar', *Cem. Concr. Res.* **30**(7), 2000, 1047-1055.
- [113] Glass, G. K., and Buenfeld, N. R., 'Chloride-Induced Corrosion of Steel in Concrete', *Prog. Struct. Engrg. Mater.* **2**(4), 2000, 448-458.
- [114] Angst, U., Elsener, B., Larsen, C. K., and Vennesland, Ø., 'Critical Chloride Content in Reinforced Concrete – A Review', *Cem. Concr. Res.* **39**, 2009, 1122-1138.
- [115] Ann, K. Y., Song, H.-W., 'Chloride Threshold Level for Corrosion of Steel in Concrete', *Corros. Sci.* **49**, 2007, 4113-4133.
- [116] Kayyali, O. A., and Hague, M. N., 'Chloride Penetration and the Ratio of  $Cl^-/OH^-$  in the Pores of Cement Paste', *Cem. Concr. Res.* **18**, 1988, 895-900.

- [117] Yonezawa, T., Ashworth, V., and Procter, R. P. M., 'Pore Solution Composition and Chloride Effects on the Corrosion of Steel in Concrete', *Corros.* **44**(7), 1988, 489-493.
- [118] Breit, W., 'Critical Chloride Content - Investigations of Steel in Alkaline Chloride Solutions', *Mater. Corros.* **49**(6), 1998, 539-550.
- [119] Li, L., and Sagüés, A. A., 'Chloride Corrosion Threshold of Reinforcing Steel in Alkaline Solutions - Open-Circuit Immersion Tests', *Corros.* **57**(1), 2001, 19-28.
- [120] Li L, and Sagüés AA. *Metallurgical Effects on Chloride Ion Corrosion Threshold of Steel in Concrete.* , final Report for the Florida Department of Transportation. Tallahassee, FL, Report No. WPI 0510806, November 2001.
- [121] Hartt, W. H., and Nam, J., 'Effect of Cement Alkalinity on Chloride Threshold and Time-to-Corrosion of Reinforcing Steel in Concrete', *Corros.* **64**(8), 2008, 671-680.
- [122] Dehwah, H. A. F., Maslehuddin, M., and Austin, S. A., 'Effect of Cement Alkalinity on Pore Solution Chemistry and Chloride-Induced Reinforcement Corrosion', *ACI Mater. J.* **99**(3), 2002, 227-235.
- [123] Hassain, S. E., Al-Gahtani, A. S., and Rasheeduzzafar, 'Chloride Threshold for Corrosion of Reinforcement in Concrete', *ACI Mater. J.* **93**(6), 1996, 1-5.
- [124] Moreno, M., Morris, W., Alvarez, M. G., and Duffó, G. S., 'Corrosion of Reinforcing Steel in Simulated Concrete Pore Solutions – Effect of Carbonation and Chloride Content', *Corros. Sci.* **46**, 2004, 2681-2699.
- [125] Cros, P., Hartt, W. H., and Yu, H., 'Effects of Reinforcement on Chloride Intrusion into Concrete and Time-to-Corrosion', in *Proceedings of the 16<sup>th</sup> International Corrosion Congress*, September 22-26, 2005, Beijing, China.
- [126] Monfore, G. E., and Verbeck, G. J., 'Corrosion of Prestressed Wire in Concrete', *ACI Mater. J.* **57**(5), 1960, 491-497.
- [127] Söylev, T. A., and Francois, R., 'Corrosion of Reinforcement in Relation to Presence of Defects at the Interface between Steel and Concrete', *J. Mater. Civ. Engrg.* **17**(4), 2005, 447-455.
- [128] Yu, H., Himiob, R. J., and Hartt, W. H., 'Effects of Reinforcement and Coarse Aggregates on Chloride Ingress into Concrete and Time-to-corrosion: Part 2: Spatial Distribution of Coarse Aggregates', *Corros.* **63**(10), 2007, 924-931.
- [129] Yu, H., Shi, X., Hartt, W. H., and Lu, B., 'Laboratory Investigation of Reinforcement Corrosion Initiation and Chloride Threshold Concentration for Self-compacting Concrete', *Cem. Concr. Res.* **40**(10), 2010, 1507-1516.
- [130] Hansen, E. J., and Saouma, V. E., 'Numerical Simulation of Reinforced Concrete Deterioration: Part I: Chloride Diffusion', *ACI Mater. J.* **96**(2), 1999, 173-180.
- [131] Yu, Y., and Hartt, W. H., 'Effect of Reinforcement and Coarse Aggregates on Chloride Ingress into Concrete and Time-to-Corrosion: Part I - Spatial Chloride Distribution and Implications', *Corros.* **63**(9), 2007, 843–850.
- [132] Oh, B. H., and Jang, B. S., 'Chloride Diffusion Analysis of Concrete Structures Considering Effects of Reinforcing', *ACI Mater. J.* **100**(2), 2003, 143–149.
- [133] Kranc, S.C., Sagüés, A. A., and Presuel-Moreno, F. , 'Decreased Corrosion Initiation Time of Steel in Concrete Due to Reinforcing Bar Obstruction of Diffusional Flow', *ACI Mater. J.* **99**(1), 2002, 51–53.

- [134] Berman, H. A., 'Determination of Chloride in Hardened Portland Cement Paste, Mortar, and Concrete', *J. Mater.* **7**(3), 1972, 330–335.
- [135] Harald, J., 'A Review of Chloride Binding in Cementitious Systems', *Nordic Concr. Res.* **21**, 1998, 1–6.
- [136] Anik, D., Jacques, M., Jean-Pierre, O., Simone, J., and Kati, H., 'Chloride Binding Capacity of Various Hydrated Cement Systems', *Adv. Cem. Bas. Mater.* **6**, 1997, 28–35.
- [137] Buenfeld, N. R., Glass, G. K., Hassanein, A. M., and Zhang, J.-Z., 'Chloride Transport in Concrete Subjected to an Electric Field', *J. Mater. Civ. Engrg.* **10**(4), 1998, 220–228.
- [138] Suryavanshi, A. K., Scantlebury, J. D., and Lyon, S. B., 'Corrosion of Reinforcement Steel Embedded in High Water–Cement Ratio Concrete Contaminated with Chloride', *Cem. Concr. Compos.* **20**(3), 1998, 263–269.
- [139] Glass, G. K., and Buenfeld, N. R., 'The Influence of Chloride Binding on the Chloride-Induced Corrosion Risk in Reinforced Concrete', *Corros. Sci.* **42**(2), 2000, 329–344.
- [140] Reddy, B., Glass, G. K., Lim, P. J., and Buenfeld, N. R., 'On the Corrosion Risk Presented by Chloride Bound in Concrete', *Cem. Concr. Compos.* **24**(1), 2002, 1–5.
- [141] Shi, X., Nguyen, T.A., Kumar, P., and Liu, Y., 'A Phenomenological Model for the Chloride Threshold of Pitting Corrosion of Steel in Simulated Concrete Pore Solutions', *Anti-Corros. Meth. Mater.* 2010, in review.
- [142] Neville, A., 'Chloride Attack of Reinforced Concrete: an Overview', *Mater. Struct.* **28**, 1995, 63–70.
- [143] Traetteberg, A., *The Mechanism of Chloride Penetration in Concrete*, SINTEF Report STF65 A77070, 1977, 51 pp.
- [144] Tritthart, J., 'Chloride Binding in Cement II. The Influence of the Hydroxide Concentration in the Pore Solution of Hardened Cement Paste on Chloride Binding', *Cem. Concr. Res.* **19**(5), 1989, 683–691.
- [145] Rasheeduzzafar, Hussain, S. E., and Al-Saadoun, S. S., 'Effect of Cement Composition on Chloride Binding and Corrosion of Reinforcing Steel in Concrete', *Cem. Concr. Res.* **21**(5), 1991, 777–794.
- [146] Andrade, C., and Page, C. L., 'Pore Solution Chemistry and Corrosion in Hydrated Cement Systems Containing Chloride Salts: A Study of Cation Specific Effects'. *Br. Corros. J.* **21**(1), 1986, 49–53.

## CHAPTER 2. LABORATORY INVESTIGATION

This chapter presents the methodology, results and discussion pertinent to the laboratory investigation of mortar and concrete samples. Various laboratory tests were conducted to investigate the compressive strength of and chloride diffusivity in mortar and concrete samples with cement partially replaced by various minerals (class F and class N FA, UFFA, SF, MK and GGBFS), the porosity of mineral concretes, the freeze-thaw resistance of mineral mortars in the presence of deicers, and the effect of SCMs on the chloride binding and chemistry of the pore solution in mortar.

### 2.1. Experimental

#### 2.1.1. Sample Preparation

In light of the representative concrete mixes and chloride exposure conditions in California, a preliminary design for the laboratory investigation was developed, in the form of a matrix of 18 concrete mix designs that need to be evaluated (see Table 2-2). All these concrete mix designs feature a  $w/cm$  ratio of 0.40. The concrete mix design without any mineral admixtures is used as a control. These mix designs were determined in close consultation with the Caltrans Corrosion Technology Branch staff. On the basis of Table 2-2, multiple trials were conducted in order to achieve reasonable workability of fresh concrete (slump) for each mix design. For this study, an ASTM specification C150-07 Type I/II low-alkali Portland cement from the Ash Grove Montana City Plant (Clancy, MT) was used and its chemical composition and physical properties are provided in Appendix E7. The properties of the mineral admixtures used are provided in Appendices E1-E6. Coarse aggregates (with maximum size of 3/4" or 19 mm) and fine aggregates (clean, natural silica sand) were purchased from the JTLGroup (Belgrade, MT). Glenium 3030<sup>TM</sup> and Micro-Air<sup>TM</sup> were used as the ASTM C 494 Type A/F water reducing agent and the ASTM C 260 air-entraining agent respectively and at the dosage per the instructions.

After the trials, the two Class N fly ash designs (at 25% replacement level) were excluded from further investigation with approval of the Caltrans technical panel, since these two mixes could not achieve desired slump and air content with the specified  $w/cm$  ratio of 0.4 even with the excessive amounts of multiple water-reducers. This left 16 concrete mixes for the study as shown in Table 2-3. These concrete mixes had a coarse-aggregate-to-cementitious-materials ratio varying between 2.17 and 2.86 and a coarse-to-fine-aggregates ratio between 1.51 and 1.54. Such variations were necessary in order to achieve reasonable slump and air content, similar to the field construction scenarios during batching operations. Note that the actual air content achieved deviated from the target air content in Table 2-2 in spite of the multiple trials for each mix design. It was also noticed that concrete made using a smaller lab mixer with same formulation usually had lower air content than using a larger lab mixer.

For each mix design, at least three replicate 12 " by 6 " (diameter 305 mm × height 152 mm) concrete cylinders and at least three replicate 4" by 8" (diameter 102 mm × height

203 mm) compression cylinders were prepared. The coarse aggregates and fine aggregates were oven-dried and then potable water was added in the amount twice as much as their absorption capacity (e.g., 1.8%). The aggregates were then soaked for 24 hours to ensure that they had fully absorbed moisture and had moisture in excess of the surface-saturated-dry (SSD) condition. The saturated aggregates and the excessive water were used in the mix, taking into account the excessive water when calculating the w/c ratio. The fine and coarse aggregates were added to the 2-cubic-foot (57-L) mixer and mixed until a homogeneous mixture was obtained. Then the cement was added and mixed again until a homogeneous mixture was obtained. Next, water was added from a graduated cylinder and mixed until the concrete is homogeneous and of the desired consistency. The batch was remixed periodically during the casting of the test specimens and the mix container was covered to prevent evaporation. Slump and air content measurements were performed by the ASTM C 143 and C 173 methods respectively, to check the workability and quality of the freshly mixed concrete; and the data are shown in Table 2-3. Fresh concrete was cast into hollow poly(vinyl chloride) piping cylinders and then carefully compacted to minimize the amount of entrapped air. The cylindrical samples were demolded after curing for 24 hours with over 90% relative humidity. After demolding, the samples were cured in the moist cure room (with over 90% relative humidity) for another 359 days before the accelerated chloride migration test. For testing of chloride diffusivity, slice specimens with diameter of 2" (51 mm) and thickness of 1" (25 mm) were cored from the center of cured cylinders to minimize possible effects of surface evaporation and air entrapment on the permeability of slice specimen. Cores were removed from the concrete according to the ASTM C42/C 42 M (2004) *Standard Test Method of Obtaining and Testing Drilled Cores and Sawed Beams of Concrete*. The specimen thickness was chosen based on two considerations. It is thick enough to reasonably represent the heterogeneity nature of the concrete and to consider the maximum aggregate size (3/4"). It is not too thick so that the accelerated chloride migration test can be completed in reasonable time frame.

Furthermore, nine mortar mixes were prepared, i.e., mixes 1, 3, 5, 7, 9, 11, 13, 15, and 17 in Table 2-3 without any coarse aggregates, water-reducer, or air-entraining agent. The w/cm ratio of the mortar samples was set at 0.45 instead of 0.40, in light of workability concerns. For each mix design, at least three replicate 2" by 4" (diameter 51 mm × length 102 mm) cylinders for diffusivity testing, at least sixteen replicate 1 7/8" by 1 1/2" (height 48 mm × diameter 38 mm) cylinders for freeze-thaw testing, and at least nine replicate 2" by 4" (diameter 51 mm × length 102 mm) compression cylinders were prepared. This aims to shed light on the role of coarse aggregates and to better interpret the chloride diffusion data in concrete containing various types and amounts of mineral admixtures. For mortar samples, cement is mixed with water at a low speed hand mixer for 5 minutes. Subsequently, fine aggregates, with a maximum size of 1.18 mm in diameter, were added, after which the slurries were stirred for 3 minutes. The fine aggregates were prepared to SSD condition in advance. All the slurries were cast into hollow poly(vinyl chloride) piping cylinders and then carefully compacted to minimize the amount of entrapped air. The cylindrical samples were demolded after curing for 24 hours with over 90% relative humidity. After demolding, the samples were cured with over 90% relative humidity for another 89 days before the accelerated chloride migration

test. For testing of chloride diffusivity, slice specimens with a thickness of 8 mm were cut from the center of cured cylinders to minimize possible effects of surface evaporation and air entrapment on the permeability of slice specimen. This was done using a low-speed saw equipped with a diamond blade.

TABLE 2-2 Preliminary design of experiments to study the influence of concrete mix design parameters on the chloride penetration resistance and durability of concrete, including type and amount of mineral replacement and entrained air content.

Concrete Test Matrix <sup>1</sup>							
Cement <sup>4</sup> (% by Mass)	Mineral Admixtures (% by Mass)						Entrained Air Content (%) <sup>7</sup>
	Flyash (Class F) <sup>2</sup>	Flyash (Class N) <sup>2</sup>	SF <sup>3</sup>	MK <sup>4</sup>	UFFA <sup>5</sup>	GGBFS <sup>6</sup>	
100 (control)	0	0	0	0	0	0	0
100 (control)	0	0	0	0	0	0	6
75	25	0	0	0	0	0	0
75	25	0	0	0	0	0	6
75	0	25	0	0	0	0	0
75	0	25	0	0	0	0	6
75	20	0	5	0	0	0	0
75	20	0	5	0	0	0	6
75	20	0	0	5	0	0	0
75	20	0	0	5	0	0	6
90	0	0	10	0	0	0	0
90	0	0	10	0	0	0	6
90	0	0	0	10	0	0	0
90	0	0	0	10	0	0	6
90	0	0	0	0	10	0	0
90	0	0	0	0	10	0	6
50	0	0	0	0	0	50	0
50	0	0	0	0	0	50	6

Notes:

- (1) All mix designs consist of 400 kg/m<sup>3</sup> total cementitious material. Mineral admixture quantities are added as a cement replacement. Water-to-cementitious material ratio is 0.40. See Note (4) for additional guidance. Review and approval of actual mix designs is required prior to start of project.
- (2) ASTM Designation: C618 Standard Specification for Coal Flyash and Raw or Calcined Natural Pozzolan for use in Concrete.
- (3) ASTM Designation: C1240, Standard Specification for Silica Fume Used in Cementitious Mixtures.
- (4) S8-C04(90CORR), Corrosion Control for Portland Cement Concrete., California Department of Transportation – Structure Reference Specification., June 2001.
- (5) Boral Technologies Micron 3 Ultra Fine Flyash Materials Product Sheet., Boral Technologies, August 2003.
- (6) ASTM Designation: C989, Standard Specification for Ground Granulated Blast-Furnace Slag for Use in Concrete and Mortars.
- (7) S8-C05, Freezing Condition Requirements., California Department of Transportation – Standard Special Provisions (SSP), November 2003

TABLE 2-3 Mix design parameters and the properties of concrete samples containing various types and amounts of mineral admixtures.

Ingredients	Mix Number							
	1	2	3	4	7	8	9	10
Portland Cement (lb)	75	75	56	56	56	56	56	56
Fly Ash (Class F) (lb)			19	19	15	15	15	15
Silica Fume (lb)					4	4		
Metakaolin (lb)							4	4
Ultra Fine Fly Ash (lb)								
Blast Furnace Slag (lb)								
Micro Air (ml)		22		33		33		33
Glenium 3030 (ml)	150	165	33	24	133	44	200	133
Water (lb)	28	25	28	28	24	26	25	24
Fine Aggregate (lb)	106.05	129.5	139.3	127.3	139.13	127.22	139.41	127.5
Moisture Content (%)	3.6	3.6	3.6	3.6	3.6	3.6	3.6	3.6
Course Aggregate (lb)	162.4	199.3	210.3	192.8	214.5	194	213.5	196.4
Moisture Content (%)	0.55	2.106	0.667	0.96	2.769	1.66	2.089	2.708
Slump (in)	2.5	3	2.5	3.5	3	4	4.5	3.5
Air Content (%)	2.5	6.5	2.5	5.5	3.75	5.6	2.75	6.5
Volume (ft <sup>3</sup> )	3	3	3	3	3	3	3	3
Strength @ 90 days (psi)	10367	7834	9404	5654	10020	5841	9557	6833
Standard Deviation (psi)	152	283	201	28	233	261	251	337

Ingredients	Mix Number							
	11	12	13	14	15	16	17	18
Portland Cement (lb)	68	68	68	68	68	68	38	38
Fly Ash (Class F) (lb)								
Silica Fume (lb)	8	8						
Metakaolin (lb)			8	8				
Ultra Fine Fly Ash (lb)					8	8		
Blast Furnace Slag (lb)							38	38
Micro Air (ml)		22		22		21		22
Glenium 3030 (ml)	266	238	255	238	150	150	155	166
Water (lb)	28	28	28	28	25	25	27	27
Fine Aggregate (lb)	140.3	128.4	140.86	128.95	140.74	128.83	140.4	128.49
Moisture Content (%)	3.6	3.6	3.6	3.6	3.6	3.6	3.6	3.6
Course Aggregate (lb)	211.8	194	212.8	195.1	216.2	197.9	213	195.1
Moisture Content (%)	0.647	0.712	0.718	0.886	2.397	2.43	1.133	1.248
Slump (in)	2.25	2	4	3.5	4	4	2	5.25
Air Content (%)	2.25	5.75	2.5	6	1.75	7	2.5	6
Volume (ft <sup>3</sup> )	3	3	3	3	3	3	3	3
Strength @ 90 days (psi)	9848	7869	11623	7070	10335	6476	8560	5544
Standard Deviation (psi)	324	453	323	252	127	147	335	181

### 2.1.2. Mechanical Testing

All the compression strength testing of mortar and concrete samples was conducted in accordance with ASTM C873 / C873M - 04e1 *Standard Test Method for Compressive Strength of Concrete Cylinders*. The compressive strength of concrete samples were first calculated by dividing the measured ultimate strength by the area of specimen cross-section, then multiplied by the Length/Diameter correction factor when necessary, and finally presented in the unit of psi, or pounds per square inch. The concrete cylinders were 4" by 8" (diameter 102 mm × height 203 mm) and cured for 90 days before testing, whereas the mortar cylinders were 2" by 4" (diameter 51 mm × length 102 mm) and cured for 1 day and 28 days respectively, prior to the compression testing. The compressive strength of each mix design was obtained by averaging the data from at least three replicate cylinders. Young's modulus (in GPa) and modulus of toughness (in KJ/m<sup>3</sup>) were also analyzed for mortar samples based on the stress-strain curve.

### 2.1.3. Electro-migration and Natural Diffusion

To rapidly measure the chloride diffusivity in the high-quality concrete and mortar samples, a modified version of RMT and RCPT, i.e., *Accelerated Chloride Migration Test (ACMT)* was conducted. The ACMT periodically measures the accumulative chloride ion concentration in the destination compartment using a calibrated chloride sensor. This test was originally developed by Truc et al. [1] and improved by the WTI Corrosion and Sustainable Infrastructure Laboratory [2, 3]. In addition, for a few selected concrete mixes (mixes 1, 2, 3, 7, 8, 10, 12, and 13), the migration test without the externally applied electric field, i.e., natural diffusion, was also conducted. Prior to such chloride diffusivity tests, the 8-mm thick mortar disc and 25-mm thick concrete disc specimens were polished to achieve a uniform surface roughness and thickness, using silicon carbide sandpapers from grit sizes from 400 to 800.

The ACMT, or electro-migration test is designed to rapidly measure the apparent diffusion coefficient,  $D_{app}$ , of chloride through *water-saturated* cementitious samples (including hardened cement paste, mortar, or concrete), using the experimental setup with a two-compartment cell shown in Figure 2-1. The detailed standard operating procedures are provided in Appendix D1. In summary, the experimental setup features a disc-shaped concrete specimen that separates the chloride anion source (a solution of 3% NaCl and 1% NaOH) and the chloride anion destination (a 1% NaOH solution). Each of the two compartments will contain one 316L stainless steel mesh electrode with a given exposed surface area (~ 15 cm<sup>2</sup>). A disc specimen (paste, mortar or concrete) was sandwiched between two plastic compartments. Solution leakage between the plastic rim and the disk specimen was prevented by the use of washers, nuts, bolts, rubber gaskets, and silicone sealer. Once the concrete disc, electrolytes, and electrodes are in place, a *30-volt* DC electric field will be maintained across the disc through the two mesh electrodes in the two compartments. During the test, readings of chloride concentration in the destination compartment are taken periodically using a *calibrated* chloride sensor, on a 2-hour interval or more frequently if necessary. In addition, the electric current in the circuit is periodically measured in order to calculate the amount of electric charge passing through

the disc during the electro-migration test. The chloride sensor is periodically calibrated using known solutions and the readings from them will be converted to units of molarity and plotted as a function of time.

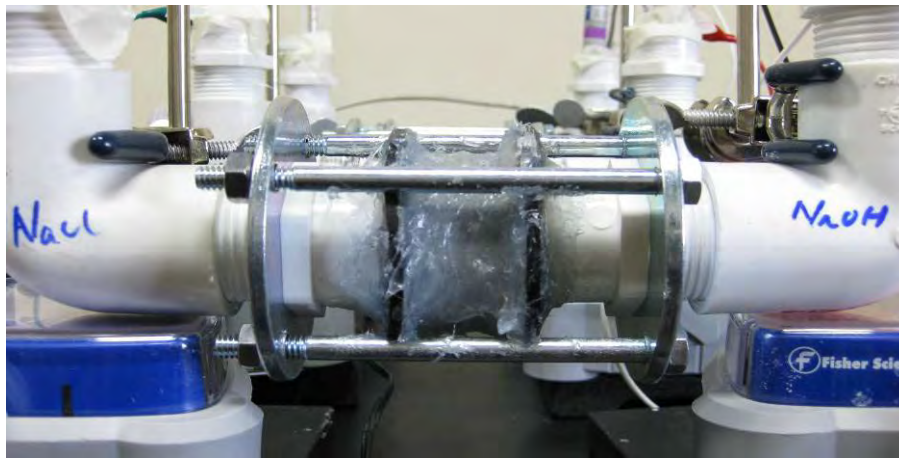
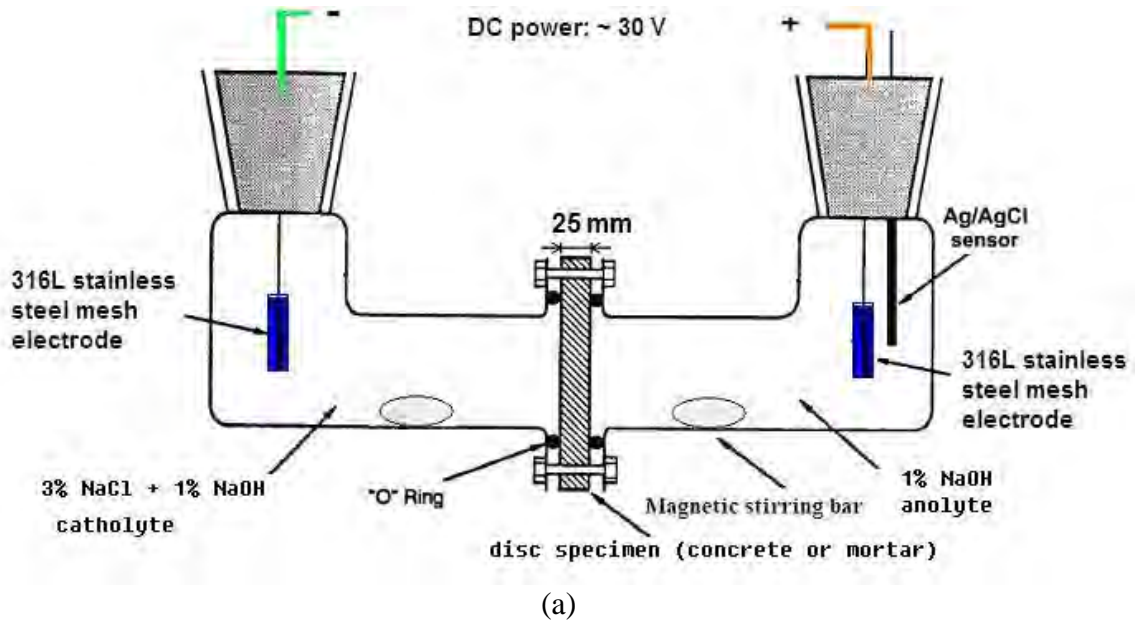


FIGURE 2-1 Schematic illustration (a) and photo (b) of the experimental setup for the electro-migration test (Note: for the natural diffusion samples, there is no external electric field applied).

A snapshot for the electro-migration tests is presented in Figure 2-2(a). Similar apparatus was used to test the natural diffusion in order to validate the  $D$  data obtained from electro-migration test, as shown in Figure 2-2(b).

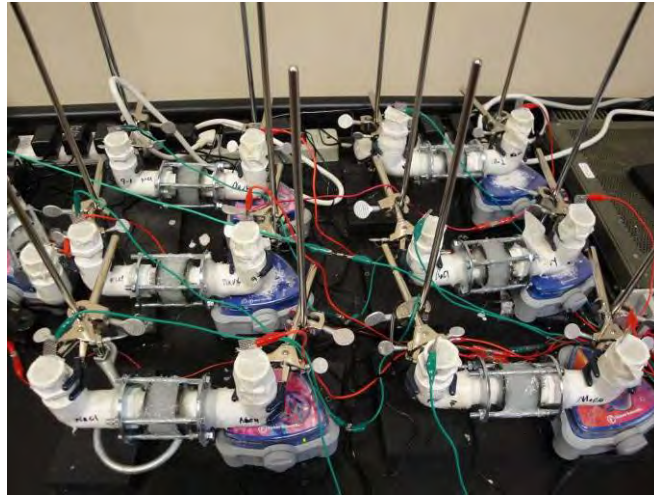


FIGURE 2-2 Photos of the migration tests: (a) electro-migration and (b) natural diffusion.

Diffusion of ionic species in cementitious materials depends heavily on the amount of aqueous solutions in the pore space. It is thus important to minimize the possible influence of chloride penetration mechanisms other than diffusion (e.g., wicking) on the measured chloride diffusion coefficient. To this end, after the disc specimens were taken out of the moist curing environment (for mortar) or cored from the moist-cured sample (for concrete), they were further saturated with de-ionized water for 2 hours using the two-compartment cell prior to migration testing

In order to accelerate the electro-migration tests, eight electro-migration assemblies were concurrently used in parallel to a DC power supply. Custom-made chloride sensors were prepared by electroplating clean silver wires, using the computer-controlled potentiostat to apply 1, 0.2, 0.5, and 0.1mA/cm<sup>2</sup> for plating about 30, 30, 30 and 100 minutes, respectively. This process helps to form a dense Ag/AgCl sensing layer on the surface of

silver wires and improve their resistance to the oxidation attack by the highly alkaline solutions. There should be a very strong correlation between the open circuit potential (OCP) of the custom-made chloride sensor and logarithm of chloride concentration. As such, they were always calibrated before being used to periodically measure the chloride concentration in the destination compartments.

Figure 2-3 illustrates the typical results obtained from the electro-migration test. The breakthrough time  $t_0$  is the point after which the  $\text{Cl}^-$  concentration in the destination solution (anolyte) shows a significant linear increase with time, i.e., the intersection of the two fitted straight lines. The electro-migration test can be terminated when the chloride concentration in the destination compartment shows a clear bilinear pattern (typically falls in the 20-50 mM range).

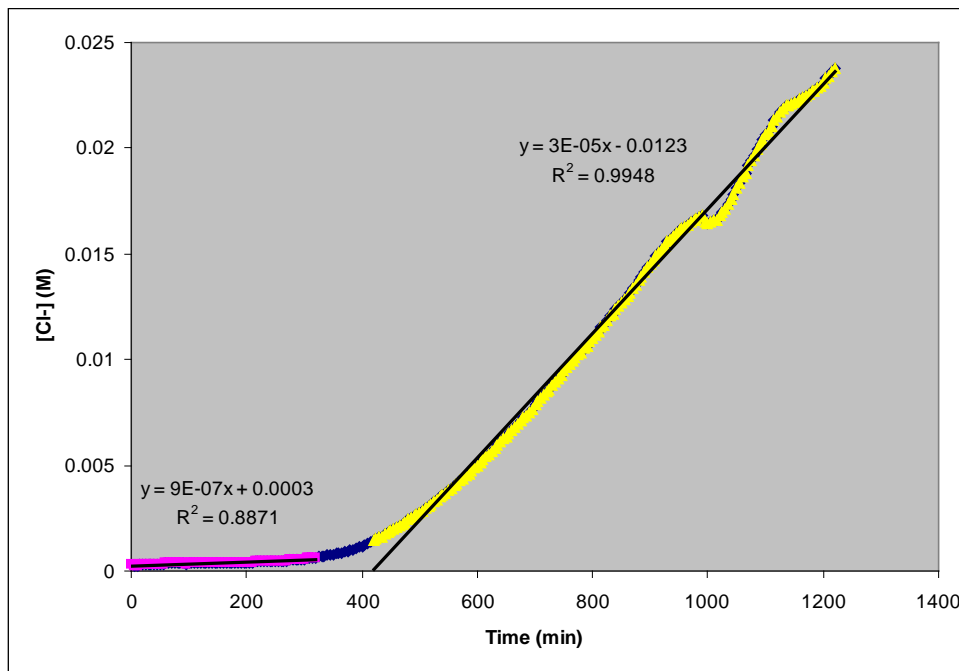


FIGURE 2-3 Temporal evolution of chloride concentration in the destination compartment, with data obtained from the electro-migration test of 3% NaCl through a Portland cement mortar specimen.

The method used to calculate the steady-state diffusion coefficient ( $D_s$ ) of  $\text{Cl}^-$  in cement paste, mortar or concrete samples is described as follows. Under an externally applied electric field with an intensity of  $E$ , the velocity of chloride ions ( $v$ ) can be described by the Nernst-Einstein equation:

$$v = \frac{zFD}{RT} \quad (1)$$

where  $z$ ,  $F$ ,  $R$  and  $T$  are charge number, Faraday constant, gas constant and absolute temperature, respectively. The velocity of chloride ions can also be calculated from:

$$v = \frac{d}{t_0 E} \quad (2)$$

where  $t_0$  is the time required for the chloride front to penetrate a depth  $d$  of the sample. Such a quantity can be estimated from the measured  $\text{Cl}^-$  concentration profiles in the anolyte (destination solution) by locating the point after which the  $\text{Cl}^-$  concentration in the anolyte increases dramatically with time. The diffusion coefficient  $D_s$  can be estimated from Equations 1 and 2 as follows [3]:

$$D = \frac{dRT}{t_0 zEF} \quad (3)$$

The electro-migration test lasts until significant chloride ion concentration is detected in the destination compartment, i.e.,  $t_0$  can be readily estimated from the chloride concentration profile over time. This could be hours, days, or weeks depending on the thickness and quality of the test specimen and the applied voltage.

#### 2.1.4. Electrochemical Impedance Spectroscopy (EIS) Measurements

EIS is a non-destructive means of providing fundamental information on interfaces as well as on the properties of mortar or concrete [2]. Before and after the electro-migration tests, the Gamry Reference 600™ Potentiostat/Galvanostat/ZRA instrument was utilized to take the EIS measurements so as to quantitatively characterize the microstructural characteristics of the concrete specimen, as detailed in Appendix D1. In summary, the two stainless steel mesh electrodes in the two compartments served as the working electrode and the counter electrode respectively, whereas a saturated calomel electrode (SCE) placed in the anolyte served as the reference electrode. By applying sinusoidal perturbations with a frequency from 300 kHz to 5 MHz, the working electrode was polarized by  $\pm 10$  mV around its OCP and the current response vs. the applied voltage was recorded to produce the EIS spectrum. Subsequently, the Gammy Echem Analyst™ software was used to analyze the EIS data using the electrical equivalent circuit shown in Figure 2-4. The equivalent circuit model contains  $R_{cement}$  and  $Q_{cement}$  to characterize the electrical resistance and capacitance of the cementitious disc specimen.  $n_{cement}$  is defined as the fitting coefficient for  $Q_{cement}$ , with 0 and 1 corresponding to the worst and the best capacitor respectively. The circuit also includes a Warburg impedance (W) indicative of the diffusion process through an interface and  $R_1$  and  $R_2$  indicative of the solution resistance and the charge transfer resistance on the working electrode respectively.

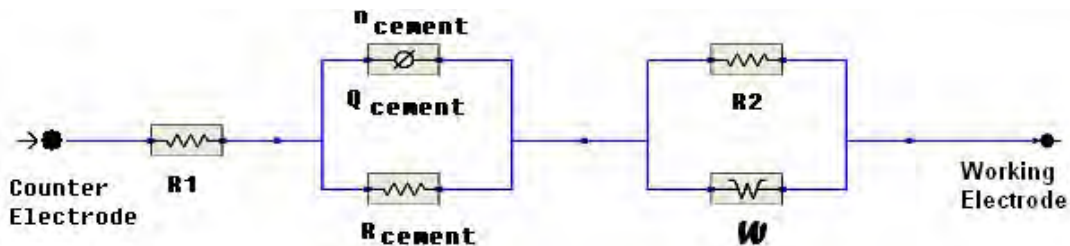


FIGURE 2-4 The equivalent circuit used for fitting the EIS data of mortar and concrete

### 2.1.5 Chloride Binding Capacity and Pore Solution Chemistry of Mortar Samples

The chloride binding capacity of mortar samples incorporating various types and amounts of mineral admixtures was measured, following the method by Delagrave et al. [4]. First, the 90-day mortar samples were dried and grounded into powder. The powder was then screened through a 150- $\mu\text{m}$  sieve, oven-dried at 80 °C overnight and cooled to room temperature. For each mix design, 5 kinds of chloride-containing simulated pore solutions were prepared for subsequent binding tests, with sodium chloride (NaCl) concentration of 1000, 5000, 10000, 20000 and 30000 mg/L respectively. 10 grams of dry mortar powders were added into 50 mL of chloride solution, after which sufficient time was allowed so that the equilibrium between the solution and solid phase could be established. The residual chloride concentration for each test was then measured by chloride sensors.

For pore solution chemistry testing, the pore solutions tested were not extracted from the mortar samples; instead, they were prepared by adding 10 grams of mortar powders into 50 ml of de-ionized water and allowing the solution to sit in a high purity nitrogen atmosphere for 24 hours for equilibrium. Subsequently, the pH of the solution was tested and its chemistry was analyzed using Ion Chromatography-Inductively Coupled Plasma (IC/ICP). Hydroxyl ion concentrations of the extracted solutions were determined by titration using ethylenediaminetetraacetic acid (EDTA) and hydrochloric acid (HCl) solutions. The titration to determine the pore solution pH was conducted in a high purity nitrogen atmosphere, in order to avoid the exposure of test solution to the atmospheric carbon dioxide [5].

### 2.1.6 Porosity Measurements of Concrete Samples

Porosity is the ratio of the void volume to the total sample volume. The technique to characterize porosity in cementitious materials relies on impregnation of the sample with water, as detailed in Appendix D2. Before experiments, the concrete samples were thoroughly dried in oven. During water infiltration into the concrete specimen, the pores were evacuated of air by boiling the water that contained the specimen. The volume of pore space is calculated by subtracting the dry weight of the specimen from its saturated weight. *The volume of permeable voids (%)* of the concrete is determined by the Archimedean principle, i.e. the total volume is calculated by subtracting the weight of the sample suspended in water from its weight in air. The percentage porosity can be calculated as follows [6]:

$$p = \frac{(W_s - W_d)}{(W_s - W_w)} \times 100\% \quad (4)$$

where  $p$  is the percent porosity,  $W_s$  is the weight of the saturated sample,  $W_d$  is the weight of the dry sample, and  $W_w$  is the weight of the saturated sample suspended in water. For each concrete mix, at least two specimens were tested.

### 2.1.7 Freeze-thaw Resistance of Mortar Samples

While compressive strength is the most widely accepted parameter used to judge the quality of concrete, corrosion properties of concrete can be more important to the service life of concrete. For reinforced concrete, freeze-thaw resistance can be another aspect of durability in addition to chloride-induced corrosion of rebar, especially in the cold-climate regions. In this study, mortar samples used for the freeze-thaw were 1 $\frac{7}{8}$ " by 1 $\frac{1}{2}$ " (height 48 mm  $\times$  diameter 38 mm) cylinders. Laboratory measurements of changes to mortar samples through freeze/thaw testing in the presence of various chloride solutions were conducted following the SHRP H205.8 test method entitled "Test Method for Rapid Evaluation of Effects of Deicing Chemicals on Concrete" with minor modifications. The SHRP H205.8 test evaluates the effects of chemical deicing formulations and freeze/thaw cycling on the structural integrity of small test specimens of non-air-entrained concrete. The method quantitatively evaluates degradation of the specimen through weight loss measurements and thus sheds light on the durability of the mortar samples with or without various SCMs admixed. Note that the test results from this method may not be suitable for predicting the field performance of concrete, considering its short duration.

Once moist-cured for 90 days, the mortar specimens were allowed to dry overnight and weighed. The freeze-thaw resistance of each mortar mix was tested in the presence of four solutions, including: de-ionized water, 23% NaCl, 30% calcium chloride (CaCl<sub>2</sub>) and 30% magnesium chloride (MgCl<sub>2</sub>). The last three are the main ingredients of deicers used for winter highway operations at their application concentration for snow and ice control, whereas the de-ionized water is used as a control. For each solution, four concrete specimens were placed on a cellulose sponge inside a dish containing 310 ml of the solution and then covered with plastic wrap to avoid water evaporation and to slightly compress each test specimen into the sponge. For the first round of testing, the deicers were used at their application concentrations respectively, without any dilution. One end of each test specimen was in full contact with the sponge. The test specimens (along with the deicer sponge and dish) were placed in the freezer for 16 to 18 hours at  $-17.8 \pm 2.7^{\circ}\text{C}$  ( $-0.04^{\circ}\text{F}$ ). Subsequently, the specimens (along with the deicer sponge and dish) were placed in the laboratory environment at  $23 \pm 1.7^{\circ}\text{C}$  ( $73.4^{\circ}\text{F}$ ) and with a relative humidity ranging from 45 to 55 percent for 6 to 8 hr, at which temperature every deicer tested thawed once it was taken out of the freezer for some time. This cycle was repeated 10 times. The average heating rate and cooling rate was observed to be  $0.4^{\circ}\text{C}/\text{min}$  and  $1.2^{\circ}\text{C}/\text{min}$ , respectively. After complete thawing following the tenth cycle, test specimens were carefully removed from the dish, individually rinsed under running tap water, and hand-crumbled to remove any material loosened during the freeze/thaw cycling. The largest intact part of each test specimen was then placed in open air to dry for 24 hr at  $23 \pm 1.7^{\circ}\text{C}$  ( $73.4^{\circ}\text{F}$ ) and a relative humidity ranging of 45-55%. After drying, test specimens are weighed. The test specimens were then immersed in de-ionized water for 24 hours to allow any possible salt contamination to leach out, and then dried and weighed. For the second round of testing, each liquid deicer solution was further diluted by de-ionized water from their application concentration at a 3% by volume. The specimens were subjected to another ten temperature cycles as described above and their final dry weights were also recorded.

## 2.2. Results and Discussion

### 2.2.1 Mechanical Properties of Mortar and Concrete Samples and Correlation with Chloride Diffusivity

Table 2-4 presents the mechanical results of mortar samples containing various types and amounts of mineral admixtures. It can be seen that the partial replacement of cement by 20% class F FA and 5% SF, by 20% class F FA and 5% MK, or by 25% class F FA alone greatly reduced the 1-day compressive strength of mortar samples, whereas the partial replacement of cement by 10% MK, 10% SF, 10% UFFA, 50% GGBFS, or 25% class N FA improved the 1-day strength to various degrees. The combined addition of class F and MK dramatically reduced the 7-day compressive strength of mortar samples, followed by the use of GGBFS or SF, whereas the addition of most other minerals (except MK) also decreased the 7-day strength to various degrees. The combined addition of class F and MK increased the 28-day compressive strength of mortar samples, whereas the addition of most other minerals (except GGBFS) decreased the 28-day strength to various degrees. All the SCMs dramatically reduced the 1-day Young's modulus of mortar samples, but they showed mixed effect on the 7-day and 28-day Young's modulus. All the SCMs dramatically reduced the 7-day and 28-day modulus of toughness, but they showed mixed effect on the 1-day modulus of toughness. The reduction in the moduli of concrete is beneficial as it renders the concrete less prone to shrinkage cracking, which in turn, reduces the risk of rapid chloride ingress.

According to the EIS measurements after the ACMT using 90-day old mortar samples, all the SCMs dramatically increased the electrical resistivity of the mortar samples in the electrolyte while most SCMs (except GGBFS) decreased the electrical capacitance of the mortar to various degrees.

Table 2-4 also shows the effect of partially replacing cement with SCMs on the steady-state diffusion coefficient ( $D_s$ ), obtained from the ACMT using 90-day old mortar samples. The results indicate that the use of 20% class F FA and 5% SF as cement replacement significantly increased the chloride diffusivity in mortar and the use of 10% MK or 50% GGBFS significantly decreased it, whereas other SCMs decreased the  $D_s$  to various degrees.

TABLE 2-4 Mechanical properties, EIS data and chloride diffusivity of mortar samples containing various types and amounts of mineral admixtures.

Mix No.	Mineral Admixtures	Average Compressive Strength (psi)			Average Young's Modulus (GPa)			Average Modulus of Toughness (kJ/m <sup>3</sup> )			90-day EIS results			90-day ACMT
		1d	7d	28d	1d	7d	28d	1d	7d	28d	$R_{\text{mortar}}$ (K $\Omega$ cm <sup>2</sup> )	$Q_{\text{mortar}}$ ( $\mu$ Scm <sup>-2</sup> )	$n_{\text{mortar}}$	$D_s$ (m <sup>2</sup> /s)
1	None	904	3863	5105	1.38	1.58	2.69	30.9	189.3	229.7	10.6±0.3	273.5±2.6	0.83±0.008	1.77E-11
3	FA F	752	3035	4025	0.36	1.20	2.53	23.4	114.8	114.2	56.1±0.3	202.0±8.8	0.78±0.003	1.50E-11
5	FA N	934	2900	4204	1.01	2.45	3.10	24.7	89.5	136.2	53.2±0.4	262.0±4.8	0.79±0.13	1.55E-11
7	FA F + SF	613	3480	4435	0.50	2.50	3.07	27.2	89.6	126.3	43.5±2.0	130.3±3.3	0.81±0.010	2.98E-11
9	FA F + MK	690	1439	5613	0.89	0.97	3.02	26.0	51.0	171.6	77.0±4.1	204.2±5.2	0.79±0.008	1.28E-11
11	SF	1056	2491	4859	0.72	1.78	3.44	42.3	119.6	147.7	125.6±17.1	111.0±5.1	0.89±0.007	1.30E-11
13	MK	1106	3850	4675	0.62	2.20	3.28	47.1	122.0	160.2	42.1±3.9	219.7±17.1	0.83±0.02	8.42E-12
15	UFFA	992	2887	4726	0.48	1.88	2.08	53.6	139.3	139.1	123.3±0.1	116.2±1.0	0.84±0.001	1.43E-11
17	GGBFS	950	2148	5109	0.44	1.61	2.82	28.6	84.8	167.0	69.8±8.0	317.4±39.1	0.90±0.03	1.09E-11

TABLE 2-5 The properties of mortar samples and concrete containing various types and amounts of mineral admixtures.

Mix No.	Mineral Admixtures	Mortar				Non-Air-Entrained Concrete				Air-Entrained Concrete			
		Average Compressive Strength (psi)			90-day ACMT	Properties			360-day ACMT	Properties			360-day ACMT
		1d	7d	28d	$D_s$ ( $10^{-11}$ m <sup>2</sup> /s)	Coarse-aggregate-to-cm ratio	Coarse-to-fine ratio	90 d compressive strength (psi)	$D_s$ ( $10^{-13}$ m <sup>2</sup> /s)	Coarse-aggregate-to-cm ratio	Coarse-to-fine ratio	90 d compressive strength (psi)	$D_s$ ( $10^{-13}$ m <sup>2</sup> /s)
1 & 2	None	904	3863	5105	1.77	2.17	1.53	10367	2.50	2.66	1.54	7834	2.74
3 & 4	FA F	752	3035	4025	1.50	2.80	1.51	9404	2.36	2.57	1.51	5654	3.77
5 & 6	FA N	934	2900	4204	1.55	NA	NA	NA	NA	NA	NA	NA	NA
7 & 8	FA F + SF	613	3480	4435	2.98	2.86	1.54	10020	2.99	2.59	1.52	5841	3.25
9 & 10	FA F + MK	690	1439	5613	1.28	2.85	1.53	9557	3.27	2.62	1.54	6833	3.14
11 & 12	SF	1056	2491	4859	1.30	2.79	1.51	9848	3.80	2.55	1.51	7869	3.96
13 & 14	MK	1106	3850	4675	0.84	2.80	1.51	11623	2.90	2.57	1.51	7070	3.70
15 & 16	UFFA	992	2887	4726	1.43	2.84	1.54	10335	3.71	2.60	1.54	6476	3.77
17 & 18	GGBFS	950	2148	5109	1.09	2.80	1.52	8560	3.52	2.57	1.52	5544	2.35

The extremely low  $D_s$  values of concrete specimens tested are indirectly confirmed by the natural diffusion test results. For mixes 1, 2, 3, 7, 8, 10, 12 and 13, the migration test was conducted without the externally applied electric field, i.e., through natural diffusion. Even after 280 days, the chloride concentration in the destination compartment of all natural diffusion test cells generally remained well below 5 mM, indicating that the diffusion front of chloride ions had not penetrated across the 25-mm concrete specimens.

Table 2-5 presents the properties of the concrete mixes, including their average 90-day compressive strength and the  $D_s$  obtained from the ACMT using 360-day old concrete samples. There is no clear trend related to the effect of SCMs on the 90-day compressive strength of concrete or the chloride diffusivity in the 360-day concrete samples. Nonetheless, the chloride diffusivity is much lower in the concrete mixes than in their corresponding mortar mixes, with the  $D_s$  values in the order of  $10^{-13}$  m<sup>2</sup>/s in concrete and of  $10^{-11}$  m<sup>2</sup>/s in mortar. This highlights the important role of coarse aggregates in slowing down the chloride ingress into concrete. Furthermore, Table 2-5 indicates that all the mortar mixes had a 28-day compressive strength above 4,000 psi (27.6 MPa) whereas the non-air-entrained concrete mixes at 90 days on average featured twice as high a compressive strength. Such extremely high strength values suggest that the hardened concrete had outstanding microstructure, which is consistent with their extremely low  $D_s$  values indicative of chloride diffusivity. The compressive strength of air-entrained concrete was consistently lower than that of their non-air-entrained counterpart, yet the differences in their chloride diffusivity were not as appreciable.

With the  $D_s$  values obtained from the ACMT, it is possible to evaluate the time required for chloride ions to migrate across concrete samples in the natural diffusion state. The penetration of chlorides across concrete is a dynamic process driven by the chloride concentration gradients. Assuming that the boundary conditions and diffusion coefficient are constant with respect to time and space, the solution of Fick's second law is given as follows:

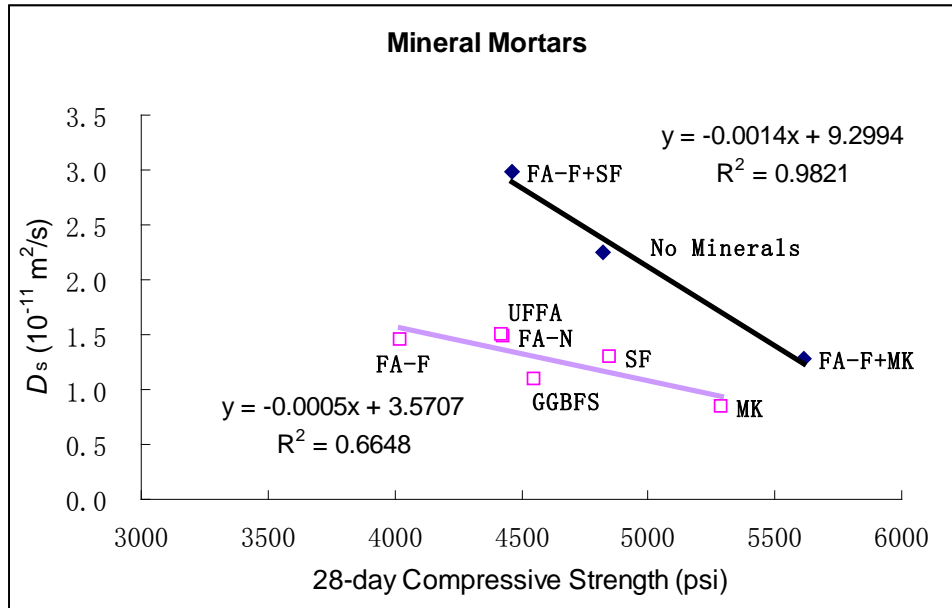
$$C(x, t) = C_s \left[ 1 - \operatorname{erf} \left( \frac{x}{2\sqrt{Dt}} \right) \right] \quad (5)$$

where  $C_s$  is the chloride concentration in the source solution;  $x$  is the thickness of concrete samples;  $D$  is the diffusion coefficient for chloride;  $t$  is time. Given the  $D_s$  values of mixes 1, 2, 3, 7, 8, 10, 12 and 13 (averaging  $2.98 \times 10^{-13}$  m<sup>2</sup>/s, see Table 2-5), it would take about 2 years to penetrate the 25-mm concrete specimen to reach a concentration of 5 mM in the destination compartment. The natural diffusion results thus indirectly confirmed the order of magnitude of  $D_s$  values of concrete specimens obtained from the ACMT.

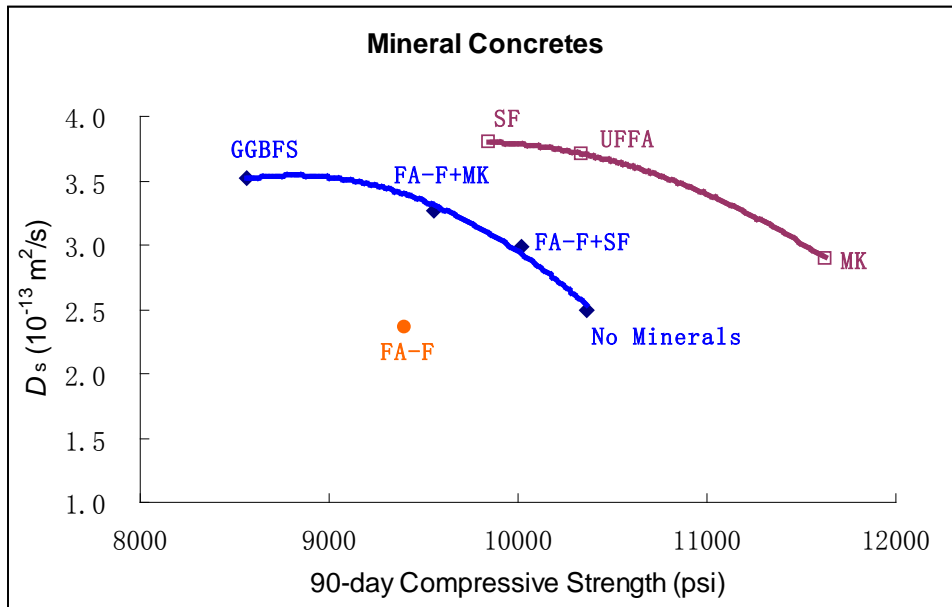
Figure 2-5(a) illustrates the relationship between the compressive strength of the mortar samples and the chloride diffusion coefficient in them, whereas Figure 2-5(b) illustrates such relationship for the concrete samples. Generally speaking, the lower  $D_s$  values corresponded to the higher compressive strength values, as both indicate high quality of the mortar or concrete. This is consistent with the tendency reported by Gao et al. [7]. Nonetheless, such correlations did not hold across all the mixes as the type and amount of SCMs in them varied. For both mortar and concrete, there is the lack of a single correlation for all the mixes. Instead, there are at least two distinct correlations between the compressive strength and the chloride diffusivity. This may be partially related to the slow hydration kinetics of some mortar mixes containing mineral admixtures as well as the effect of certain mineral admixtures on chloride binding, which merit further investigation.

Figure 2-6(a) presents the relationship between the  $D_s$  values in mortar samples and those in their non-air-entrained concrete counterparts. Generally speaking, the lower  $D_s$  values

in mortar corresponded to the lower  $D_s$  values in the non-air-entrained concrete, indicating that chloride diffusion in the mortar phase contributed to the overall chloride diffusion in the concrete which consisted of the mortar phase, the coarse aggregate phase, and possibly the paste-aggregate interfacial transition zone (ITZ). For the control concrete mix or the mixes with 20% class F FA and 5% SF or with 25% class F FA, the mortar phase seemed to play a significant role in their chloride diffusivity; whereas for the other concrete mixes the role of mortar phase is less significant.

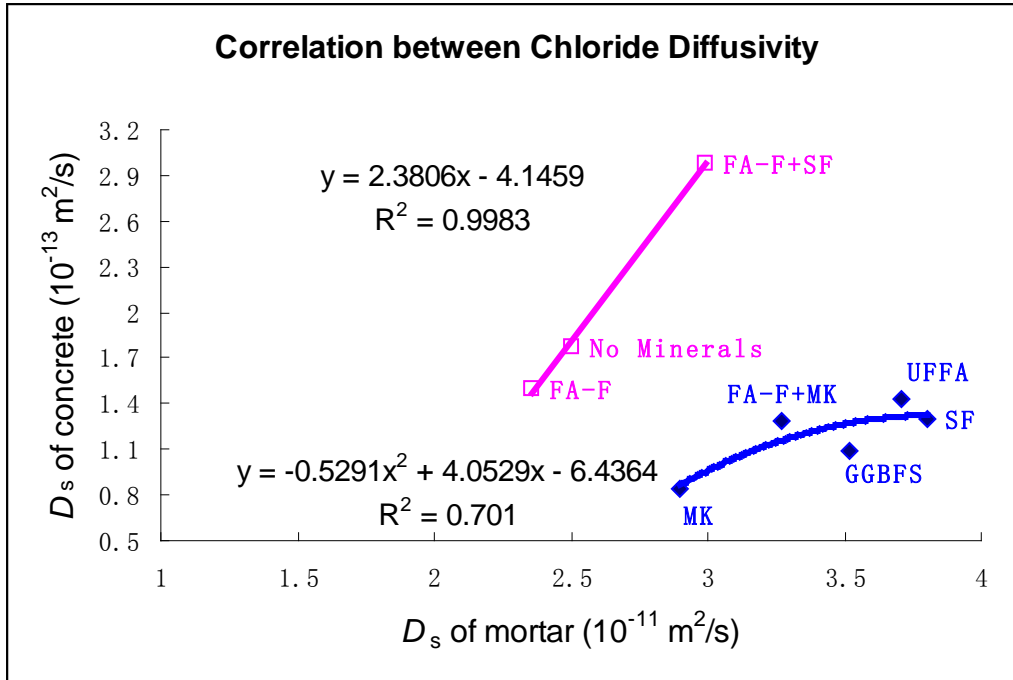


(a)

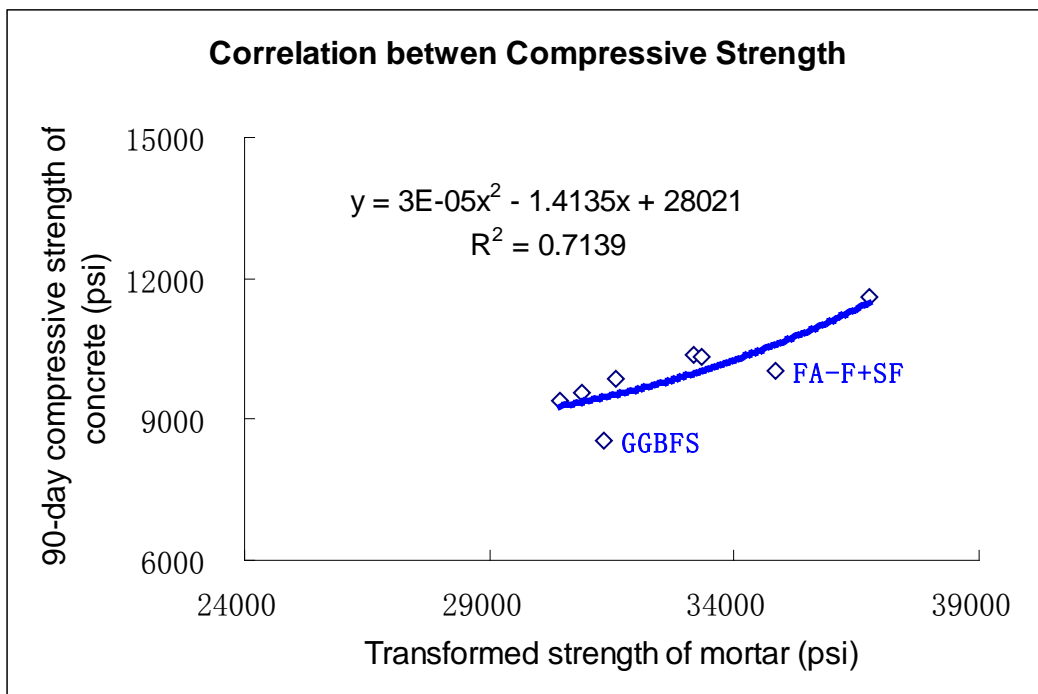


(b)

FIGURE 2-5 Relationship between compressive strength and chloride diffusion coefficients: (a) mortar samples and (b) concrete samples.



(a)



(b)

FIGURE 2-6 Relationship between: (a) chloride diffusivity in mortar and that in non-air-entrained concrete; (b) transformed strength of mortar and 90-day compressive strength of concrete.

Figure 2-6(b) presents the relationship between the transformed strength of mortar samples and the 90-day compressive strength of their non-air-entrained concrete counterparts. The transformed mortar strength (TMS) is calculated by the following equation:

$$\text{TMS} = (7\text{-day compressive strength} + 28\text{-day compressive strength}) \times (\text{coarse-aggregate-to-cementitious-materials ratio} + \text{coarse-to-fine-aggregates ratio}) \quad (6)$$

There is a strong proportional correlation between the TMS and the concrete strength, suggesting that the mortar phase is an integral component of the heterogeneous concrete matrix and greatly contributes to its compressive strength. Note that the definition of TMS was proposed based on the experimental data obtained from this specific research and on the existing knowledge that higher levels of coarse aggregates in concrete generally lead to higher strength of the concrete.

### 2.2.2 Electro-migration Data and Correlation with Porosity

Shown in Figure 2-7(a) is the temporal evolution of chloride concentration in the destination compartment for some concrete mixes during the ACMT, where each curve generally features two stages. The first stage is characterized by a negligible amount of chloride that has migrated into the anolyte, which corresponds to the time-lag period for chlorides to penetrate the concrete sample. Such a stage is followed by a subsequent steady-state period, in which the flux of chloride ions is almost constant. This period is evidenced by a sudden rise in the  $\text{Cl}^-$  concentration, indicating the arrival of a relative significant amount of  $\text{Cl}^-$  ions in the destination compartment. The transition time,  $t_0$ , utilized to distinguish such two processes can be defined by the point around which the  $\text{Cl}^-$  concentration slope changes dramatically in the destination solution, which can be located by the intercept from the tangent lines and the abscissa in Figure 2-7(a).

The current evolution curve contains abundant information on the transport of all the ions present in the pore solution of mortar or concrete specimens. Figure 2-7(b) shows four typical electric current density curves in the electrical circuit against time. Such curves are characterized by rapid increase in the initial state, followed by plateaus with steady-state values. The evolution of electric current over time was used to calculate the amount of electric charge ( $Q_{\text{Charge}}$ ) passing across the concrete samples, which is given by:

$$Q_{\text{Charge}} = \int_0^t J(t) A dt \quad (7)$$

where  $J(t)$  is the current density;  $A$  is the sample area;  $t$  is time; the integration is performed over the whole experiments. Note that the standard RCPT test (AASHTO T 277 or ASTM C 1202) classifies the chloride permeability of concrete based on the charge in the first 6 hours. As shown in Figure 2-7(b), for high-quality concrete, the more appropriate time frame for a 25-mm thick specimen would be in the hundreds of hours, instead of 6 hours.

The variation of chloride diffusion coefficients obtained from the electro-migration test is strongly correlated with the physiochemical characteristics of the test specimen, thereby

allowing a systematic study of the influence of mix design on chloride diffusivity. Figure 2-8(a) illustrates a linear correlation between the porosity of concrete and its chloride diffusion coefficient, which shows that the chloride diffusivity generally increases with the volume of permeable voids in concrete. This is reasonable considering the more porous microstructure of concrete leads to a longer zigzag diffusion path for the diffusion of chloride. The relatively low R-square of this correlation may be derived from the experimental errors as well as the fact that chloride diffusion is not only affected by the physical properties of concrete but also the chemical interactions between ionic species and the pore solution.

The correlation between the cumulative charge and the chloride diffusion coefficients is presented in Figure 2-8(b), where the cumulative charge generally increases with chloride diffusion coefficients. This is reasonable since both parameters have been used to assess the chloride permeability of concrete. A less permeable concrete is expected to feature a low  $D_s$  value and less electric charge passing through it in a given time period, as suggested by our previous research [2].

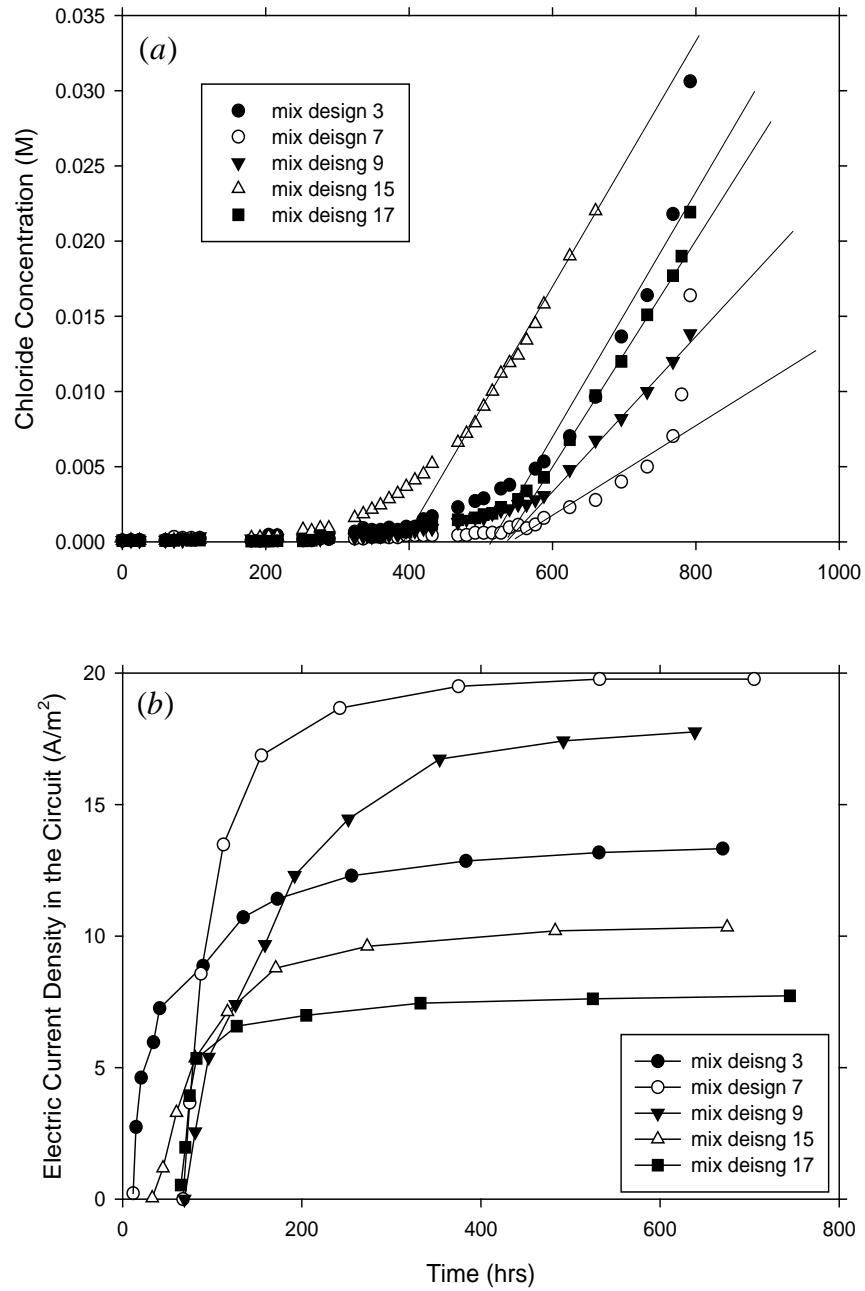


FIGURE 2-7 Temporal evolution of: (a) chloride concentration in destination compartment; and (b) electric current density during the ACMT of concrete samples.

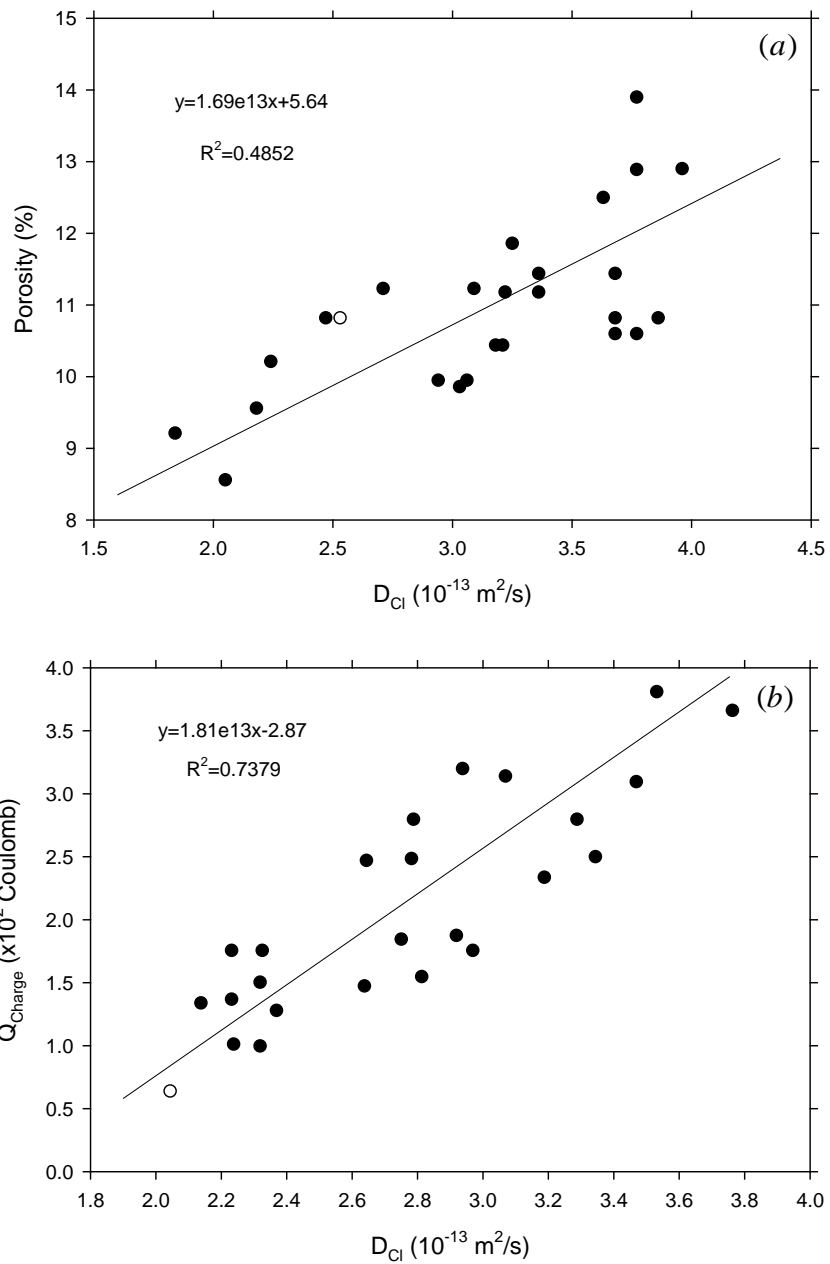


FIGURE 2-8 Correlation between: (a) porosity and chloride diffusion coefficient for concrete samples; (b) cumulative electrical charge and chloride diffusion coefficient.

### 2.2.3. EIS Data of Concrete and Correlation with Chloride Diffusivity

In this study, the EIS measurements were conducted to non-destructively characterize the microstructural properties of the concrete specimens before and after the ACMT. The complex impedance of the concrete/electrolyte interface was dependent on the frequency of the applied AC polarization signal. The equivalent circuit shown in Figure 2-4 was used to model the interfaces between the counter electrode and the working electrode.

Figures 2-9(a) and (b) present the fitted equivalent circuit parameters,  $Q_{\text{cement}}$  and  $R_{\text{cement}}$ , both of which seems to be somewhat correlated with the chloride diffusion coefficient obtained from the ACMT. These correlations, however, were much weaker as those reported in our previous research [2]. The results indicate that both the electrical capacitance ( $Q_{\text{cement}}$ ) and the electric resistivity ( $R_{\text{cement}}$ ) of the concrete specimen generally increase with its chloride diffusivity. It is intuitive that a less permeable concrete (featuring high  $D_s$ ) generally has more refined microstructure and thus low  $Q_{\text{cement}}$  and high  $R_{\text{cement}}$  values. In this study, the relationship between  $D_s$  and  $Q_{\text{cement}}$  greatly deviated from this, likely due to the chloride binding and pore solution chemistry changes induced by the mineral admixtures.

Figures 2-9(a) and (b) also show that the electrical resistivity of concrete generally decreased after the electro-migration test whereas its electrical capacitance generally increased. This is likely attributable to the coarsening of the microstructure of concrete induced by the externally applied electric field as well as the enriching of ionic species in the pore solution of the concrete.

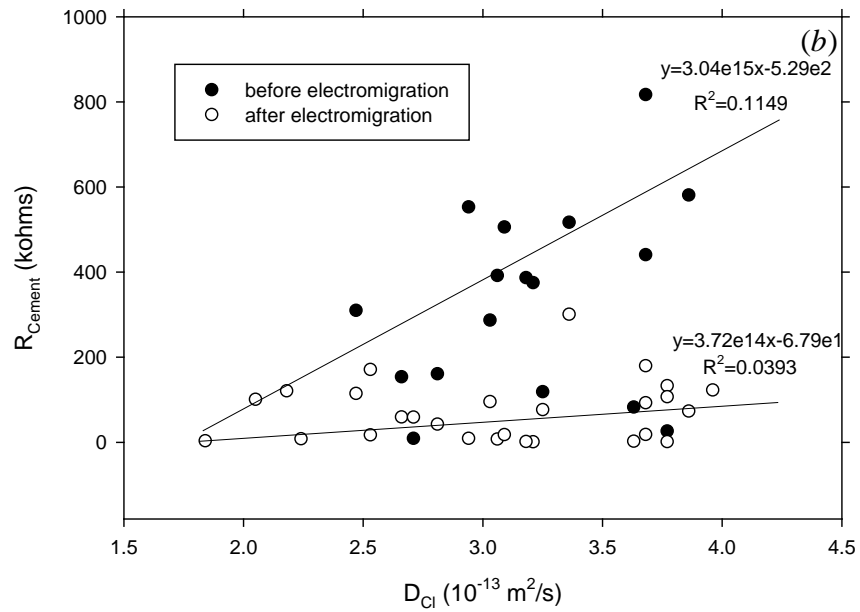
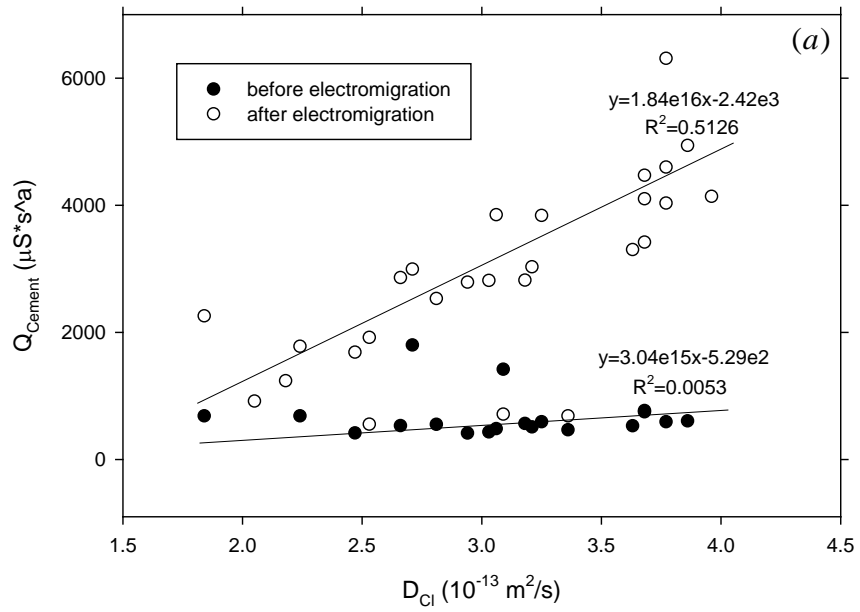


FIGURE 2-9 Correlation between the measured  $Q_{\text{cement}}$  (a) and  $R_{\text{cement}}$  (b) against chloride diffusion coefficients.

#### 2.2.4. Chloride Binding of Mortar and Influence of Mineral Admixtures

The relationship between free and bound chloride is generally non-linear. In order to describe the experimental results with analytical expressions, a Langmuir isotherm for chloride binding is utilized in this study, which follows [8]:

$$C_b = \frac{aC_f}{1 + bC_f} \quad (8)$$

where  $C_b$  and  $C_f$  stand for the bound and free chloride concentrations, respectively.  $a$  and  $b$  are the binding parameters to be evaluated by the least-square regression. Such parameters reflect the influence from such factors as type and amount of mineral admixtures. Table 2-6 provides the Langmuir isotherm parameters obtained from experimental data of the 9 mortar mixes. The experimental data for four kinds of mortars, as well as the isothermal chloride binding curves, are provided in Figure 2-10.

The chloride binding capability against mix design is depicted in Figure 2-11, which represents the chloride binding percentage at various initial chloride concentrations ( $C_0$ ). Mix design 9 (20% class F FA + 5% MK) and mix design 11 (10% SF) had the lowest binding capacity, whereas mix designs 1 (100% cement), 7 (10% UFFA) and 9 (50% GGBFS) had generally high chloride binding capacity relative to other mixes. These results are consistent with previous study that suggests silica fume to reduce chloride binding capability of concrete [9]. GGBFS has been reported to increase the chloride binding capability, as it promotes the formation of more Friedel's salt [11].

Nonetheless, the results from this work suggest the ordinary fly ash (both class F and class N) and metakaolin additions to reduce chloride binding capacity of mortar samples, which contradicts the previous knowledge on these minerals. Fly ash is considered to possess much higher capability for chloride binding, as it features much higher amount of active alumina compared with Portland cement [10]. In addition, MK was also found to significantly increase the chloride binding ability when used to partially replace cement in concrete [12]. These discrepancies may be a result of testing the chloride binding capacity with different methods (e.g., the sample preparation and the chloride concentrations used).

Table 2-7 provides the pore solution chemistry of mortar samples containing various types and amounts of mineral admixtures, shown as changes in the key elements that affect the ionic transport in such mineral concretes, i.e., Na, K, Ca, Mg, Fe as well as OH<sup>-</sup>.

While the metallic elements were measured using the IC/ICP, the pH of pore solution was measured using the chemical titration method. All the pH values were lower than 13.0, likely due to the contamination of airborne carbon dioxide into the small mortar specimens. Nonetheless, the pH data suggest that all the mineral admixtures reduced the alkalinity of the pore solution in the mortar samples, regardless of their type and amount.

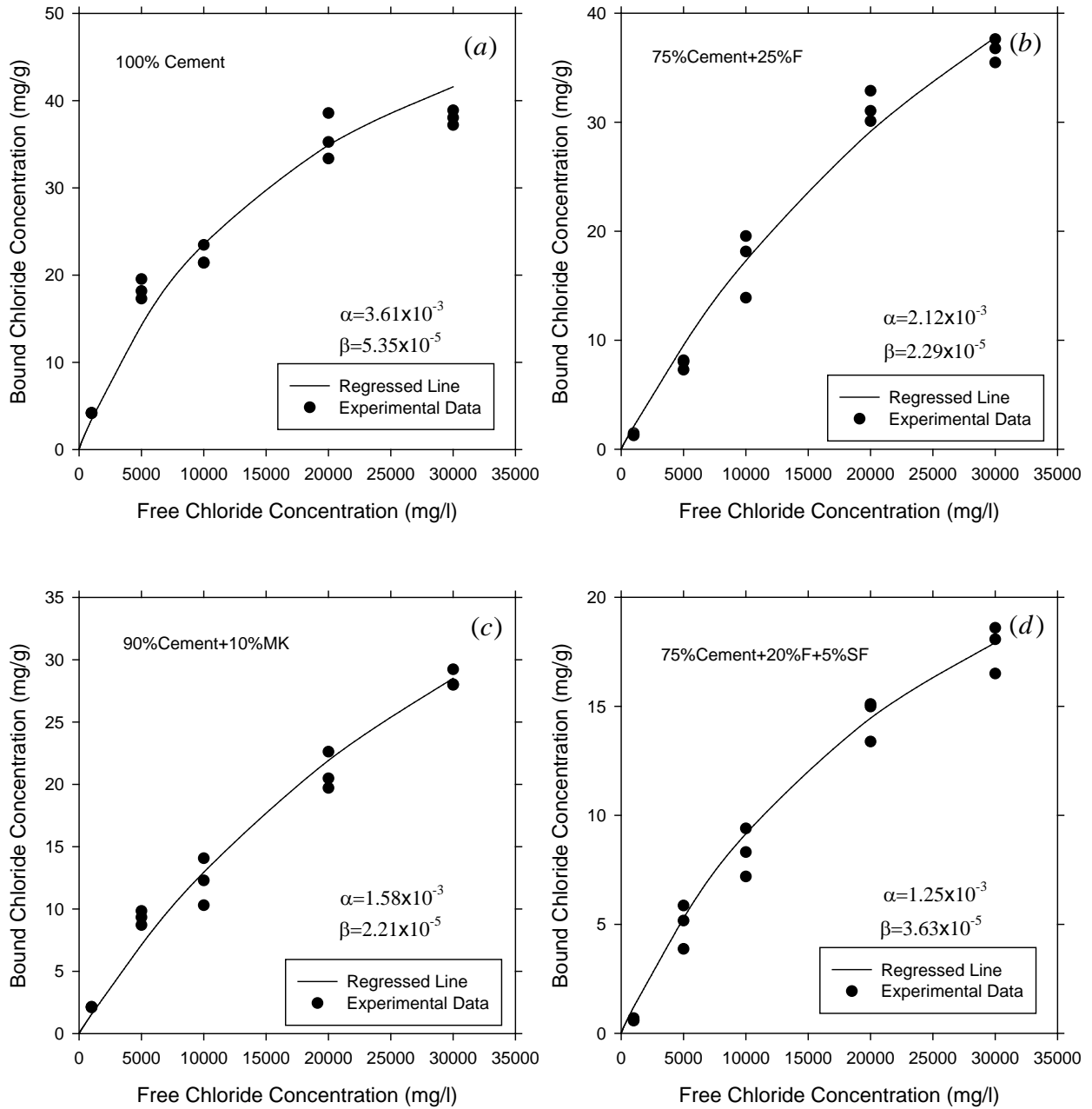


FIGURE 2-10 Chloride binding isotherms for four kinds of mortar samples.

TABLE 2-6 Chloride binding parameters measured from the mortar samples containing various mineral admixtures.

Mix Design	Constituents	$\alpha$ ( $10^{-3}$ L/mg)	$\beta$ ( $10^{-5}$ L/mg)
1	100% Cement	3.61	5.35
3	75% Cement, 25% FA-F	2.12	2.29
5	75% Cement, 25% FA-N	2.13	4.04
7	75% Cement, 20% FA-F, 5% SF	1.25	3.63
9	75% Cement, 20% FA-F, 5% MK	1.25	1.77
11	90% Cement, 10% SF	2.18	4.12
13	90% Cement, 10% MK	1.58	2.21
15	90% Cement, 10% UFFA	2.95	3.75
17	50% Cement, 50% GGBFS	2.16	4.08

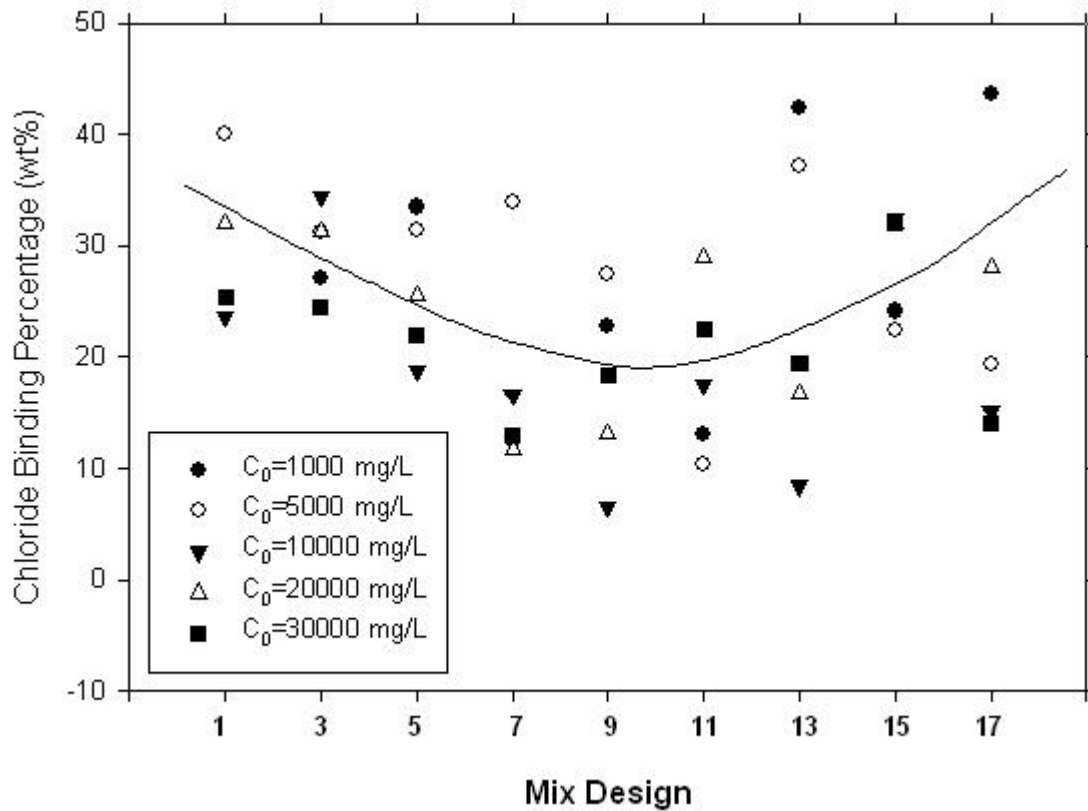


FIGURE 2-11 Chloride binding percentage with respect to mix designs of different mortar samples.

TABLE 2-7 Pore solution chemistry in mortar samples containing various types and amounts of mineral admixtures.

Mix No.	Mix Design	Na (ppm)	K (ppm)	Ca (ppm)	Mg (ppm)	Fe (ppm)	pH
1	100% Cement	1510	738	416	0.134	1.23	12.70
3	75% Cement, 25% FA-F	3430	1440	142	0.129	0.74	12.08
5	75% Cement, 25% FA-N	1460	687	271	0.022	0.64	12.34
7	75% Cement, 20% FA-F, 5% SF	2340	754	269	0.171	1.06	12.21
9	75% Cement, 20% FA-F, 5% MK	2170	903	157	0.159	0.83	12.43
11	90% Cement, 10% SF	920	313	669	< 0.010	1.50	12.51
13	90% Cement, 10% MK	1700	849	389	< 0.010	0.89	12.44
15	90% Cement, 10% UFFA	1560	1090	306	0.166	1.16	12.18
17	50% Cement, 50% GGBFS	929	838	385	0.280	1.06	12.46
	<i>ICP detection limit</i>	<i>40</i>	<i>20</i>	<i>30</i>	<i>0.010</i>	<i>0.30</i>	

#### 2.2.6. Freeze-thaw Resistance of Mortar in the Presence of Chlorides

After ten temperature cycles in the presence of concentrated deicers (23% NaCl, 30% CaCl<sub>2</sub>, and 30% MgCl<sub>2</sub>) and de-ionized water, it was observed that all the mortar samples had insignificant changes in their weight. As such, they were subjected to another ten temperature cycles in the presence of diluted deicers, with each deicer further diluted from their application concentration at a 3% by volume. This 3-to-100 ratio was chosen to simulate the field dilution of liquid or solid deicers once applied onto the pavement for some time. The average weight loss of mortar specimens after the two rounds of testing is presented in Figure 2-12. The results indicate that the weight loss of mortar specimens was the greatest in the presence of diluted NaCl solution, followed by the diluted CaCl<sub>2</sub>, and then by the diluted MgCl<sub>2</sub> solution, whereas the mortar deterioration in the de-ionized water was negligible. In the presence of diluted NaCl solution, the mix designs, the mix designs 13 (10% MK), 15 (10% UFFA) and particularly 17 (50% GGBFS) showed less weight loss relative to the control, whereas other SCMs exacerbated the freeze-thaw damage with the mix designs 5 (25% class N FA) and particularly 7 (20% class F FA + 5% SF) being the worst. In the presence of diluted CaCl<sub>2</sub> and MgCl<sub>2</sub> solutions, the effect of mineral admixtures on the freeze-thaw resistance of mortar followed a trend similar to that seen in the presence of diluted NaCl solution, yet with the mix designs 5 (25% class N FA) and 7 (20% class F FA + 5% SF) being the worst respectively. In summary, the partial replacement of cement by 50% GGBFS is most beneficial for the freeze-thaw resistance of mortar, followed by the 10% UFFA or 10% MK replacement; whereas the use of ordinary fly ash and silica fume seems to undermine the freeze-thaw resistance of mortar in the presence of various diluted chloride solutions.

It is postulated that the air-entrained concrete would have better freeze-thaw resistance than their mortar counterparts for two reasons. First, the concrete matrix contains less

cement paste phase than its mortar counterpart and is thus less prone to the physical attack by temperature cycling and chemical attack by deicers. Second, the air entrainment introduces microstructure that can mitigate the internal stress due to ice formation and thawing inside the concrete.

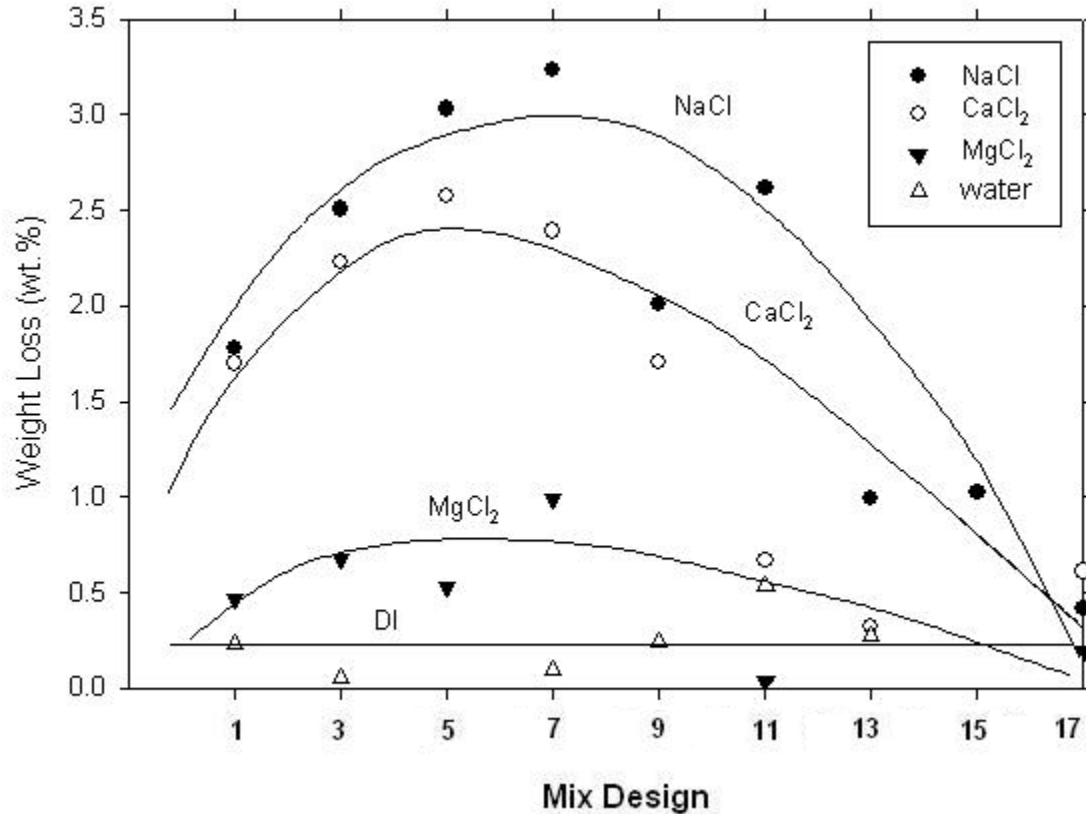


FIGURE 2-12 Weight loss of concrete specimens after freeze-thaw tests in the presence of various chlorides

### 2.3. Conclusions

Various laboratory tests were conducted to investigate the properties of mortar and concrete samples with cement partially replaced by various minerals (class F and class N FA, UFFA, SF, MK and GGBFS). These include: the compressive strength, Young's modulus, and modulus of toughness of mortar samples at 1-d, 7-d and 28-d; the compressive strength and porosity of concrete samples at 90-d; the chloride diffusivity and EIS measurements of hardened mortar and concrete samples; the natural diffusion of chloride into select concrete samples; the freeze-thaw resistance of mortars in the presence of chloride deicers; and the effect of mineral admixtures on the chloride binding and chemistry of the pore solution in mortar.

The accelerated chloride migration test of hardened concrete specimens found them to feature unusually low chloride diffusivity ( $D_s$  values in the order of  $10^{-13}$  m<sup>2</sup>/s vs. the commonly reported  $10^{-12}$  m<sup>2</sup>/s), corresponding to very high compressive strength. The

research findings imply that these high-quality concrete samples tested likely had little or no interfacial transitional zone (ITZ) in them. The chloride diffusivity in high-strength concretes was largely determined by the use of coarse aggregates whereas the effect of mineral admixtures was relatively small. The research also implies the importance of quality assurance in the processes and procedures used in the new construction, in order to achieve the great potential of reinforced concrete as a construction material and to manage corrosion risks pro-actively.

## 2.4. References

- [1] Truc O., Ollivier J.P., Carcassès M. A new way for determining the chloride diffusion coefficient in concrete from steady state migration test. *Cement and Concrete Research*, 30, 2000, 217-226.
- [2] Yang, X. Shi, A. T. Creighton, M. M. Peterson, Effect of styrene-butadiene rubber latex on the chloride permeability and microstructure of Portland cement mortar, *Construction and Building Materials*, 23(6), 2009, 2283-2290.
- [3] T. Pan, T. A. Nguyen, X. Shi, Assessment of Electrical Injection of Corrosion Inhibitor for Corrosion Protection of Reinforced Concrete, *Transportation Research Record*, 2044, 2008, 51-60.
- [4] Delagrave A., Marchand J., Ollivier J.-P., Julien S., Hazrati K. Chloride binding capacity of various hydrated cement paste systems. *Advn Cem Bas Mat* 6 (1997) 28-35.
- [5] G. Sergia, G. K. Glassb, A method of ranking the aggressive nature of chloride contaminated concrete, *Corrosion Science*, 42(12), 2000, 2043-2049.
- [6] C. Hall, W. D. Hoff, *Water transport in brick, stone and concrete*, Spon Press, Oct. 28, 2002.
- [7] P. Gao, M. Deng, N. Feng, The influence of superplasticizer and superfine mineral powder on the flexibility, strength and durability of HPC, *Cement and Concrete Research*, 31(5), 2001, 703-706.
- [8] L. Tang, L. Nilsson, Chloride binding capacity and binding isotherms of OPC pastes and mortars, *Cement and Concrete Research*, 23(2), 1993, 247-253.
- [9] P. S. Mangat, B. T. Molloy, Chloride binding in concrete containing PFA, GBS or silica fume under sea-water exposure, *Magazine of concrete research*, 47(171), 1995, 129-141.
- [10] T. Cheewaket, C. Jaturapitakkul, W. Chalee, Long term performance of chloride binding capacity in fly ash concrete in a marine environment, *Construction and Building Materials*, 24(8), 2010, 1352-1357.
- [11] R. Luo, Y. Cai, C. Wang, X. Huang, Study of chloride binding and diffusion in GGBS concrete, *Cement and Concrete Research*, 33(1), 2003, 1-7.
- [12] E. Vejmelková, M. Pavlíková, M. Keppert, Z. Keršner, P. Rovnaníková, M. Ondráček, M. Sedlmajer, R. Černý, High performance concrete with Czech metakaolin: Experimental analysis of strength, toughness and durability characteristics, *Construction and Building Materials*, 24(8), 2010, 1404-1411.

## CHAPTER 3. STOCHASTIC MODELING OF SERVICE LIFE OF REINFORCED CONCRETE IN CHLORIDE-LADEN ENVIRONMENTS

This chapter presents the methodology, results and discussion pertinent to the service life modeling of reinforced concrete in chloride-laden environments. The important features of ionic transport in concrete (with a focus on chloride diffusion) were explored and a two-dimensional finite-element-method (FEM) model was developed. The stochastic nature of model inputs is taken into consideration. Specifically, the surface chloride concentrations and concrete cover depth follow the normal distribution, whereas the diffusion coefficients and the chloride threshold follow the gamma distribution and the triangular distribution respectively. The nonlinear partial differential equations (PDEs) to characterize the spatial and temporal evolution of ionic species are numerically solved, the results of which are utilized to elucidate the influence of various factors on the service life of reinforced concrete, such as mix design (i.e., partial replacement of cement by mineral admixtures), surface chloride concentration, crack level, coarse aggregate and concrete cover depth.

### 3.1. Introduction

Due to its high strength, flexibility in geometries and variability in mechanical properties, reinforced concrete has been the most widely used construction material for infrastructures across the world. Concrete pore solution can have pH values well above 12, which allows rebar surface to be covered with a thin, passive and impermeable oxide film [1-2]. In addition, the dense concrete cover forms a physical barrier to reduce the penetration of deleterious species. Under such protective environments within concrete, steel rebars do not corrode spontaneously, which prevents anodic reactions from occurring and makes steel inert from active corrosion.

Chloride-induced degradation in concrete structures is a common occurrence in the United States due to the use of deicers in cold-climate states and the chloride environments in coastal areas. By capillary effect and diffusion, chloride ions can migrate into concrete. Although capillary movement is fast, it is less favored by the discontinuous pore system in concrete. Diffusion thus provides a practical manner for chloride ions to migrate across concrete cover and reach rebar surface, and the transport of chloride ions through concrete cover to rebar surface is a major cause of concrete degradation, the results of which lead to serious economic and safety implications. Chloride ions are responsible for the breakdown of passive film and the initiation of corrosion [3-4]. Reliable predictions for existing rebar performance are indispensable, which can take into account the extent of deterioration, the expected remaining service life, and the optimum repair strategy. A well-defined procedure allows sufficient information to be obtained for timely rehabilitation and replacement of reinforced concrete structures.

Although research in reinforcement corrosion in concrete has been extensively documented in the past decades [5-8], the current state of knowledge in corrosion initiation remains unsatisfactory. In traditional service life modeling, the concerns are addressed with the stochastic technique, with only the diffusion of chlorides taken into

consideration. Such treatments [9-10] fail to adequately describe concrete degradation due to mutual interactions among multiple ionic species, thereby underestimating or overestimating the risk of chloride contamination. In this study, a stochastic model is presented to simulate the service life of concrete structures subject to chloride ingress, the goal of which is to develop a reliable technique to predict structural deterioration and assess life performance of concrete infrastructures for typical aggressive chloride environments. Within the mathematical framework and the numerical implementation, input parameters are assumed to follow normal, gamma and triangular distributions respectively. Combined with the chloride binding isotherms, the algorithm of service life assessment is depicted for concrete infrastructures, the methodology for which can be used as a value tool for structural engineers and asset managers to estimate the appropriate timing of concrete maintenance and rehabilitation.

### 3.2. Methodology

Provided that the chloride-induced rebar corrosion is the major durability issue, the service of concrete structures (denoted by  $t_s$ ) can be described as [10]:

$$t_s = t_i + t_p \quad (1)$$

where  $t_i$  is the period within which a sufficient amount of chlorides can accumulate on rebar surface and  $t_p$  is the time for rebar corrosion to reach an unacceptable condition.

Although capillary movement is another manner by which chloride species can migrate into concrete, the discontinuous and zigzag nature of concrete pore systems does not favor this process.  $t_i$  can thus be assumed solely related to the penetration process in concrete cover by diffusion, and Fick's law is capable of predicting the chloride concentration evolution on the rebar surface. The initiation period is mainly influenced by diffusion coefficients of ionic species, concrete cover depth, surface chloride concentration, and critical chloride concentration on the rebar surface. Such variables are in principle stochastic, as corrosion damage is highly dependent on environmental parameters. Thus, the service life is best presented by a range of distribution rather than a single value. The degradation process, in which rebar experiences active corrosion, is complex and strongly depends on external conditions, such as temperature and humidity. However,  $t_p$  is generally accepted to be around 4~6 years. Such a short duration can be neglected for service life modeling, compared with the relative long time frame of corrosion initiation (~100 years).

In what follows, the mathematical model to be used for service life prediction is based on the conservation laws with fundamental model parameters related to the concrete characteristics and the environment to which the system is subject. Unlike the traditional treatment where only chloride diffusion is taken into consideration, the physical and chemical interactions among ionic species and cement phases are fully explored in this study.

### 3.2.1. Model for Multi-Species Transport (Method A)

From the modeling perspective, concrete structures can be divided into three physical domains, i.e. aggregate, porosity and paste/mortar. Aggregate is a dense and hard reinforcing component in concrete materials, in which the diffusivities of ionic species are negligible, while the pore system provides the zigzag diffusion path through which ionic species can migrate. Depending on cement types and additive varieties, multiple ionic species can be present in pore solutions, among which  $\text{Na}^+$ ,  $\text{K}^+$ ,  $\text{Ca}^{2+}$ ,  $\text{Cl}^-$ , and  $\text{OH}^-$  are most frequently encountered. Chloride ions in concrete are either free or bound. The free ones are water-soluble and can attack the passive film on the rebar surface to initiate pitting corrosion, whereas the bound ones exist in the form of chloride-aluminates, making them unavailable for free transport. In the traditional service life prediction of concrete structures, only chloride ions are taken into consideration. Although this treatment is simple and can be successfully applied to various scenarios, it fails to elucidate material degradation due to ionic and mineral interactions. There is thus a necessity to incorporate all the ionic species present in the system, and reformulate the model methodology to reflect the real scenario.

To describe the ionic transport in a porous system, the technique of homogenization is indispensable, which is rooted at the microscopic scale with the subsequent integration over a representative elementary volume [11]:

$$p \frac{\partial C_i}{\partial t} + (1-p) \frac{\partial S_i}{\partial t} + \nabla \cdot (pJ_i) = 0 \quad (2)$$

where  $C_i$  and  $S_i$  are the free and bound concentrations of species  $i$ , respectively;  $p$  is porosity;  $t$  is time;  $J_i$  is the flux of species  $i$ . The flux of each species in the pore solution can be given by [12]:

$$J_i = -D_i \nabla C_i - \frac{D_i}{RT} C_i F Z_i \nabla \phi \quad (3)$$

where  $D_i$  and  $Z_i$  are the diffusion coefficient and valence number for species  $i$ , respectively;  $F$  is Faraday constant;  $R$  is gas constant,  $T$  is temperature;  $\phi$  is electric potential.

From the practical point of view, only chloride binding is considered in this work, which is assumed to follow the Langmuir isotherm as follows [13]:

$$S_{Cl} = \frac{\alpha C_{Cl}}{1 + \beta C_{Cl}} \quad (4)$$

where  $\alpha$  and  $\beta$  are the binding parameters to be evaluated from measured free and bound chloride concentrations.

For saturated concrete where there is no external voltage, ionic species transport through the pore system under the electro-neutrality condition. At typical concentrations, the influence of non-ideality of electrolytic solution on the ionic fluxes is negligible, which indicates that the chemical activity of each species can be approximated by its corresponding concentration. Under an internally-induced electric field, all the ionic

species in the pore solution contribute to the electro-neutrality condition. Since the electric current in an electrolyte results from the movement of charged particles, the current density can be formulated as the fluxes of all the species as follows [12]:

$$i = pF \sum_{i=1}^n Z_i (-D_i \nabla C_i - \frac{Z_i F D_i}{RT} C_i \nabla \phi) \quad (5)$$

With the zero-flux boundary condition, the electro-neutrality condition can be formulated as [12]:

$$\nabla \cdot i = 0 \quad (6)$$

which serves as a supplemental equation to correlate the electric interaction among various species.

The concentrations of ionic species and the internal electric field constitute the degrees of freedom in the model, with which to describe the mass transfer and reactive diffusion. The model is accomplished by dividing the computation into two stages for each time step. The first stage is to investigate the transport of ionic species alone, with the chemical interaction being ignored. The second stage is to check local solubility constraints so that a certain amount of calcium carbonate can precipitate from pore solution and locally alter the pore fraction. Such two stages constitute a numeric time step during modeling, where the temporal scale should be set as small as possible to approach real and spontaneous local equilibrium.

### 3.2.2. Model for Single-Species Transport (Method B)

Based on the measured materials properties, the service life prediction can be obtained using a reliability analysis with only chloride species. Assuming chloride diffusion is the only physical process under consideration, the chloride content in concrete can be described by [15]:

$$\frac{\partial C_{Cl}}{\partial t} = D \frac{\partial^2 C_{Cl}}{\partial x^2} \quad (7)$$

where  $C_{Cl}$  is the chloride content in  $\text{kg/m}^3$ ;  $D$  is the chloride diffusion coefficient;  $x$  is the depth from the concrete surface;  $t$  is the time. When the surface chloride concentration is a constant and the diffusion problem is described for a one-dimensional finite depth, the analytical solution for Eqn. (7) can take the following form [4]:

$$C_{Cl} = C_0 (1 - \text{erf}(\frac{x}{2\sqrt{Dt}})) \quad (8)$$

where  $C_0$  is the surface chloride concentration; erf is the error function. When calculating the service of concrete infrastructure,  $C_{Cl}$  is treated as the corrosion initiation concentration. With given values of  $C_{Cl}$ ,  $C_0$ ,  $D$  and  $x$  based on their own statistical distribution, the time for corrosion initiation can be conveniently evaluated.

### 3.2.3. Input Parameters

As domain or boundary parameters, surface concentrations, concrete cover depth, diffusion coefficients, and chloride threshold values are random variables that have a stochastic nature. Once such model parameters have been identified either from lab measurement or field practice, a random number generator based on normal, triangle and gamma distributions to sample such stochastic values will be utilized, which can be linked with finite element analysis to retrieve information on the time for repair and rehabilitation. In order to reflect this peculiarity, a solution to Equations 2 to 6 should be sampled extensively so as to reflect the probabilistic nature of the input variables. The number of samplings is a compromise between the time for the simulation and the acceptability of the simulation results. As the number of samplings increases, the confidential interval for predicted service life becomes less sensitive with respect to the stochastic nature of input variables. The precision of the predictions can thus represent the range of service life. To this end, the simulation for each computational study in this work is explored by 10000 times. Based on the results of such trials, the 95% confidence intervals for the predicted time to repair and rehabilitation are evaluated.

The surface chloride concentration is an important parameter to characterize the driving force for chloride diffusion, the value of which depends on geographic locations and structure types. In order to estimate service life in extreme conditions, various surface chloride concentrations (from 2 to 8 kg/m<sup>3</sup>) are utilized. Note that these concentrations are in the weight of free Cl<sup>-</sup> ions per volume of solution. As the surface chloride concentrations vary with temperature, local humidity, and season alternation, a normal distribution is adopted in the simulation, which follows:

$$f(x) = \frac{1}{\sqrt{2\pi\sigma^2}} e^{-\frac{(x-\mu)^2}{2\sigma^2}} \quad (9)$$

where  $\sigma$  and  $\mu$  are the mean and standard deviation, respectively. The mean values for chlorides are set to 2, 4, 6 and 8 kg/m<sup>3</sup>, with a standard deviation of 0.2 kg/m<sup>3</sup> for all the cases investigated. Such a standard deviation is also applied for other ionic concentrations involved in the simulation. The spectrum distributions for various chloride concentrations are presented in Figure 3-13.

Diffusion coefficients of chloride and other species are highly dependent on materials characteristics and environments. In order to reflect the stochastic nature of diffusion coefficients in concrete structures, the diffusion coefficients are assumed to follow the gamma distribution given by:

$$f(x : k, \theta) = x^{k-1} \frac{e^{-x/\theta}}{\theta^k \Gamma(k)} \quad (10)$$

where  $x > 0$  and  $k, \theta > 0$ ;  $k = 27.05$  and  $\theta = 1.42$  for chloride diffusion in concrete, respectively. A graphical representation of the chloride diffusion coefficient distribution is provided in Figure 3-14, the tendency of which is also applied for other diffusion coefficients and mix designs.

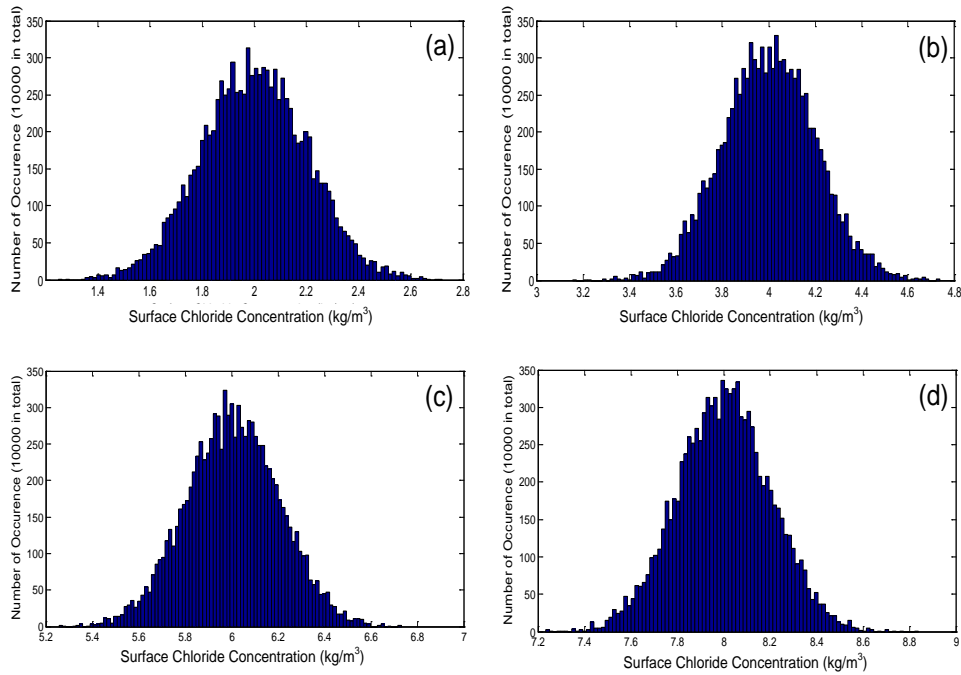


FIGURE 3-13 Surface chloride concentration distribution according to the normal distribution: (a) 2 kg/m<sup>3</sup>; (b) 4 kg/m<sup>3</sup>; (c) 6 kg/m<sup>3</sup> and (d) 8 kg/m<sup>3</sup>.

The actual chloride threshold in concrete is dependent on various parameters, such as cement type, composition, moisture content, and temperature. The triangular distribution is a continuous distribution with lower limit  $a$ , mode  $c$  and upper limit  $b$ , mathematically expressed as:

$$f(x, a, b, c) = \begin{cases} \frac{2(x-a)}{(b-a)(c-a)} & \text{for } a \leq x \leq c \\ \frac{2(b-x)}{(b-a)(c-a)} & \text{for } c \leq x \leq b \\ 0 & \text{otherwise} \end{cases} \quad (11)$$

In this work, the chloride threshold value is assumed to follow the symmetric triangular distribution, the shape of which is weighted towards to the center of a range of values. The upper limit is set as 5 kg/m<sup>3</sup>, while the lower limit remains at 0.6 kg/m<sup>3</sup>, as illustrated in Figure 3-15. Concrete cover depths in infrastructures feature natural variability, the change of which was found to follow the normal distribution from a survey on bridge decks in Virginia. For all the concrete cover depth utilized in this work, a standard deviation of 5 mm is assumed, the probability for the thickness distribution is shown in Figure 3-16 for concrete cover depths with a mean value of 50 mm.

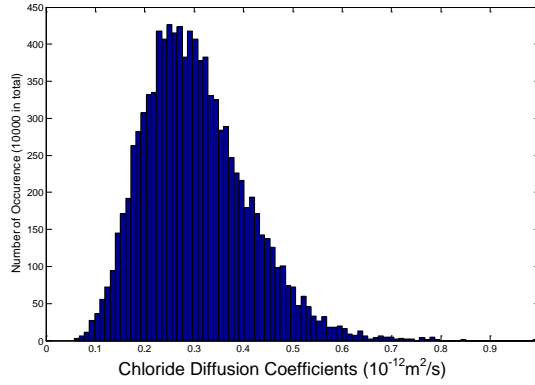


FIGURE 3-14 Chloride diffusion coefficient distribution according to the gamma distribution.

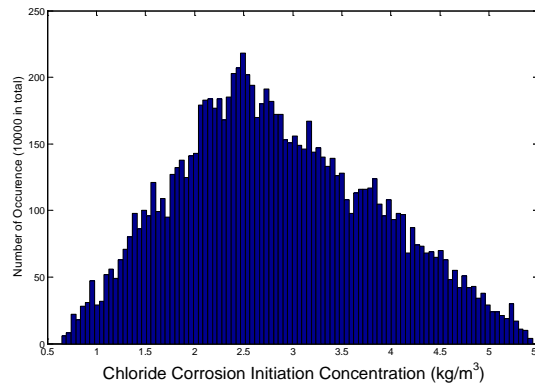


FIGURE 3-15 Chloride corrosion initiation concentration distribution according to the triangular distribution.

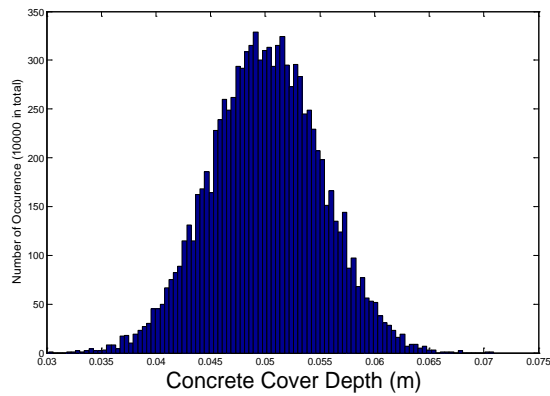


FIGURE 3-16 Concrete cover depth distribution according to the normal distribution.

In order to cover a wide range of design configurations, 14 concrete mix designs were considered, the details of which can be found in Table 2-2. A water-to-cementitious-materials ratio of 0.40 was specified for all the mix designs. The chloride diffusion coefficients of 360-day concrete samples were measured using an accelerated chloride migration test as detailed in our previous work [16], whereas the testing procedures of chloride binding capacity of concrete are detailed in the reference [17] and the laboratory investigation chapter. Diffusion coefficients other than chlorides were taken from the work of Wang et al. [11]. Note that this work pertains to the concrete reinforced with “black bar” (uncoated mild steel bar), instead of epoxy-coated rebar or corrosion-resistant rebar.

### **3.3. Results and Discussion**

#### *3.3.1. Effect of Mix Design on Service Life*

Chloride diffusion in concrete materials strongly depends on the environment, as such species will either chemically or physically interact with cement phases. Chloride transport through concrete materials will thus be eventually influenced by the pore structure, the physical or chemical binding and the inclusion of the supplementary materials. Using the proposed two methods, transport of chloride ions in various mix design is simulated, the results of which are presented in Table 2.

It is interesting to note that all concrete mixes investigated had a 50%-probability service life of 114 years or longer (with a surface chloride concentration of  $6 \text{ kg/m}^3$  and concrete cover of 50 mm), which highlights the great potential of reinforced concrete as a construction material when the concrete is made using the best practices of construction and curing and is free of cracking. The data in Table 3-8 also suggest that when the concrete is made using the best practices, partially replacing cement with class F FA, SF, MK, or GGBFS tends to decrease the service life of reinforced concrete or at least show little benefits to its service life. This trend contradicts what have been generally reported in published literature, and is likely attributable to the fact that the PCC made without any mineral admixtures (mixes 1 and 2) featured unusually low chloride diffusion coefficients in the order of  $10^{-13} \text{ m}^2/\text{s}$ . While the chloride diffusion coefficients did not differ greatly among the concrete mixes investigated, the predicted service life of reinforced concrete showed a certain degree of variations. Finally, for all these high-quality concrete mixes, the effects of air entrainment on the chloride diffusivity in concrete and the service life of reinforced concrete were not dramatic and did not show a clear trend.

As mentioned above, the rate of chloride migration depends on not only the diffusion rate of chloride ions but also the chloride binding capability of concrete materials. It is evident from Table 3-8 that for the 10, 50 and 90% likelihood of corrosion initiation, the service life predicted from multi-species model (method A) is generally longer than that obtained from single-species model (method B), which is due to the incorporation of chloride binding in the former case.

TABLE 3-8 Predicted service life for various mix designs, with a surface chloride concentration of 6 kg/m<sup>3</sup> and concrete cover of 50 mm

Mix Design	D (10 <sup>-13</sup> m <sup>2</sup> /s)	Chloride Binding Parameters $\alpha$ and $\beta$ (L/mg)	Service Life from method A (years) (10, 50 and 90%)	Service Life from method B (years) (10, 50 and 90%)
1	2.50	3.61×10 <sup>-3</sup> ; 5.35×10 <sup>-5</sup>	103;285;624	95;182;521
2	2.74	3.61×10 <sup>-3</sup> ; 5.35×10 <sup>-5</sup>	91;179;584	79;168;523
3	2.36	2.12×10 <sup>-3</sup> ; 2.29×10 <sup>-5</sup>	102;174;628	87;157;593
4	3.77	2.12×10 <sup>-3</sup> ; 2.29×10 <sup>-5</sup>	64;136;348	53;121;326
7	2.99	1.25×10 <sup>-3</sup> ; 3.63×10 <sup>-5</sup>	79;114;405	65;107;384
8	3.25	1.25×10 <sup>-3</sup> ; 3.63×10 <sup>-5</sup>	83;159;481	77;143;438
9	3.27	1.25×10 <sup>-3</sup> ; 1.77×10 <sup>-5</sup>	94;168;498	83;152;467
10	3.14	1.25×10 <sup>-3</sup> ; 1.77×10 <sup>-5</sup>	83;171;458	73;148;412
11	3.80	2.18×10 <sup>-3</sup> ; 4.12×10 <sup>-5</sup>	62;157;371	53;135;348
13	2.90	1.58×10 <sup>-3</sup> ; 2.21×10 <sup>-5</sup>	71;184;532	67;167;481
14	3.70	1.58×10 <sup>-3</sup> ; 2.21×10 <sup>-5</sup>	62;148;397	53;136;356
15	3.71	2.95×10 <sup>-3</sup> ; 3.75×10 <sup>-5</sup>	59;163;328	52;151;305
17	3.52	2.16×10 <sup>-3</sup> ; 4.08×10 <sup>-5</sup>	53;167;324	48;145;296
18	2.35	2.16×10 <sup>-3</sup> ; 4.08×10 <sup>-5</sup>	116;237;603	97;193;541

### 3.3.2. Effect of Surface Chloride Concentration on Service Life

Concrete structures located in different regions are exposed to varying degrees of corrosivity, as the amount and frequency of salt usage in northern snow states vary significantly and the attack from marine environments in coastal states differs geographically. Such variations are reflected on the surface chloride concentrations for chlorides to migrate into concrete structures. The chloride concentrations on concrete surface serve as the driving force for chloride ingress, thus showing a significant effect on service life prediction. To investigate the effect of surface chloride concentration on concrete service life prediction, numerical predictions are conducted with four levels of surface chloride concentrations, i.e. 2, 4, 6 and 8 kg/m<sup>3</sup>. A concrete cover depth measuring 50 mm in thickness is laid over the rebar surface for all the cases studied, after which the computational investigation is conducted to explore the long term protection. The initial conditions for concentrations of Na<sup>+</sup>, K<sup>+</sup>, Ca<sup>2+</sup>, and OH<sup>-</sup> within the concrete domain are 2, 2, 3, and 7 kg/m<sup>3</sup>, respectively, and the boundary conditions for such species also remain at those values. To determine whether the chloride threshold concentration for active corrosion has been reached on rebar surface, the chloride content on rebar surface is monitored against time, and a randomly generated chloride threshold value is used as a reference to identify the service life. Based on the evolution of such curves against time, the value of  $t_f$  is determined, which is considered to be the time for active corrosion. The current treatment incorporates the influence of mutual interaction between chloride and hydroxyl ions on chloride threshold values.

The effect of surface chloride concentration is explored by comparing the predicted service life spectrum for four scenarios in Figure 3-17. However, it is noted that the surface chloride concentration and the chloride threshold value are random numbers. Once the chloride threshold value is higher than the surface chloride concentration, the resulted time for diffusion is trivial, as sufficient chlorides will never be present at the rebar depth for corrosion to initiate. Based on the modeling results, chloride inward-diffusion with the lowest surface chloride concentration is the most sluggish process. With the surface chloride concentration increasing, the service life decreases significantly. For the case in which the surface chloride concentration of mix design 1 remains at  $6 \text{ kg/m}^3$ , the 90% likelihood of corrosion initiation is around 600 years. The above discussion is based on the assumption that concrete is fully saturated with water. However, alternate wetting and drying cycles can change the chloride content on concrete surface. For a concrete cover with a depth of 50 mm, the time for chlorides to arrive at the chloride threshold level is from 150 to 600 years under various exposure conditions in Figure 3-17. It is obvious that with the current concrete cover depth, it is likely to obtain a reliable protection against chloride attack, where the chloride concentrations on rebar surface can be well below the critical threshold value for corrosion initiation even after 100 years.

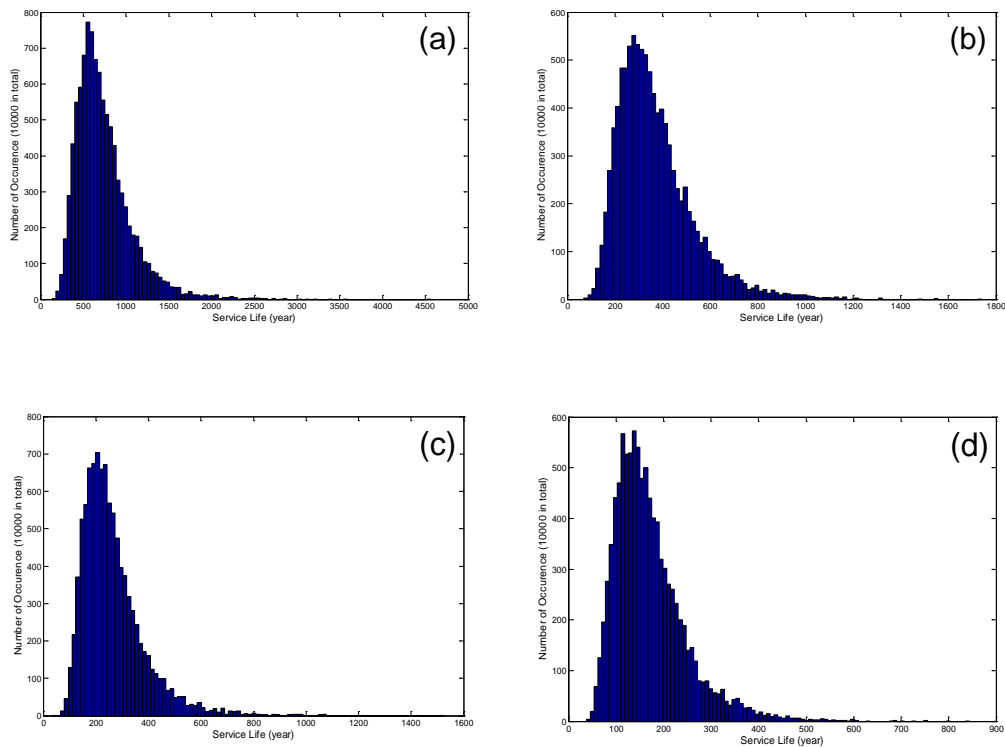


FIGURE 3-17 Predicted service life for concrete structures with surface chloride concentrations being (a)  $2 \text{ kg/m}^3$ , (b)  $4 \text{ kg/m}^3$ , (c)  $6 \text{ kg/m}^3$  and (d)  $8 \text{ kg/m}^3$ .

### 3.3.3. Effect of Cracking Level on Service Life

Concrete structures are subject to environmental loadings (e.g., freeze/thaw cycles) and periodic traffic load under normal service conditions, leading to cracks characterized by various densities. Poor practices during construction and curing can also lead to the initiation and propagation of cracks in concrete. The effect of crack density has practical implication for infrastructures. Chloride transport through cracks over long period of time is of the primary concern for performance evaluation. Durability of concrete infrastructures is significantly affected by the presence of cracks, as they can facilitate the chloride ingress by act as preferential channel. This consensus has been universally accepted, but a quantitative description is still lacking. Francois et al. [19] conducted a corrosion study by exposing loaded reinforced concrete beams to salt fog for twelve years. They found that the tensile micro-cracking in concrete as a result of service loading was responsible for accelerating chloride penetration whereas the existence and width of micro-cracks (with width less than 0.5 mm) did not influence the development of the rebar corrosion.

The simulation domains are established in Figure 3-18 to investigate the effects of crack on service life, where four levels of crack configurations are presented, i.e. 50, 80, 145 and 207  $\text{m}^{-1}$ . Here, the crack density is defined as the total crack length per unit area. The initial conditions for  $\text{Na}^+$ ,  $\text{K}^+$ ,  $\text{Ca}^{2+}$  and  $\text{OH}^-$  are chosen as 2, 2, 3 and 2  $\text{kg}/\text{m}^3$ , respectively, with the boundary conditions for such species having the same values. The surface chloride concentration remains at 5  $\text{kg}/\text{m}^3$ , and the multi-species model is utilized. Diffusion coefficients for ionic species in cracks are taken from the work of Li and Gregory [18].

The effect of crack density on service life is evaluated by comparing the predicted chloride concentration profiles on rebar surface. It is noted that due to the presence of cracks in the two-dimensional domains, the distribution of chlorides on rebar surface is not uniform. Based on the modeling results, average chloride concentrations on rebar surface are utilized as the indicator, i.e. the chloride surface concentration after the introduction of cracks is determined by integration of the chloride concentration across the rebar surface and then divided by the rebar surface area. The time to corrosion initiation is presented in Figure 3-19, where the model outputs as a function of crack density are given.

As shown in Figure 3-19, the service life of reinforced concrete decreases as the cracking level of the concrete increases. The actual diffusion path traveled by ionic species in a cracked concrete is shorter than in crack-free solid. For the case in which the crack fraction is low, the short circuit path is far apart. Upon increasing of crack density, the distance for chloride ingress among various diffusion channels decreases. Based on the modeling results, chloride diffusion in crack-free concrete is the slowest process. With the crack density increasing, more chlorides are accumulating around rebar surface. It is interesting to note that when the crack density is over 200  $\text{m}^{-2}$ , the service life shows no significant dependence on further increase on crack density, which is attributable to the forming of continuous net-like configuration in the concrete domain.

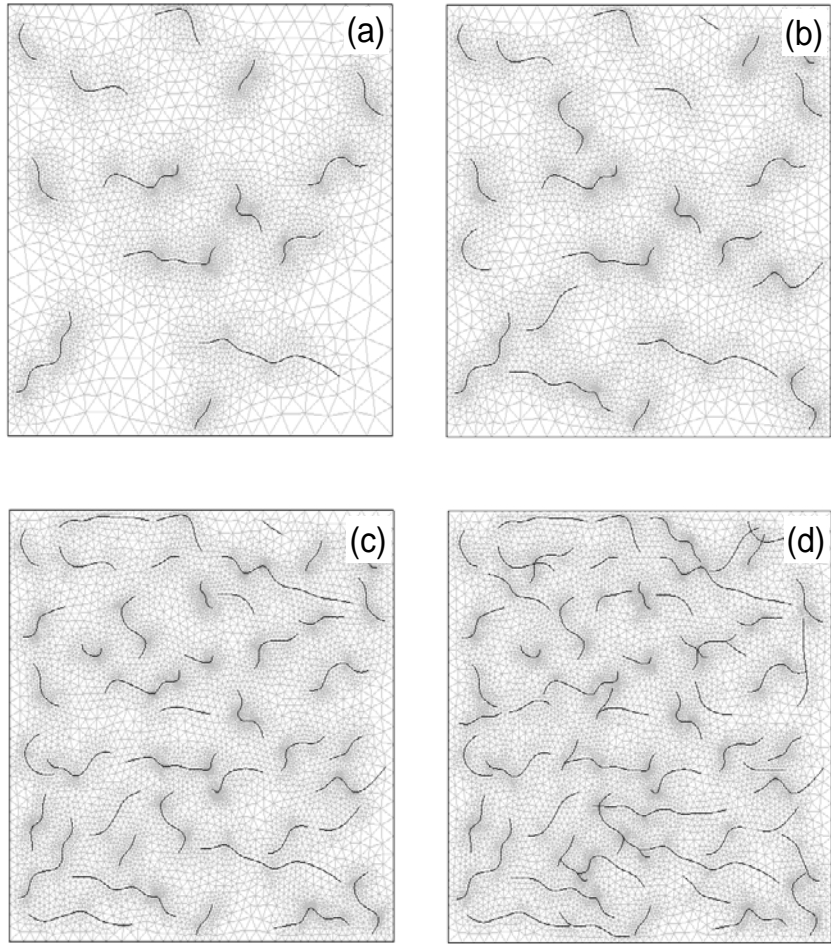


FIGURE 3-18 Crack configurations with various densities for service life prediction: (a)  $50 \text{ m}^{-1}$ ; (b)  $80 \text{ m}^{-1}$ ; (c)  $145 \text{ m}^{-1}$  and (d)  $207 \text{ m}^{-1}$ .

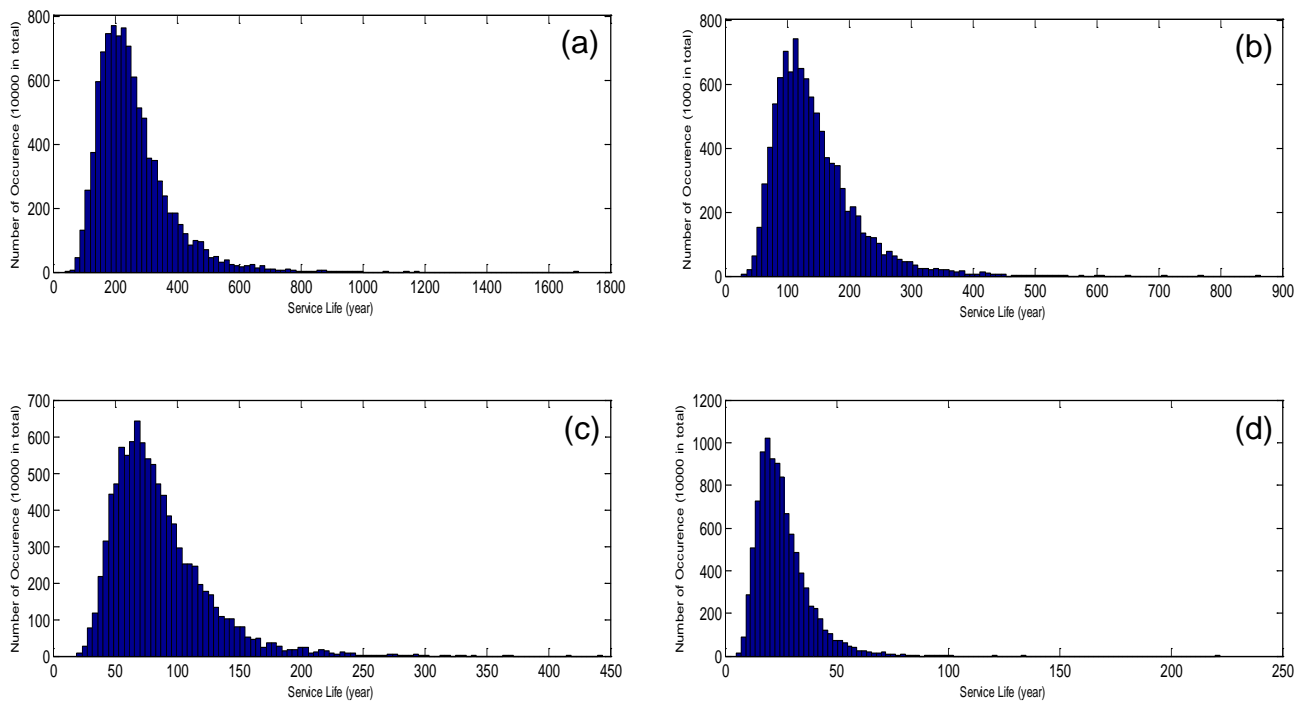


FIGURE 3-19 Effect of crack densities on service life prediction: (a)  $50 \text{ m}^{-1}$ ; (b)  $80 \text{ m}^{-1}$ ; (c)  $145 \text{ m}^{-1}$  and (d)  $207 \text{ m}^{-1}$ .

### 3.3.4. Effect of Coarse Aggregates on Service Life

From the practical point of view, concrete can be treated as a structure having two main constituents: cement paste and aggregates. Aggregates are a dense phase that is randomly distributed within continuous cement matrix. When concrete is water-saturated, the pores in cement matrix form a continuous channel system, within which chlorides diffuse and transport towards rebar surface. The diffusivity of ionic species in aggregates is typically very small, which leads to appreciable heterogeneities of chloride diffusion within concrete. The diffusion coefficient of chloride ions in aqueous solutions [20], cement paste [21] and marble [22] has the order of  $10^{-9} \text{ m}^2/\text{s}$ ,  $10^{-12} \text{ m}^2/\text{s}$  and  $10^{-15} \text{ m}^2/\text{s}$ , respectively. Accordingly, it can be assumed that diffusion of chloride ions in coarse aggregates of concrete is negligible.

Traditionally, concrete is considered to have a heterogeneous interfacial transition zone (ITZ) with about  $30 \text{ }\mu\text{m}$  of porosity gradient on the surface of each coarse aggregate, featuring high localized  $w/cm$  ratio and high porosity relative to the cement paste phase [23-24]. This, however, is debatable since “the higher porosity present initially is significantly diminished by the migration of ions during hydration” [25] and “the extra space produced by the wall effect is filled in by CH deposits” [26]. In our opinion, it is possible to eliminate the presence of ITZ through best practices of construction and

curing, such as the use of surface-saturated-dry aggregates and high-speed stirring during mixing of fresh concrete.

If we ignore the presence of paste-aggregate ITZ, the diffusion coefficients in paste and mortar can be combined with the amount of aggregates to predict transport properties of concrete. To gain an acceptable description for chloride diffusion in concrete structures, the mean field theory is adopted to evaluate the effective diffusion coefficients, where a two-dimensional simulation domain with the same size as mentioned above is utilized. To gain a phenomenological description of chloride diffusion in hetero-structural concrete, the effective diffusion coefficient for a two-phased structure can be described by [27]:

$$D_{eff} = D_c \frac{D_a + K_a D_c + K_a \phi (D_a - D_c)}{D_a + K_a D_c - \phi (D_a - D_c)} \quad (12)$$

where  $D_c$  stands for the chloride diffusion coefficients in cement paste, while  $D_a$  is that for aggregates,  $\phi$  and  $K_a$  are the volume fraction and the shape factor for the aggregates. For spherical aggregates,  $K_a = 2$ . For impermeable coarse aggregates,  $D_a$  is assumed to be 1/1000 of the averaged  $D_c$ . The formula (12) is utilized in this work to extrapolate diffusion coefficients with various aggregate fractions from the measured chloride diffusion coefficients in concrete samples.

For the simulation, a rectangular domain dimensioned by 50×50 mm is taken from a semi-infinite concrete with its left surface exposed to chloride-containing solution. The multi-species model is utilized. Four volume fractions of aggregate are used, i.e. 0.2, 0.4, 0.6 and 0.8. For convenience, the diffusion coefficients of ionic species in aggregate are set to zero. Four kinds of concrete mix designs are utilized for simulation, and the cumulative percentage of corroded structures for different aggregate volume fraction are shown in Figure 3-20. All the curves share the same pattern across the entire temporal domain. The large difference in diffusion rate between aggregates and cement paste complicates concrete service life prediction. For concrete structures with aggregates, the chloride diffusion rate was found to be quite different from its corresponding homogeneous medium. The overall flux decreases as the volume fraction of aggregates increases. The same behavior is also observed for other aggregate fractions, but shifted with respect to time and positions.

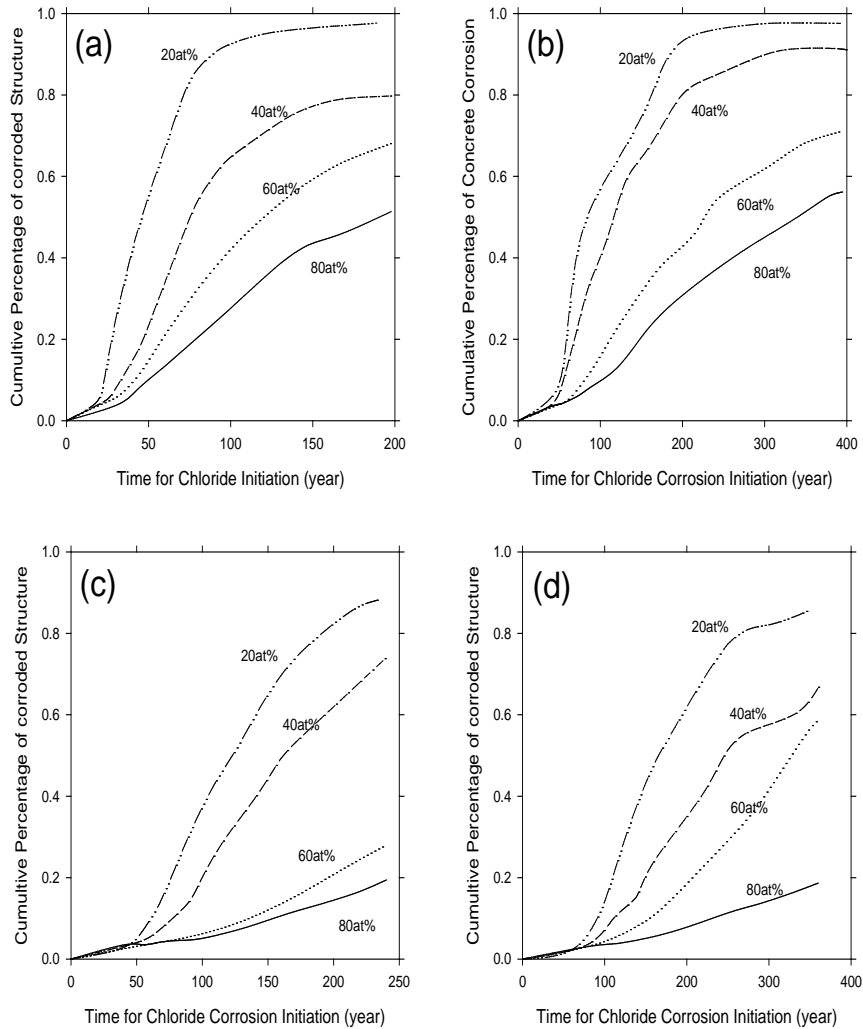


FIGURE 3-20 Effect of aggregate fraction on chloride-induced corrosion (a) mix design 2, (b) mix design 4, (c) mix design 8 and (d) mix design 11.

### 3.3.5. Effect of Concrete Cover Depth on Service Life

Concrete cover serves as a physical barrier to retard the ingress of deleterious species. Usually, an increase in the thickness of the concrete cover leads to beneficial effects, because it increases the barrier to the various aggressive species moving towards the reinforcement and increases the time for corrosion to initiate. In reality, however, the cover thickness cannot exceed certain limits, for mechanical and practical reasons [28].

To ensure the durability of concrete structures for a specific service life, concrete cover depths need to be evaluated with a theoretical method. According to the numerical method for multi-species diffusion, the relation between service life and concrete cover depth is predicted, the results of which are shown in Figure 3-21. Such profiles provide

qualitative information to predict service life against a given concrete cover depth. As the model incorporates probability distribution of input variables, the predictions can be used not only for a particular structure but also for a large population of bridges. As shown in Figure 3-21, for all the mineral concrete mixes investigated, as the concrete cover depth increases, the time to corrosion initiation of rebar in concrete is predicted to increase exponentially, highlighting the importance of cover depth in extending the service life of reinforced concrete exposed to external chlorides. According to the model calculations, it would take more than 100 years for the chloride ions in an aggressive environment (with surface chloride content of  $8 \text{ kg/m}^3$ ) to reach the threshold level at a depth of 60 mm. It should be cautioned that the chloride diffusivity data used for the model were measured using specimens cored from the center of a large concrete sample. In field construction, the top layer of the concrete cover is likely to have much higher chloride diffusivity than the interior of the concrete, in light of the possible defects derived from bleeding and water evaporation etc. at the top layer. Furthermore, the field construction is unlikely to achieve the same level of detailed quality assurance as implemented in the laboratory study and cracking cannot be fully eliminated for the service life prediction considerations. In this context, a thicker-than-predicted concrete cover is needed for the target service life of concrete structures in the field environment and the importance of good construction and curing practices can not be overemphasized.

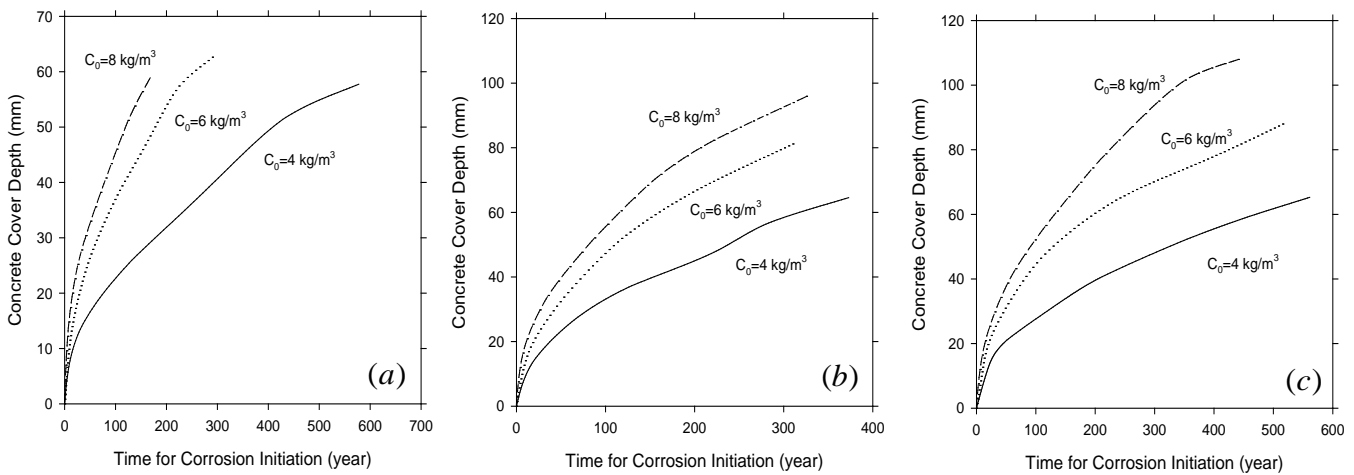


FIGURE 3-21 Variation of service life with respect to concrete cover depth. (a) mix design 2, (b) mix design 4 and (c) mix design 8.

### 3.4. Concluding remarks

Chloride ingress into concrete is a complex process, which in the highway environment is further complicated by the freeze-thaw cycles and wet-dry cycles experienced by roadways and bridges. While there are numerous existing experimental or modeling studies related to the transport of chlorides in concrete, the measurement of chloride ingress into concrete is technically challenging. Furthermore, it is also difficult to assess the durability of reinforced concrete from its chloride diffusivity, partially owing to the heterogeneous nature of the concrete matrix, the difficulty in fabricating concrete in a

reproducible manner, and the inherently probabilistic nature of species transport in concrete and of chloride-induced corrosion of steel rebar in concrete. In this context, modeling is a useful tool to provide quantitative understanding of key processes and their interactions that define the service life of reinforced concrete in chloride-laden environments.

A two-dimensional FEM model, coupled with the stochastic technique, was developed to study the service life of concrete structures under various conditions. In order to provide a reliable and statistical method to predict service life of concrete structures, concrete cover depth, chloride diffusion coefficients, surface chloride concentration, cracks and aggregates are taken into consideration, which are stochastically sampled. Starting from the equation of mass balance, the model incorporates the effect of various internal and external factors, and then explores the important features of ionic transport in concrete.

The technique developed in this work (e.g., multi-species transport model) may prove to be very effective in predicting chloride migration and generating statistical conclusions about the service life of reinforced concrete, which allows the civil engineers to estimate the rate of chloride ingress and speculate the deterioration risk of reinforced concrete. Future improvements could be made to the model so that it takes into account the time-dependency of transport properties of concrete [29, 35], the repair or replacement of concrete cover [15], the corrosion propagation [30], the chloride penetration mechanisms other than diffusion (e.g., wicking) [31], the structure geometry [32], the environmental humidity and temperature fluctuations and the decay of structures under coupled physical, chemical, and mechanical deterioration processes [33, 34] etc. With continued improvements on such models, they could also be used for life cycle costing and for the timing of repair or rehabilitation strategies.

### 3.5. References

- [1] G. Fasjardo, G. Escadeillas, G. Arliguie, Electrochemical chloride extraction from steel-reinforced concrete specimens contaminated by 'artificial' sea-water, *Cement and Concrete Research*, 32(2), 2002, 323-326.
- [2] J. C. Orellan, G. Escadeillas, G. Arliguie, G., Electrochemical chloride extraction: efficiency and side effects, *Cement and Concrete Research*, 31(1), 2003, 116-125.
- [3] G. K. Glass, and N. R. Buenfeld. Chloride-induced corrosion of steel in concrete, *Progress in Structural Engineering and Materials*, 2, 2000, 448-458.
- [4] O. E. Gjrv, . Vennesland, Diffusion of chloride ions from seawater into concrete, *Cement and Concrete Research*, 9, 1979, 229-238.
- [5] L. Basheer, J. Kropp, D. Cleland, Assessment of the durability of concrete from its permeation properties: a review, *Construction and Building Materials*, 15, 2001, 93-103.
- [6] G. K. Glass and N. R. Buenfeld, The presentation of the chloride threshold level for corrosion of steel in concrete, *Corrosion Science*, 39(5), 1997, 1001-1013.
- [7] G. K. Glass, N. R. Buenfeld, The influence of chloride binding on the chloride induced corrosion risk in reinforced concrete, *Corrosion Science*, 42(2), 2000, 329-344.

- [8] M. Thomas, Chloride thresholds in marine concrete, *Cement and Concrete Research*, 26(4), 1996, 513-519.
- [9] R. P. Khatri, V. Sirivivatnanon, Characteristic service life for concrete exposed to marine environments, *Cement and Concrete Research*, 34, 2004, 745-752.
- [10] P. Konecny, P. J. Tikalsky, D. G. Tepke, Performance Evaluation of Concrete Bridge Deck Affected by Chloride Ingress: Simulation-based Reliability Assessment and Finite Element Modeling, *Transportation Research Record*, No. 2028, 2007, 3-8.
- [11] W. Wang, L. Y. Li, C. L. Page, A two-dimensional model of electrochemical chloride removal from concrete, *Computational Materials Science*, 20, 2001, 196-212.
- [12] A. M. Hassanein, G. K. Glass, N. R. Buenfeld, A mathematical model for electrochemical removal of chloride from concrete structures, *Corrosion*, 54(4), 1998, 323-332.
- [13] X. Lu, C. Li, H. Zhang, Relationship between the free and total chloride diffusivity in concrete, *Cement and Concrete Research*, 32, 2002, 323-326.
- [14] N. R. Buenfeld, G. K. Glass, Al. M. Hassanein, J. Zhang, Chloride transport in concrete subjected to electric field, *Journal of Materials in Civil Engineering*, 10(4), 1998, 220-228.
- [15] Song, H.-W., Shim, H.-B., Petcherdchoo, A., and Park, S.-K., 'Service Life Prediction of Repaired Concrete Structures under Chloride Environment Using Finite Difference Method', *Cem. Concr. Compos.* 31, 2009, 120-127.
- [16] Z. Yang, X. Shi, A. T. Creighton, M. M. Peterson, Effect of styrene-butadiene rubber latex on the chloride permeability and microstructure of Portland cement mortar, *Construction and Building Materials*, 23(6), 2009, 2283-2290.
- [17] R.S. Barneyback Jr., S. Diamond, Expression and analysis of pore fluids from hardened cement pastes and mortars, *Cement and Concrete Research*, 11(2), 1981, 279-285.
- [18] Y. Li, S. Gregory, Diffusion of ions in sea water and in deep-sea sediments, *Geochimica et Cosmochimica Acta* 1974; 38: 703-714.
- [19] Francois R., G. Arliguie, and A. Castel. Influence of Service Cracking on Service Life of Reinforced Concrete, in: *Concrete under severe conditions 2: environment and loading: Proceedings of the 2nd International Conference on Concrete Under Severe Conditions, CONSEC'98, Tromsø, Norway, June 21-24, 1998. pp.143-152.*
- [20] Lee S.H., J. C. Rasiaiah. *Journal of Physical Chemistry* 1996; 100: 1420-1425.
- [21] Castellote M., C. Alonso, C. Andrade, G. A. Chadbourn, C. L. Page. *Cement and Concrete Research* 2001; 31: 621-625.
- [22] Hobbs D.W. *Cement and Concrete Research* 1999; 29: 1995-1998.
- [23] Diamond S., and J. Huang. The ITZ in Concrete – a Different View Based on Image Analysis and SEM Observations, *Cem Concr Compos* 2001; 23(2-3): 179-188.
- [24] Scrivener K.L., A.K. Crumbie, and P. Laugesen. The Interfacial Transition Zone (ITZ) Between Cement Paste and Aggregate in Concrete, *Interf Sci* 2004; 12(4); 411-421.
- [25] Ollivier J.P., J. C. Maso, and B. Bourdette. Interfacial Transition Zone in Concrete, *Adv Cem Bas Mater* 1995; 2(1): 30-38.

- [26] M. G. Alexander, G. Arliguie, G. Ballivy, A. Bentur and J. Marchand. Engineering and Transport Properties of the Interfacial Transition Zone in Cementitious Composites - State-of-the-Art Report of RILEM TC 159-ETC and 163-TPZ. 404 pp. 1999. <http://www.rilem.net/repContents.php?rep=rep020>, last accessed on January 15, 2010.
- [27] Zeng Y. Modeling of Chloride Diffusion in Hetero-Structured Concretes by Finite Element Method, *Cem Concr Compos* 2007; 29: 559-565.
- [28] Bertolini L, Elsener B, Pedeferra P, Polder R. Corrosion of steel in concrete: Prevention, diagnosis, repair. Wiley-VCH, Verlag GmbH & Co. KGaA, Weinheim. 2004.
- [29] Thomas, M.D.A.; Bamforth, P. B. Modelling Chloride Diffusion in Concrete: Effect of Fly Ash and Slag, *Cem Concr Res* 1999, 29(4): 487-495.
- [30] Pettersson, K. Service Life of Concrete Structure Including the Propagation Time. In: Concrete under severe conditions 2: environment and loading: Proceedings of the 2nd International Conference on Concrete Under Severe Conditions, CONSEC'98, Tromsø, Norway, June 21-24, 1998. pp.489-498.
- [31] Boddy, A., E. Bentz, M.D.A. Thomas, and R.D. Hooton. *Cement and Concrete Research* 1999; 29(6): 827-837.
- [32] Kranc S.C., and A.A. Sagues. Advanced Analysis of Chloride Ion Penetration Profiles in Marine Substructures, prepared for the Florida Department of Transportation. 2003.
- [33] Lin G., Y. Liu, and Z. Xiang. Numerical Modeling for Predicting Service Life of Reinforced Concrete Structures Exposed to Chloride Environments, *Cem Concr Compos* 2010; 32(9): 571-579.
- [34] Chen D. Computational Framework for Durability Assessment of Reinforced Concrete Structures Under Coupled Deterioration Processes. Dissertation. Ph.D. in Civil Engineering. Vanderbilt University. August 2006.
- [35] Nokken M., A. Boddy, R.D. Hooton, and M.D.A. Thomas. Time Dependent Diffusion in Concrete – Three Laboratory Studies, *Cem Concr Res* 2006; 36(1): 200-207.

## CHAPTER 4. CONCLUSIONS AND RECOMMENDATIONS FOR IMPLEMENTATION

Corrosion of reinforced and prestressed concrete structures is a major and increasing problem worldwide. The remediation of concrete bridges in the United States, undertaken as a direct result of chloride-induced corrosion of the reinforcing steel, would cost the US highway departments \$5 billion per year (FHWA, 1999). The cost of maintenance and rehabilitation required to preserve the structural integrity and overall safety of highway concrete structures is phenomenal. Repeated rehabilitation and repair also incur a significant environmental toll, as well as the delays caused by closing roads or bridges. On the other hand, appropriate design for corrosion protection would generate substantial cost savings for the DOTs by minimizing the premature rehabilitation or failure of highway bridges and reducing the construction costs.

DOTs spend billions of dollars each year on the construction and maintenance of highway bridges, and the national bridge inventory includes numerous structures with exposure to corrosive salt conditions in marine environments and in ice-prone regions of the country. With extended service life and reduced need for costly and difficult repair and rehabilitation of bridge structures, the implementation of better design practices will have immediate positive impacts on the nation's highway system, including cost savings, enhanced traveler safety, reduced traveler delays, and minimized environmental impacts.

### 4.1. Conclusions

Various laboratory tests were conducted to investigate the properties of mortar and concrete samples with cement partially replaced by various minerals (class F and class N FA, UFFA, SF, MK and GGBFS). These include: the compressive strength, Young's modulus, and modulus of toughness of mortar samples at 1-d, 7-d and 28-d; the compressive strength and porosity of concrete samples at 90-d; the chloride diffusivity and EIS measurements of hardened mortar and concrete samples; the natural diffusion of chloride into select concrete samples; the freeze-thaw resistance of mortars in the presence of chloride deicers; and the effect of mineral admixtures on the chloride binding and chemistry of the pore solution in mortar.

The accelerated chloride migration test of hardened concrete specimens found them to feature unusually low chloride diffusivity ( $D_s$  values in the order of  $10^{-13}$  m<sup>2</sup>/s vs. the commonly reported  $10^{-12}$  m<sup>2</sup>/s), corresponding to very high compressive strength. The research findings imply that these high-quality concrete samples tested likely had little or no interfacial transitional zone (ITZ) in them. The chloride diffusivity in high-strength concretes was largely determined by the use of coarse aggregates whereas the effect of mineral admixtures was relatively small.

Some detailed findings are provided as follows.

1. The partial replacement of cement by 20% class F FA and 5% SF, by 20% class F FA and 5% MK, or by 25% class F FA alone greatly reduced the 1-day compressive

strength of mortar samples, whereas the partial replacement of cement by 10% MK, 10% SF, 10% UFFA, 50% GGBFS, or 25% class N FA improved the 1-day strength to various degrees.

2. The combined addition of class F and MK dramatically reduced the 7-day compressive strength of mortar samples, followed by the use of GGBFS or SF, whereas the addition of most other minerals (except MK) also decreased the 7-day strength to various degrees.
3. The combined addition of class F and MK increased the 28-day compressive strength of mortar samples, whereas the addition of most other minerals (except GGBFS) decreased the 28-day strength to various degrees.
4. All the SCMs dramatically reduced the 1-day Young's modulus of mortar samples, but they showed mixed effect on the 7-day and 28-day Young's modulus. All the SCMs dramatically reduced the 7-day and 28-day modulus of toughness, but they showed mixed effect on the 1-day modulus of toughness. The reduction in the moduli of concrete is beneficial as it renders the concrete less prone to shrinkage cracking, which in turn, reduces the risk of rapid chloride ingress.
5. According to the EIS measurements after the ACMT using 90-day old mortar samples, all the SCMs dramatically increased the electrical resistivity of the mortar samples in the electrolyte while most SCMs (except GGBFS) decreased the electrical capacitance of the mortar to various degrees.
6. The effect of partially replacing cement with SCMs on the steady-state diffusion coefficient ( $D_s$ ) obtained from the ACMT was evaluated using 90-day old mortar samples. The results indicate that the use of 20% class F FA and 5% SF as cement replacement significantly increased the chloride diffusivity in mortar and the use of 10% MK or 50% GGBFS significantly decreased it, whereas other SCMs decreased the  $D_s$  to various degrees. Note that the  $D_s$  values were all very low (in the order of  $10^{-13}$  m<sup>2</sup>/s), and the chloride diffusivity differences between these highly impermeable concrete samples could be related to the workability and construction practices of the fresh concrete mixes.
7. There is no clear trend related to the effect of SCMs on the 90-day compressive strength of concrete or the chloride diffusivity in the 360-day concrete samples. Nonetheless, the chloride diffusivity is much lower in the concrete mixes than in their corresponding mortar mixes, with the  $D_s$  values in the order of  $10^{-13}$  m<sup>2</sup>/s in concrete and of  $10^{-11}$  m<sup>2</sup>/s in mortar. This highlights the important role of coarse aggregates in slowing down the chloride ingress into concrete.
8. All the mortar mixes had a 28-day compressive strength above 4,000 psi (27.6 MPa) whereas the non-air-entrained concrete mixes at 90 days on average featured twice as high a compressive strength. Such extremely high strength values suggest that the hardened concrete had outstanding microstructure, which is consistent with their extremely low  $D_s$  values indicative of chloride diffusivity. The compressive strength of air-entrained concrete was consistently lower than that of their non-air-entrained counterpart, yet the differences in their chloride diffusivity were not as appreciable.

9. The natural diffusion results indirectly confirmed the order of magnitude of  $D_s$  values of concrete specimens obtained from the ACMT.
10. Generally speaking, the lower  $D_s$  values corresponded to the higher compressive strength values, as both indicate high quality of the mortar or concrete. The lower  $D_s$  values in mortar corresponded to the lower  $D_s$  values in the non-air-entrained concrete, indicating that chloride diffusion in the mortar phase contributed to the overall chloride diffusion in the concrete.
11. There is a strong proportional correlation between the transformed mortar strength and the concrete strength, suggesting that the mortar phase is an integral component of the heterogeneous concrete matrix and greatly contributes to its compressive strength.
12. The chloride diffusivity generally increases with the volume of permeable voids in concrete.
13. The cumulative charge generally increases with chloride diffusion coefficients.
14. The electrical resistivity of concrete generally decreased after the electro-migration test whereas its electrical capacitance generally increased.
15. Mix design 9 (20% class F FA + 5% MK) and mix design 11 (10% SF) had the lowest binding capacity, whereas mix designs 1 (100% cement), 7 (10% UFFA) and 9 (50% GGBFS) had generally high chloride binding capacity relative to other mixes.
16. The pH data suggest that all the mineral admixtures reduced the alkalinity of the pore solution in the mortar samples, regardless of their type and amount.
17. The weight loss of mortar specimens was the greatest in the presence of diluted NaCl solution, followed by the diluted CaCl<sub>2</sub>, and then by the diluted MgCl<sub>2</sub> solution, whereas the mortar deterioration in the de-ionized water was negligible. In the presence of diluted NaCl solution, the mix designs, the mix designs 13 (10% MK), 15 (10% UFFA) and particularly 17 (50% GGBFS) showed less weight loss relative to the control, whereas other SCMs exacerbated the freeze-thaw damage with the mix designs 5 (25% class N FA) and particularly 7 (20% class F FA + 5% SF) being the worst. In the presence of diluted CaCl<sub>2</sub> and MgCl<sub>2</sub> solutions, the effect of mineral admixtures on the freeze-thaw resistance of mortar followed a trend similar to that seen in the presence of diluted NaCl solution, yet with the mix designs 5 (25% class N FA) and 7 (20% class F FA + 5% SF) being the worst respectively. In summary, the partial replacement of cement by 50% GGBFS is most beneficial for the freeze-thaw resistance of mortar, followed by the 10% UFFA or 10% MK replacement; whereas the use of ordinary fly ash and silica fume seems to undermine the freeze-thaw resistance of mortar in the presence of various diluted chloride solutions.

A two-dimensional FEM model, coupled with the stochastic technique, was developed to study the service life of reinforced concrete as a function of various influential factors. The FEM model stochastically sampled its inputs. Specifically, the surface chloride

concentrations and concrete cover depth follow the normal distribution, whereas the diffusion coefficients and the chloride threshold follow the gamma distribution and the triangular distribution respectively. The nonlinear partial differential equations (PDEs) to characterize the spatial and temporal evolution of ionic species were numerically solved. Some key findings are provided as follows.

1. All concrete mixes investigated had a 50%-probability service life of 114 years or longer (with a surface chloride concentration of  $6 \text{ kg/m}^3$  and concrete cover of 50 mm), which highlights the great potential of reinforced concrete as a construction material when the concrete is made using the best practices of construction and curing and is free of cracking. The modeling also suggest that when the concrete is made using the best practices, partially replacing cement with class F FA, SF, MK, or GGBFS tends to decrease the service life of reinforced concrete or at least show little benefits to its service life. This trend contradicts what have been generally reported in published literature, and is likely attributable to the fact that the PCC made without any mineral admixtures (mixes 1 and 2) featured unusually low chloride diffusion coefficients in the order of  $10^{-13} \text{ m}^2/\text{s}$ . Finally, for all these high-quality concrete mixes, the effects of air entrainment on the chloride diffusivity in concrete and the service life of reinforced concrete were not dramatic and do not show a clear trend.
2. Based on the modeling results, chloride inward-diffusion with the lowest surface chloride concentration is the most sluggish process. With the surface chloride concentration increasing, the service life decreases significantly.
3. The service life of reinforced concrete decreases as the cracking level of the concrete increases. When the crack density is over  $200 \text{ m}^{-2}$ , the service life shows no significant dependence on further increase on crack density, which is attributable to the forming of continuous net-like configuration in the concrete domain.
4. Assuming negligible diffusion of chloride ions in coarse aggregates and absence of ITZ, the chloride diffusion rate in concrete was found to be quite different from its corresponding homogeneous medium. The overall flux decreases as the volume fraction of aggregates increases.
5. For all the mineral concrete mixes investigated, as the concrete cover depth increases, the time to corrosion initiation of rebar in concrete is predicted to increase exponentially, highlighting the importance of cover depth in extending the service life of reinforced concrete exposed to external chlorides. According to the model calculations, it would take more than 100 years for the chloride ions in an aggressive environment (with surface chloride content of  $8 \text{ kg/m}^3$ ) to reach the threshold level at a depth of 60 mm. It should be cautioned that the chloride diffusivity data used for the model were measured using specimens cored from the center of a large concrete sample. In field construction, the top layer of the concrete cover is likely to have much higher chloride diffusivity than the interior of the concrete, in light of the possible defects derived from bleeding and water evaporation etc. at the top layer. Furthermore, the field construction is unlikely to achieve the same level of detailed quality assurance as implemented in the laboratory study and cracking cannot be fully eliminated for the service life

prediction considerations. In this context, a thicker-than-predicted concrete cover is needed for the target service life of concrete structures in the field environment and the importance of good construction and curing practices can not be overemphasized.

6. The technique developed in this work (e.g., multi-species transport model) was found to be very effective in predicting chloride migration and generating statistical conclusions about the service life of reinforced concrete, which allows the civil engineers to estimate the rate of chloride ingress and associated deterioration risk of reinforced concrete. Future improvements could be made to the model so that it takes into account the time-dependency of transport properties of concrete, the corrosion propagation, the chloride penetration mechanisms other than diffusion (e.g., wicking), the structure geometry, the environmental humidity and temperature fluctuations and the decay of structures under coupled physical, chemical, and mechanical deterioration processes etc.

#### **4.2. Recommendations for Implementation**

In light of the research findings from this project, we provide the following recommendations for implementation:

1. The accelerated chloride migration test (ACMT) used in this work should be considered by the Caltrans corrosion technology branch for implementation. When testing the concrete with unusually low chloride diffusivity ( $D_s$  values in the order of  $10^{-13}$  m<sup>2</sup>/s), the test could last up to 2 months using a 30-V applied voltage and a 25-mm thick disc specimen. Nonetheless, for most concrete mixes prepared in the field construction, the chloride diffusivity is expected to be much higher and the test typically would last no more than 2 weeks. An unusually high compressive strength can serve as a warning sign that the concrete may be highly impermeable. In general, the ACMT is anticipated to help Caltrans and other DOTs to make the transition from prescriptive specifications of concrete mixes to more performance-based specifications, which then would allow more innovation and flexibility in the materials selection of concrete and likely facilitate the paradigm shift from conventional PCC to EFCs.
2. If coupled the ACMT with the model developed in this work or the simplistic Life-365 software, this would provide a rapid, reliable method for determining the amount of concrete cover needed, based on the amount of chlorides present in the service environment and the required design life. With further improvements on the service life model, it could also be used for life cycle costing and for the timing of repair or rehabilitation strategies.
3. Caltrans should consider additional research phases for this work, such as the development and field evaluation of various types of high performance corrosion-resistant concretes. The research findings from such work should be shared with the DOT Design Engineers, as it may lead to improvements to the current Bridge Design Specifications in mitigating chloride-induced corrosion and deterioration.

4. The research findings imply that the chloride diffusivity in high-strength concretes largely determined by the use of coarse aggregates instead of the mineral admixtures. As such, the role of coarse aggregates in concrete durability should be further explored. The existing ASTM standard on the proportioning of aggregates may be further optimized for conventional and unconventional concrete mixes, in light of their important role in dramatically slowing down chloride ingress. Similarly, how the preparation of aggregates affects the durability of concrete merit further investigation, as it may benefit the internal curing of concrete and minimize its early-age cracking.
5. The processes and procedures used in the new construction should be closely supervised under a systematic quality assurance program, in order to achieve the great potential of reinforced concrete as a construction material and to manage corrosion risks pro-actively. The importance of good construction and curing practices can not be overemphasized, as they greatly reduce the risk of rebar corrosion in concrete.
6. Continued research is needed to explore the effect of partially replacing cement with mineral admixtures on the durability of concrete. The results from this study imply that for concrete with ordinary quality, the mineral admixtures may have great potential in increasing its electric resistivity, enhancing its chloride binding (e.g., the use of 10% UFFA or 50% GGBFS), reducing its chloride diffusivity (e.g., the use of 10% MK or 50% GGBFS), and improving its resistance to freeze-thaw in the presence of diluted deicers (e.g., the use of 50% GGBFS, 10% UFFA, or 10% MK). The use of fly ash and slag etc. may translate to cost savings and reduced energy use, greenhouse gas emissions and landfill waste, without sacrificing quality and long-term performance of the concrete.

## Appendices: Table of Contents

<b>APPENDIX A. CHLORIDE TRANSPORT IN CONCRETE AND SERVICE LIFE OF REINFORCED CONCRETE – A MODELING PERSPECTIVE .....</b>	<b>A-1</b>
<b>A1. THEORETICAL MODELING OF TRANSPORT BEHAVIOR IN CONCRETE .....</b>	<b>A-1</b>
<i>A1.1. Diffusion in Aqueous Solutions</i>	2
<i>A1.2. Ionic Diffusion in Water-saturated Concrete</i>	4
<i>A1.3. Ionic Diffusion in Water-unsaturated Concrete</i>	7
<b>A2. SERVICE LIFE MODELING OF REINFORCED CONCRETE IN CHLORIDE-LADEN ENVIRONMENTS.....</b>	<b>A-9</b>
<b>A3. CONCLUDING REMARKS .....</b>	<b>A-12</b>
<b>A4. REFERENCES.....</b>	<b>A-13</b>
<b>APPENDIX B. A PHENOMENOLOGICAL MODEL FOR THE CHLORIDE THRESHOLD OF PITTING CORROSION OF STEEL IN SIMULATED CONCRETE PORE SOLUTIONS .....</b>	<b>A-16</b>
<b>B1. INTRODUCTION .....</b>	<b>A-16</b>
<b>B2. EXPERIMENTAL.....</b>	<b>A-17</b>
<i>B2.1. Materials and Preparation</i>	18
<i>B2.2. Electrochemical Testing</i>	18
<b>B3. MODELING TECHNIQUE.....</b>	<b>A-19</b>
<b>B4. RESULTS AND DISCUSSION.....</b>	<b>A-20</b>
<i>B4.1. Electrochemical Characterization of Pitting Risk</i>	20
<i>B4.2. Performance of the ANN Model</i>	23
<i>B4.3. Relative Importance of Variables</i>	24
<i>B4.4. Effect of Chloride Concentration and Chloride Binding on Pitting Risk</i>	25
<i>B4.5. Effect of pH and DO on Pitting Risk</i>	26
<i>B4.6. Effect of [Cl<sup>-</sup>]/[OH<sup>-</sup>] Ratio on Pitting Risk</i>	29
<i>B4.7. Limitations and Practical Implications of Research Findings</i>	32
<b>B5. CONCLUSIONS .....</b>	<b>A-33</b>
<b>B6. REFERENCES .....</b>	<b>A-33</b>

<b>APPENDIX C. MODELING CATHODIC PREVENTION FOR UNCONVENTIONAL CONCRETE</b>	
<b>IN SALT-LADEN ENVIRONMENT .....</b>	<b>A-38</b>
<b>C1. INTRODUCTION .....</b>	<b>A-38</b>
<b>C2. METHODOLOGY .....</b>	<b>A-40</b>
<i>C2.1. Experimental</i> 40	
<i>C2.2. Model Description</i> 42	
<b>C3. RESULTS .....</b>	<b>A-44</b>
<b>C4. DISCUSSION .....</b>	<b>A-49</b>
<i>C4.1. Effect of Voltage Magnitude and Direction on Cathodic Prevention</i> 49	
<i>C4.2. Effect of Surface Chloride Concentration on Cathodic Prevention</i> 50	
<i>C4.3. Effect of Concrete Constituents on Cathodic Prevention</i> 50	
<i>C4.4. Effect of Voltage Interruption on Cathodic Prevention</i> 53	
<b>C5. CONCLUSIONS .....</b>	<b>A-54</b>
<b>C6. REFERENCES .....</b>	<b>A-55</b>
<b>APPENDIX D. STANDARD OPERATING PROCEDURES .....</b>	<b>A-58</b>
<b><i>D1. ELECTRICALLY ACCELERATED TEST OF CHLORIDE DIFFUSION COEFFICIENT IN</i></b>	
<b><i>CONCRETE SPECIMENS .....</i></b>	<b>A-58</b>
<b>D2. TESTING PROCEDURES FOR CONCRETE POROSITY .....</b>	<b>A-67</b>
<b>APPENDIX E. DATA OF MINERAL ADMIXTURES AND CEMENT.....</b>	<b>A-69</b>
<b>E1. ASTM C 618 CLASS F FLY ASH.....</b>	<b>A-69</b>
<b>E2. ASTM C 618 CLASS N FLY ASH - NATURAL POZZOLAN .....</b>	<b>A-70</b>
<b>E3. ASTM C 1240 SILICA FUME.....</b>	<b>A-73</b>
<b>E4. ASTM C 618 (CLASS N) CALCINED NATURAL POZZOLAN – METAKAOLIN .....</b>	<b>A-75</b>
<b>E5. ULTRA-FINE FLY ASH (UFFA) .....</b>	<b>A-78</b>
<b>E6. ASTM C 989 GGBFS - GROUND GRANULATED BLAST-FURNACE SLAG .....</b>	<b>A-84</b>
<b>E7. TYPE I/II LOW-ALKALI PORTLAND CEMENT .....</b>	<b>A-85</b>

## APPENDIX A. CHLORIDE TRANSPORT IN CONCRETE AND SERVICE LIFE OF REINFORCED CONCRETE – A MODELING PERSPECTIVE

This appendix chapter provides the results of a comprehensive literature review on topics relevant to this study. Specifically, it synthesizes the information on existing research related to the computational models to simulate the transport of species in aqueous solution, water-unsaturated and water-saturated cementitious materials, and the service life modeling of reinforced concrete in chloride-laden environments.

### A1. Theoretical Modeling of Transport Behavior in Concrete

The testing and modeling of chloride ingress into concrete has been extensively studied in the last decades and there are recent conferences dedicated to this topic [1,2]. Chloride ingress into concrete can occur by a number of mechanisms, including diffusion due to a concentration gradient, migration in an electric field, absorption, electro-osmosis, and wick action [3]. Diffusion is considered the basic mechanism on the assumption that the concrete is generally moist [4]. Chloride penetration from the environment produces a profile in the concrete characterized by high chloride content near the external surface and decreasing contents at greater depth. The natural diffusion of chloride ions from one dimension is governed by Fick's second law:

$$\frac{\partial c(x,t)}{\partial t} = \frac{\partial}{\partial x} \left( D \frac{\partial c(x,t)}{\partial x} \right) \quad (1)$$

where  $c(x,t)$  is the  $\text{Cl}^-$  concentration at depth  $x$  beneath the exposed surface after exposure time  $t$ , and  $D$  is the diffusion coefficient. Given reasonable assumptions, an analytical solution to Equation (1) is proposed to describe the kinetics of a non-stationary diffusion process [5]:

$$\frac{c(x,t) - c_0}{c_s - c_0} = 1 - \text{erf} \left( \frac{x}{2\sqrt{Dt}} \right) \quad (2)$$

where  $c_0$ ,  $c_s$  is the  $\text{Cl}^-$  concentration in initial concrete and at the external surface at time  $t$ , respectively, and erf is a Gaussian error function defined by:

$$\text{erf}(z) = \frac{2}{\sqrt{\pi}} \int_0^z e^{-t^2} dt \quad (3)$$

Active corrosion of steel in concrete does not commence until the chloride content at the reinforcement surface exceeds a critical value, known as the chloride threshold. In normal circumstances, the chloride threshold content may vary from 0.2% to 0.5% by weight of cement [6].

In addition to empirical models, mechanistic models are also used for quantitative analysis of the chloride ingress process. Recent research [7] employed the finite element method to predict the chloride concentration profiles of a coastal concrete structure, which agreed favorably with the measured data.

When cathodic protection is provided to the reinforced concrete structure, the theoretical modeling of chloride transport in concrete can be further complicated. More details are provided in reference [8] and Appendix C for the modeling under such scenarios.

### ***A1.1. Diffusion in Aqueous Solutions***

#### *A1.1.1. In the Absence of an External Electric Field*

Ions in electrolytic solutions are subjected to various types of interactions that complicate the mathematical treatment of this problem. For example, the diffusion coefficient for each species present does not have the same value, and thus the various ions attempt to reach different speeds in electrolytic solutions. An induced internal electrical field is then created by the species of opposite sign so that the faster ions will be slowed down and the slower ones will be accelerated. Eventually, all the ions will move at the same average speed that predominantly depends on the diffusion coefficient of each species.

In a non-ideal ionic solution, the extended Nernst-Planck equation describing the flux of each species is given by [9]:

$$J_i = -D_i \nabla C_i - \frac{Z_i F D_i}{RT} C_i \nabla \phi + C_i u - C_i \nabla \ln \gamma_i \quad (4)$$

where  $i$  denotes for the type of species (e.g.,  $\text{Na}^+$ ,  $\text{K}^+$ ,  $\text{Cl}^-$  and  $\text{OH}^-$ ) and  $J$ ,  $D$ ,  $C$ ,  $\gamma$  and  $Z$  are the flux, diffusion coefficient, concentration, activity, and valence number of that specific species respectively;  $F$  is the Faraday constant,  $R$  is the ideal gas constant,  $T$  is temperature,  $\phi$  is the induced electrical potential.

For each ionic species, the law of mass conservation leads to [10]:

$$\frac{\partial C_i}{\partial t} = -\nabla \cdot J_i \quad (5)$$

To complete the system of equations, a supplemental relation is needed to account for the electrical potential that is inherently induced by the movement of all ions. According to the literature, three methods can determine the magnitude of  $\phi$  in Equation (4).

✧ Electroneutrality: [11]

$$\sum Z_i C = 0 \quad (6)$$

✧ Null Current: [12]

$$\sum Z_i J_i = 0 \quad (7)$$

✧ Poisson Equation: [13]

$$-\varepsilon \nabla \cdot \nabla \phi = F \sum Z_i C_i \quad (8)$$

where  $\varepsilon$  is the dielectric constant. The summation in Equations (6-8) is taken over all the species present in the ionic solutions. The Poisson equation, which relates the electrical potential to the electrical charge in space, is developed based on the assumption that the electromagnetic signal travels much faster than ions in solutions.

In order to calculate the activity of each species in electrolytic solutions, the model developed by Pitzer and his co-workers can be used. According to this model, the activity coefficient of cation  $i$  can be obtained from the following equation [14]:

$$\begin{aligned} \ln \gamma_i = & z_M^2 G + \sum_{a=1}^{Na} m_a (2B_{Ma} + ZC_{Ma}) + \sum_{c=1}^{Nc} m_c (2\phi_{Mc} + \sum_{a=1}^{Na} m_a \phi_{Mca}) \\ & + \sum_{a=1}^{Na-1} \sum_{a'=a+1}^{Na} m_a m_{a'} \phi_{aa'} M + |Z_M| \left[ \sum_{c=1}^{Nc} \sum_{a=1}^{Na} m_c m_a C_{ca} + \sum_{n=1}^{Nn} m_n (2\lambda_{nM}) \right] \end{aligned} \quad (9)$$

where the subscript  $a$  and  $c$  are related to the other cations in ionic solutions and  $G$  is the extend Debye-Hückel model. All the other parameters are evaluated through experiments to represent the short-range interactions between the various species. Pitzer developed two similar equations to calculate the activity coefficients of anions and neutral species in ionic solutions. Given the complexity of these equations, they can hardly be implemented in a computer program for simulation purpose.

Samson et al. recently proposed a new equation to account for chemical activity effect in ionic solutions [15]:

$$\ln \gamma_i = -\frac{Az_i^2 \sqrt{I}}{1 + a_i B \sqrt{I}} + \frac{(0.2 - 4.17 \cdot 10^{-5} I) Az_i^2 I}{\sqrt{1000}} \quad (10)$$

where  $I$  is the ionic strength of electrolytic solutions,  $A$  and  $B$  are temperature-dependent parameters, and  $a_i$  is a parameter that varies with the ionic species considered. Given its relative simplicity, Equation (10) can be easily implemented in a numerical code aimed at modeling ionic transport phenomena in electrolytic solutions.

It has been reported that the effect of the nonideality of electrolytic solutions on the ionic fluxes is negligible. If this conclusion is valid, the chemical activity of each species can be well approximated by its corresponding concentration, and the last term in Equation (4) can be omitted. With the null current flux assumption in Equation (7) used, the combination of Equations (4-6) leads to [16]:

$$\nabla \phi = \frac{RT}{F} \frac{\sum_{i=1}^N Z_i D_i \nabla C_i}{\sum_{i=1}^N Z_i^2 D_i C_i} \quad (11)$$

#### *A1.1.2. In the Presence of an External Electric Field*

With the nonideality of electrolytic solutions ignored, the combination of Equations (4-5) gives [17]:

$$\frac{\partial C_i}{\partial t} + \nabla \cdot (-D_i \nabla C_i - \frac{Z_i F D_i}{RT} C_i \nabla \phi + C_i u_i) = R_i \quad (12)$$

where  $R_i$  denotes the reaction rate term.

As mentioned above, Equation (12) introduces one more variable for the electric potential  $\phi$  that can be solved by the electroneutrality condition. From Equation (12), one can get the following expression [18]:

$$F \sum_{i=1}^n Z_i \frac{\partial C_i}{\partial t} + \nabla \cdot (F \sum_{i=1}^n Z_i J_i) = F \sum_{i=1}^n Z_i R_i \quad (13)$$

where  $J_i$  is the flux vector defined in Equation (4).

The first term in Equation (13) is zero by taking the time derivative of the electroneutrality condition. The term under the divergence operator can be identified as the total current density vector defined by [19]:

$$i = F \sum_{i=1}^n Z_i (-D_i \nabla C_i - \frac{Z_i F D_i}{RT} C_i \nabla \phi) \quad (14)$$

It should be noted that no convective term is included in the expression of the current density which is also a result of the electroneutrality condition.

For simplicity, Equation (13) can be written in the form of conservation of electric charge [20]:

$$\nabla \cdot i = F \sum_{i=1}^n Z_i R_i \quad (15)$$

The ionic conductivity, which is defined in the absence of concentration gradients, is implicitly given by [21]:

$$k = F^2 \sum_{i=1}^n \frac{Z_i^2 C_i}{RT} \quad (16)$$

Based on the assumption that the electromagnetic signal travels much more rapidly than ions in the solution, it is possible to use the following equation to calculate the electric potential  $\phi$  [22-23].

$$\nabla \cdot i = 0 \quad (17)$$

Inserting the current density expression in Equation (17), one can get:

$$\nabla \cdot i = \nabla \cdot (F \sum_{i=1}^n Z_i (-D_i \nabla C_i - \frac{Z_i F D_i}{RT} C_i \nabla \phi)) = 0 \quad (18)$$

The arrangement of Equation (18) results in [24]:

$$\nabla \cdot (-F^2 \sum_{i=1}^n Z_i^2 D_i \nabla C_i) = \nabla \cdot F \sum_{i=1}^n Z_i D_i \nabla C_i \quad (19)$$

### ***A1.2. Ionic Diffusion in Water-saturated Concrete***

Hydrated cement paste is generally believed to be a kind of composite material with a large porosity, in which the pores are filled with water and ions can transport within the pore solution. Comparatively, the diffusion coefficients of ions in the solid phases are so small that they can be ignored. However, the solid phases can capture ions either physically or chemically. When chloride ions penetrate into concrete, some of them will

be captured by the hydrated products. Therefore, chloride in cementitious materials can have free and bound components. Free chloride ions can move from one place to another and destroy the passive film on the surface of the steel bar to initiate corrosion. The bound chlorides are generally harmless to the reinforcement and exist in the form of chloro-aluminates, making them unviable for free transport. Since only free chloride is involved in the corrosion of the reinforcement, chloride binding will effectively reduce the amount of free chlorides available to initiate the deterioration process, which can retard the transport process of free chloride ions.

The mechanism of chloride binding is not quite clear, but chemical and physical bindings are believed to occur. Accordingly, the free and bound chlorides under equilibrium conditions are expressed by empirical equations. The total amount of chloride concentration in cementitious materials can be divided into free and bound components as below [25]:

$$C_t = C_b + C_f \quad (20)$$

where  $C_t$  represents the total chloride concentration,  $C_b$  denotes the bound chloride concentration, and  $C_f$  is the free chloride concentration. In real cementitious materials, the relationship between the free, bound and total amount of chlorides can be either linear or non-linear. Four kinds of scenarios are referenced as follows.

✓ Linear isotherm [26]

Arya et al. proposed a linear relationship for bound and free chloride:

$$C_b = \alpha \cdot C_f + \beta \quad (21)$$

where  $\alpha$  and  $\beta$  are constant. Although this equation fit their experimental data fairly well, it could not explain the physical meaning of  $C_b = \beta$  at  $C_f = 0$ . For instance, if a chloride-free concrete is exposed to a chloride-free solution, bound or total chloride should not be  $\beta$ , but zero. Therefore, Equation (21) is not applicable for low free chloride concentrations.

✓ Langmuir isotherm [27]

In fact, the linear relationship holds well only in a limited range of free chloride concentration. In most cases, the relationship between bound and free chlorides is nonlinear. Owing to this non-linearity, Pereira et al. [25] suggested a Langmuir isotherm for describing chloride binding:

$$C_b = \frac{\alpha \cdot C_f}{1 + \beta \cdot C_f} \quad (22)$$

where  $\alpha$  and  $\beta$  are constant.

✓ Freundlich isotherm [28]

Sometimes, the Freundlich isotherm can be sued:

$$C_b = a \cdot C_f^\beta \quad (23)$$

where the parameters  $\alpha$  and  $\beta$  in the Freundlich equation are purely empirical coefficients from a non-linear regression.

✓ Modified BET isotherm [29]

Recently, a modified BET equation was proposed for describing chloride binding:

$$\frac{C_b}{C_{bm}} = \frac{\alpha \frac{C_f}{C^s} [1 - (1 - \beta)(1 - \beta \frac{C_f}{C^s})^2]}{\beta(1 - \beta \frac{C_f}{C^s}) [1 - \beta \frac{C_f}{C^s} + \alpha \frac{C_f}{C^s} (1 - \beta \frac{C_f}{C^s} + \frac{C_f}{C^s})]} \quad (24)$$

where  $C^s$  is the free chloride concentration in a saturated solution,  $\alpha$  relates to the difference between the adsorption energy at the first layer and those at the second or higher layers, and  $\beta$  denotes the difference between the adsorption energy at the second layer and those at the third or higher layers. It is found that both Freundlich equation and the modified BET equation correspond very well when the free chloride concentrations are lower than 1mol/l.

The porosity of a material, a commonly used parameter for the description of diffusion in porous materials, is defined as [30]:

$$p = \frac{\text{void volume}}{\text{total volume}} \quad (25)$$

This parameter is non-dimensional and does not provide information on the geometrical features of the pores or their size distribution.

A proper way to describe the movement of ions in the pore solution of cementitious materials is based on the homogenization technique. To obtain the concentration profiles, the continuity equation has to be computed for each species, but some considerations about the binding of different species are needed. The following two scenarios are most commonly used.

1) Only Chloride can be bound

It can be assumed that only chlorides can be bound to the solid phase in concrete. However, for each chloride ion bound, one hydroxide ion is released to keep the electroneutrality of the pore solution. For example, consider the pore solution which only contains chloride, sodium, potassium and hydroxide. The mass balance equations for the considered species take the following format [31]:

$$p \frac{\partial C_f}{\partial t} + (1 - p) \frac{\partial C_b}{\partial t} = - \frac{\partial J_f}{\partial x} \quad (26)$$

$$p \frac{\partial C_{Na^+}}{\partial t} = - \frac{\partial J_{Na^+}}{\partial x} \quad (27)$$

$$p \frac{\partial C_{K^+}}{\partial t} = - \frac{\partial J_{K^+}}{\partial x} \quad (28)$$

The concentration of hydroxide can be obtained from the electroneutrality condition that must be followed in any volume of the diffusion medium:

$$C_{OH^-} = C_{Na^+} + C_{K^+} - C_f \quad (29)$$

## 2) All the species present can be bound

In some cases, specific chemical interactions can happen between dissolved substances and the porous matrix. For example, chloride, sulfate and carbonate ions can all react with hydrated cementitious minerals. During capillary absorption, these ions can be removed from pore solutions by chemical or physical combination. It is possible to take the binding of all the cations and anions into consideration. A proper way to handle such a condition, based on the homogenization technique, can be achieved via the following equation [32]:

$$(1-p)\frac{\partial C_{ib}}{\partial t} + p\frac{\partial C_{if}}{\partial t} = \nabla \cdot (pJ_i) \quad (30)$$

where  $C_{ib}$  stands for the concentration of species  $i$  in the solid phase, and  $C_{if}$  represents its corresponding part in the pore solutions.

In both cases, the size of pores is considered as independent of time, which is generally reached under long steady-state flow. Actually, the size of pores varies with the progress of physical or chemical interactions of all sorts. However for modeling purpose, the size and distribution of pores can be assumed unchanged with time.

Equation (30) should be used carefully to ensure that the pore solutions and the solid cement phases are in the state of electroneutrality, respectively. A procedure similar to Equation (26) can be used to achieve this purpose. In addition, the Poisson equation used to calculate the electric potential can be written as [33]:

$$-\frac{\partial}{\partial x} \left( p\varepsilon \frac{\partial \phi}{\partial x} \right) = pF \sum_{i=1}^N Z_i C_i \quad (31)$$

### ***A1.3. Ionic Diffusion in Water-unsaturated Concrete***

In many cases, concrete structures exposed to ionic solutions are frequently subjected to wetting and drying cycles. While the transport of chloride in water-saturated concrete has been relatively well understood, recent reports have underlined the complexity of ionic transport in water-unsaturated concrete. The transport of water can accelerate concrete degradation, and its kinetics is a very important factor for durability evaluation.

The kinetics of water-unsaturated concrete deterioration is based on the penetration of water and aggressive ions carried by water into the pores of concrete. In unsaturated materials, the stress acting on the liquid arises not from external pressure differences but from the effects of capillarity. The macroscopic velocity of the fluid appearing in Equation (4) as  $u$  can be described by [34]:

$$u = -D_w \frac{\partial \theta}{\partial x} \quad (32)$$

where  $D_w$  is called the capillary diffusivity, and  $\theta$  is the volumetric water content in the pores.

To accomplish the model, the mass conservation on the liquid phase must be taken into account [35]:

$$\frac{\partial \theta}{\partial t} = \frac{\partial}{\partial x} \left( D_w \frac{\partial \theta}{\partial x} \right) \quad (33)$$

The capillary diffusivity in Equation (33) depends heavily on  $\theta$  in porous materials so that the water content profile is steep-fronted. It is often useful to represent the wetted region by a rectangular profile, which is the so-called sharp front approximation. Equation (33) is known as Richard equation. While Richard equation is commonly accepted among scientists, its use over the past decades has led to some confusion on moisture transport mechanism in unsaturated porous materials.

The application of homogenization technique to the law of mass conservation results in the following relation [36]:

$$\frac{\partial((1-p)C_{is})}{\partial t} + \frac{\partial(p\theta C_{if})}{\partial t} = \frac{\partial}{\partial x} \left( p\theta D_i \frac{\partial C_{if}}{\partial x} + p\theta \frac{D_i Z_i F}{RT} C_{if} \frac{\partial \theta}{\partial x} + p\theta D_i C_{if} \frac{\partial \ln \gamma_i}{\partial x} - C_{if} u \right) \quad (34)$$

where  $p$  is the porosity of the material,  $C_{is}$  is the concentration of species  $i$  in the solid phase,  $C_{if}$  is the corresponding part of  $C_{is}$  in the pore solutions, and  $D_i$  is the diffusion coefficient of species  $i$  at the macroscopic level. For the water-unsaturated cementitious materials, the Poisson equation, which relates the electrical potential to the concentration of each ionic species, can be expressed with Equation (31).

In the above, the fluid velocity is not explicitly considered. The convective transport of a fluid in concrete can occur under a pressure gradient. In the absence of gravity and for the isotropic case, the filtration velocity of a fluid, subjected to the pressure gradient is governed by Darcy's law [37]:

$$u = -\frac{k}{p} \nabla h \quad (35)$$

where  $u$  is the fluid velocity,  $k$  is the intrinsic permeability,  $p$  is the porosity, and  $h$  is the pressure head.

Darcy's law, linearly relating a flow velocity to a pressure gradient, is well suitable to model laminar liquid flow through porous materials, but is not capable of accurately modeling fluid flows where non-zero fluid velocity is maintained at the solid-fluid interface. Because of such slippage at the solid-liquid interface, the rate of mass flow through the material exceeds that predicted from Darcy's law.

It should be noted that Darcy's law is a phenomenological equation derived from empirical observations. It describes the bulk flow of a fluid through a porous medium without any reference to the microstructure characteristics of the material. From this perspective, Darcy's law is analogous to Fourier's law for heat conduction and Ohm's law for electricity conduction.

In the presence of fluid movement, the conservation equation can be written as:

$$\frac{\partial C_i}{\partial t} + u \cdot \nabla C_i = -\nabla \cdot J_i \quad (36)$$

Inserting the expression for the flux of each species in Equation (4), as well as the fluid velocity in Equation (35), one can obtain the governing equations to describe the transport of each species in the presence of pressure gradient.

Specifically, if only chloride is considered in the calculation, the governing equation involving both convection and diffusion simply becomes [38]:

$$\frac{\partial C_{cl}}{\partial t} = D_{cl} \frac{\partial^2 C_{cl}}{\partial x^2} - u \frac{\partial C_{cl}}{\partial x} \quad (37)$$

The analytic solution to this differential equation is:

$$\frac{C_{cl}}{C_{cl}^s} = 0.5 \left[ \operatorname{erfc} \left( \frac{x-ut}{2\sqrt{D_{cl}t}} \right) + \exp \left( \frac{ux}{D_{cl}} \right) \operatorname{erfc} \left( \frac{x+ut}{2\sqrt{D_{cl}t}} \right) \right] \quad (38)$$

## A2. Service Life Modeling of Reinforced Concrete in Chloride-laden Environments

Through the use of concrete deterioration models, cost-effective decisions can be made concerning the appropriate time to repair or replace existing structures, and the most effective corrosion control strategies. There are software packages available to aid in concrete modeling and service life forecasting, such as 4SIGHT and CONLIFE available from the National Institute of Standards and Technology [39], Life-365<sup>TM</sup> ([www.life-365.org/](http://www.life-365.org/)), as well as conventional Finite Difference Method (FDM) applications. Khatri and Sirivivatnanon [40] proposed a model for predicting the service life of reinforced concrete structures, where the acceptable level of deterioration is related to the presence of chloride ions on the rebar surface. As such, the service life is defined as the time required for transport processes to raise the chloride content at the depth of the rebar to the threshold level for pitting corrosion. It should be mentioned that the service life is not a fixed value as calculated by a deterministic model, but instead it is a range of values determined by material characteristics, cover depth, and severity of service environments.

The diffusion of chloride ions in water-saturated cementitious materials is a complex process involving various physical and chemical interactions. The chloride ions can be bound either physically or chemically by cement paste, thereby lowering the fraction of free chlorides that can diffuse freely in the pore solutions. In addition, the internal electric field formed by the cations and anions will speed up the ions that have low diffusion coefficients and slow down the ions that have high diffusion coefficients to maintain the electro-neutrality condition. If we ignore such complex internal processes and treat the diffusion problem phenomenologically, the temporal and spatial evolution of chloride-ion concentration can be calculated based on Fick's second law in Equation (39) [4, 17], which has been used extensively by many researchers to calculate the chloride concentrations for various concrete cover depths at different exposure time intervals:

$$\frac{\partial C}{\partial t} = D_c \frac{\partial^2 C}{\partial x^2} \quad (39)$$

where  $C$  is the concentration ( $\text{mol m}^{-3}$ );  $t$  is the time (s);  $D$  is the chloride diffusion coefficient ( $\text{m}^2\text{s}^{-1}$ );  $\chi$  is the position (m). In most work, the service life or the length of the corrosion initiation stage is approximated with the following simplified assumptions:

- The concrete is initially chloride-free, and the concrete acts as a physical barrier to protect the rebar. The rebar corrosion is triggered only when the concrete in contact with the steel becomes contaminated with chloride ions exceeding a threshold concentration value.
- Chloride ions progress inward from the external surface of the concrete, which is covered by aqueous solutions of chlorides. Therefore, the concrete immediately below the surface acquires a surface chloride concentration that remains unchanged in the simulation.
- Chloride ions progress inward by simple diffusion, driven by the gradient of the concentration of chloride ions in the concrete. The effective diffusion coefficient is constant with time and space, and is a property of the concrete between the concrete surface and the steel rebar.

Based on these assumptions, an analytical solution exists to predict the spatial and temporal evolution of chloride concentration profiles in concrete, which is given by [4, 40, 41]:

$$C_t = C_s [1 - \text{erf}(\frac{x}{2\sqrt{D_c t}})] \quad (40)$$

where  $x$  is the concrete cover depth;  $C_t$  is the chloride concentration at cover depth;  $C_s$  is the surface chloride concentration;  $t$  is time;  $D_c$  is the effective diffusion coefficient in concrete;  $\text{erf}$  is the Gaussian error function as below:

$$\text{erf}(z) = \frac{2}{\sqrt{\pi}} \int_0^z e^{-t^2} dt \quad (41)$$

Equation (40) can be used to calculate the service life of a reinforced concrete structure, provided that  $C_t$ ,  $C_s$ ,  $D_c$  and  $x$  are known.

Boddy et al. [42] developed a multi-mechanistic transport model for chloride penetration which considers diffusion, permeability, chloride binding and wicking as well as the time-dependent nature of concrete properties (e.g., diffusivity). Sagüés and Kranc [43, 44] developed service life models for marine substructures that incorporate statistical stochastics and take preexisting cracks, strong localized corrosion spots, and/or structure geometry into account.

Concrete is a multiphase porous composite consisting of cement paste and aggregates, in both of which phases pores exist. Chloride ions can only diffuse in the pore solutions. Effective diffusion coefficients of chloride, characterizing the resistance of concrete to diffusive ingress of chlorides, are therefore considered to be a function of the characteristics of the cement paste and the aggregates. The rate at which chloride ions penetrate into water-saturated concrete depends on the diffusion coefficients in cement paste and aggregates as well as the aggregates fraction. Additionally, the rate of ingress is also influenced by the cement paste/aggregate interfacial (ITZ) zones and internal cracks.

Prediction of effective chloride diffusion coefficients in concrete based on its mixture proportions is needed for service life evaluation. If the roles of ITZ and internal cracks on chloride ingress can be ignored, the effective diffusion coefficient of chloride in water-saturated concrete can be calculated by the following equation:

$$D_c = \frac{[(D_a - D_p)V_a + (D_p + D_a)]D_p}{(D_p + D_a) + (D_p - D_a)V_a} \quad (42)$$

where  $D_p$  and  $D_a$  are the chloride ion diffusion coefficients in the cement paste and aggregates, respectively, and  $V_a$  is the aggregate volume fraction.

If the aggregates have a lower diffusion coefficient than the cement paste, the concrete will have a lower diffusion coefficient than the cement paste. Therefore, chloride ion ingress will decrease with the increase in the aggregate volume, and controls are necessary on the quantity of cement paste and aggregates to achieve a specified service life. The diffusion coefficient of chloride ions in aqueous solutions [45], cement paste [46] and marble [47] has the order of  $10^{-9}$  m<sup>2</sup>/s,  $10^{-12}$  m<sup>2</sup>/s and  $10^{-15}$  m<sup>2</sup>/s, respectively. Accordingly, it can be assumed that diffusion of chloride ions in aggregates of concrete is negligible, leading to:

$$D_c = \frac{(1 - V_a)}{(1 + V_a)} D_p \quad (43)$$

For instance, at  $V_a = 0.7$ , the effective diffusion coefficient predicted from Equation (43) is:

$$D_c = 0.1765 D_p \quad (44)$$

The chloride threshold value is required in the assessment of service life when chloride-induced corrosion is the failure mechanism. Choosing an accurate value for  $C_t$  is a great challenge as this parameter varies over a wide range of reported values, as detailed in Appendix B.

Time-to-corrosion of reinforcement in concrete ( $T_i$ ) and  $C_t$  are important service life determinants for reinforced concrete structures in chloride-laden environments. Numerous literatures have discussed, through experimental or modeling approaches, these two determinants in conventional PCC and their relationships with the type of cement and reinforcement, mix design, exposure conditions, and other factors. It should be cautioned, however, that these relationships feature a probabilistic nature [48, 49]. Williamson et al. [50] validated a probabilistic model that predicts the time to first repair (2% deterioration) of bridge decks under various chloride exposure conditions, using data gathered from 10 bare steel bridge decks constructed in Virginia between 1965 and 1968. A recent study confirmed and analyzed the probabilistic distribution of  $T_i$  and  $C_t$  for both regular concrete and self-compacting concrete (SCC) slabs, and the air voids at the rebar-concrete interface were also found to contribute the uncertainty inherent in the service life of reinforced concrete in chloride-laden environments [49].

Note that the models discussed above assume rapid propagation of rebar corrosion once it is initiated in the concrete and thus focus only on the initiation period for chloride-induced corrosion. Pettersson [179] argued that the propagation period could be as long as 50 years or more for high performance concrete featuring high electric resistivity and very limited oxygen availability.

The service life of reinforced concrete in the field environment can be very difficult to predict or model, as it depends on not only the chloride-related durability but also on mechanical properties of the concrete. For instance, the cracking of concrete (due to environmental or mechanical stresses) can greatly affect the ingress of chlorides and other deleterious species from the surrounding environment and the durability and serviceability of the concrete. Francois et al. [52] conducted a corrosion study by exposing loaded reinforced concrete beams to salt fog for twelve years. They found that the tensile micro-cracking in concrete as a result of service loading was responsible for accelerating chloride penetration whereas the existence and width of micro-cracks (with width less than 0.5 mm) did not influence the development of the rebar corrosion.

Lin et al. [53] presented a deterministic service life FEM model of reinforced concrete structures, which incorporates chloride binding, diffusion and convection, environment humidity and temperature fluctuations, and the decay of structural performance. As such, the model considers the interactions between the transport of moisture and chloride and the decay of structures under coupled physical, chemical, and mechanical deterioration processes. Chen [54] presented a probabilistic service life FEM model that also considers the coupled deterioration processes, including heat transfer and associated expansion and contraction, moisture transport and associated wetting expansion and drying shrinkage, carbon dioxide transport and associated carbonation, chloride penetration and associated rebar corrosion and rust expansion, and subsequent crack initiation and propagation. Chen [54] also suggested future improvements for the model could consider additional deterioration processes such as freeze-thaw cycling, sulfate attack, alkali-aggregate reactions, leaching of concrete constituents, etc.

### **A3. Concluding remarks**

Chloride ingress into concrete is a complex process, which in the highway environment is further complicated by the freeze-thaw cycles and wet-dry cycles experienced by roadways and bridges. While there are numerous existing experimental or modeling studies related to the transport of chlorides in concrete, the measurement of chloride (and inhibitor) ingress into concrete is technically challenging. Furthermore, it is also difficult to assess the durability of reinforced concrete from its chloride diffusivity, partially owing to the heterogeneous nature of the concrete matrix, the difficulty in fabricating concrete in a reproducible manner, and the inherently probabilistic nature of species transport in concrete and of chloride-induced corrosion of rebar or dowel bars in concrete.

In this context, modeling is a useful tool to provide quantitative understanding of key processes and their interactions that define the service life of reinforced concrete in chloride-laden environments.

#### A4. References

- [1] C. Andrade and J. Kropp. Testing and Modelling the Chloride Ingress into Concrete. 2000. 519p. RILEM Proceedings Pro019. <http://www.rilem.net/proContents.php?pro=pro019> (last accessed on June 1, 2010).
- [2] C. Andrade and J. Kropp. Testing and Modelling the Chloride Ingress into Concrete. 2004. 462p. RILEM Proceedings Pro038. <http://www.rilem.net/proContents.php?pro=pro038> (last accessed on June 1, 2010).
- [3] Buenfeld N.R., G.K. Glass, A.M. Hassanein, and J.Z. Zhang, *Journal of Materials in Civil Engineering* 11(1998):220.
- [4] Erdoğan S., I.L. Kondratova, and T.W. Bremner, 'Determination of Chloride Diffusion Coefficient of Concrete Using Open-Circuit Potential Measurements', *Cem. Concr. Res.* **34**(4), 2004, 603-609.
- [5] Hartt W.H., G.P. Rodney, L. Virginie, and D.K. Lysogorski (2004). A Critical Literature Review of High-Performance Corrosion Reinforcements in Concrete Bridge Applications. FHWA-HRT-04-093.
- [6] Mehta P.K. (1977). Effect of cement composition on corrosion of reinforcing steel in concrete. In *Chloride Corrosion of Steel in Concrete*, Philadelphia, ASTM STP 629, pp.12-19.
- [7] Shin C.B., and E.K. Kim, *Cement and Concrete Research* 32(2002): 757.
- [8] Liu, Y., and Shi, X. Cathodic Protection Technologies for Reinforced Concrete: Introduction and Recent Developments. *Reviews in Chemical Engineering* 2009, 25(5-6), 339-388.
- [9] Marcotte T. et al., *Cement and Concrete Research* 29(1999): 1561-1568.
- [10] Stanish, K., M. Thomas, *Cement and Concrete Research* 33(2003), 55-62
- [11] Buenfeld, N., *Journal of Materials in Civil Engineering* 11(1998): 220-228
- [12] Samson, E., J. Marchand, J. Beaudoin, *Cement and Concrete Research* 30(2000): 1895-1902
- [13] Stanish, K., R. Hooton, M. Thomas, *Cement and Concrete Research* 34(2004): 43-49
- [14] Pitzer, K., *Journal of Physical Chemistry* 77(1973): 268-277
- [15] Samson, E. et al., *Computational Material Science* 15(1999): 285-294
- [16] Samson, E., J. Marchand, *Journal of Colloid and Interface Science* 215(1999):1-8
- [17] Zhang, J., Mcloughlin, I., and Buenfeld, N., 'Modelling of Chloride Diffusion into Surface-Treated Concrete', *Cem. Concr. Compos.* **20**(4), 1998, 253-261.
- [18] Yu, S., C. Page, *British Corrosion Journal* 31(1996):73-76
- [19] Shin, C., E. Kim, *Cement and Concrete Research* 32(2002):757-762
- [20] Ait-Mokhtar, A., *Cement and Concrete Composites* 26(2004):339-345
- [21] Hassanein, A., G. Glass, N. Buenfeld, *Corrosion Science*, 55(1999): 840-850
- [22] Keister, J., *Journal of Membrane Science*, 29(1986):155-167

- [23] Wang, Y., L. Li, C. Page, *Computational Material Science* 20(2001):196-212
- [24] Masi, M., *Cement and Concrete Research* 27(1997):1591-1601
- [25] Truc, O., J. Ollivier, L. Nilsson, *Cement and Concrete Research* 30(2000):1581-1592
- [26] Arya, C., J. Newman, *Materials and Structures* 23(1990):319-330
- [27] Pereira, C., L. Hegedus, *Proceedings of the 8<sup>th</sup> International Symposium on Chemical Reaction Engineering*, 87, 427-438
- [28] Tangtermsirikul, S., T. Maruya, Y. Matsuoka, *Taisei Kensetsu Gijutsu kenkyu*, 24(1991):377-382
- [29] Tang, L., Chloride Transport in Concrete-Measurement and Prediction, Thesis, Chalmers University of technology.
- [30] Siegwart, M., J. Lyness, B. Mcfarland, *Cement and Concrete Research* 33(2003):1211-1221
- [31] Boddy, A., E. Bentz, M. Thomas, R. Hooton, *Cement and Concrete Research* 29(1999): 827-837
- [32] Hassanein A, G. Glass, N. Buenfeld, *Corrosion* 54(1997):323-332
- [33] Johannesson, B., *Cement and Concrete Research* 29(1999):1261-1270
- [34] Samson, E., J. Marchand, K. Snyder, J. Beaudoin, *Cement and Concrete Research* 35(2005):141-153
- [35] Xi, Y., A. Ababneh, *ICACS* 17-19(2003) : 354-364
- [36] Marchand, J., *Materials and Structures* 34(2001):195-200
- [37] Chung J., G. Consolazio, *Cement and Concrete Research* 35(2005):597-608
- [38] Freeze, R.A., and J. Cherry (1979). *Groundwater*, Prentice-Hall, Inc., New Jersey.
- [39] NIST (2005). Publicly Available Computer Models, Lastly accessed in Feb. 2005, at: <http://ciks.cbt.nist.gov/~bentz/phpct/cmml.html>.
- [40] Khatri, R. P., and Sirivivatnanon, V., 'Characteristic Service Life for Concrete Exposed to Marine Environments', *Cem. Concr. Res.* **34**(5), 2004, 745-752.
- [41] Kirkpatrick, T. J., Weyers, R. E., Anderson-Cook, C. M., and Sprinkel, M. M., 'Probabilistic Model for the Chloride-Induced Corrosion Service Life of Bridge Decks', *Cem. Concr. Res.* **32**(12), 2002, 1943-1960.
- [42] Boddy, A., Bentz, E., Thomas, M. D. A., and Hooton, R. D., 'An Overview and Sensitivity Study of a Multimechanistic Chloride Transport Model', *Cem. Concr. Res.* **29**(6), 1999, 827-837.
- [43] Kranc S.C., and A.A. Sagues (2003). Advanced Analysis of Chloride Ion Penetration Profiles in Marine Substructures, prepared for the Florida Department of Transportation.
- [44] Sagues A.A., S.C. Kranc et al. (2001). Corrosion Forecasting for 75-Year Durability Design of Reinforced Concrete, prepared for the Florida Department of Transportation.
- [45] Lee, S. H., and Rasaiah, J. C., 'Molecular Dynamics Simulation of Ion Mobility. 2. Alkali Metal and Halide Ions Using the SPC/E Model for Water at 25 °C', *J. Phys. Chem.* **100**(4), 1996, 1420-1425.
- [46] Castellote, M., Alonso, C., Andrade, C., Chadbourn, G. A., and Page, C. L., 'Oxygen and Chloride Diffusion in Cement Pastes As a Validation of Chloride Diffusion Coefficients Obtained by Steady-State Migration Tests', *Cem. Concr. Res.* **31**(4), 2001, 621-625.

- [47] Hobbs, D. W., 'Aggregate Influence on Chloride Ion Diffusion into Concrete', *Cem. Concr. Res.* **29**(12), 1999, 1995-1998.
- [48] Englund, S., and Sørensen, J. D., 'A Probabilistic Model for Chloride-Ingress and Initiation of Corrosion in Reinforced Concrete Structures', *Structural Safety* **20**(1), 1998, 69-89.
- [49] Yu, H., Shi, X., Hartt, W. H., and Lu, B. Laboratory investigation of reinforcement corrosion initiation and chloride threshold concentration for self-compacting concrete. *Cement and Concrete Research* 2010; 40(10): 1507-1516.
- [50] Williamson, G. S., Weyers, R. E., Brown, M. C., Ramniceanu, A., and Sprinkel, M. M., 'Validation of Probability-Based Chloride-Induced Corrosion Service-Life Model', *ACI Mater. J.* **105**(4), 2008, 375-380.
- [51] Pettersson, K. Service Life of Concrete Structure Including the Propagation Time. In: Concrete under severe conditions 2: environment and loading: Proceedings of the 2nd International Conference on Concrete Under Severe Conditions, CONSEC'98, Tromsø, Norway, June 21-24, 1998. pp.489-498.
- [52] Francois R., G. Arliguie, and A. Castel. Influence of Service Cracking on Service Life of Reinforced Concrete. In: Concrete under severe conditions 2: environment and loading: Proceedings of the 2nd International Conference on Concrete Under Severe Conditions, CONSEC'98, Tromsø, Norway, June 21-24, 1998. pp.143-152.
- [53] Lin G., Y. Liu, and Z. Xiang. Numerical Modeling for Predicting Service Life of Reinforced Concrete Structures Exposed to Chloride Environments. *Cement and Concrete Composites* 2010; 32(9): 571-579.
- [54] Chen D. Computational Framework for Durability Assessment of Reinforced Concrete Structures Under Coupled Deterioration Processes. Dissertation. Ph.D. in Civil Engineering. Vanderbilt University. August 2006.

## **APPENDIX B. A PHENOMENOLOGICAL MODEL FOR THE CHLORIDE THRESHOLD OF PITTING CORROSION OF STEEL IN SIMULATED CONCRETE PORE SOLUTIONS**

This appendix chapter presents a systematic study aimed to provide quantitative understanding of the fundamental factors that influence the chloride threshold of pitting corrosion of steel in concrete, by conducting a set of laboratory tests to assess the corrosion potential ( $E_{\text{corr}}$ ) and pitting potential ( $E_{\text{pit}}$ ) of steel coupons in simulated concrete pore solutions. With the aid of artificial neural network (ANN), the laboratory data were then used to establish a phenomenological model correlating the influential factors (total chloride concentration, chloride binding, solution pH, and dissolved oxygen concentration) with the pitting risk (characterized by  $E_{\text{corr}} - E_{\text{pit}}$ ). Three-dimensional response surfaces were then constructed to illustrate such predicted correlations and to shed light on the complex interactions between various influential factors. The results indicate that the threshold  $[\text{Cl}^-]/[\text{OH}^-]$  of steel rebar in simulated concrete pore solutions is a function of dissolved oxygen concentration, pH and chloride binding, instead of a unique value. The limitations and practical implications of the research findings were also discussed.

### **B1. Introduction**

The chloride threshold of rebar in concrete,  $Cl_{\text{th}}$ , can be defined as the content of chloride at the depth of the rebar that is necessary to sustain localized breakdown of its passive film and hence initiate its active corrosion [1]. The  $Cl_{\text{th}}$  is an important parameter in modeling and predicting the time to corrosion for rebar in concrete and subsequently in assessing the service life of reinforced concrete in chloride-laden environments [2,3].

The  $Cl_{\text{th}}$  data in published literature scatter over a wide range of values [4,5,6]. One possible reason is that different definitions and measurement methods are applied to quantify the “chloride threshold” [6,7,8]. The chloride-to-hydroxyl ionic concentration ratio ( $[\text{Cl}^-]/[\text{OH}^-]$ ) traditionally has been considered to be a more reliable indicator than the chloride concentration (often expressed as total chloride content by the weight of cement or concrete or free chloride concentration in concrete pore solution), considering that the competition between aggressive  $\text{Cl}^-$  and inhibitive  $\text{OH}^-$  governs the pitting and repassivation of steel. Research in aqueous solutions has indicated that for chloride-contaminated concrete the pitting corrosion occurs only above a critical  $[\text{Cl}^-]/[\text{OH}^-]$  ratio [9]. Through a probability simulation model, the threshold  $[\text{Cl}^-]/[\text{OH}^-]$  for corrosion of bare steel rods in high pH solutions was once predicted to be 0.66 in the presence of oxygen bubbles attached to the steel and 1.4 in the case of air. Such result agreed favorably with experimental data. In the same model, it was concluded that the threshold ratio should be about 1.4 for typical reinforced concrete and in excess of 3 for high-quality concrete with minimal air voids [10]. A number of studies [3,11,12,18,25] exposed reinforcing steel bars to simulated concrete pore solutions and revealed that the threshold  $[\text{Cl}^-]/[\text{OH}^-]$  ratio increased with increasing pH. Higher results (1.17-3.98) have been reported for the threshold  $\text{Cl}/\text{OH}$  ratio in mortars than was found in synthetic pore solution (0.25-0.8) [5]. Recently, Ann and Song [8] argued that the ratio of total chloride content to acid neutralization capacity,  $[\text{Cl}^-]/[\text{H}^+]$ , best presents the chloride threshold

level since it takes into account “all potentially important inhibitive (cement hydration products) and aggressive (total chloride) factors”.

The lack of universally accepted chloride threshold value is also attributable to the numerous factors that affect steel corrosion in concrete, such as: the pH of concrete pore solution, the electrochemical potential of the steel, and the physical condition of the steel/concrete interface. The pH of concrete pore solution depends mainly upon the type of cement and additions and the carbonation level of concrete [13,14,15,16]. The potential of the steel is not only related to the steel type and surface condition (e.g., roughness) but also on the availability of oxygen at the steel surface; the latter is affected by the moisture content of concrete [17,18,19]. The physical condition of the steel/concrete interface (especially entrapped air void content) was found to be more dominant in defining the  $Cl_{th}$  than chloride binding or buffering capacity of the cement matrix or binders [8]. Voids that normally can be found in real structures due to incomplete compaction may weaken the layer of cement hydration products deposited at the steel/concrete interface and thus may favor local acidification required for sustained propagation of pits. The presence of air voids, as well as crevices and microcracks, may decrease the chloride threshold [20,21,22,23]. In addition, the presence of sulfate ions, the temperature and the concrete mix proportions and quality may affect the chloride threshold [6,7,23,24]. Li and Sagüés [25] listed a wide array of internal and external factors defining the  $Cl_{th}$ , such as: the composition, surface condition, and configuration of rebar; the concrete chemistry (type and amount of cement and admixtures, type and porosity of aggregates,  $w/c$  ratio, degree of hydration, etc.); the type and source of chloride; and the service environment (humidity, temperature, cracking of concrete, etc.). Angst et al. [7] summarized the state of the art in the  $Cl_{th}$  research in a recent review.

Furthermore, it has been argued that the  $Cl_{th}$  should be treated as a distributed parameter represented by a probability function, in light of the statistical nature of the processes involved (e.g., chloride ingress and pitting initiation) and the inherent heterogeneities of the concrete matrix [22,23,25]. Li and Sagüés [25] suggested the incorporation of a  $Cl_{th}$  variability term in the service life prediction procedures and durability models.

Despite the multitude of studies undertaken, the factors defining the  $Cl_{th}$  of steel rebar and their interactions merit further investigation. This work presents a systematic study aimed to provide quantitative understanding of the fundamental factors that influence the chloride threshold of pitting corrosion of steel in concrete, by conducting a set of laboratory tests to assess the corrosion potential ( $E_{corr}$ ) and pitting potential ( $E_{pit}$ ) of steel coupons in simulated concrete pore solutions.

## **B2. Experimental**

This work involves exposing polished and pre-passivated steel coupons to various alkaline solutions and electrochemically measuring their  $E_{corr}$  and  $E_{pit}$ . As the steel in concrete is assumed to be passive if its  $E_{pit}$  is nobler than its  $E_{corr}$ , in this study the difference between the two, ( $E_{corr} - E_{pit}$ ), serves as a quantitative measure of the

susceptibility of the steel rebar to pitting in simulated concrete pore solutions; the greater the difference, the greater the risk of pitting.

### ***B2.1. Materials and Preparation***

To enhance the reliability of experimentally obtained data of ( $E_{\text{corr}} - E_{\text{pit}}$ ), at least five replicate steel coupons were tested in each alkaline solution of interest. The steel coupons were 15-cm long specimens cut from rust-free Nucor Steel - Utah 10/#3 Rebar (ASTM A615M-09 GR 40), with a diameter of 3/8 inches (0.95 cm) and the following chemical composition by weight: 0.16% C; 0.22% Si; 0.72% Mn; 0.043% Mo; 0.3% Cu; 0.041% S; 0.014% P; 0.014% Ni; 0.22% Cr; the balance Fe. The steel coupon was first cleaned with acetone to remove oil and grease; then polished to provide a specific level of uniform surface roughness, using first #600 then #1000 grit size SiC sandpapers with tap water on a metallographic grinding disc. After polishing, the coupons were rinsed with running tap water to remove any remaining grit; rinsed by de-ionized water; cleaned in ethanol using 5-min ultra-sonication; and then dried. Prior to electrochemical testing, the steel coupons were immersed in a NaOH solution of pH 13 for seven days to allow for their pre-passivation and then washed with ethanol and dried.

Sixty-two simulated concrete pore solutions were prepared for this study, featuring various levels of chloride contamination, carbonation, and aeration. The dissolved oxygen concentration in the solutions was controlled by using either oxygen bubbles, air bubbles, or none. The initial pH of the solutions was controlled at five levels as follows: pH 9: 0.3 M NaHCO<sub>3</sub> + 0.1 M Na<sub>2</sub>CO<sub>3</sub>, pH 10.63: 0.1 M NaHCO<sub>3</sub> + 0.1 M Na<sub>2</sub>CO<sub>3</sub>, pH 11.0: ~ 0.1M Na<sub>2</sub>CO<sub>3</sub>, pH 12.27: 0.3M Na<sub>2</sub>CO<sub>3</sub>, and pH 13.9: 0.9M NaOH.

To explore the effect of chloride binding on the  $Cl_{\text{th}}$ , various types and amounts of dry powder of cementitious paste were added to the alkaline solutions. The paste specimens were prepared with a water-to-cementitious-materials ratio of 0.45 and with the Portland cement replaced by a class C fly ash at 0%, 15% and 30% by weight respectively. After de-molding, the paste specimens were cured in saturated Ca(OH)<sub>2</sub> solution for 27 days before being dried and ground into powder. The powder was then screened through a 150- $\mu\text{m}$  sieve, oven-dried at 80°C overnight and cooled to room temperature. Depending on the experimental design, 2, 8 and 40 grams of various dry paste powders were added into 100 ml of the alkaline solution respectively and allowed 48 hours for sufficient chloride binding and pH equilibration.

### ***B2.2. Electrochemical Testing***

Once the dry paste powder had been added into the alkaline solution for 48 hours, the final pH and dissolved oxygen concentration (DO) of the test solution were measured using an Accumet model AB15 pH meter and a Sper Scientific DO meter respectively. The free chloride concentration of the solution was measured by a Nexsens model WQ-CL chloride sensor, which was then used to calculate the chloride binding (i.e., percent of bound chloride) and  $[\text{Cl}^-]/[\text{OH}^-]$  ratio as follows.

$$\text{Chloride binding} = (Cl_{TT} - Cl_f) / Cl_{TT} \times 100\% \quad (1)$$

$$[Cl^-] / [OH^-] = Cl_f / 10^{(14 - pH)} \quad (2)$$

where  $Cl_{TT}$  and  $Cl_f$  were the initial known chloride concentration and the final measured free chloride concentration, respectively.

Subsequently, the electrochemical behavior of steel rebar was assessed using a three-electrode electrochemical cell and a Gamry Instruments<sup>®</sup> Potentiostat with an 8-channel Electrochemical Multiplexer. The working electrode was the rebar immersed in the alkaline solution for 3 cm, resulting in a nominal exposure surface area of 8.55 cm<sup>2</sup>. The counter electrode used was a stainless steel mesh, and the reference electrode was a saturated calomel electrode (SCE). The  $E_{corr}$  of steel rebar in each alkaline solution was derived from the potentiodynamic weak polarization measurements, during which the steel was polarized from -30mV to +30 mV relative to its open circuit potential (OCP) using a scan rate of 0.2 mV/s. The  $E_{pit}$  of steel rebar in each alkaline solution was derived from the cyclic polarization measurements, during which the steel was polarized from -0.6V to +0.9V relative to SCE (anodic scan) and from +0.9V to -0.6 V relative to SCE (cathodic scan), using a scan rate of 0.5 mV/s. The  $E_{pit}$  was determined as the electrochemical potential at which a sudden increase in the electric current is observed (in the anodic scan curve).

### B3. Modeling Technique

To explore the complex relations between the solution properties and the resultant pitting risk to steel rebar, artificial neural network (ANN) was chosen to be the modeling tool. ANNs provide a non-parametric, self-adaptive approach to information processing and are powerful in tackling complex, non-linear problems where conventional modeling techniques (e.g., multiple regression) fail. A multi-layer feed-forward ANN was adopted for modeling, a typical architecture of which is shown in Figure 1. The nodes in the input and output layers consist of independent variables and response variable(s), respectively. The detailed description of error propagation algorithm is provided elsewhere [26].

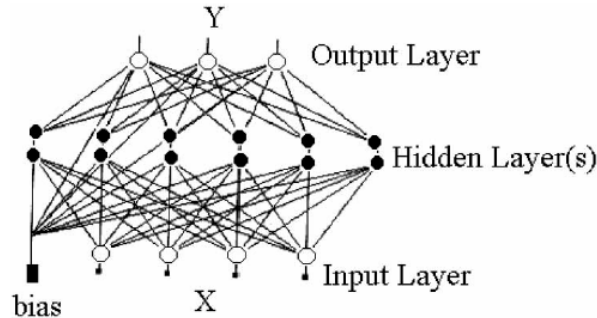


FIGURE 22 A typical multi-layer feed-forward ANN architecture

ANNs have been successfully utilized to predict the compressive strength of concrete, to predict the electrochemical behavior of steel in various chloride solutions and the chloride binding, chloride profiles, and chloride permeability in concrete, to recognize the OCP behavioral pattern of steel in concrete, to predict the time to onset of rebar corrosion

and the life of concrete structures, and to model the ingress of chlorides into concrete and its corrosion implications [27].

In this study, a modified back propagation (BP) algorithm was employed for the ANN training in which a sigmoid function in Equation (3) was used as the nonlinear transfer function and the sum of the mean squared error (SMSE) in the output layer as the convergence criteria.

$$f(x) = \left(1 + e^{-x}\right)^{-1} \quad (3)$$

All the data for input and output were normalized based on Equation (4), where  $X_i$  and  $NX_i$  are the  $i^{\text{th}}$  value of factor  $X$  before and after the normalization, and  $X_{\min}$  and  $X_{\max}$  are the minimum and maximum value of factor  $X$ , respectively.

$$NX_i = \frac{(x_i - x_{\min} + 0.1)}{(X_{\max} - X_{\min} + 0.1)} \quad (4)$$

## **B4. Results and Discussion**

### ***B4.1. Electrochemical Characterization of Pitting Risk***

Table 1 presents the experimentally obtained electrochemical data of the ASTM A615 steel rebar in the 62 alkaline solutions. Note that each record was averaged from five replicate steel coupons; and when there was significant variability in the data, more replicate steel coupons were tested to identify and remove outliers.

TABLE 1 Electrochemical data of the ASTM A615 steel rebar in alkaline solutions.

$Cl_{\pi}$ (M)	Cl-binding	pH	DO (ppm)	$E_{corr}$ (mV/SCE)	$E_{pit}$ (mV/SCE)	$E_{corr}-E_{pit}$ (mV), measured	$E_{corr}-E_{pit}$ (mV), modeled
0.0005	36%	10.17	0.97	-77.59	547.78	-625.37	-624.44
0.0005	4%	10.6	1.4	-82.77	-233.17	150.40	140.72
0.0005	85%	13.49	5.32	-334.33	319.84	-654.17	-893.23
0.0007	59%	10.52	0.58	-306.56	629.48	-936.04	-972.75
0.0007	71%	13.45	5.2	-457.36	-217.63	-239.73	-324.57
0.0009	71%	13.65	7.9	-366	360	-726.00	-978.01
0.0012	36%	10.93	1.35	-87.09	730.07	-817.16	-811.24
0.0012	54%	13.55	8.41	-596.76	396.67	-993.43	-973.63
0.0019	45%	10.55	2.45	-105.54	750.2	-855.74	-757.70
0.0019	76%	12.57	18.54	-8.94	380.35	-389.29	-390.79
0.0022	2%	12.95	0.8	-463.93	317.13	-781.06	-772.90
0.0022	78%	11.76	1.39	-37.37	-232.23	194.86	200.37
0.0034	70%	10.55	1.4	-35.23	736.19	-771.42	-775.99
0.0034	32%	12.98	3.98	-465.76	10.1	-475.86	-454.59
0.0042	54%	10.52	3.56	-56.97	736.76	-793.73	-715.67
0.0042	74%	13.71	20	-440.22	-269.89	-170.33	-555.42
0.0053	80%	13.91	0.46	-43.51	-142.07	98.56	109.45
0.0053	36%	10.95	1.32	42.47	-18.13	60.60	62.69
0.0053	36%	11.74	1.32	-341.04	632.91	-973.95	-973.45
0.0053	64%	12.7	5.01	-52.55	-245.31	192.76	221.23
0.0130	39%	11.78	1.32	-123.67	-205.74	82.07	83.71
0.0130	33%	12.95	2.98	-428.19	543.83	-972.02	-947.20
0.0224	66%	11.71	1.24	-120.49	-245.05	124.56	154.83
0.0476	39%	13.66	1.06	-289.29	-129.03	-160.26	-152.09
0.0476	41%	10.68	15.65	85.35	-30.05	115.40	117.15
0.0640	27%	12.7	4.98	-238.75	114.64	-353.39	-355.03
0.0930	36%	11.84	1.21	89.75	-147.97	237.72	248.81
0.0930	50%	12.65	5.65	-285.05	622.03	-907.08	-861.00
0.1230	39%	12.7	0.5	-43.58	-231.91	188.33	207.77

TABLE 1 Electrochemical data of the ASTM A615 steel rebar in alkaline solutions (continued, with the testing data set highlighted).

$Cl_{\pi}$ (M)	Cl-binding	pH	DO (ppm)	$E_{corr}$ (mV/SCE)	$E_{pit}$ (mV/SCE)	$E_{corr}-E_{pit}$ (mV), measured	$E_{corr}-E_{pit}$ (mV), modeled
0.1230	27%	12.7	5.02	-43.49	-125.62	82.13	93.16
0.2002	79%	13.85	3.25	-473.36	214.76	-688.12	-850.63
0.2002	36%	12.73	3.61	-77.25	10.31	-87.56	-87.78
0.2002	55%	13.22	4.89	-417.67	63.33	-481.00	-21.94
0.2002	19%	12.61	5.07	-244.93	663.63	-908.56	-870.71
0.2002	62%	13.61	7.77	-167.44	-241	73.56	113.64
0.2410	29%	13.64	0.98	-322.8	628.2	-951.00	-941.16
0.2410	39%	12.7	16.1	52.39	-131.67	184.06	195.01
0.3000	2%	13.8	4.4	-249.96	-48.88	-201.08	-183.83
0.3000	47%	12.4	5.6	-23.83	-185.83	162.00	164.91
0.3987	52%	13.75	1.31	-384.5	200	-584.50	-64.19
0.3987	54%	13.75	1.31	-467.33	158.34	-625.67	-193.15
0.3987	45%	13.77	1.31	-52.07	-197.75	145.68	112.06
0.3987	57%	12.93	1.7	-37.81	-230.98	193.17	176.49
0.3987	66%	12.71	2	-106.77	-146.41	39.64	40.53
0.3987	39%	13.63	20	-336.33	176.67	-513.00	-582.79
0.4980	40%	12.9	0.78	-6.59	-193.64	187.05	189.72
0.4980	30%	13.63	1.01	-30.81	-153.29	122.48	161.16
0.4980	36%	9.59	3.5	-102.05	-84.95	-17.10	-6.75
0.5989	14%	13.82	0.46	-68.36	78.31	-146.67	-16.40
0.5989	80%	14.03	3.25	-464.76	49.24	-514.00	-314.07
0.5989	79%	13.82	6.17	-481.53	336.14	-817.67	-651.95
0.5989	20%	13.88	7.25	-228.84	33.51	-262.35	272.06
0.5989	45%	13.35	20	-76.61	164.95	-241.56	-141.32
0.9538	32%	13.56	0.7	-436.21	40.24	-476.45	-477.57
0.9538	21%	12.68	2.58	-44.35	-238.39	194.04	175.45
0.9538	32%	10.9	17.01	81.41	-202.11	283.52	276.56
0.9538	12%	11.56	5.69	22.74	-216.04	238.78	208.12
0.0005	31%	10.92	1.38	-5.97	-61.83	55.86	62.24
0.0007	78%	10.94	1.45	48.17	-200.39	248.56	247.48
0.0053	39%	12.96	20	-233.23	77.02	-310.25	-301.50
0.0640	39%	12.96	20	-86.92	22.31	-109.23	-98.13
0.4980	22%	12.64	13.5	81.11	-120.12	201.23	195.17

Figure 2a and Figure 2b illustrate the relationships between  $E_{pit}$  and  $E_{corr}$  and the pitting risk respectively, the latter of which is indicated by  $(E_{corr} - E_{pit})$ . It can be seen that there is a strong correlation between  $E_{pit}$  and the pitting risk and a much weaker correlation between  $E_{corr}$  and the pitting risk. In general, higher  $E_{pit}$  values and lower  $E_{corr}$  values correspond to lower pitting risk for the steel rebar investigated. Both  $E_{pit}$  and  $E_{corr}$  are affected by the quality of the passive film on the steel rebar and the electrolyte it is exposed to, even though  $E_{pit}$  is shown to be a more sensitive indicator for evaluating its

resistance to pitting corrosion. Li and Sagüés [25] conducted an extensive study of chloride corrosion threshold of rebar in alkaline solutions and found that “the average value of  $E_{pit}$  in replicate tests decreased with solution  $Cl^-$  concentration, specimen size, and steel surface roughness but increased with solution pH and passive film maturity”.

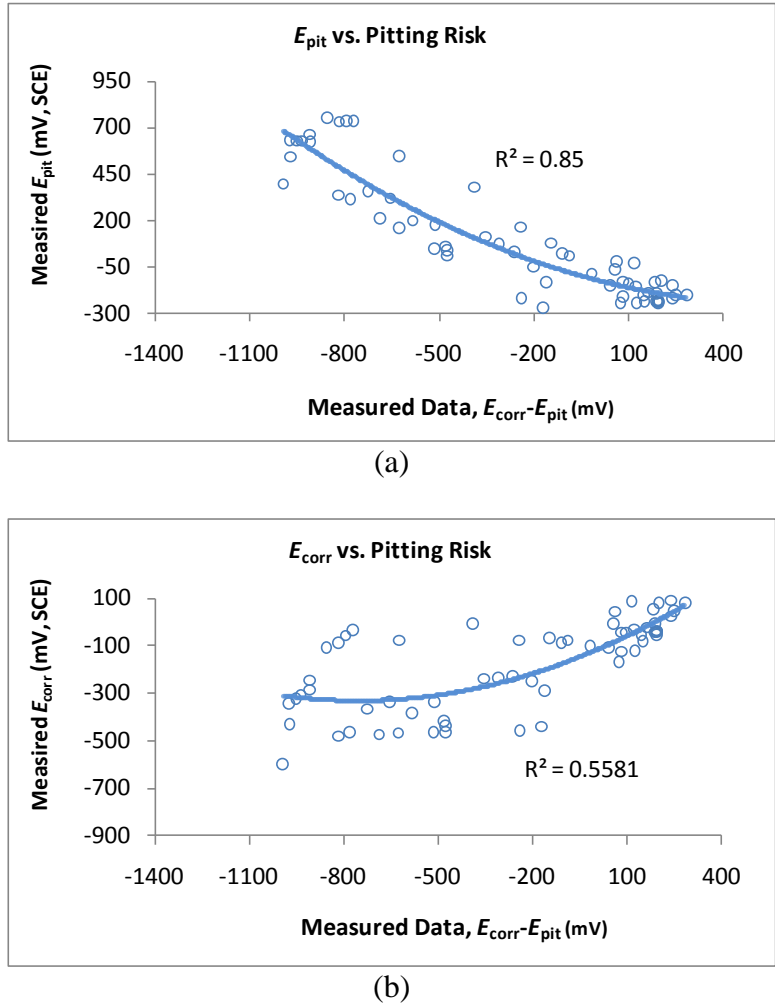


FIGURE 23 Relations between (a)  $E_{pit}$  and (b)  $E_{corr}$  and the pitting risk

#### ***B4.2. Performance of the ANN Model***

As shown in Table 1, the experimental data were divided randomly into a training set (56 records, 90%) and a testing set (6 records, 10%) for the ANN model. Through trial and error, a 4-9-1 BP ANN was chosen to model the relationship between the four independent variables ( $Cl_{TT}$ , chloride binding, pH and DO) and the response variable ( $E_{corr} - E_{pit}$ ). The model was trained to allow for a reasonable training error and a reasonable testing error (SMSE of 0.086 and 0.059 respectively), implying acceptable disparities between the measured data and the modeled data. In addition, Figure 3 confirms that the established ANN model has good “memory” and the trained matrices of

interconnected weights and bias (“building blocks” of the neural network) reflected the hidden functional relationships well.

As such, once the empirical ANN model was trained and tested, it was used to predict the  $(E_{\text{corr}} - E_{\text{pit}})$  as a function of various independent variables. Such predictions were made with each independent variable over the range of the training data, since ANNs are not suitable for extrapolation. As the  $(E_{\text{corr}} - E_{\text{pit}})$  exceeds 0 mV, the steel rebar is likely to make the transition from passive state to transpassive state.

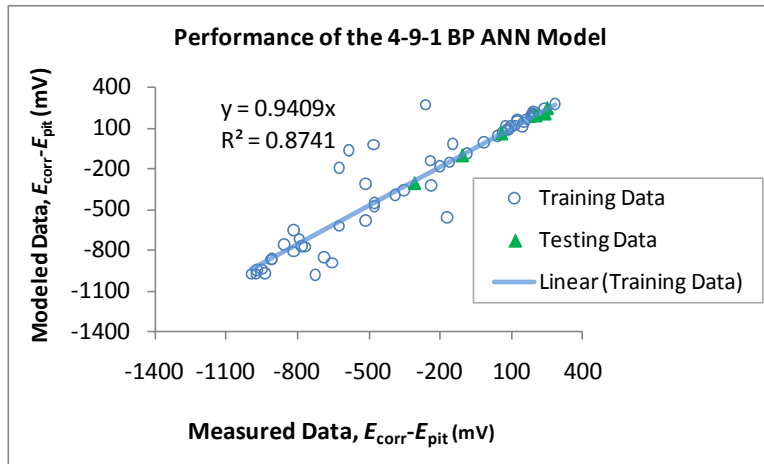


FIGURE 24 Relationship between experimental and modeled pitting risk

#### ***B4.3. Relative Importance of Variables***

The relative importance of each independent variable was assessed by predicting the change in  $(E_{\text{corr}} - E_{\text{pit}})$  when the variable was assigned the minimum and maximum values in its typical range and the other variables were kept at the median level. The results (shown in Table 2) suggest that, under the conditions investigated, the total chloride concentration has the largest effect on the pitting risk, with an increase in  $Cl_{\text{TT}}$  significantly increasing the  $(E_{\text{corr}} - E_{\text{pit}})$  of the steel rebar. According to the model predictions, a significant decrease in the  $(E_{\text{corr}} - E_{\text{pit}})$  of the steel rebar also occurs with an increase in the pH of the alkaline solution. The percent of bound chloride and the dissolved oxygen concentration had a less significant effect on the pitting risk of the steel rebar, with a decrease in chloride binding or increase in DO increasing the  $(E_{\text{corr}} - E_{\text{pit}})$ . It should be cautioned, however, the data in Table 2 show only the overall trend with independent variables maintained at specific levels. As discussed later, the influence of these variables and their interactions on the pitting risk of steel in simulated concrete pore solutions is in fact very complex.

TABLE 2 Effect of each variable on the pitting risk of steel rebar in alkaline solutions.

Independent Variable		$E_{\text{corr}} - E_{\text{pit}}$			
Type	Range*	Predicted data (mV)	Change (mV)	Normalized data**	% Change
$Cl_{\text{TT}}$	0.002 → 0.30M	-699.6 → 123.2	822.8	0.23 → 0.87	280%
Chloride binding	2% → 64%	164.5 → -175.7	-340.2	0.91 → 0.64	-29%
pH	9.6 → 13.8	226.1 → 688.0	-914.1	0.96 → 0.24	-75%
DO	0.5 → 20 ppm	-76.8 → 192.5	269.3	0.72 → 0.93	29%

\* Other variables at the median level:  $Cl_{\text{TT}}$  0.151M, chloride binding 33%, pH 12.7 and DO 5 ppm.

\*\* All data were normalized between 0 and 1 using the experimentally obtained min. and max., i.e., ( $E_{\text{corr}} - E_{\text{pit}}$ ) of -993.4 mV and 283.5 mV respectively.

#### B4.4. Effect of Chloride Concentration and Chloride Binding on Pitting Risk

As shown in Figure 4, the established ANN model was used to construct a response surface illustrating the effect of chloride concentration and chloride binding on the pitting risk of the steel rebar. With pH and DO set at 12.5 and 5 ppm respectively, the pitting risk is predicted to increase noticeably as  $Cl_{\text{TT}}$  increases from 0.002 M to 0.18 M and then level off as  $Cl_{\text{TT}}$  exceeds 0.18 M. At low chloride concentrations, the predicted pitting risk increases as the percent of bound chloride decreases from 64% to 2%; this effect, however, diminishes at high chloride concentrations.

These model predictions confirm the known deleterious role of  $Cl^-$  ions, as they serve as catalyst for the anodic half-reaction of steel corrosion. Moreno et al. [12] suggested that “a passivity breakdown process took place above a certain potential that decreases with the chloride concentration”. From a kinetics perspective, as the  $Cl_{\text{TT}}$  increases or chloride binding decreases, the free chloride concentration increases. This may shift the anodic polarization curve (indicative of the iron oxidation half-reaction) to the negative direction and reduce both the  $E_{\text{corr}}$  and  $E_{\text{pit}}$ . Relative to the  $E_{\text{corr}}$ , the  $E_{\text{pit}}$  is expected to decrease much more significantly with the increase in free chloride concentration [6,19,31,32]. As such, there is a possibility for the steel to move from the passive state ( $E_{\text{corr}} < E_{\text{pit}}$ ) to the transpassive state ( $E_{\text{corr}} > E_{\text{pit}}$ ), i.e., increasing the pitting risk. From a mechanistic perspective, higher chloride concentration is expected to “increase the number of sites where corrosion initiates” and “reduce initiation time for the onset of corrosion” [62].

In concrete, chlorides can exist either in the pore solution, chemically bound to hydration products, or physically held to the surface of hydration products [33,34,35]. Chloride binding removes chloride ions from the pore solution and slows down the rate of

penetration [36]. While previous studies [37,38] suggest that only free chloride ions in the pore solution are responsible for initiating corrosion of the steel, Glass et al. [4,39,40] indicated that bound chlorides also may present a significant risk to steel.

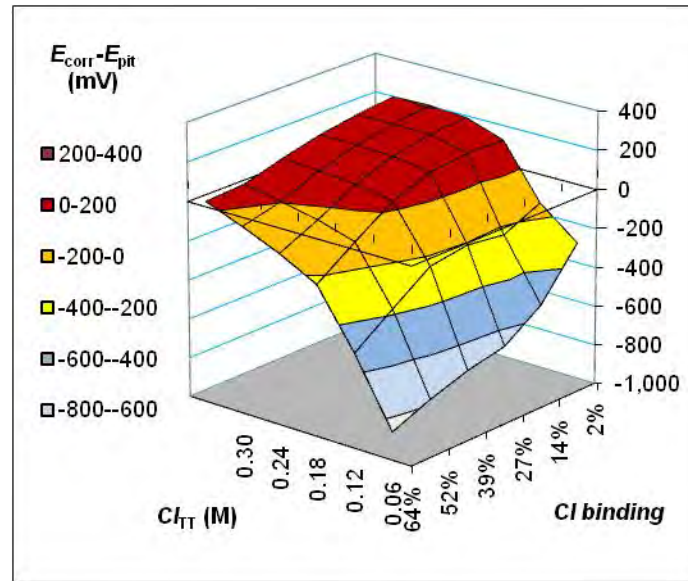


FIGURE 25 Predicted pitting risk as a function of  $Cl_{TT}$  and chloride binding, with pH and DO set at 12.5 and 5 ppm respectively.

#### B4.5. Effect of pH and DO on Pitting Risk

As shown in Figure 5, the established ANN model was used to construct a response surface illustrating the effect of chloride concentration and pH on the pitting risk of the steel rebar. With the percent of bound chloride and DO set at 33% and 5 ppm respectively, the pitting risk is predicted to increase significantly as pH decreases from 13.8 to 9.6. At high pH, the predicted ( $E_{corr} - E_{pit}$ ) is well below zero regardless of the chloride concentration, indicating no pitting risk. When both pH and  $Cl_{TT}$  are high, there may be unstable micropits that would not develop to macro-pits on the steel surface. At intermediate pH, the predicted pitting risk increases noticeably as  $Cl_{TT}$  increases from 0.002 M to 0.18 M and then levels off as  $Cl_{TT}$  exceeds 0.18 M. The effect of  $Cl_{TT}$  on the pitting risk becomes insignificant at low pH values.

The predicted effect of pH on pitting risk agrees well with the existing knowledge. For instance, according to the well-known Pourbaix diagram for Fe-H<sub>2</sub>O system, as pH decreases from highly alkaline (near 14) to neutral, the steel can move from the thermodynamically passive region to the thermodynamically active region and initiate the dissolution of its passive film. According to Moreno et al. [12], “a critical acidification is necessary to render repassivation unlikely and sustain pit activity”. In this study, the lower the pH value of alkaline solutions, the more unstable was the passive film on the steel. As pH decreases from 8 to 2 in calcium chloride solutions, the  $E_{pit}$  of AISI 434, 201, and 301 steels has been reported to decrease, indicative of an increase in their risk of pitting [28].

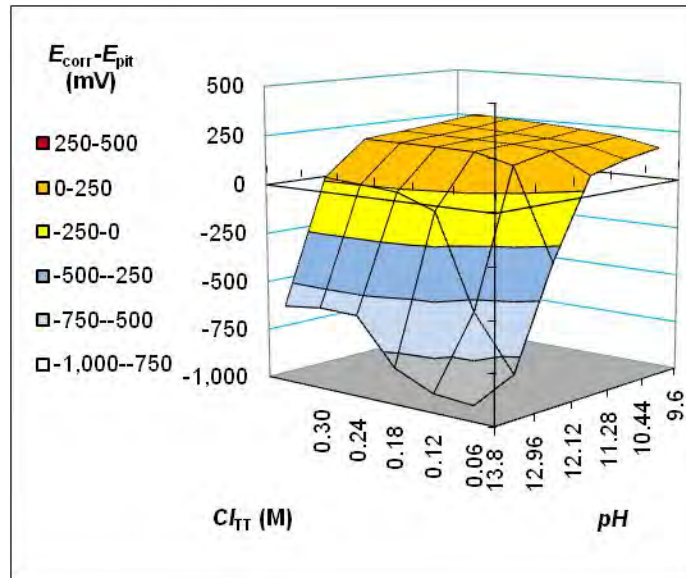


FIGURE 26 Predicted pitting risk as a function of  $Cl_{TT}$  and pH, with the chloride binding and DO set at 33% and 5 ppm respectively.

As is shown in Figure 6, the established ANN model was used to construct a response surface illustrating the effect of chloride concentration and DO on the pitting risk of the steel rebar. With the percent of bound chloride and pH set at 33% and 12.7 respectively, the pitting risk is predicted to increase noticeably as DO increases from 0.5 ppm to 20 ppm or as  $Cl_{TT}$  increases from 0.002 M to 0.18 M.

The predicted effect of DO on pitting risk agrees well with existing knowledge. Dissolved oxygen is an essential reactant in the electrochemical processes of steel corrosion in alkaline solutions, since its reduction is the cathodic half-reaction that enables corrosion to occur in the typical potential range. In the case where DO is extremely low (such as in submerged concrete structures), no active corrosion of the steel rebar could occur and the risk of pitting is negligible. This corresponds to the case of DO less than 1 ppm (as shown in Figure 6), where the  $(E_{corr} - E_{pit})$  is very negative regardless of the chloride concentration. As DO increases from 0.01 to 10 ppm in high-purity water, the  $E_{corr}$  of AISI 304 stainless steel has been reported to increase greatly [29], likely accompanying an increase in its risk of pitting. As DO decreases from 8 to 1 ppm in an alkaline solution, both the corrosion rate and  $E_{corr}$  of carbon steel SA-178A have been reported to decrease greatly, accompanying the formation and stability of the passive film once DO drops below 2 ppm [30]. Oxygen is also known to affect the rate of corrosion dramatically once active corrosion is initiated [62].

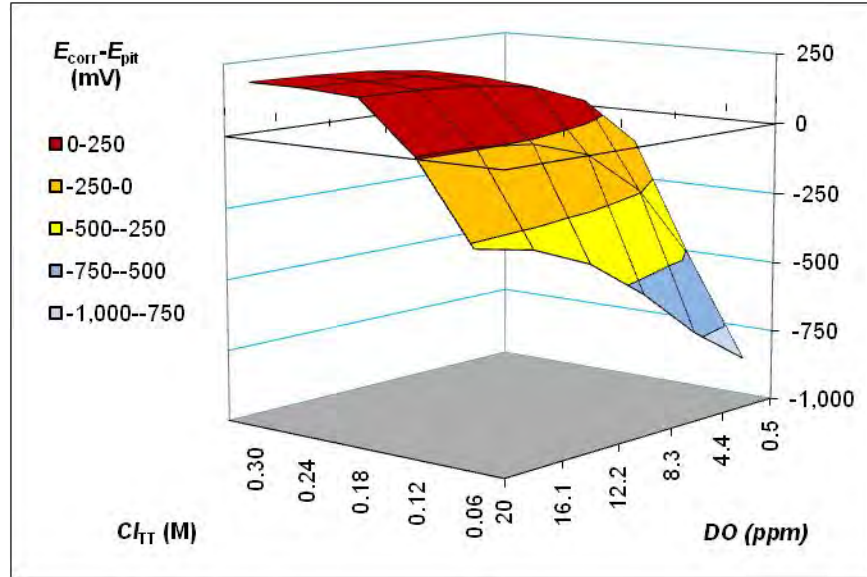


FIGURE 27 Predicted pitting risk as a function of  $Cl_{TT}$  and DO, with the chloride binding and pH set at 33% and 12.7 respectively.

As shown in Figure 7, the established ANN model was also used to construct a response surface illustrating the effect of pH and DO on the pitting risk of the steel rebar. With the  $Cl_{TT}$  and percent of bound chloride set at 0.151 M and 33% respectively, the pitting risk is predicted to be high once the solution pH drops below 11.4, regardless of the dissolved oxygen concentration. The pitting risk is predicted to be the lowest when the solution pH exceeds 13.0 and DO drops below 1 ppm.

From the kinetics perspective,  $E_{corr}$  is the electrochemical potential at which the anodic curve (indicative of the iron oxidation half-reaction) and cathodic curve (indicative of the oxygen reduction half-reaction) intersect. As pH decreases or DO increases, the cathodic curve shifts to the positive potential direction (in light of the Nernst equation for the cathodic reaction:  $2H_2O + 4e + O_2 \rightarrow 4OH^-$ ), there is a possibility for the steel to move from the passive state ( $E_{corr} < E_{pit}$ ) to the transpassive state ( $E_{corr} > E_{pit}$ ), i.e., with increased pitting risk.

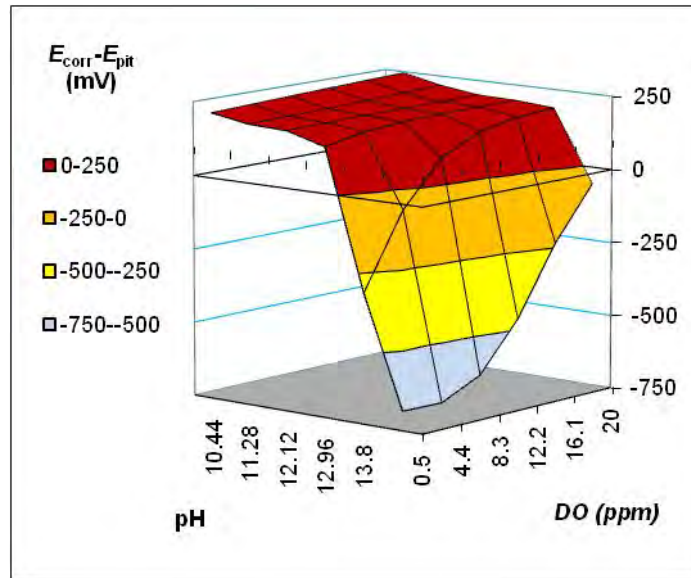


FIGURE 28 Predicted pitting risk as a function of pH and DO, with the  $Cl_{\text{TT}}$  and chloride binding set at 0.151 M and 33% respectively.

#### ***B4.6. Effect of $[Cl^-]/[OH^-]$ Ratio on Pitting Risk***

Figure 8 illustrates the pitting risk of the steel rebar as a function of DO and the  $[Cl^-]/[OH^-]$  ratio, with the  $Cl_{\text{TT}}$  and chloride binding set at 0.151 M and 33% respectively. The threshold  $[Cl^-]/[OH^-]$  ratio is defined the maximum ratio at which  $E_{\text{pit}}$  is nobler than its  $E_{\text{corr}}$ . As shown in Figure 8, at all DO levels, the predicted  $(E_{\text{corr}} - E_{\text{pit}})$  first increases greatly with the increase in the  $[Cl^-]/[OH^-]$  ratio and then gradually levels off. The predicted threshold  $[Cl^-]/[OH^-]$  ratio increases from 0.22 to 2.72 as the dissolved oxygen concentration of the alkaline solution decreases from 20 ppm to 0.5 ppm.

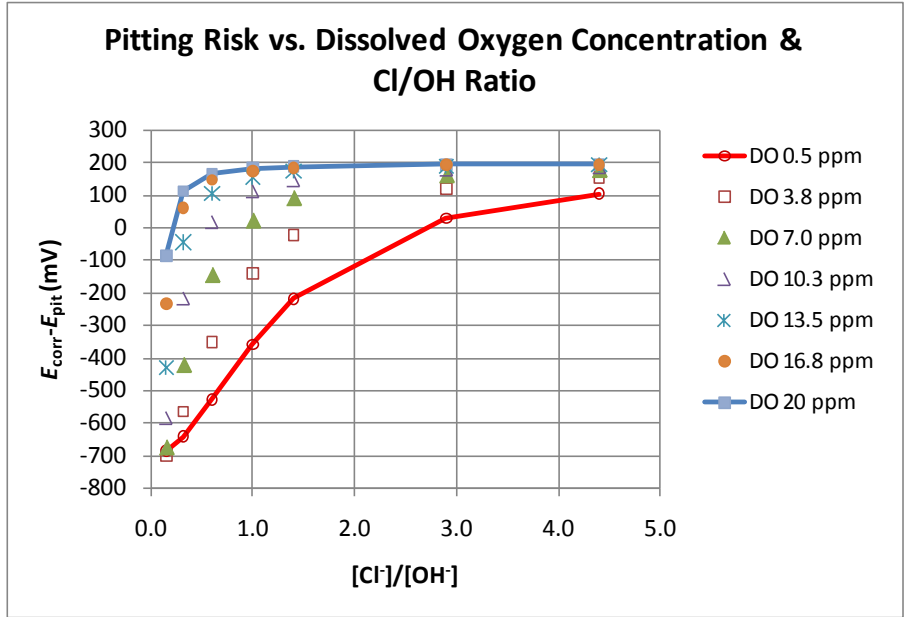


FIGURE 29 Predicted pitting risk as a function of DO and  $[Cl^-]/[OH^-]$ , with the  $Cl_{TT}$  and chloride binding set at 0.151 M and 33% respectively

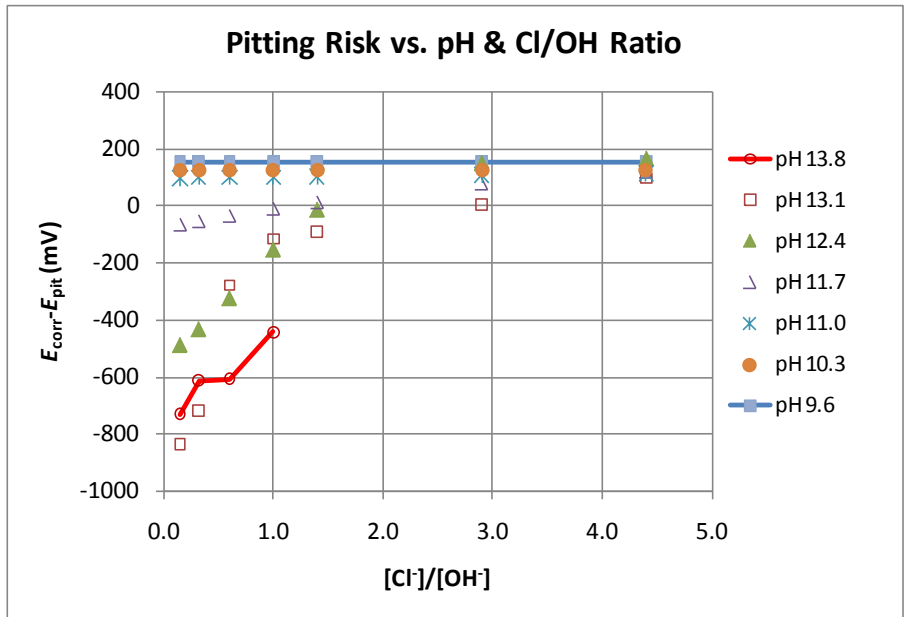


FIGURE 30 Predicted pitting risk as a function of pH and  $[Cl^-]/[OH^-]$ , with DO and chloride binding set at 5 ppm and 33% respectively

Figure 9 illustrates the pitting risk of the steel rebar as a function of pH and the  $[Cl^-]/[OH^-]$  ratio, with DO and chloride binding set at 5 ppm and 33% respectively. As shown in Figure 9, at intermediate pH levels, the predicted ( $E_{corr} - E_{pit}$ ) first increases greatly with the increase in the  $[Cl^-]/[OH^-]$  ratio and then gradually levels off. The predicted threshold  $[Cl^-]/[OH^-]$  ratio increases from 1.2 to 2.8 as the solution pH increases from 11.7 to 13.1.

Such a threshold increase with pH is consistent with the previous studies in simulated concrete pore solutions [3,11,12,18,25], suggesting a stronger inhibiting effect of OH<sup>-</sup> ions at higher concentrations. When the solution pH drops below 11.7, the pitting risk is always high and insensitive to the [Cl<sup>-</sup>]/[OH<sup>-</sup>] ratio. At the very high pH (13.8), it was infeasible to derive the threshold [Cl<sup>-</sup>]/[OH<sup>-</sup>] ratio using the reasonable chloride concentrations.

Figure 10 illustrates the pitting risk of the steel rebar as a function of chloride binding and the [Cl<sup>-</sup>]/[OH<sup>-</sup>] ratio, with the  $Cl_{TT}$  and DO set at 0.151 M and 5 ppm respectively. As shown in Figure 10, at all chloride binding levels, the predicted ( $E_{corr} - E_{pit}$ ) first increases greatly with the increase in the [Cl<sup>-</sup>]/[OH<sup>-</sup>] ratio and then gradually levels off. The predicted threshold [Cl<sup>-</sup>]/[OH<sup>-</sup>] ratio increases from 0.5 to 2.1 as the percent of bound chloride increases from 2% to 54% and then levels off as the chloride binding exceeds 54%.

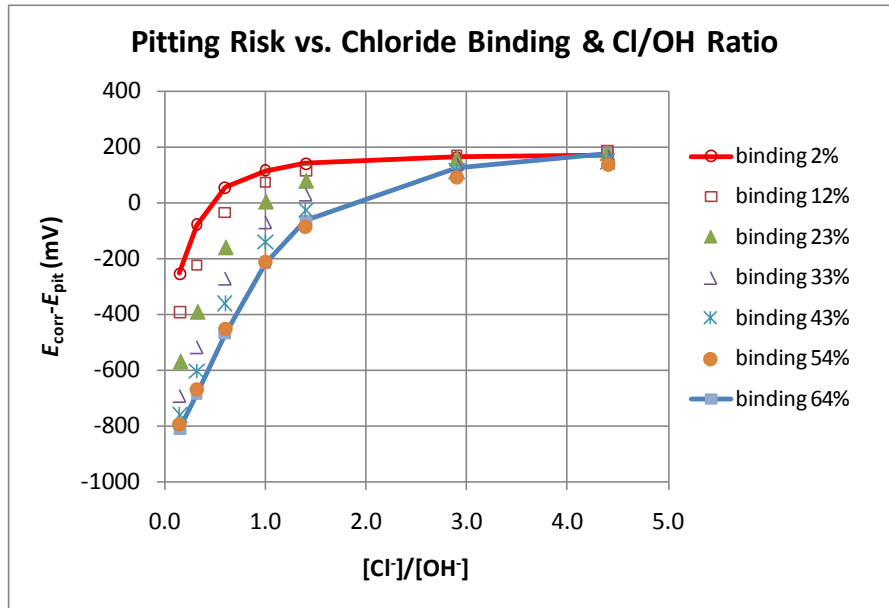


FIGURE 31 Predicted pitting risk as a function of chloride binding and [Cl<sup>-</sup>]/[OH<sup>-</sup>], with  $Cl_{TT}$  and DO set at 0.151 M and 5 ppm respectively

The results discussed above indicate that the threshold [Cl<sup>-</sup>]/[OH<sup>-</sup>] of steel rebar in simulated concrete pore solutions is a function of solution DO, pH and chloride binding, rather than a unique value. In this study, the polishing and subsequent pre-passivation of the rebar surface likely improved the threshold chloride threshold values by removing defects where micropits could initiate, as suggested by previous studies [6,25,42,61]. The chloride threshold also depends on the type of reinforced alloy being used [43,44]. Hurley et al. [45] measured the chloride threshold of various rebar in saturated Ca(OH)<sub>2</sub> solutions containing NaCl and found that the 316LN stainless steel rebar had a much higher threshold [Cl<sup>-</sup>]/[OH<sup>-</sup>] (> 20) than carbon steel (0.25-0.34). The exposed area and roughness of the rebar, pre-passivation time (thus passive film maturity), and scan rate

during potentiodynamic polarization measurements all had an impact on the measured pitting risk and thus the derived threshold  $[Cl^-]/[OH^-]$  of steel rebar [25].

#### ***B4.7. Limitations and Practical Implications of Research Findings***

Cement hydrates in concrete can produce hydroxyls for the concrete pore solution and provide buffering capacity to resist to possible pH drop in the electrolyte. Such pH drop could be the result of concrete carbonation, active corrosion of rebar, or ingress of deleterious species. In concrete, there is often the separation of anode and cathode areas on the rebar surface and the electrical resistivity of concrete thus plays a significant role in both the pitting initiation and pitting propagation on the steel surface. The buildup of corrosion products at the anode areas (and subsequent localized acidification) or the availability of oxygen at the cathode areas on the rebar in concrete can differ greatly from the case in the solutions. The chloride threshold,  $Cl_{th}$ , is typically higher for mortars and concretes than for solutions [6,12]. As such, while this study sheds light on the factors defining the chloride threshold of steel corrosion in concrete, the application of such knowledge to reinforced concrete should take into account the complications discussed above.

Another limitation of the findings from this study arises from the assumption used to simplify the model predictions, i.e., the effect of two independent variables could be examined and set other variables set at a specific level (e.g., Figures 4, 5, 7, 9 and 10). In real concrete, it would be unrealistic to expect a constant chloride binding level with varying pH or vice versa. It has been observed that the pH of NaCl-containing alkaline solution increases as the chloride binding increases [34]. Reducing the pH in concrete may destabilize the chloroaluminate and thus reduce the percent of bound chloride [8], and carbonation of concrete can reduce the chloride binding capacity [46] and facilitate the chloride intrusion [47]. It has been reported also that an increase in the pH above 12.6 produces a remarkable decrease in the level of the bound chloride [48,49].

Despite of these limitations, the findings from this study can still provide useful guidance in the effort of managing the chloride-induced corrosion of steel rebar in concrete. For reinforced concrete in chloride-laden environments, the time-to-active-corrosion of rebar ( $t_{in}$ ) and  $Cl_{th}$ , are two inter-related parameters that define its service life. The mix proportions, curing regime, construction quality and exposure history of concrete determine its physical microstructure (especially the tortuous pore structure of cement paste and interfacial transition zone adjacent to the aggregates surface) and chemical composition (including the amount of pore solution in the matrix), which in turn, determine the rate of chloride ingress into the concrete and thus the  $t_{in}$  [41]. The physiochemical properties of the concrete also determine the chloride binding capacity of the cementitious paste phase, the pH of the pore solution, the oxygen transport from the service environment and the physical condition of the steel/concrete interface. As discussed earlier, all of these factors significantly affect the  $Cl_{th}$  of a given rebar (with known composition, surface condition, and configuration) and thus the  $t_{in}$ . Furthermore, the physiochemical properties of the concrete determine its electrical resistivity which, along with oxygen availability, control the rate of rebar corrosion after initiation [41].

To enhance the chloride threshold of rebar and thus extend the service life of reinforced concrete, the following measures should be applied: (1) reduce the total chloride content at the rebar depth, by controlling the source of chloride and slowing down the chloride ingress (e.g., minimizing the application of deicing salts and using the less permeable concrete mixes); (2) increase the percent of bound chloride, which is affected by the  $C_3A$  and alkali contents of cement [50], use of supplementary cementitious materials (e.g., ground granulated blastfurnace slag and fly ash), temperature, and degree of hydration [34]; (3) increase the pH of concrete and minimize its carbonation; and (4) improve the physical condition of the steel/concrete interface and minimize the DO at the interface, by eliminating the bleeding/settlement/segregation of concrete and minimizing its cracking or by applying cement-based coating on rebar, etc. Note that the use of mineral admixtures in concrete affects the  $Cl_{th}$  and  $t_{in}$  through multiple mechanisms. The addition of fly ash or slag generally leads to the formation of less porous microstructure (and thus slowing down the ingress of chloride and oxygen), improvement in chloride binding, and reduction of pore solution pH [6,41,51-58], and likely increases the electrical conductivity of the concrete. The addition of silica fume into concrete reduces the pore solution pH and the chloride binding, but also slows down the chloride ingress and reduces the DO in concrete [58-61].

## B5. Conclusions

This work presents a systematic study aimed to provide quantitative understanding of the fundamental factors that influence the chloride threshold of pitting corrosion of steel in concrete, by conducting a set of laboratory tests to assess the corrosion potential ( $E_{corr}$ ) and pitting potential ( $E_{pit}$ ) of steel coupons in simulated concrete pore solutions. With the aid of an artificial neural network (ANN), the laboratory data were then used to establish a phenomenological model correlating the influential factors (total chloride concentration, chloride binding, solution pH, and dissolved oxygen concentration) with the pitting risk (characterized by  $E_{corr} - E_{pit}$ ). Three-dimensional response surfaces were then constructed to illustrate such predicted correlations and to shed light on the complex interactions between various influencing factors. The results indicate that the threshold  $[Cl^-]/[OH^-]$  of steel rebar in simulated concrete pore solutions is a function of solution DO, pH and chloride binding, and is not a unique value. The limitations and practical implications of the research findings were also discussed.

## B6. References

- [1] Schiessl P, Raupach M. Influence of concrete composition and microclimate on the critical chloride content in concrete, in: C. L. Page, K. W. J. Treadaway, P. B. Bamforth (Eds.), *Corrosion of Reinforcement in Concrete*, Elsevier Applied Science, London UK, 1990, pp. 49–58.
- [2] Stratfull RF. The Corrosion of Steel in a Reinforced Concrete Bridge, *Corros* 1956; 13(3): 173-178.
- [3] Gouda VK, Corrosion and Corrosion Inhibition of Reinforcing Steel, *Br Corros J* 1970; 5(2): 198-202.

- [4] Glass GK, Buenfeld NR. The Presentation of the Chloride Threshold Level for Corrosion of Steel in Concrete, *Corros Sci* 1997; 39(5): 1001-1013.
- [5] Alonso C, Andrade C, Castellote M, Castro P. Chloride Threshold Values to Depassivate Reinforcing Bars Embedded in A Standardized OPC Mortar, *Cem Concr Res* 2000; 30(7): 1047-1055.
- [6] Glass GK, Buenfeld NR. Chloride-induced Corrosion of Steel in Concrete, *Prog Struct Engng Mater* 2000; 2: 448-458.
- [7] Angst U, Elsener B, Larsen CK, Vennesland Ø. Critical Chloride Content in Reinforced Concrete – A Review, *Cem Concr Res* 2009; 39: 1122-1138.
- [8] Ann KY, Song H-W. Chloride Threshold Level for Corrosion of Steel in Concrete, *Corros Sci* 2007; 49: 4113-4133.
- [9] Kayyali OA, Hague MN. Chloride Penetration and the Ratio of  $\text{Cl}^-/\text{OH}^-$  in the Pores of Cement Paste, *Cem Concr Res* 1988; 18: 895-900.
- [10] Hausmann DA. A Probability Model of Steel Corrosion in Concrete, *Mater Perform* 1998; 37(10): 64-68.
- [11] Yonezawa T, Ashworth V, Procter RPM. Pore Solution Composition and Chloride Effects on the Corrosion of Steel in Concrete, *Corros* 1988; 44(7): 489-493.
- [12] Breit W. Critical Chloride Content - Investigations of Steel in Alkaline Chloride Solutions, *Mater Corros* 1998; 49(6): 539-550.
- [13] Hartt WH, Nam J. Effect of Cement Alkalinity on Chloride Threshold and Time-to-Corrosion of Reinforcing Steel in Concrete, *Corros* 2008; 64(8): 671-680.
- [14] Dehwah HAF, Maslehuddin M, Austin, SA. Effect of Cement Alkalinity on Pore Solution Chemistry and Chloride-Induced Reinforcement Corrosion, *ACI Mater J* 2002; 99(3): 227-235.
- [15] Hassain SE, Al-Gahtani AS, Rasheeduzzafar. Chloride Threshold for Corrosion of Reinforcement in Concrete, *ACI Mater J* 1996; 93(6): 1-5.
- [16] Moreno M, Morris W, Alvarez MG, Duffó GS. Corrosion of Reinforcing Steel in Simulated Concrete Pore Solutions – Effect of Carbonation and Chloride Content, *Corros Sci* 2004; 46: 2681-2699.
- [17] Cros P, Hartt WH, Yu H. Effects of reinforcement on chloride intrusion into concrete and time-to-corrosion, in: Proceedings of the 16<sup>th</sup> International Corrosion Congress, September 22-26, 2005, Beijing, China.
- [18] Li L, Sagüés AA. Chloride Corrosion Threshold of Reinforcing Steel in Alkaline Solutions - Open-Circuit Immersion Tests, *Corros* 2001; 57(1): 19-28.
- [19] Alonso C, Castellote M, Andrade C. Chloride Threshold Dependence of Pitting Potential of Reinforcements, *Electrochim Acta* 2002; 47: 3469-3481.
- [20] Monfore GE, Verbeck GJ. Corrosion of Prestressed Wire in Concrete, *ACI Mater J* 1960; 57(5): 491-497.
- [21] Söylev TA, Francois R. Corrosion of Reinforcement in Relation to Presence of Defects at the Interface between Steel and Concrete, *J Mater Civil Eng* 2005; 17(4): 447-455.
- [22] Yu H, Himiob RJ, Hartt WH. Effects of Reinforcement and Coarse Aggregates on Chloride Ingress into Concrete and Time-to-corrosion: Part 2: Spatial Distribution of Coarse Aggregates, *Corros* 2007; 63(10): 924-931.

- [23] Yu H, Shi X, Hartt WH, Lu B. Laboratory Investigation of Reinforcement Corrosion Initiation and Chloride Threshold Concentration for Self-compacting Concrete, *Cem Concr Res* 2010; 40(10): 1507-1516.
- [24] Bertolini L, Elsener B, Pedferri P, Polder R. Corrosion of Steel in Concrete: Prevention, Diagnosis, Repair. Wiley-VCH, Verlag GmbH & Co. KgaA, Weinheim. 2004.
- [25] Li L, Sagüés AA. Metallurgical effects on chloride ion corrosion threshold of steel in concrete. Final Report for the Florida Department of Transportation. Tallahassee, FL. Report No. WPI 0510806. November 2001.
- [26] Shi X, Schillings P, Boyd D. Applying Artificial Neural Networks and Virtual Experimental Design to Quality Improvement of Two Industrial Processes, *Intl J Prdn Res* 2004; 42(1): 101-108.
- [27] Shi X, Liu Y, Mooney M, Berry M, Hubbard B, Nguyen TA. Laboratory Investigation and Neural Networks Modeling of Deicer Ingress into Portland Cement Concrete and Its Corrosion Implications, *Corros Rev* 2010; 28(3-4): 105-153.
- [28] Hospadaruk V, Petrocelli JV. The Pitting Potential of Stainless Steels in Chloride Media, *J Electrochem Soc* 1966; 113(9): 878-883.
- [29] Huijbregts WMM. Oxygen and Corrosion Potential Effects on Chloride Stress Corrosion Cracking, *Corros* 1986; 42(8): 456-462.
- [30] Kim HT, Paik CH, Cho WI, Cho BW, Yun KS, Kim YH, Ju JB, Kim JS, Kang MS, Ha JS, Kim KY. Effect of Dissolved Oxygen and Hydrogen Ion on Corrosion Rate and Passivation of Carbon Steel Boiler Tube, *J Ind Eng Chem* 1997; 3(1): 51-55.
- [31] Al-Kharafi FM, Ateya BG, Abdallah RM. Electrochemical Behaviour of Low Carbon Steel in Concentrated Carbonate Chloride Brines, *J Appl Electrochem* 2002; 32(12): 1363-1370.
- [32] Leckie HP, Uhlig HH. Environmental Factors Affecting the Critical Potential for Pitting in 18-8 Stainless Steel, *J Electrochem* 1966; 113(12): 1262-1267.
- [33] Berman HA. Determination of Chloride in Hardened Portland Cement Paste, Mortar, and Concrete, *J Mater* 1972; 7(3): 330-335.
- [34] Harald J. A Review of Chloride Binding in Cementitious Systems, *Nordic Concr Res* 1998; 21: 1-6.
- [35] Anik D, Jacques M, Jean-Pierre O, Simone J, Kati H. Chloride Binding Capacity of Various Hydrated Cement Systems, *Adv Cem-Based Mater* 1997; 6: 28-35.
- [36] Buenfeld NR, Glass GK, Hassanein AM, Zhang J.-Z. Chloride Transport in Concrete Subjected to an Electric Field, *J Mater Civ Eng* 1998; 10(4): 220-228.
- [37] Kayyali OA, Haque MN. The  $Cl^-: OH^-$  Ratio in Chloride-Contaminated Concrete – A Most Important Criterion, *Mag Concr Res* 1995; 47: 235-242.
- [38] Suryavanshi AK, Scantlebury JD, Lyon SB. Corrosion of Reinforcement Steel Embedded in High Water-Cement Ratio Concrete Contaminated with Chloride, *Cem Concr Compos* 1998; 20(3): 263-269.
- [39] Glass GK, Buenfeld NR. The Influence of Chloride Binding on the Chloride-Induced Corrosion Risk in Reinforced Concrete. *Corros Sci* 2000; 42(2): 329-344.

- [40] Reddy B, Glass GK, Lim PJ, Buenfeld NR. On the Corrosion Risk Presented by Chloride Bound in Concrete, *Cem Concr Compos* 2002; 24(1): 1–5.
- [41] Hansson CM, Sørensen B. The threshold concentration of chloride in concrete for the initiation of reinforcement corrosion, in: N.S. Berke, V. Chaker, and D. Whiting (Eds.), *Corrosion Rates of Steel in Concrete*, ASTM STP 1065, American Society for Testing and Materials, Philadelphia, USA, 1990, pp. 3-16.
- [42] Pillai RG, Trejo D. Surface Condition Effects on Critical Chloride Threshold of Steel Reinforcement, *ACI Mater J* 2005; 102(2): 103-109.
- [43] Treadaway KWJ, Brown BL, Cox RN. Durability of galvanized steel in concrete, in: D.E. Tonini, J.M. Gaidis (Eds.), *Corrosion of Reinforcing Steel in Concrete*, ASTM STP 713, 1978, pp. 102–131.
- [44] Stark D. Measurement techniques and evaluation of galvanized reinforcing steel in concrete structures in Bermuda, in: D.E. Tonini, J.M. Gaidis (Eds.), *Corrosion of Reinforcing Steel in Concrete*, ASTM STP 713, 1978, pp. 132–141.
- [45] Hurley MF, Scully JR. Threshold Chloride Concentrations of Selected Corrosion-Resistant Rebar Materials Compared to Carbon Steel, *Corros* 2006; 62(10): 892-904.
- [46] Neville A. Chloride Attack of Reinforced Concrete: an Overview, *Mater Struct* 1995; 28: 63-70.
- [47] Traetteberg A. The mechanism of chloride penetration in concrete, SINTEF Report STF65 A77070, 1977, 51 pp.
- [48] Tritthart J. Chloride Binding: II. The Influence of the Hydroxide Concentration in the Pore Solution of Hardened Cement Paste on Chloride Binding, *Cem Concr Res* 1989; 19: 683–691.
- [49] Glass GK, Hassanein NM, Buenfeld NR. Neural Network Modelling of Chloride Binding, *Mag Concr Res* 1997; 49: 323–335.
- [50] Rasheeduzzafar, Hussain SE, Al-Saadoun SS. Effect of Cement Composition on Chloride Binding and Corrosion of Reinforcing Steel in Concrete, *Cem Concr Res* 1991; 21(5): 777-794.
- [51] Arya C, Buenfeld, NR, Newman JB. Factors Influencing Chloride Binding in Concrete, *Cem Concr Res* 1990; 20(2): 291–300.
- [52] Dhir RK, Jones MR. Development of Chloride-Resisting Concrete Using Fly Ash, *Fuel* 1999; 78: 137-142.
- [53] Diamond S. Two Danish Flyashes on Alkali Contents of Pore Solutions of Cement-Flyash Pastes, *Cem Concr Res* 1981; 11: 383–394.
- [54] Kawamura M, Kayyali OA, Haque MN. Effect of Flyash on Pore Solution Composition in Calcium and Sodium Chloride-Bearing Mortars, *Cem Concr Res* 1988; 18: 763–773.
- [55] Dhir RK, El-Mohr MAK, Dyer TD. Chloride Binding in GGBS Concrete, *Cem Concr Res* 1996; 26: 1767–1773.
- [56] Luo R, Cai YB, Wang CY, Huang XM. Study of Chloride Binding and Diffusion in GGBS Concrete, *Cem Concr Res* 2003; 33: 1–7.
- [57] Cheng A, Huang R, Wu J-K, Chen C-H. Influence of GGBS on Durability and Corrosion Behavior of Reinforced Concrete, *Mater Chem Phys* 2005; 93: 404-411.

- [58] Byfors K. Influence of Silica Fume and Flyash on Chloride Diffusion and pH Values in Cement Paste, *Cem Concr Res* 1987; 17: 115–130.
- [59] Page CL, Vennesland Ø. Pore Solution Composition and Chloride Binding Capacity of Silica Fume-Cement Pastes, *Mater Struct* 1983; 19: 19-25.
- [60] Page CL, Havdahl J. Electrochemical Monitoring of Corrosion of Steel in Microsilica Cement Pastes, *Mater Struct* 1985; 18: 41-47.
- [61] Manera M, Vennesland Ø, Bertolini L. Chloride Threshold for Rebar Corrosion in Concrete with Addition of Silica Fume, *Corros Sci* 2008; 50: 554-560.
- [62] Escalante E, Ito S. Measuring the rate of corrosion of steel in concrete, in: N.S. Berke, V. Chaker, and D. Whiting (Eds.), *Corrosion Rates of Steel in Concrete*, ASTM STP 1065, American Society for Testing and Materials, Philadelphia, USA, 1990, pp. 86-102.

## APPENDIX C. MODELING CATHODIC PREVENTION FOR UNCONVENTIONAL CONCRETE IN SALT-LADEN ENVIRONMENT

Currently there is a void of knowledge base regarding the use of cathodic prevention (CPre) to protect reinforced concrete structures from chloride attack, especially when the concrete is made with mineral admixtures partially replacing cement. This appendix chapter aims to provide a modeling perspective relevant to the use of CPre for unconventional concrete in salt-laden environment. Based on the experimentally obtained concrete resistivity and chloride diffusion coefficient data, numerical studies with the Nernst-Planck equations were conducted to investigate the influence of applied voltage (magnitude, direction, and interruption), surface chloride concentration, and concrete mix design on the effectiveness of cathodic prevention and the distribution of ionic species in protected concrete. The modeling results revealed that the direction of applied electric voltage has significant effect on the distributions of electrical potential and hydroxyl ions in the reinforced concrete, confirming the benefits of cathodic prevention in significantly increasing hydroxyl concentration near rebar and in slowing down the ingress of chloride ingress into concrete. The performance of intermittent CPre was found to be constrained by the variations in concrete resistance from the anode to the cathode. The model was also useful in illustrating the temporal and spatial evolutions on rebar surface in terms of oxygen, hydroxyl and chloride concentrations on and electrical potential of top rebar as well as such evolutions in concrete domain in terms of concrete resistivity and current density for each mix design. The results reported herein shed light on the fundamental processes defining the performance of CPre for new unconventional concrete in salt-laden environment.

### C1. Introduction

As an economical and durable composite, steel reinforced concrete has been widely utilized in construction projects worldwide. Chlorides, from road salts used in cold-climate regions for winter service, from marine environments, or from raw materials used to make concrete, pose significant risk to the steel reinforcement in concrete (Gjørsv and Vennesland, 1979; Enevoldsen *et al.* 1994; Manera *et al.* 2008; Liu and Shi, 2009a; Shi *et al.* 2009). Chloride-induced corrosion of steel may cause premature and difficult-to-predict failure of reinforced concrete and compromise their durability and reliability, with tremendous economic and safety implications. While the reinforcing steel is normally protected by a nanometer-thin oxide/hydroxide passive film formed in the highly alkaline concrete environment, such passive film can be broken down locally once sufficient airborne carbon dioxide penetrates into the concrete to significantly reduce its alkalinity or once sufficient chloride anions reach the rebar surface (Thomas 1996; Sergi and Glass 2000; Orlikowski *et al.* 2004; Ann and Song 2007; Zornoza *et al.* 2008; Poursaee and Hansson 2009). The corrosion process generally consists of a cathodic half-reaction (e.g.,  $2\text{H}_2\text{O} + \text{O}_2 + 4\text{e}^- \rightarrow 4\text{OH}^-$ ) and an anodic half-reaction (e.g.,  $\text{Fe} + 2\text{Cl}^- \rightarrow \text{FeCl}_2 + 2\text{e}^-$ ), among other possible chemical reactions (e.g.,  $\text{Fe}^{+2} + 2\text{H}_2\text{O} \rightarrow \text{Fe}(\text{OH})_2 + 2\text{H}^+$  and  $4\text{Fe}(\text{OH})_2 + \text{O}_2 \rightarrow 4\gamma\text{-FeOOH} + 2\text{H}_2\text{O}$ ). The corrosion of reinforcing steel in concrete can be divided into two main stages: first the time for aggressive species to penetrate the heterogeneous concrete matrix in order to

depassivate the rebar surface and then the time for corrosion propagation in concrete. Once the localized corrosion of steel (pitting) is initiated, the corrosion products start to form on the rebar surface and exert expansive stresses that ultimately crack the concrete surrounding the rebar. As such, the corrosion of rebar not only leads to its section loss in a localized manner, but more importantly the loss of rebar/concrete bond and aggravated ingress of deleterious species into concrete (Andrade *et al.* 2001), all of which accelerates the deterioration of concrete.

Cathodic protection (CP) has proven to be a non-destructive technique to mitigate chloride-induced corrosion of rebar in concrete by providing a cathodic current so that the rebar potential ( $E$ ) is shifted to a more negative value (Liu and Shi 2009b). The cathodic polarization of rebar is designed to induce protecting effects both thermodynamically and kinetically, by reducing the driving force for the anodic process (i.e., the difference between corrosion potential and equilibrium potential,  $E_{\text{cor}} - E_{\text{eq}}$ ) and by reducing the corrosion rate of the anodic process (as steel is brought from activity to passivity zone) (Pedferri 1996; Bertolini *et al.* 1998 and 2002). CP can also consume the oxygen and produce  $\text{OH}^-$  ions on the rebar surface and oppose the penetration of  $\text{Cl}^-$  ions into concrete, thus causing the following beneficial effects: widening of the passive region, depolarization of the cathodic process, and hindering localized acidification and thus affecting pitting initiation and propagation (Pedferri 1994). Furthermore, CP is known to potentially cause the degradation of concrete containing alkali-reactive aggregates, to affect the adhesion of non-ribbed rebars to concrete, or to cause hydrogen embrittlement of high strength steels in concrete that is overprotected and/or has very low oxygen availability (with the following cathodic half-reaction:  $\text{H}^+ + \text{e} \rightarrow \text{H}^\circ$ ).

Extensive studies since 1970s have been dedicated to the use of CP to control corrosion rate of chloride-contaminated concrete (Liu and Shi 2009b), whereas the use of CP on new concrete structures (referred to as cathodic prevention, or CPre) in salt-laden environments has been much less investigated despite some published studies since 1990s (Pedferri 1996; Bertolini *et al.* 1993, 1998, 1999 and 2002; Bertolini 2000). CPre works by principles similar to conventional CP and the two share the “4h 100 mV potential decay” empirical criterion for verifying the actual protection achieved in reinforced concrete (Bertolini *et al.* 1998 and 2002) but feature significantly different levels of protective current required ( $i_p$ , relative to rebar surface area). Conventional CP aims to either reduce the rate of pitting propagation or restore the rebar passivity after active pitting has initiated, with  $i_p$  of up to  $15 \text{ mA m}^{-2}$  or with  $i_p$  of  $20 \text{ mA m}^{-2}$  or more respectively for aerial concrete structures. CPre aims to ensure that pitting does not initiate by applying the protective current from the early stage of service life when the chloride-induced corrosion has not initiated (Pedferri 1996), with  $i_p$  lower than  $2 \text{ mA m}^{-2}$  for aerial concrete structures and as low as  $0.2 \text{ mA m}^{-2}$  for immersed concrete structures. In CPre systems, the protective current in the range of 1 to  $2 \text{ mA m}^{-2}$  can produce a potential drop of at least 100-200 mV and thus enhances the threshold chloride content (to initiate rebar pitting in concrete) by at least one order of magnitude (Bertolini *et al.* 1998). CPre also features protective potentials typically 200 mV more positive than those for conventional CP, posing less demand on anodes. Finally, CPre

can extend its beneficial effects “to rebars at remarkable distances from the anode” whereas conventional CP has its effects “usually limited to distances of a few tens of centimeters” (Bertolini *et al.* 2002).

The last decade has seen a paradigm shift from conventional Portland cement concrete (PCC) to so-called environmentally friendly concretes (EFCs) with reduced environmental footprint, generally by incorporating recycled materials or industrial byproducts. One type of EFCs that have gradually entered the engineering practice is the ones with mineral admixtures to partially replace Portland cement in concrete. The use of mineral admixtures such as fly ash, silica fume, slag and metakaolin has been shown to enhance concrete durability (Toutanji and Delatte 2001; Gruber *et al.* 2001; Choi *et al.* 2006), by increasing chloride binding (Lu *et al.* 2002), decreasing chloride permeability (Thomas *et al.* 1999; Choi *et al.* 2006), elevating threshold chloride content (Manera *et al.* 2008), and/or improving the distribution of pore size and shape of concrete matrix (Yang and Cho 2003). Since some of these materials are cheaper than Portland cement, there is also an economic advantage to wider use. For a concrete mix with water-to-cementitious-materials ( $w/cm$ ) ratio of 0.37, the addition of fly ash (35% cement replacement) and silica fume (27% cement replacement) reduced the chloride diffusion coefficient from  $3.48 \times 10^{-12} \text{ m}^2/\text{s}$  to  $7.35 \times 10^{-13} \text{ m}^2/\text{s}$  and  $1.01 \times 10^{-12} \text{ m}^2/\text{s}$ , but also reduced the pore water pH from 13.84 to 13.39 and 13.47, respectively (Hartt *et al.* 1999). Concrete mixes with high-volume fly ash have demonstrated good workability and high compressive strength, in addition to excellent durability behavior (Collepardi *et al.* 2000).

Currently there is a void of knowledge base regarding the use of CPre to protect reinforced concrete structures from chloride attack, especially when the concrete is made with mineral admixtures partially replacing cement. Traditionally, laboratory or field exposure tests have been used to characterize the corrosion behavior of rebar in concrete and to evaluate the effectiveness of CPre. Such tests, however, tend to produce findings that are not transferrable to other experimental conditions. To mitigate this, computational modeling based on physically sound principles can be utilized to provide quantitative information to estimate service performance and to provide guidance for practical applications (Kranc and Sagues 1993 and 2001; Rabiot *et al.* 1999; Riemer and Orazem 2005; Dridi *et al.* 2006). As such, this work aims to provide a modeling perspective relevant to the use of cathodic prevention for unconventional concrete in salt-laden environment, with a focus on how various operating parameters affect the CPre effectiveness and the distribution of ionic species in protected concrete.

## **C2. Methodology**

### ***C2.1. Experimental***

Three duplicate cylindrical concrete samples were constructed for each of the three mixes (75% Portland cement-25% Class F fly ash; 90% Portland cement-10% silica fume; or 90% Portland cement-10% metakaolin), featuring a  $w/cm$  ratio of 0.40. Table 1 presents their mix designs and fresh concrete properties.

TABLE 1 Mix design and properties of concrete samples containing various types and amounts of mineral admixtures

Ingredients	Mix Number		
	A	B	C
Portland Cement (lb)	56	68	68
Fly Ash (Class F) (lb)	19	-	-
Silica Fume (lb)	-	8	-
Metakaolin (lb)	-	-	8
Micro Air™ (ml)	33	-	22
Glenium 3030™ (ml)	24	266	238
Water (lb)	28	28	28
Fine Aggregate (lb)	127.3	140.3	128.95
Moisture Content (%)	3.6	3.6	3.6
Course Aggregate (lb)	192.8	211.8	195.1
Moisture Content (%)	0.96	0.647	0.886
Slump (inches) by ASTM C 143	3.5	2.25	3.5
Air Content (%) by ASTM C173	5.5	2.25	6
Volume (ft <sup>3</sup> )	3	3	3

In the first 24 hours of molding, the concrete specimens were placed on a rigid surface under ambient temperature and at a relative humidity of about 50 percent and covered to prevent excessive evaporation of water. Next, the specimens were de-molded and cured in a moist cure room with relative humidity of 98% for 90 days. Once out of the moisture room, each concrete sample was ponded with distilled water for 2 hours to be fully saturated. Thereafter, a direct voltage of 8 volts was applied across the 6-inch (152-mm) distance between the two ends of the concrete cylinder, with the external anode (stainless steel mesh with a diameter of 8 or 203 mm) and the external cathode (galvanized steel plate with a diameter of 12 or 305 mm) ponded by weekly -replaced 3% NaCl and simulated concrete pore solution (0.32 mol/L KOH, 0.17 mol/L NaOH, and 0.07 mol/L Ca(OH)<sub>2</sub> in distilled water) respectively. The electric current flowing through the two external electrodes was monitored by measuring the potential drop over a 100-ohm

standard resistor connecting the external anode with the external cathode. All readings were taken every day in the early days and gradually down to two or three times per week. As such, the concrete resistivity for each unconventional concrete mix (with three duplicates) was periodically measured for 40 days. The apparent chloride diffusion coefficient for each concrete mix (with three duplicates) was measured using a modified Rapid Chloride Permeability Test, the details of which have been reported elsewhere (Yang *et al.* 2009).

## C2.2. Model Description

The electron transfer between anodic and cathodic sites establishes the electric current flow necessary for electrochemical corrosion. The key element to successful modeling of such corrosion demands the quantitative understanding of electrode kinetics and current flow through the electrolyte. Assuming that the electrolyte in concrete is dilute enough so that the activity of each species is equivalent to its concentration, the diffusion flux of species  $i$  in a pore solution can be described by the extended Nernst-Planck equation as follows (Andrade *et al.* 1995; Yu and Page 1996; Hassanein *et al.* 1998; Samson *et al.* 2000; Wang *et al.* 2001; Gardner *et al.* 2004):

$$J_i = -D_i \nabla C_i - \frac{D_i}{RT} C_i F Z_i \nabla \phi \quad (1)$$

where  $D_i$  is the diffusion coefficient of species  $i$ ;  $C_i$  is the concentration of species  $i$  in pore solution;  $F$  is the Faraday constant;  $Z_i$  is the charge of species  $i$ ; and  $\phi$  is the electric potential.

The macroscopic description of mass conservation relies on the homogenization technique, where physical quantities are averaged over a representative elementary volume. Based on such treatment, all the equations are written on the microscopic scale, the application of which yields the following relation (Wang *et al.* 2001):

$$p \frac{\partial C_i}{\partial t} + (1-p) \frac{\partial S_i}{\partial t} + \nabla \cdot (p J_i) = 0 \quad (2)$$

where  $p$  is the porosity;  $S_i$  is the bound concentration of species  $i$  that follows a Langmuir relation with the corresponding free concentration. For simplicity, only chloride binding is considered in this work. In the model, seven ionic species, i.e.  $\text{Na}^+$ ,  $\text{K}^+$ ,  $\text{Ca}^{2+}$ ,  $\text{Mg}^{2+}$ ,  $\text{Fe}^{2+}$ ,  $\text{OH}^-$  and  $\text{Cl}^-$ , are taken into consideration.

Under an externally applied electric field, the current density is contributed by the fluxes of all the cations and anions in the pore solution, which is characterized by (Wang *et al.* 2001):

$$i = pF \sum_{i=1}^n Z_i \left( -D_i \nabla C_i - \frac{Z_i F D_i}{RT} C_i \nabla \phi \right) \quad (3)$$

The evolution of electrical potential can be described by:

$$\nabla \cdot (-k \nabla \phi) = 0 \quad (4)$$

where  $k$  is the electric conductivity.

Under the natural corrosion state, the presence of dissolved oxygen around rebar plays a vital role for the active corrosion of rebar, in light of the common cathodic half-reaction ( $2\text{H}_2\text{O} + \text{O}_2 + 4\text{e} \rightarrow 4\text{OH}^-$ ). The migration and distribution of oxygen molecules in pore solution can be described by the mass conservation law as:

$$p \frac{\partial C_o}{\partial t} + \nabla \cdot (-pD_o \nabla C_o) = 0 \quad (5)$$

where  $C_o$  is the oxygen concentration;  $D_o$  is the oxygen diffusion coefficient.

The boundary of the simulation domain is defined by the surface area of the anode and cathode as well as the external surface of the concrete. The metal dissolution and oxygen consumption reactions are accompanied by local current exchange on electrode surface, where chemical species can be produced or consumed. Boundary conditions at the rebar surface can be formulated from the electrochemical reactions, which describe the rate of oxidation and reduction processes and can be expressed mathematically as nonlinear relations with the current density and potential.

Provided that the active corrosion on rebar is controlled by oxygen supply, the boundary condition can be formulated as follows (Riemer and Orazem 2005):

$$\frac{i}{4F} = D_{O_2} \frac{\partial C_{O_2}}{\partial n} \quad (6)$$

where the factor 4 arises from the number of electrons in the reduction reaction with one mole of  $\text{O}_2$ .

At the rebar surface, the metal dissolution and oxygen reduction need to be modeled, taking into account the polarization behaviors. Formulations based on anodic and cathodic reactions follow (Kranc and Sagues 2001):

$$i_a = i_{0a} e^{\frac{E_{0a} - \phi_s}{\beta_a}} \quad (7)$$

$$i_c = i_{0c} \frac{C_{O_2}}{C_{O_2}^0} e^{-\frac{\phi_s - E_{0c}}{\beta_c}} \quad (8)$$

where  $i_{0a}$  and  $i_{0c}$  are the exchange current density for the anodic and cathodic reactions respectively;  $C_{O_2}^0$  is the critical oxygen concentration on rebar surface;  $\beta_a$  and  $\beta_c$  are the Tafel slopes for the anodic and cathodic reactions, respectively;  $\phi_s$  is the surface potential of rebar. The net current density on steel surface is thus the summation of the partial anodic and cathodic current, which follows (Dridi et al. 2006):

$$i = i_a + i_c \quad (9)$$

In the vicinity of rebar surface, the concentrations of  $\text{Fe}^{2+}$  and  $\text{OH}^-$  are governed by local equilibrium, as their concentrations cannot change independently. As such, the rate of  $\text{Fe}(\text{OH})_2$  formation is assumed to be large enough so that local equilibrium is maintained as follows:

$$C_{\text{OH}^-}^2 \cdot C_{\text{Fe}^{2+}} = k_{\text{Fe}(\text{OH})_2} \quad (10)$$

where  $k_{Fe(OH)_2}$  is the equilibrium constant for  $Fe(OH)_2$ .

In the absence of external electric field, the boundary conditions on rebar surface are such that the normal fluxes of  $Na^+$ ,  $K^+$ ,  $Ca^{2+}$ ,  $Mg^{2+}$  and  $Cl^-$  are zero, while the normal fluxes of  $Fe^{2+}$  and  $O_2$  are described by:

$$n \cdot \vec{J}_{Fe} = -\phi_a \quad (11)$$

$$n \cdot \vec{J}_{O_2} = 0.5\phi_c \quad (12)$$

In addition, it follows that:

$$i = 0 \quad (\phi_a = \phi_c) \quad (13)$$

$$\phi_s = E_{Corr} \quad (14)$$

$$i_a = -i_c = i_{corr} \quad (15)$$

where  $E_{Corr}$  and  $i_{corr}$  are the corrosion potential and corrosion current, respectively.

### C3. Results

As shown in Fig. 1, a concrete domain measuring  $0.12 \times 0.02 \times 0.08$  m is constructed to computationally model CPre, with rebars featuring a diameter of 0.01 m embedded through the length-height cross section of the simulation domain. A thick concrete cover thickness of 0.045 m is assumed for the immersed concrete structure. Under an externally applied electrical field, all the ionic species in the concrete pore solution contribute to the total current flux. To determine the electrochemical response of a concrete system, the finite element method (FEM) investigation needs to account for each of the seven ionic species ( $Na^+$ ,  $K^+$ ,  $Ca^{2+}$ ,  $Mg^{2+}$ ,  $Fe^{2+}$ ,  $OH^-$ , and  $Cl^-$ ) as well as dissolved oxygen ( $O_2$ ). The computational simulation is accomplished by specifying initial conditions within concrete domains and boundary conditions at the internal and external surfaces. The initial values for concentrations of  $Na^+$ ,  $K^+$ ,  $Ca^{2+}$ ,  $Mg^{2+}$ ,  $Fe^{2+}$ ,  $OH^-$ ,  $Cl^-$ , and  $O_2$  are chosen as: 100, 100, 50, 50, 0, 400, 0 and 0 mol/m<sup>3</sup>, respectively. The effective chloride diffusion coefficient ( $D_{eff}$ ) for mix design A, B, and C is taken as  $4.0 \times 10^{-13}$  m<sup>2</sup>/s, which for each mix design was averaged from apparent chloride diffusion coefficient ( $D_{app}$ ) measured with three duplicate concrete disc specimens. The diffusion coefficients of  $Na^+$ ,  $K^+$ ,  $Ca^{2+}$ ,  $Mg^{2+}$ ,  $Fe^{2+}$ ,  $OH^-$  are taken from the work of Kranc and Sagues (2001) and Wang *et al.* (2001). The concrete conductivity is a material property necessary for simulation, which is essential to reflect the constituents and microstructures of concrete. In this study, the experimentally obtained resistivity data over the 40-day monitoring time period were fed into the FEM model for each unconventional concrete mix. The parameters to characterize the polarization response of rebar are taken from the work of Kranc and Sagues (2001). The top boundary in Fig. 1 is adjacent to an electrolyte solution in which species are maintained at constant concentrations for  $Na^+$ ,  $K^+$ ,  $Ca^{2+}$ ,  $Mg^{2+}$ ,  $Fe^{2+}$ ,  $OH^-$ ,  $Cl^-$  and  $O_2$ , i.e. 100, 100, 50, 50, 0, 300, 100 and 0 mol/m<sup>3</sup>, respectively. The left-hand, right-hand, front and rear boundaries are treated with periodic boundary conditions, assuming that the concrete domain being analyzed is from a concrete structure that includes multiple identical domains. The Neumann boundary condition is applied to the bottom boundary with zero fluxes for all the ionic species. As for  $OH^-$  ions on rebar, the Neumann boundary

condition is such that the amount of hydroxyl ion flux generated on rebars corresponds to the current flux.

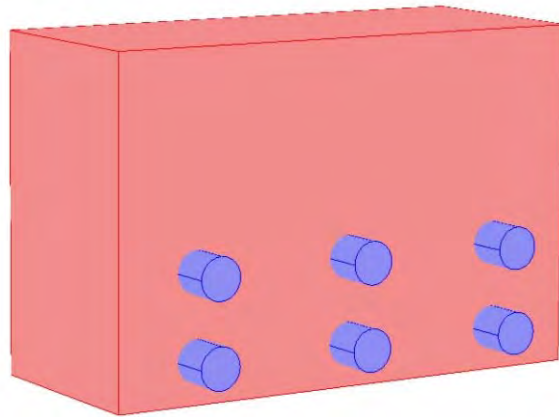
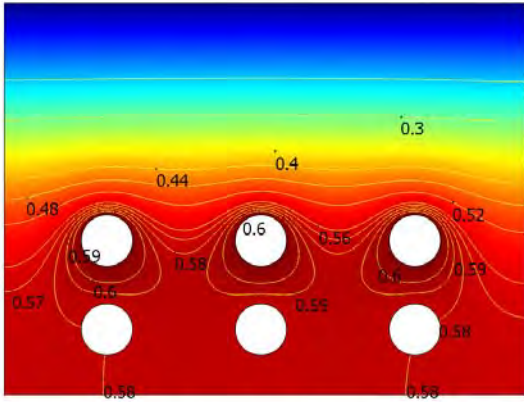
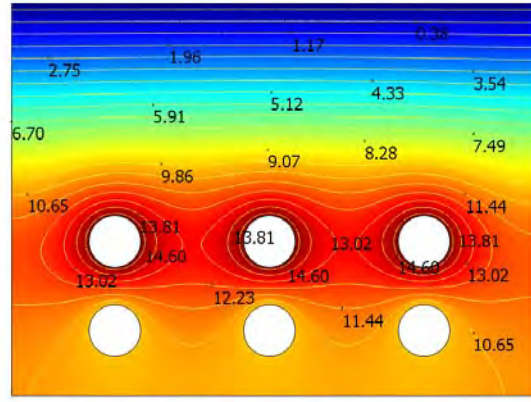


FIGURE 1 Model setup for the cathodic prevention (with concrete domain in red and rebar domain in blue)

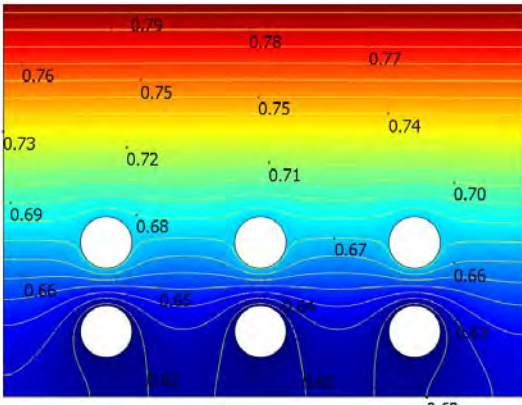
To explore the effect of voltage magnitude and direction on cathodic prevention, electric potential and hydroxyl ion distributions are predicted at three levels of voltages (800, 0 and -800 mV) applied for one year on concrete with mix design A. Such a combination of applied voltage, treatment time and ionic species distribution leads to a comprehensive computational investigation with the aid of FEM. Considering that the anodic and cathodic currents on steel rebar will be significantly different when different external voltage is applied, the potential distribution profiles were obtained, using the governing equations described above. The distribution of electric potential and hydroxyl ions is shown in Fig. 2.



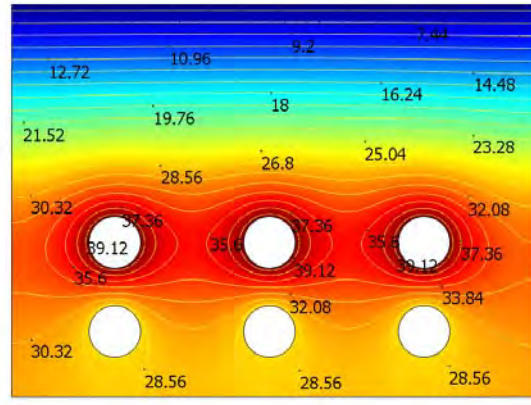
(a) Electrical Potential (0 mV)



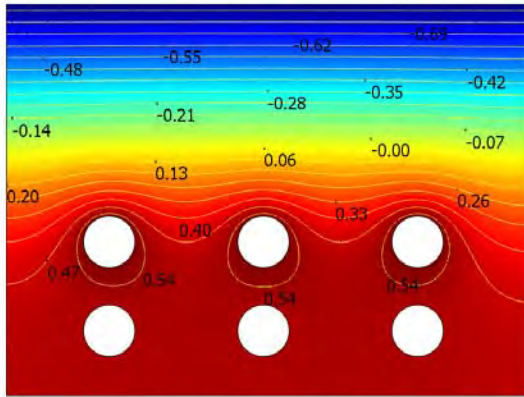
(b)  $\text{OH}^-$  ( $C_{\text{OH}^-} = 400 \text{ mM}$ , 0 mV)



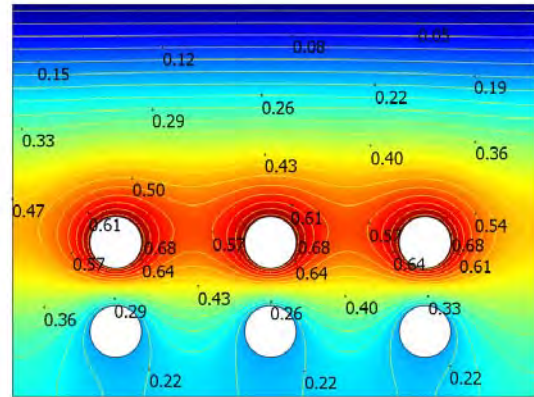
(c) Electrical Potential (800 mV)



(d)  $\text{OH}^-$  ( $C_{\text{OH}^-} = 400 \text{ mM}$ , 800 mV)



(e) Electrical Potential (-800 mV)

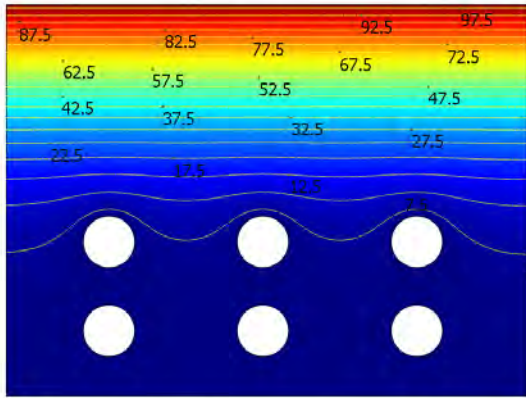


(f)  $\text{OH}^-$  ( $C_{\text{OH}^-} = 400 \text{ mM}$ , -800 mV)

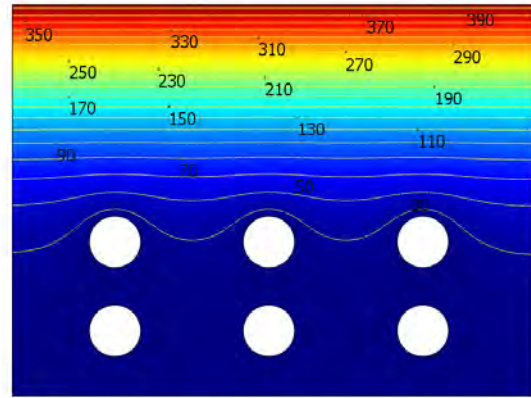
FIGURE 2 Distributions of the electrical potential and hydroxyl ion concentration under various polarization conditions.

To explore the effect of surface chloride concentration on cathodic prevention, Fig. 3 depicts the chloride distribution in concrete from mix design A treated with 0, 500 and 800 mV for 8 years, where the concrete top boundary is characterized by a chloride concentration of 100 and 400 mol/m<sup>3</sup>, respectively. The effect of concrete constituents on cathodic prevention is studied by exploring the FEM-predicted system properties. Simulation results obtained using three different concrete mix designs are shown in Fig. 4 with the external top surface polarized to 800 mV, where the calculated integral and local quantities are presented. The integral is performed across the concrete domain while the local characteristics are evaluated on the top rebar surface. The integral quantities include concrete resistivity and current density against time, while the local characteristics comprise oxygen concentration, chloride concentration, hydroxyl concentration, and electrical potential on top rebar surface.

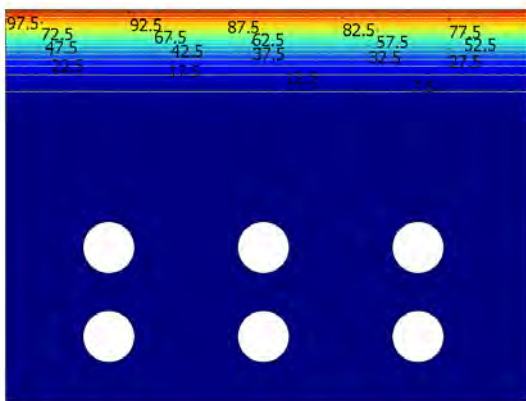
To explore the effect of voltage interruption on cathodic prevention, the spatial distribution of Na<sup>+</sup>, K<sup>+</sup>, OH<sup>-</sup> and Cl<sup>-</sup> as a distance from the two rebar rows is presented in Fig. 5. While the applied potential is switched off periodically, the migration of oxygen is not influenced. As such, for a prolonged period in CPre, the dissolved oxygen throughout the concrete domain can be treated as homogeneous. When the CPre is periodically switched off, dissolved oxygen is responsible for active corrosion on rebar surface or passive film disruption with the arrival of chloride ions.



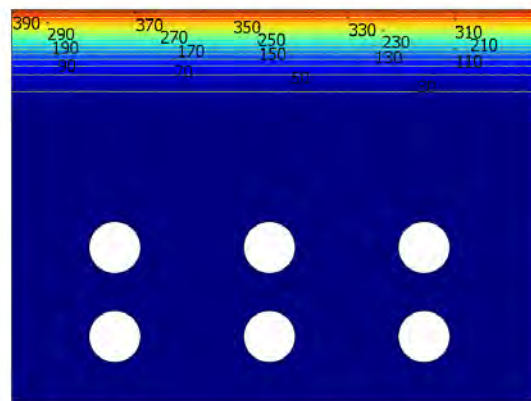
(a)  $\text{Cl}^-$  (0 mV, 100 mM  $\text{Cl}^-$ )



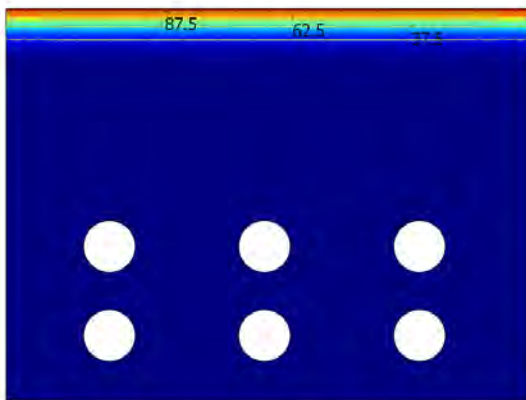
(b)  $\text{Cl}^-$  (0 mV, 400 mM  $\text{Cl}^-$ )



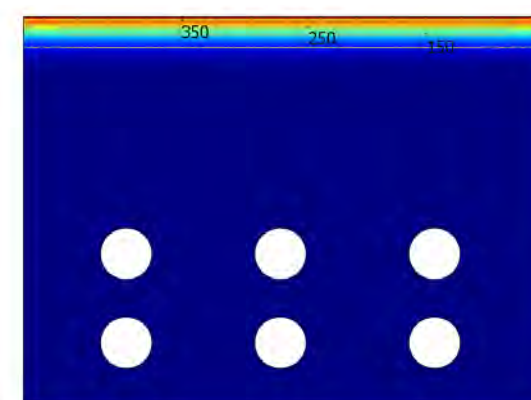
(c)  $\text{Cl}^-$  (500 mV, 100 mM  $\text{Cl}^-$ )



(d)  $\text{Cl}^-$  (500 mV, 400 mM  $\text{Cl}^-$ )



(e)  $\text{Cl}^-$  (800 mV, 100 mM  $\text{Cl}^-$ )



(f)  $\text{Cl}^-$  (800 mV, 400 mM  $\text{Cl}^-$ )

FIGURE 3 Effect of surface chloride concentration on cathodic prevention imposed on a concrete system for 8 years.

## C4. Discussion

### *C4.1. Effect of Voltage Magnitude and Direction on Cathodic Prevention*

Fig. 2 illustrates that the direction of applied electric voltage has significant effect on the distributions of electrical potential and hydroxyl ions in the reinforced concrete, confirming the benefits of cathodic prevention. The occurrence of rebar corrosion in concrete depends on the relative electric potential of rebars as well as the amount of protective hydroxyl ions and deleterious chloride ions. When there is no external voltage, the sum of all the partial currents around the active and passive regions on rebar should be zero. Fig. 2(a) shows the potential distribution within the concrete domain for the natural corrosion. Evidently, the natural corrosion with the aid of oxygen reduction and anodic dissolution gives rise to a potential of around 580 mV on rebar surface. Although the potential established on rebar surface contributes null net current in the concrete domain, the ionic species in concrete pore solutions can be drifted with the electric gradient developed in concrete domain, until an opposite electric field is established to offset the one imposed by electrodes. When the external electrode is set to be 800 mV in Fig. 2(c), the rebar potential is shifted to a more negative value by 59 mV, leading to an expectable decrease in rebar corrosion. Such a negative shift does not meet the 100 mV polarization criterion for adequate cathodic protection. However, under CPre, the potential of rebar can reach the values at which the anodic dissolution is no longer appreciable when sufficiently large driving voltage is applied. When the external electrode is set to be -800 mV in Fig. 2(e), the potential of rebar is shifted to a more positive value by 35 mV, which indicates an enhanced anodic dissolution that facilitates rebar degradation.

Among the three cases presented, the hydroxyl ion concentration in concrete exhibits distinct characteristics. The distribution of hydroxyl ions features a peak in Figs. 2(b) and 2(d) and a valley in Fig. 2(f) in the vicinity of rebar, due to the combined effect of diffusion and electromigration. Under the natural corrosion state, the hydroxyl ions are generated by the oxygen reduction, which depends on the oxygen supply from the external surrounding and the local equilibrium constrained by  $\text{Fe}(\text{OH})_2$  formation. The increase in hydroxyl ion concentration is consistent with the arrival of diffusion front for oxygen, beyond which the hydroxyl concentration remains almost unchanged, indicating a local equilibrium by  $\text{Fe}^{2+} + 2\text{OH}^- = \text{Fe}(\text{OH})_2$  in Fig. 2(b). The increase in oxygen diffusion coefficients can improve the concentration of oxygen near rebar, but shows little effect on changing hydroxyl ion concentration under the natural corrosion state. When an external voltage is applied so that the rebar is polarized to 800 mV, the generation of hydroxyl ions can be assisted with the aid of oxygen evolution on rebar surface, thereby resulting in much higher hydroxyl ion concentrations on rebar surface in Fig. 2(d). In other words, such cathodic prevention is beneficial in producing corrosion inhibitive  $\text{OH}^-$  ions near the rebar surface.

When an electric voltage of -800 mV is applied on the rebar, the evolution of hydroxyl ions on rebar surface is characterized by the arrival of  $\text{OH}^-$  formed on the external electrode in Fig. 2(f), the migration of which is facilitated by the applied electric field.

As such, such an applied voltage increases the risk of rebar corrosion by reducing the  $\text{OH}^-$  concentrations near the rebar surface.

#### ***C4.2. Effect of Surface Chloride Concentration on Cathodic Prevention***

To evaluate the risk for rebar corrosion and predict the service life of concrete structures, the chloride threshold value to initiate active rebar corrosion in concrete is a critical parameter. Chloride ions act as a catalyst in the anodic reaction to disrupt the passive film on rebar surface, once they migrate across the concrete cover and accumulate in the vicinity of rebar surface. Such depassivation of passive film on rebar surface usually leads to subsequent accelerated corrosion if no protective action is taken. Fig. 3 confirms that CPre is an effective way to retard chloride-induced corrosion by significantly slowing down the ingress of chloride into concrete. The total chloride amount is calculated by integration over the whole concrete domain based on the distribution of chloride concentration from the FEM model. For all the cases presented, the chloride content is negligible in the innermost zone, as the applied voltages impose a retarding force to hamper chloride ions from migrating inwards. As the chloride concentration on the anode boundary increases, the chloride amount that has diffused into the concrete domain also increases, reaching a trend that can be described by a quasi-parabolic manner. The ingress of chloride ions is significantly reduced under CPre conditions, as chloride ion ingress only spans a relatively thin domain. The electric potential on anodes can be adjusted to achieve the best protection level, which provides practical guidance for CPre in new concrete structures.

#### ***C4.3. Effect of Concrete Constituents on Cathodic Prevention***

Figs. 4(a), 4(b), 4(c) and 4(d) show the evolution of the oxygen concentration, hydroxyl concentration, rebar potential and chloride concentration on top rebar, respectively, where the involved curves generally increase against time. The temporal evolutions of integral concrete resistivity and current density are given in Figs. 4(e) and 4(f), respectively.

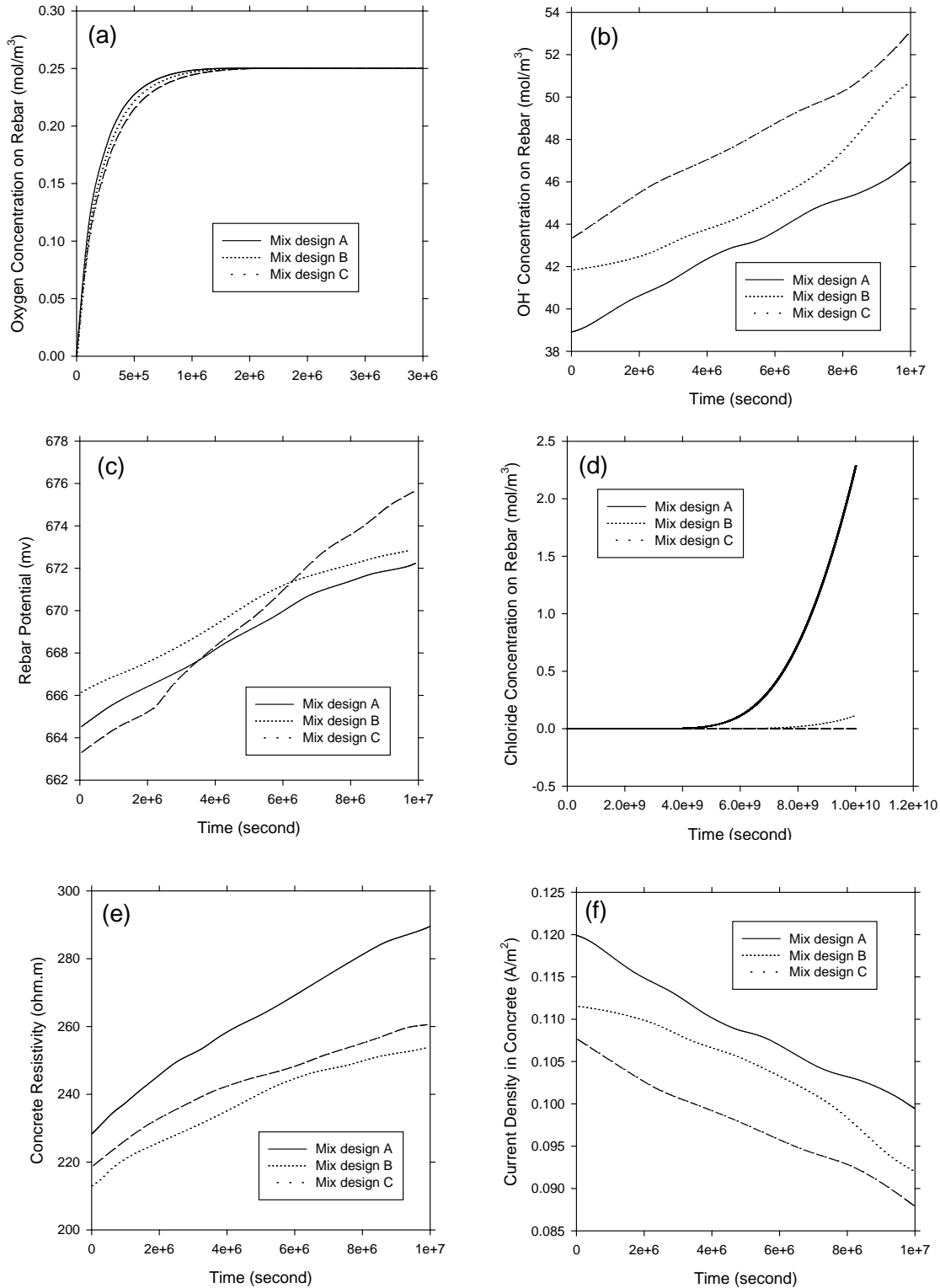


FIGURE 4 Effect of concrete mix design on cathodic prevention.

For the evolution of oxygen concentration in Fig. 4(a), there exists a stable region after a transient period in the three curves representing three concrete designs. Rebar degradation is determined by the local oxygen concentration, as its corrosion rate is limited by the oxygen flux across the steel/concrete interface. The change in the concrete microstructure is responsible for such a behavior. The variations in concrete design significantly alter the length of the transient period in which there exist oxygen concentration gradients within concrete domains, thereby serving as driving force for oxygen migration. The oxygen concentration on rebar surface increase monotonically with time until the concentration gradient in concrete domain is no longer present, when the concrete pore solution is saturated with oxygen. During the transient period, oxygen content at the rebar surface is very low. Corrosion of rebar is controlled by oxygen transport and the corrosion rate is correlated with the oxygen flux. However, when the pore solution in the vicinity of rebar is saturated with oxygen, corrosion is controlled by electrochemical reactions on rebar surface rather than the diffusion process in concrete domains. For the hydroxyl ion concentration on rebar surface in Fig. 4(b), there are two competitive factors that govern the evolution of hydroxyl ion concentration on rebar surface. One is the hydroxyl ion formation through water electrolysis and the other is the migration of hydroxyl ions away from rebar surface by diffusion and electromigration. The curves in Fig. 4(b) all increase with time, indicating that the formation process is the governing process for hydroxyl evolution on rebar surface. The evolution of electric potential on rebar surface is presented in Fig. 4(c), where the curves generally increase with time. As the electric potential on rebar surface remain unchanged at 800 mV, such an evolution reveals that the resistivity of concrete is gaining a higher value with time, which is likely due to the redistribution of ionic species within concrete domain. The change of chloride concentration on rebar surface is illustrated in Fig. 4(d), where the concrete constituents show significant effects on chloride ingress. The diffusion and electromigration of various ionic species in concrete pore solutions are interdependent, and are heavily affected by the concrete resistivity, which reflects the microstructure characteristics of each concrete mix.

The concrete resistivity and current density in concrete domain are two mutually interdependent quantities. According to the Nernst-Planck model, the concrete resistivity is given by:

$$i = -\frac{1}{r_s} \nabla \phi \quad (16)$$

where  $r_s$  is the concrete resistivity defined by:

$$r_s = \left( \frac{F^2}{RT} \sum_i z_i^2 D_i C_i \right)^{-1} \quad (17)$$

With the parameters given for partial anodic and cathodic reaction on rebar, integral concrete resistivity and integral current density can be evaluated for three concrete mix designs, the results of which are presented in Figs. 4(e) and 4(f), respectively. The integral current densities decrease with time in Fig. 4(f), as the integral concrete resistivity increases against time in Fig. 4(e). Such evolutions are consistent with the evolution of rebar potential in Fig. 4(c). The cathodic prevention of new concrete

structures generally leads to lower chloride concentrations, higher pH and polarized potentials at the rebar surface, thereby extending the service life of reinforced concrete. Through examining the temporal and spatial evolutions on rebar surface and in concrete domains, the above conclusions shed light on the long-term implications for CPre.

#### ***C4.4. Effect of Voltage Interruption on Cathodic Prevention***

During CPre, the rebars will be polarized to a more negative potential, which is accompanied by a change in local environments. Chloride removal and hydroxyl ion formation give rise to a less aggressive condition for steel. When CPre is switched off, the local evolutions depend on the diffusion of deleterious and beneficial species, which is generally slow in concrete materials. The protective environments around rebar can thus be retained even if the cathodic current is interrupted periodically, which is particularly useful for concrete infrastructures in remote areas where only solar or battery power is available. In this work, intermittent CPre is explored for concrete with mix design A, with the aim to assess the influence of current interruption. To this end, three current interruption schemes are investigated, in which the power-on duration is one, one and two days followed by power interruption for one, two and one day, respectively. As expected, the current interruption will be accompanied with depolarization and environment reduction on rebar surface.

For Fig. 5(a), when the CPre system is energized, the formation of hydroxyl ions is accompanied by the electrochemical reaction on rebar surface, characterized by water decomposition as well as oxygen and hydroxyl ion formation. During potential interruption, the oxygen in the vicinity of rebar and the pitting corrosion in active regions contribute to the formation of hydroxyl ions. However, the equilibrium  $\text{Fe}^{2+}$  ion concentration is dictated by the local hydroxyl concentration. The current interruption enhances the ingress of chloride ions in Fig. 5(b). With the increase of current interruption duration, the integral amount of chloride ions increases, which is due to the absence of a retarding force to hamper chloride ions from migrating onto rebar surface. Figs. 5(c) and 5(d) present the distribution of  $\text{Na}^+$  and  $\text{K}^+$  cations, the migration of which is facilitated by CPre. Being positively charged,  $\text{Na}^+$  and  $\text{K}^+$  ions accumulate around rebar surface with the aid of diffusion as well as electromigration. Generally, the performance of intermittent CPre is constrained by the variations in concrete resistance from the anode to the cathode. To eliminate chloride ions from concrete infrastructures, higher driving voltages can be applied so as to polarize rebars to more negative values. However, under such a condition, hydrogen embrittlement is a practical concern for high strength steel.

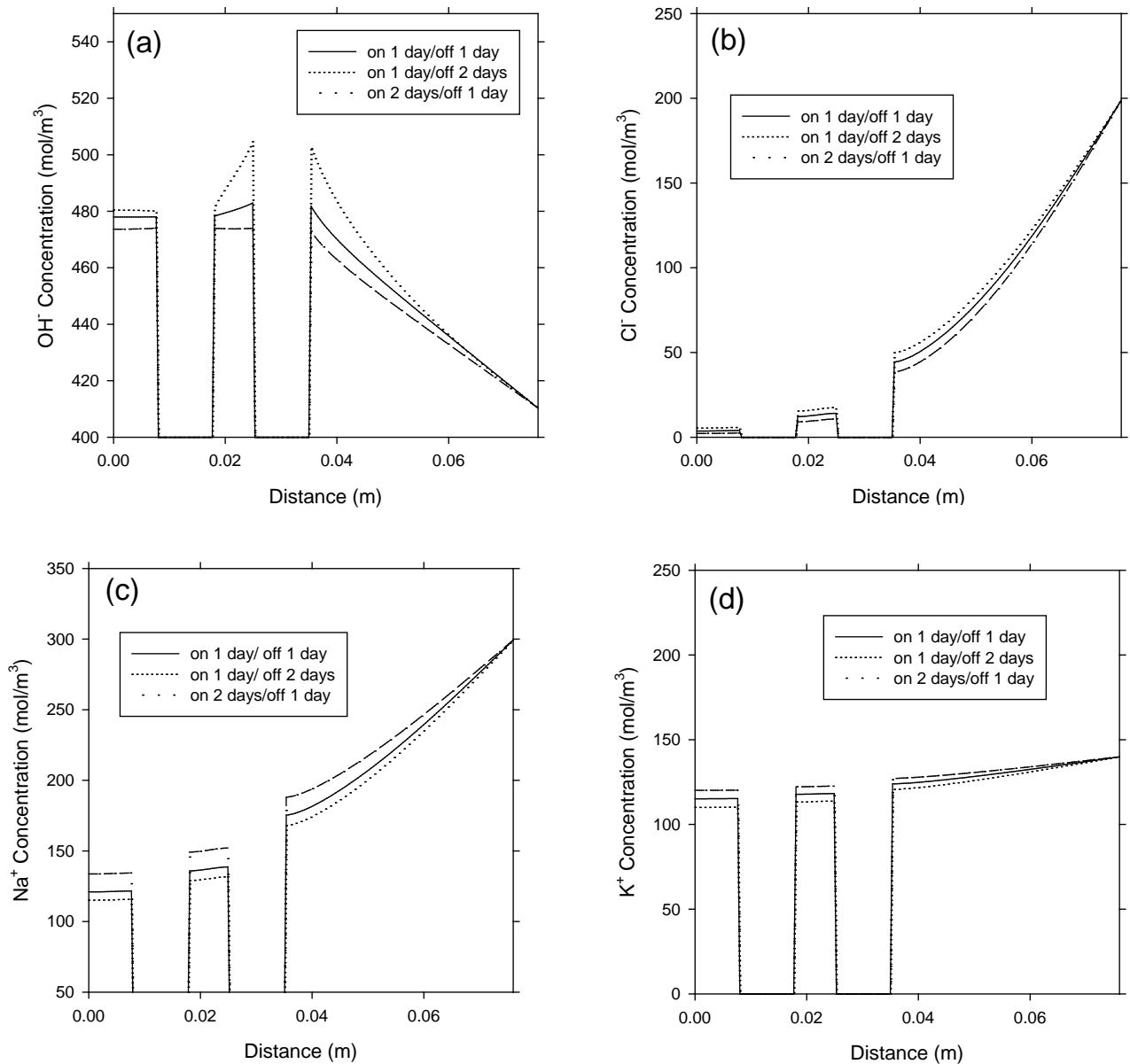


FIGURE 5 Effect of voltage interruption on the distribution of (a)  $\text{OH}^-$ , (b)  $\text{Cl}^-$ , (c)  $\text{Na}^+$  and (d)  $\text{K}^+$  in the cathodic prevention system.

### C5. Conclusions

Based on the experimentally obtained concrete resistivity and chloride diffusion coefficient data, numerical studies with the Nernst-Planck equations were conducted to investigate the influence of applied voltage (magnitude, direction, and interruption), surface chloride concentration, and concrete mix design on the effectiveness of cathodic prevention and the distribution of ionic species in protected concrete. Starting from the

mass balance law, a FEM model was established to study ionic transport for various species in concrete and electrochemical reactions on electrodes. The established FEM model was used to evaluate the behavior of CPre under various conditions. The modeling results show the great potential of CPre to effectively managing rebar corrosion in concrete if used appropriately. The applied voltage can shift the potential of rebar to a more negative value and effectively prevent the pitting initiation of rebar in concrete while excluding chloride ions and generating hydroxyl ions on the rebar surface. Such a technique can practically extend the longevity of the service life of new concrete infrastructures.

This study sheds light on the fundamental processes defining the performance of CPre for new unconventional concrete in salt-laden environment. Although the basic aspects for CPre are considered in the FEM model, there remain a number of important issues to be implemented in the future work. For example, further efforts are needed to incorporate how micro-cracks formed in the new concrete structures affects the CPre performance; how the presence of air voids at the rebar/concrete interface changes the electrochemical behaviors on the domain boundaries; how the distribution of coarse aggregates zigzags ionic transport and dictates electric field evolution within concrete domain; how the interfacial transition zone (ITZ) can be effectively represented in the model so that minimum computational resources are demanded; how a statistics-based model can be implemented to account for the inherent variability of input variables and the statistical nature of chloride-induced corrosion of steel in concrete.

## **C6. References**

- Andrade, C.; Diez, J. M.; Alaman, A.; Alonso, C. (1995), "Mathematical modelling of electrochemical chloride extraction from concrete", *Cem. Con. Res.*, Vol. 25, No. 4, pp. 727-740.
- Andrade, C.; Keddad, M.; Novoa, X. R.; Perez, M. C.; Rangel, C. M.; Takenouti, H. (2001), "Electrochemical behaviour of steel rebars in concrete: influence of environmental factors and cement chemistry", *Electrochem. Acta*, Vol. 46, pp. 3905-3912.
- Ann, K. Y.; Song, H.-W. (2007), "Chloride threshold level for corrosion of steel in concrete", *Corro. Sci.*, Vol. 49, pp. 4113-4133.
- Bertolini, L.; Bolzoni, F.; Cigada, A.; Pastore, T.; Pedferri, P. (1993), "Cathodic protection of new and old reinforced concrete structures", *Corros. Sci.*, Vol. 35, pp. 16233-1639.
- Bertolini, L.; Bolzoni, F.; Pedferri, P.; Lazzari, L.; Pastore, T. (1998), "Cathodic protection and cathodic prevention in concrete", *J. Appl. Electrochem.*, Vol. 28, No.12, pp. 1321-1331.
- Bertolini, L.; Gastaldi, M.; Pastore, T.; Pedferri, M. P.; Pedferri, P. (1999), "Cathodic protection of steel in concrete and cathodic prevention". European community, COST 521 Workshop, Annecy, 21-24 September, 1999.
- Bertolini, L. (2000), "Cathodic prevention", in: T.D. Sloan, P.A.M. Basheer (Eds.), *Proceedings of the European Workshop Corrosion of Steel in Reinforced*

- Concrete Structures, Queens University, Belfast, 28-31 August, 2000, pp. 107-115.
- Bertolini, L.; Gastaldi, M.; Pedferri, M.; Redaelli, E. (2002), "Prevention of steel corrosion in concrete exposed to seawater with submerged sacrificial anodes", *Corro. Sci.*, Vol. 44, pp. 1497-1513.
- Choi, Y.-S.; Kim, J.-G.; Lee, K.-M. (2006), "Corrosion behavior of steel bar embedded in fly ash concrete", *Corro. Sci.*, Vol. 48, No. 7, pp. 1733-1745.
- Colleparidi, S.; Corinaldesi, V.; Moriconi, G.; Bonora, G.; Colleparidi, M. (2000), *Durability of High-Performance Concretes with Pozzolanic and Composite Cements*. ACI Special Report SP 192-10, American Concrete Institute.
- Dridi, W.; Dangla, P.; Foct, F.; Petre-Lazar, I. (2006), "Modeling the influence of ionic and fluid transport on rebars corrosion in unsaturated cement systems", *J. Phys. IV France*, Vol. 136, pp. 131-140.
- Enevoldsen, J. N.; Hansson, C. M.; Hope, B. B. (1994), "Binding of chloride in mortar containing admixed or penetrated chlorides", *Cem. Con. Res.*, Vol. 24, No.8, pp. 1525-1533.
- Gardner, C. L.; Nonner, W.; Eisenberg, R. S. (2004), "Electrodifusion model simulation of ionic channels: 1D simulations", *J. Comp. Electro.*, Vol. 3, pp. 25-31.
- Gjørsv, O. E.; Vennesland, Ø. (1979), "Diffusion of chloride ions from seawater into concrete", *Cem. Con. Res.*, Vol. 9, No. 2, pp. 229-238.
- Gruber, K. A.; Ramlochan, T.; Boddy, A.; Hooton, R. D.; Thomas, M. D. A. (2001), "Increasing concrete durability with high-reactivity metakaolin", *Cem. Con. Comp.*, Vol. 23, No. 6, pp. 479-484.
- Hartt, W. H.; Charvin, S.; Lee, S. K. (1999), *Influence of Permeability Reducing and Corrosion Inhibiting Admixtures in Concrete upon Initiation of Salt Induced Embedded Metal Corrosion*, prepared for the Florida Department of Transportation.
- Hassanein, A. M.; Glass, G. K.; Buenfeld, N. R. (1998), "A mathematical model for electrochemical removal of chloride from concrete structures", *Corros.*, Vol. 54, No. 4, pp. 323-332.
- Kranc, S. C.; Sagues, A. A. (1993), "Computation of Reinforcing Steel Corrosion Distribution in Concrete Marine Bridge Substructures", in *Proceedings of NACE CORROSION 1993 Annual Meeting*, Paper No. 327.
- Kranc, S. C.; Sagues, A. A. (2001), "Detailed modeling of corrosion macrocells on steel reinforcing in concrete", *Corro. Sci.*, Vol. 43, No. 7, pp. 1355-1372.
- Liu, Y.; Shi, X. (2009a), "Electrochemical chloride extraction and electrochemical injection of corrosion inhibitor in concrete: state of the knowledge", *Corro. Rev.*, Vol. 27, No. 1-2, pp. 53-81.
- Liu, Y.; Shi, X. (2009b), "Cathodic protection technologies for reinforced concrete: introduction and recent developments", *Rev. Chem. Eng.*, Vol. 25, No. 5-6, pp. 339-388.
- Lu, X.; Li, C.; Zhang, H. (2002), "Relationship between the free and total chloride diffusivity in concrete", *Cem. Con. Res.*, Vol. 32, No. 2, pp. 323-326.
- Manera, M.; Vennesland, Ø.; Bertolini, L. (2008), "Chloride threshold for rebar corrosion in concrete with addition of silica fume", *Corro. Sci.*, Vol. 50, No. 2, pp. 554-560.

- Orlikowski, J.; Cebulski, S.; Darowicki, K. (2004), "Electrochemical investigations of conductive coatings applied as anodes in cathodic protection of reinforced concrete", *Cem. Con. Comp.*, Vol. 26, No. 4, pp. 721-728.
- Pedefferri, P. (1996), "Cathodic protection and cathodic prevention", *Const. Build. Mater.*, Vol. 10, No. 5, pp. 391-402.
- Poursae, A.; Hansson, C. M. (2009), "Potential pitfalls in assessing chloride-induced corrosion of steel in concrete", *Cem. Con. Res.*, Vol. 39, pp. 391-400.
- Rabiot, D.; Dalard, F.; Rameau, J. J.; Caire, J. P.; Boyer, S. (1999), "Study of sacrificial anode cathodic protection of buried tanks: numerical modeling", *J. Appl. Electrochem.*, Vol. 29, pp. 541-550.
- Riemer, D. P.; Orazem, M. E. (2005), "A mathematical model for the cathodic protection of tank bottoms", *Corro. Sci.*, Vol. 47, No. 3, pp. 849-868.
- Samson, E.; Marchand, J.; Beaudoin, J. J. (2000), "Modeling the influence of chemical reactions on the mechanisms of ionic transport in porous materials: an overview", *Cem. Con. Res.*, Vol. 30, No. 12, pp. 1895-1902.
- Sergi, G.; Glass, G. K. (2000), "A method of ranking the aggressive nature of chloride contaminated concrete", *Corro. Sci.*, Vol. 42, No. 12, pp. 2043-2049.
- Shi, X.; Fay, L.; Yang, Z.; Nguyen, T. A.; Liu, Y. (2009), "Corrosion of deicers to metals in transportation infrastructure: introduction and recent development", *Corro. Rev.*, Vol. 27, No. 1-2, pp. 23-52.
- Thomas, M. (1996), "Chloride thresholds in marine concrete", *Cem. Con. Res.*, Vol. 26, No.4, pp. 513-519.
- Thomas, M. D. A.; Bamforth, P. B. (1999), "Modelling chloride diffusion in concrete: Effect of fly ash and slag", *Cem. Con. Res.*, Vol. 29, No. 4, pp. 487-495.
- Toutanji, H. A.; Delatte, D. (2001), *Supplementary Materials to Enhance Bridge Deck Durability*, Prepared for University Transportation Center for Alabama.
- Wang, Y.; Li, L.; Page, C. L. (2001), "A two-dimensional model of electrochemical chloride removal from concrete", *Comp. Mater. Sci.*, Vol. 20, pp. 196-212.
- Yang, C. C.; Cho, S. W. (2003), "An electrochemical method for accelerated chloride migration test of diffusion coefficient in cement-based materials", *Mater. Phys. Chem.*, Vol. 81, No. 1, pp. 116-125.
- Yang, Z.; Shi, X.; Creighton, A. T.; Peterson, M. M. (2009), "Effect of styrene-butadiene rubber latex on the chloride permeability and microstructure of Portland cement mortar", *Const. Build. Mater.*, Vol. 23, No. 6, pp. 2283-2290.
- Yu, S. W.; Page, C. L. (1996), "Computer simulation of ionic migration during electrochemical chloride extraction from hardened concrete", *British Corro. J.*, Vol. 31, No. 1, pp. 73-75.
- Zornoza, E.; Paya, J.; Garces, P. (2008), "Chloride-induced corrosion of steel embedded in mortars containing fly ash and spent cracking catalyst", *Corro. Sci.*, Vol. 50, No. 6, pp. 1567-1575.

## APPENDIX D. STANDARD OPERATING PROCEDURES

### *D1. Electrically Accelerated Test of Chloride Diffusion Coefficient in Concrete Specimens*

The chloride electro-migration test is designed to rapidly measure the apparent diffusion coefficient,  $D_{app}$ , of chloride through *water-saturated* cementitious samples (including hardened cement paste, mortar, or concrete). In summary, the experimental setup features a disc-shaped concrete specimen that separates the chloride anion source (a solution of 3% NaCl and 1% NaOH) and the chloride anion destination (a 1% NaOH solution). Each of the two compartments will contain one 316L stainless steel mesh electrode with a given exposed surface area ( $\sim 15 \text{ cm}^2$ ). Once the concrete disc, electrolytes, and electrodes are in place, a *30-volt* DC electric field will be maintained across the disc through the two mesh electrodes in the two compartments. During the test, readings of chloride concentration in the destination compartment are taken periodically using a *calibrated* chloride sensor, on a 2-hour interval or more frequently if necessary. In addition, the electric current in the circuit is periodically measured in order to calculate the amount of electric charge passing through the disc during the electro-migration test. The chloride sensor is periodically calibrated using known solutions and the readings from them will be converted to units of molarity and plotted as a function of time. The detailed procedures are described as follows.

For cement paste or mortar samples, the test follows very similar procedures except that in step 1 the disc specimens were cut from fabricated cylinders instead of from cores.

#### *Step 1. Extracting and Preparation of Concrete Specimen*

- 1) Core at least three cores from hardened concrete for each Caltrans mix design concrete sample, using a 2" drill bit.
- 2) Cut the ends of the core specimen off as level as possible and obtain the center portion as the test specimen (1 inch thick and 2 inches in diameter).
- 3) Sand the specimen to a uniform surface finish using silicon carbide sandpaper and air-clean the specimen to remove debris.
- 4) Seal the specimen with commercial silicone but leave a circular area of 1 inch diameter exposed on both ends.
- 5) Glue the rubber gasket on the specimen in correct position and seal the exterior of the concrete specimen to prevent any water evaporation or leakage.
- 6) Let the sealed specimen dry and cure overnight.
- 7) Drill four  $\frac{3}{4}$  inch holes equally spaced in washers for bolting.
- 8) Assemble a PVC tube to each end of the specimen using the washers, bolts and nuts, and the final experimental setup should look like Figure 1.

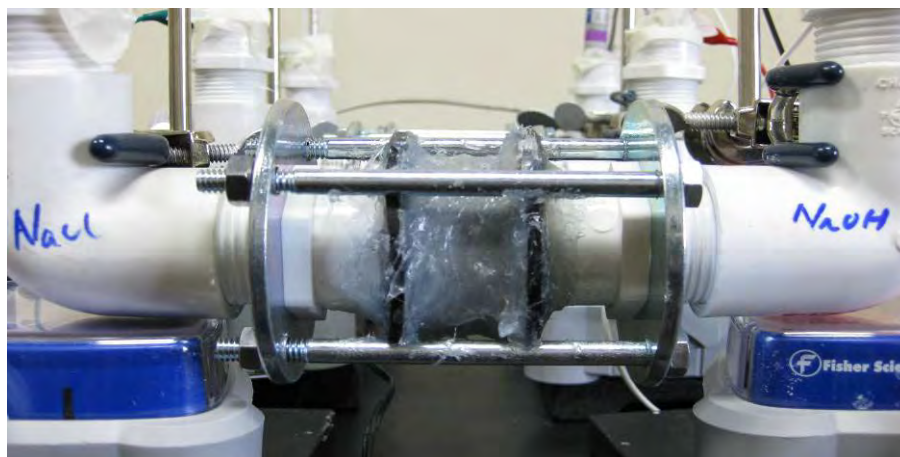


FIGURE 1 A photo of the assembled concrete specimen for electro-migration test

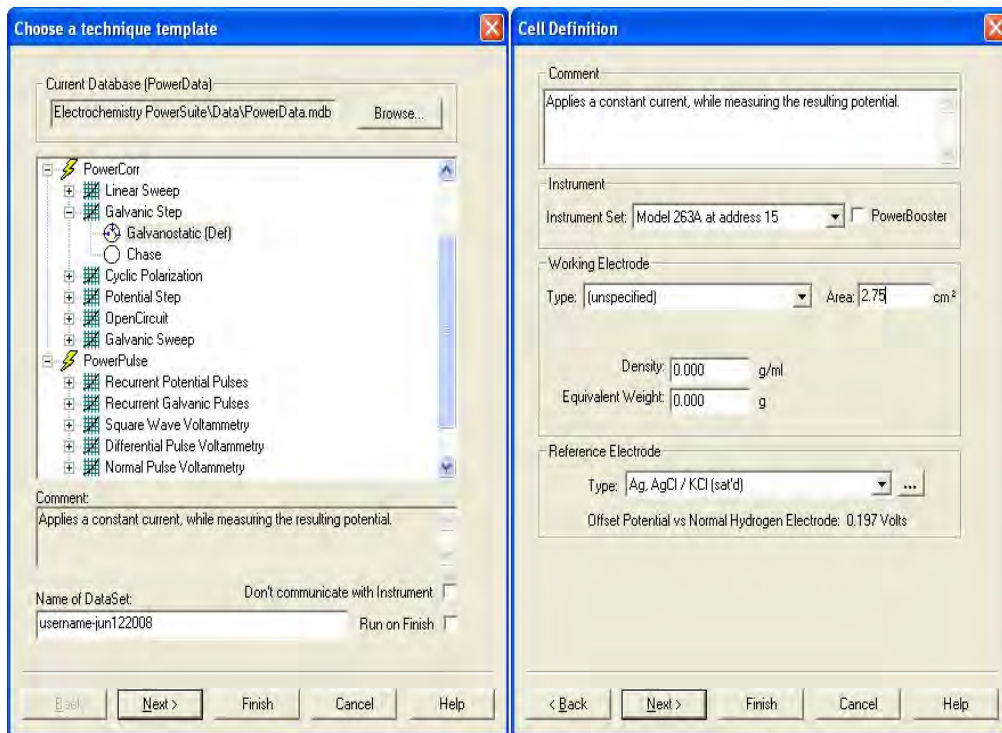
### *Step 2. Fabrication and Calibration of Chloride Sensor*

First, fabricate chloride sensors by electroplating silver wires with the Princeton Applied Research Model 263A Potentiostat/Galvanostat.

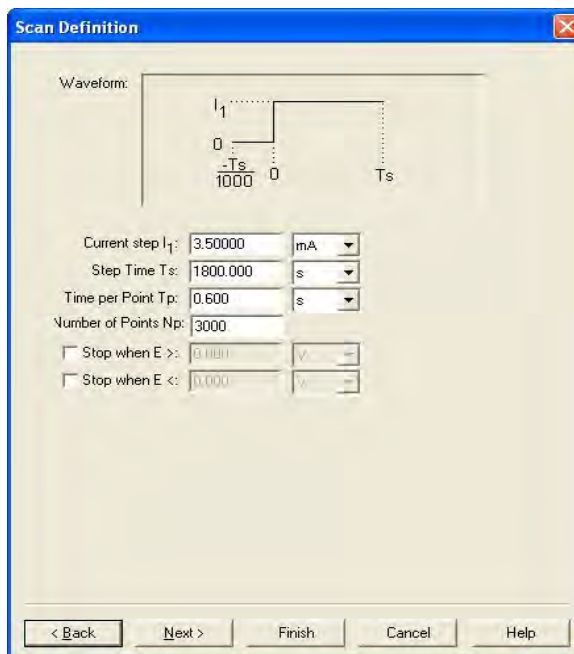
- 1) Clean the commercial silver wire with a fine-grade silicon carbide sandpaper (grit size 1000). This should be done as thoroughly and consistently as possible to achieve a uniform electroplated sensing layer of Ag/AgCl later.
- 2) Rinse the polished silver wire with acetone and then de-ionized water.
- 3) Place the clean silver wire into 1 M KCl solution with few drops of 0.1 M HCl and attach the red and white cables from the potentiostat to it. Attach the black cable from the potentiostat to ground. Attach the green cable from the potentiostat to a bare silver wire as a cathode and place it into the same solution.
- 4) Use the computer-controlled potentiostat to apply 1, 0.2, 0.5, and 0.1mA/cm<sup>2</sup> for plating about 30, 30, 30 and 100 minutes, respectively. During this electroplating process, a black deposit is formed on the silver wire.

The following sections illustrate a 30-min electroplating process using the potentiostat software.

- Launch the PowerSuite program on the computer. Go to Experiment -> New. Choose PowerCorr -> Galvanic Step -> Galvanostatic (def.) as shown, enter a name for the test, and then press Next. Enter the working electrode type as (unspecified) and enter the area (exposed area of silver wire, e.g., 2.75 cm<sup>2</sup>). Enter the reference electrode type as Ag/AgCl/KCl (saturated). Press Next.



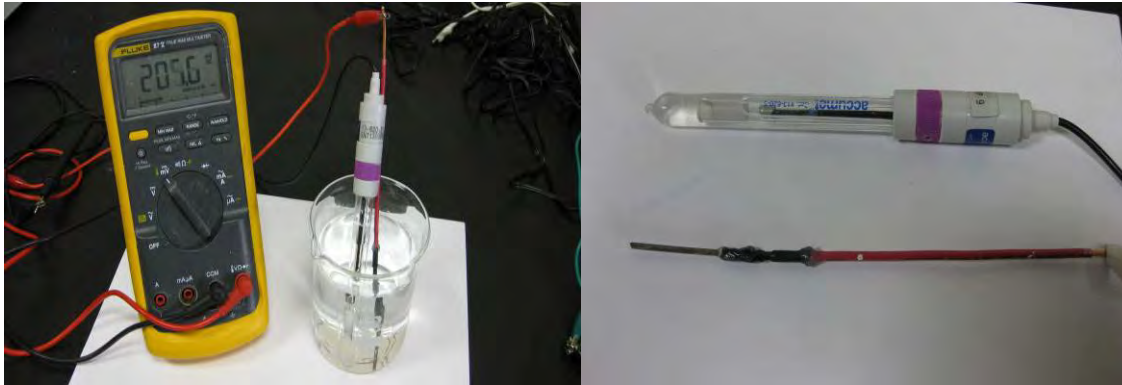
- On the next screen, enter the amperage required calculated in part A in the Current Step box (make sure to change the units to mA). In Time Step, enter 1800 seconds, and press tab. PowerSuite calculates the rest. Press Finish and power on the potentiostat. On the main window, press the go arrow.



- 5) Before use place the sensor in a beaker with 1 M KCl for a few hours to reach a stable potential. When not in use store the sensor in 1 M KCl.

Second, calibrate the custom-made chloride sensors using standard aqueous solutions of sodium chloride (NaCl).

- 1) Prepare 5 small clean beakers and label with the following NaCl concentrations: 0.001, 0.005, 0.01, 0.05, and 0.1 M. Prepare these standard solutions of NaCl. Pour a small amount of each standard solution into its respective beaker.
- 2) Pair the chloride sensor with a saturated calomel electrode (SCE) and clean them off with de-ionized water. The chloride sensor should be rinsed at least three times with de-ionized water and then the standard NaCl solution to be immersed in.
- 3) Immerse both the chloride sensor and the SCE reference electrode in the standard solutions of NaCl. Start from the solution with lowest NaCl concentration and use a multi-meter to take the open circuit potential (OCP) reading of the chloride sensor relative to the SCE. Then remove both electrodes from the NaCl solution and dry them before immersing them into the next standard solution. Continue this sequence until the OCP reading of chloride sensor is taken in all five standard solutions. Such calibration in increasing NaCl concentrations aims to minimize cross-contamination. Note that the chloride sensor takes a few minutes to stabilize in each test solution. For convenience and consistency, 2 minutes of response time are allowed for the sensor in each test solution.



- 4) The OCP reading of the chloride sensor in the five standard solutions are recorded using a chart shown in Figure 2. Such data can be used to fit a calibration curve correlating the OCP as a function of chloride concentration. There should be a very strong correlation between OCP and logarithm of chloride concentration. If R-square of the linear regression is lower than 0.9, the calibration process needs to be repeated. If the problem continues, then the chloride sensor needs to be re-fabricated.

[Cl <sup>-</sup> ] (M)	Log[Cl <sup>-</sup> ]	Readings (mV/SCE)		
		Sensor A	Sensor B	Sensor C
0.001				
0.005				
0.01				
0.05				
0.1				

FIGURE 2 Data Chart for the OCP of chloride sensor

*Step 3. Set up the electro-migration experiment*

- 1) Before setting up the electromigration cell, use a Permanent Marker to mark “NaCl” on the left compartment and “NaOH” on the right compartment.
- 2) Add 70 mL of de-ionized water in each side of the test cell and then allow the disc concrete specimen to saturate for two hours.
- 3) Rinse both sides of the test cell with a small amount of their respective solutions three times. Put the cell on two ring stands above two magnetic stir plates.
- 4) Using a glove, rinse off two small stir bars thoroughly with de-ionized water, and put one into each side of the cell. Turn the stir plates on low, making sure that the stir bars stay in the right place.
- 5) Add 70 mL of anodic solution (1% NaOH) in the anodic/right compartment. The volume of the anodic solution is kept small so that the chloride sensor placed in it can be sensitive enough to detect the increase in chloride concentration once sufficient chloride ions penetrate through the concrete disc. Yet the volume of the anodic solution is kept large enough to avoid significant change in its composition that may derive from electrochemical reaction on the mesh anode.
- 6) Add 70 mL of cathodic solution (3% NaCl and 1% NaOH) in the cathodic/left compartment. It is designed to prevent significant buildup of hydroxyl ions (due to electrochemical reaction on the mesh cathode) or significant depletion of chloride ions. The experiment creates a near constant concentration of migrating anions (Cl<sup>-</sup> and OH<sup>-</sup>) at concentrations somewhat representative of real concrete pore solution.
- 7) Insert one 316L stainless steel (S.S.) mesh electrode in each side of the test cell with a same exposed electrode surface area and make sure the S.S. mesh electrode surface is cleaned with acetone and de-ionized water and dried in advance.
- 8) Repeat this step with the other two concrete discs and wire the three discs in parallel in the same electric circuit, as shown in Figure 3.
- 9) Once the experiment is started the level of solution in the upstream and downstream compartment needs to be marked using a Permanent Marker. This is to monitor any loss of solution due to evaporation etc. Once the solution drops below the marked level it is compensated with more de-ionized water to maintain a constant volume.

Addition of the de-ionized water drops must be done before taking the chloride concentration reading every day.

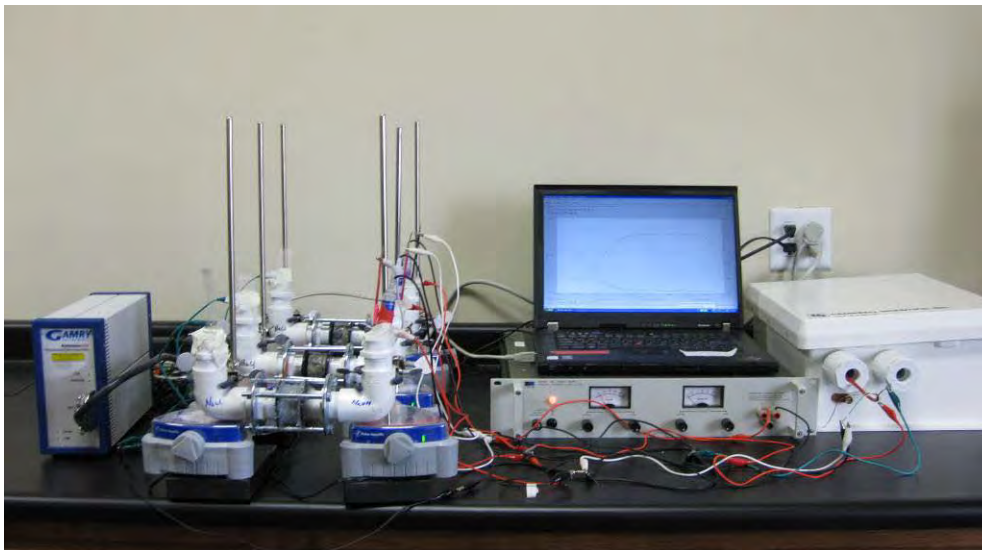


FIGURE 3 A photo of the assembled experimental setup for electro-migration test

*Step 4. Electrochemical impedance spectroscopy (EIS) measurement before electro-migration*

Once the concrete disc, electrolytes and electrodes were in place, the following EIS measurement should be done for each concrete disc specimen, immediately before running the electro-migration test.

- 1) Place the SCE reference electrode in the anodic/right compartment (which contains 1% NaOH).
- 2) Connect the cables from the potentiostat to various electrodes according to Table 1 and Figure 4 and make sure none of the wires physically touch one another.

TABLE 1 Potentiostat Connections

From...	Cable Color	Connect to...
Multi-channel Gamry Potentiostat	Red and Orange	NaCl-side S.S. mesh electrode
	Green and Blue	NaOH-side S.S. mesh electrode
	White	SCE reference electrode
	Black	Ground (any exposed metal)

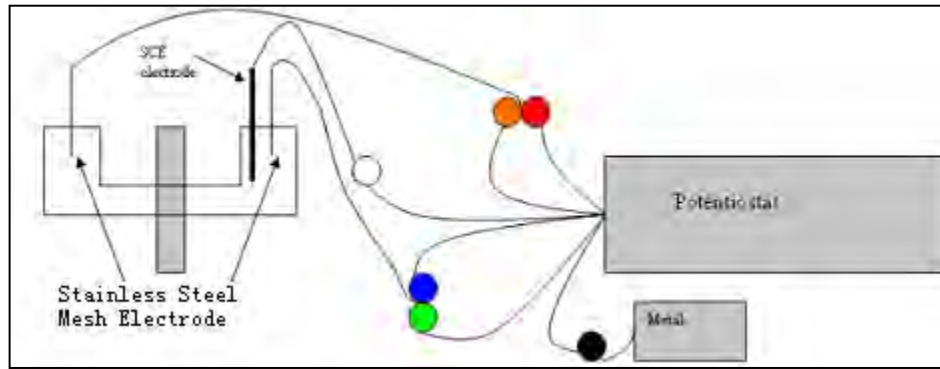


FIGURE 4 Schematics of connecting cables from the potentiostat to electrodes

- 3) Launch Gamry Framework, make sure the Gamry Potentiostat device is powered on, and go to Experiment -> G. Electrochemical Impedance -> 5. Potentiostatic EIS. Make sure the experiment is set up as follows in figure 3, changing the name as necessary being sure to include the specimen name, date, and project name such as: (Caltrans1c4-1-08): Press OK. A typical screen is shown in Figure 5.

FIGURE 5 A typical startup screen for EIS.

- 4) The EIS will run for about 30 minutes to 60 minutes. When the test is finished, the window will show "Curve done" at the bottom. Press F2 (skip) until the window closes and save it.
- 5) Disconnect all potentiostat cables from electrodes.
- 6) Any abnormality in the obtained EIS spectrum or the analyzed resistance and capacitance values would indicate inherent defects in the concrete specimen. As such, the specific concrete specimen can be replaced or the data from which be discarded.

*Step 5. Start the electro-migration test*

After the EIS measurement is completed, a 30-V DC electric field was maintained across the concrete disc through the two S.S. mesh electrodes in the two compartments, using a DC power supply. During the test, the calibrated Ag/AgCl sensor and the SCE reference electrode were periodically placed in the destination solution and its OCP reading was taken relative to the SCE. The electro-migration test continues until a bilinear trend and a significant increase in the chloride concentration are detected in the destination solution.

Furthermore, a 100-Ohm resistor is connected in the electric circuit as shown in Figure 6, in order to periodically measure the electronic current going through the circuit.

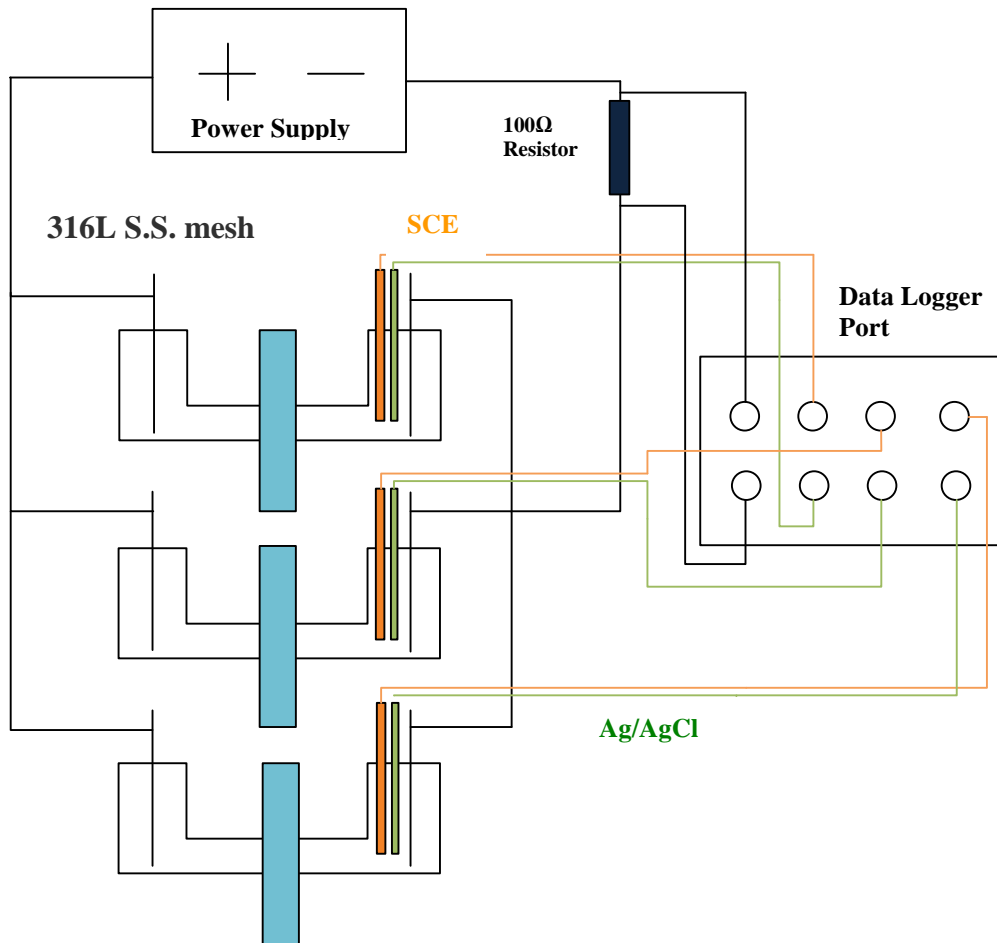


FIGURE 6 Schematics of the overall setup for electro-migration test

For concrete samples, the electro-migration test typically lasts more than 6 weeks. As such, the chloride sensor and the SCE were not continuously immersed in the destination solution, where the high alkalinity may damage both the Ag/AgCl sensing layer and the glass tip of the SCE. For cement paste or mortar samples, however, the electro-migration test typically lasts less than a few days, in which case the chloride sensor and the SCE could be continuously immersed in the destination solution and a data logger can be used

to continuously monitor both the OCP of chloride sensors and the electric current in the circuit. The following describes the procedures of using the data logger.

- Open the program Logger Net.
- The proper code should already be loaded on the computer.
- Connect the data logger to the computer and plug into outlet.
- Test the resistor to be used and input its actual resistance in the code.
- Wire the data logger to the resistors that are connected to the sample while ensuring that it is wired in series and not in parallel (see Figure 6).
- Wire other channels of the data logger to the chloride sensors and the SCE reference electrodes (see Figure 6).
- Click on the Connect tab on the Logger Net opening toolbar.
- The Connect window will appear and you will see a button that says Connect.
- Click Connect. This will begin data logging every 5 minutes for outputs.
- To see data click on the “1” in the Connect window by either Graph or Numeric tabs.

#### *Step 6. EIS measurement after electro-migration*

Once the electro-migration test is completed, remove the chloride sensors from destination solutions. Rinse off a magnetic stir bar retriever with DI water and remove both magnetic stir bars from each side of the cell. Finally, set up the EIS test as described in Step 4 and run the EIS measurement again.

#### *Step 7. Clean up the test cell*

Clean up the test cell and take the assembled test cell apart carefully. When cleaning up the cell hardware, draw several arrows on the edge on the concrete sample disk to indicate in which direction the Cl<sup>-</sup> migrated (NaCl → NaOH). Save all the hardware including PVC, washers, nuts, bolts, and rubber gaskets.

#### Some thoughts on improving this test for future experiments

From this study, we observed a few weaknesses in this test method and propose the following improvements that may be implemented for future experiments. First, it may be beneficial to add a corrosion inhibitor in the anodic compartment to minimize the corrosion of the mesh anode. The type and concentration of the inhibitor should be evaluated such that its addition would not significantly interfere the temporal evolution of chloride concentration reading in the destination solution. Second, the apparent chloride diffusion coefficient could be derived from the slope of the second line in the chloride concentration profile, instead of  $t_0$  (the intersection of the two lines). Finally, methods should be developed to enable the continuous immersion of chloride sensor and reference electrode in the destination solution over a longer time period. One possible solution would be to coat a permeable film on the chloride sensor to slow down the oxidation attack of sensing layer by hydroxyl ions. Instead of the SCE, other reference electrodes less prone to the high alkalinity (e.g., Mn/MnO<sub>2</sub> and Mo/MoO<sub>3</sub>) should be evaluated.

## D2. Testing Procedures for Concrete Porosity

The hardened Caltrans concrete samples numbered 1, 3, 4, 7, 8, 9, 10, 11, 13, 14, 15, 16, 17, and 18 were roughly 94mm in diameter and between 30mm and 40mm thick. The concrete samples 12a, 12b, and 12c were roughly 45mm in diameter and 25mm thick. These samples were first placed in an oven at 105°C in accordance with the ASTM C 642 test method entitled “Standard Test Method for Density, Absorption and Voids in Hardened Concrete”. After 24 hours a potential dry mass was measured for each concrete sample. Subsequently the samples were placed back in the 105°C oven for another 24 hours. Upon such time a second potential dry mass was measured and since the difference in the two potential dry masses was less than 0.5% the second potential dry mass was taken to be the true dry mass (A).

Next the samples were completely submerged in de-ionized water of around 21°C for a period of 24 hours. Once removed out of water, the surface of each concrete sample was patted dry and a potential immersed weight was measured. Then the samples were submerged for another 24 hours, patted dry and a second potential immersed mass was recorded. Since the difference in potential immersed weights was less than 0.5% the second potential immersed weight was recorded as the true immersed weight (B).

Then the concrete samples were submerged in de-ionized water and the water was brought to boiling temperatures for a period of 5 hours. The heat was removed and the samples were left to cool off for a period no less than 14 hours. The samples were removed out of the water when they were around 20°C, patted dry and the mass was recorded as the saturated boiled mass (C). Finally, the concrete samples were suspended by wire in water to measure an immersed apparent mass which was recorded as D.

The parameters  $g_1$  and  $g_2$  were then calculated. The bulk dry density,  $g_1$ , was found from the ASTM standard equation of  $g_1 = [A/(C-D)] \times \text{density of water}$ . The apparent density,  $g_2$ , was found by the same standard with the equation being  $g_2 = [A/(A-D)] \times \text{density of water}$ . With these the ***volume of permeable voids (%)*** could be found by the following equation  $VPV = [(g_2 - g_1) / g_2] \times 100\%$ .

Next the samples were crushed so that about 64 grams of material could be obtained after passing through a 90µm sieve (#170). Then using a Le Chateller Flask in accordance with ASTM C 188 the flask is first filled with about 250mL of kerosene to bring the kerosene level to a point between the 0 and 1 mL graduations on the cylinder. Then the flask is placed in a constant temperature (20°C) water-bath for sufficient time to reach a temperature balance throughout. Next the crushed dry powder is added carefully so as to allow all powder to fall into the kerosene with none sticking on the edges above the kerosene level. This powder is added until the kerosene level has risen to the second set of graduations on the flask between 18 and 24 mL. A glass stopper is then placed in the top of the flask and the flask is swirled and vibrated until such time that no air bubbles ascend from out of the crushed powder. The flask is then placed back in the constant temperature water-bath to return to the constant temperature. The specific gravity,  $g_3$ , is then determined from the volume change and the mass of material added to the flask. The

calculation is as follows:  $g_3 = (\text{mass of crushed sample added}) / (\text{final volume} - \text{initial volume})$ . The ***volume of total voids (%)*** can then be found by the following equation:  
 $\% \text{ total voids} = [(g_3 - g_1) / g_3] \times 100\%$ .

## APPENDIX E. DATA OF MINERAL ADMIXTURES AND CEMENT

### E1. ASTM C 618 Class F fly ash

The Class F fly ash used in this study was provided by the Headwaters Resources Inc. and originated from the Jim Bridger Power Plant near Rock Springs, Wyoming. The composition of the fly ash depends on the quality of coal, the machinery, and the method of production and may vary greatly over a given time period. It contains 6.2% to 7.5% calcium oxide by weight. One quality control measure followed is that no more than 34% of the fly ash particles can be retained on a 325 mesh sieve. The specific gravity of the fly ash was 2.30.

Typical composition of ASTM C 618 Class F and Class C fly ashes\*

Mineral Admixtures (%)	Class C Fly Ash	Class F Fly Ash
SiO <sub>2</sub> + Al <sub>2</sub> O <sub>3</sub> + Fe <sub>2</sub> O <sub>3</sub> , minimum	>70	>50
SiO <sub>3</sub> , maximum	5	5
Moisture content, Maximum	3	3
Loss on ignition, maximum	6	6
Available alkali as Na <sub>2</sub> O	1.50	1.50
Calcium content	>10%	<10%
LOI	Very low LOI of < 1%	Typically contain > 3%
Major crystalline phases	Quartz, mullite (3Al <sub>2</sub> .2SiO <sub>2</sub> ), and hematite	Anhydrite, tricalcium aluminate, lime, quartz, periclase (MgO), mullite, merwinite (Ca <sub>3</sub> Mg[Si <sub>2</sub> O <sub>8</sub> ], and ferrite

\* Scheetz BE, Olanrewaju J. Determination of the rate of formation of hydroceramic waste forms made with INEEL calcined wastes. Final report prepared for the Department of Energy. 2001.

**E2. ASTM C 618 Class N fly ash - natural pozzolan**



**Resource Materials Testing, Inc.**

171 Smith Hollow -- Murphy NC 28906 1-877-217-5147

**REPORT OF NATURAL POZZOLAN ANALYSIS**

TO: Western Pozzolan Corporation  
 Attn: Mr. Steve Beck  
 1748 Senecio Drive  
 Larkspur, CO 80118

PROJECT NO.: RMT-453  
 SAMPLE NO.: 15186  
 DATE RECEIVED: 7-14-06  
 DATE REPORTED: 9-27-06

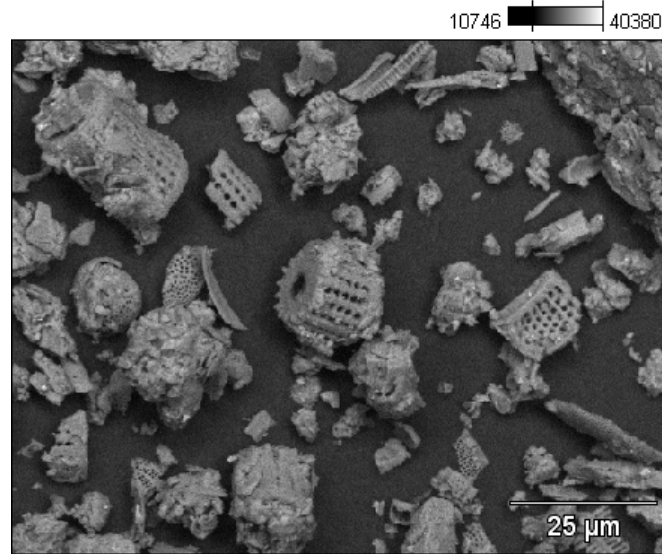
PROJECT NAME: Pozzolan Evaluation  
 SAMPLE ID: Raw Lassenite Material

<b>CHEMICAL ANALYSIS:</b>	<b>RESULTS:</b>	<b>ASTM C-618 -</b>
<b>SPEC Nat Pozz</b>		
Silicon Dioxide, SiO <sub>2</sub> , %	70.92	----
Aluminum Oxide, Al <sub>2</sub> O <sub>3</sub> , %	16.63	----
Iron Oxide, Fe <sub>2</sub> O <sub>3</sub> , %	4.85	----
Sum of SiO <sub>2</sub> , Al <sub>2</sub> O <sub>3</sub> & Fe <sub>2</sub> O <sub>3</sub> , %	92.40	70/50 Min
Calcium Oxide, CaO, %	2.84	----
Magnesium Oxide, MgO, %	0.66	----
Sodium Oxide, Na <sub>2</sub> O, %	2.03	----
Potassium Oxide, K <sub>2</sub> O, %	1.73	----
Sulfur Trioxide, SO <sub>3</sub> , %	0.34	4.0 Max
Moisture Content, %	9.39	3.0 Max
Loss on Ignition, %	4.62	10.0 Max
<b>PHYSICAL ANALYSIS:</b>	<b>RESULTS:</b>	<b>ASTM C-618 -</b>
<b>SPEC Nat Pozz</b>		
Amount Retained on No. 325 Sieve, %	32.9	34 Max
Sieve Uniformity, % Points from Ave	----	5 Max
Strength Activity Index		
Portland Cement @ 7 days, % of Control		
Portland Cement @ 28 days, % of Control	82	75 Min
Water Requirement, % of Control	106	115 Max
Autoclave Expansion, %	-0.01	0.8 Max
Density	2.28	
Density Uniformity, % from Ave	----	5 Max
Increase of Drying Shrinkage, %*	----	0.03 Max
Reactivity with Cement Alkalis, %*		
Reduction of Mortar Expansion, %	----	----
Mortar Expansion, % of LA Cement Control	0.6	100 Max
Air Entrainment of Mortar, %		
Uniformity*	----	20
Multiple Factor*	----	255 Max

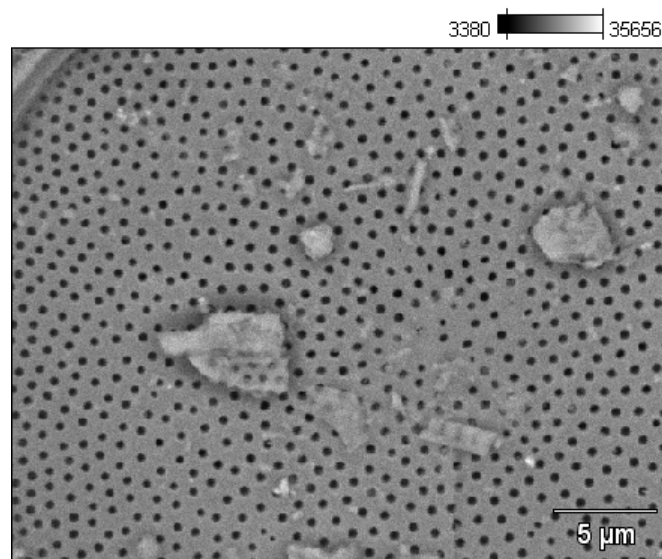
\*Optional Requirements applicable only when requested by purchaser. This material meets the requirements of ASTM C 618 for natural pozzolans.

By *Robert L. Smith*  
 Robert L. Smith, Ph.D.

**Loc 10 1000X BSE**



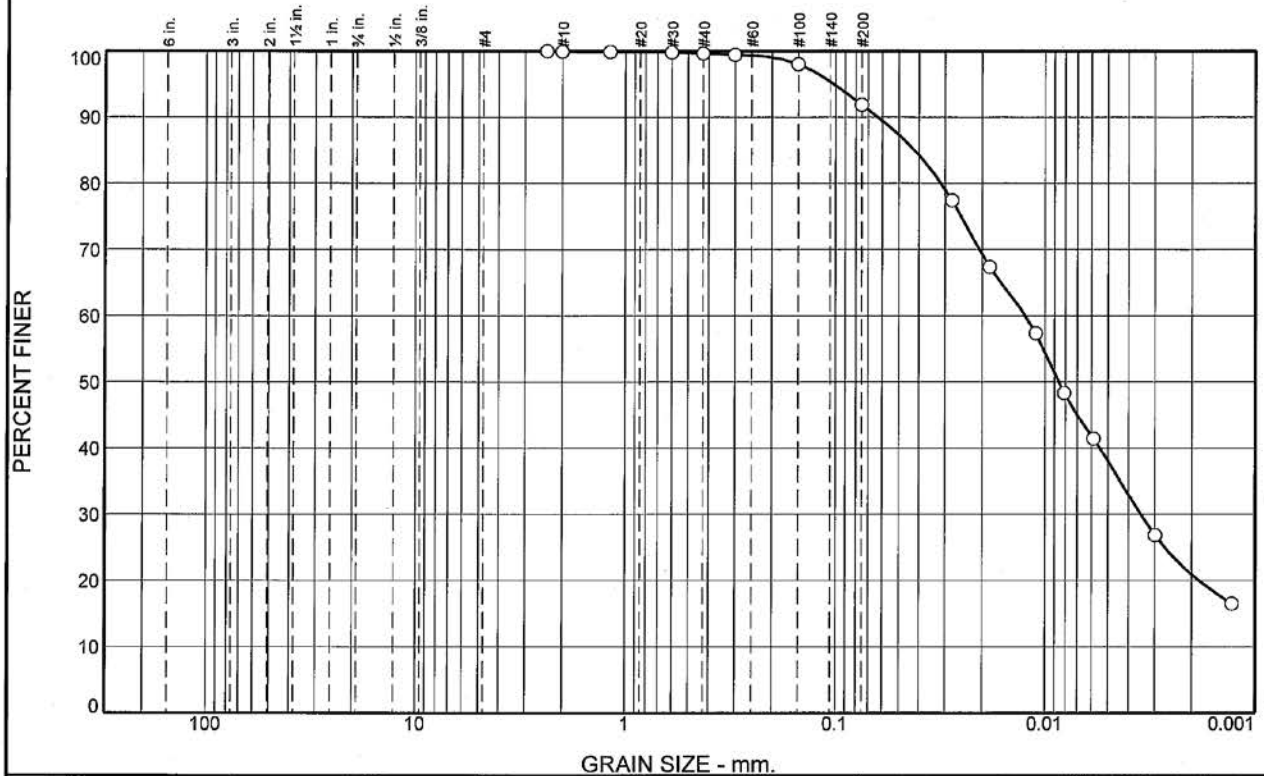
**Loc 5 3500X BSE**



**BSE Photos of the Class N Fly Ash Particles**

Generally, more than 70% (typically 83-86%) of the class N fly ash particles can pass the number 325 sieve (according to the ASTM C 430 test method). A typical particle size distribution curve is shown as follows.

# Particle Size Distribution Report



% +3"	% Gravel		% Sand			% Fines	
	Coarse	Fine	Coarse	Medium	Fine	Silt	Clay
0.0	0.0	0.0	0.1	0.3	7.7	53.8	38.1

SIEVE SIZE	PERCENT FINER	SPEC.* PERCENT	PASS? (X=NO)
#8	100.0		
#10	99.9		
#16	99.9		
#30	99.8		
#40	99.6		
#50	99.4		
#100	98.1		
#200	91.9		
0.0278 mm.	77.4		
0.0184 mm.	67.4		
0.0111 mm.	57.4		
0.0081 mm.	48.3		
0.0058 mm.	41.4		
0.0030 mm.	26.8		
0.0013 mm.	16.5		

**Soil Description**

PL=                      **Atterberg Limits**                      PI=

LL=

**Coefficients**

D<sub>85</sub>= 0.0419                      D<sub>60</sub>= 0.0124                      D<sub>50</sub>= 0.0086

D<sub>30</sub>= 0.0035                      D<sub>15</sub>=                      D<sub>10</sub>=

C<sub>u</sub>=                      C<sub>c</sub>=

USCS=                      **Classification**                      AASHTO=

**Remarks**

\* (no specification provided)

Sample No.: S1775                      Source of Sample: R325 Series                      Date: 9-18-07

Location: R325-001                      Elev./Depth:

<b>SIERRA TESTING LABS, INC.</b> El Dorado Hills, CA	Client: Western Pozzolan Project: Western Pozzolan General Testing Project No: 07-170
---	---

Tested By: MPW                      Checked By: CMW

## E3. ASTM C 1240 Silica fume



The Chemical Company

3	03 30 00	Product Data
	03 40 00	Cast-in-Place Concrete
	03 70 00	Precast Concrete Mass Concrete

### Description

Rheomac SF 100 dry, densified silica fume mineral admixture is formulated to produce extremely strong, durable concrete or mortar possessing special performance qualities. It maximizes concrete service life by providing superior resistance to attack from damaging environmental forces. Rheomac SF 100 silica fume admixture meets the requirements of ASTM C 1240, *Standard Specification for Silica Fume used in Cementitious Mixtures*.

### Applications

Recommended for use in:

- Steel-reinforced concrete structures or wet shotcrete applications exposed to deicing or airborne salts
- Parking structures, bridge decks, marine structures, mines and tunnels
- Any construction project requiring the protection provided by highly durable, low permeability concrete
- Projects requiring high-strength/high-performance concrete for reducing member size, increasing span lengths, improving structural economics and meeting other high-performance structural requirements

## RHEOMAC® SF 100

### Densified Silica Fume Mineral Admixture

#### Features

- Added cohesiveness
- Reduced bleeding
- Enhanced performance

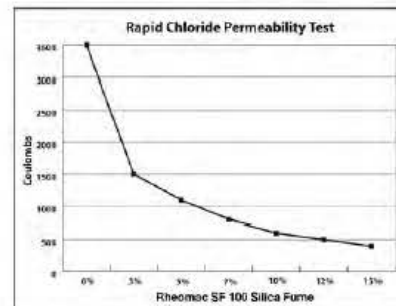
#### Benefits

- Increased concrete service life
- Improved strength
- Increased modulus of elasticity
- Reduced permeability thereby increasing durability
- Increased resistance to sulfate attack
- Increased resistance to alkali-silica reactivity

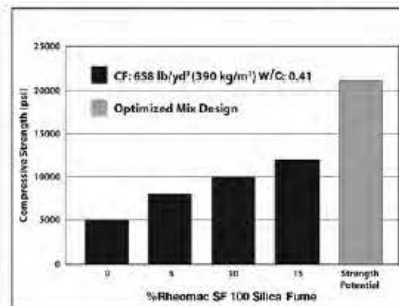
#### Performance Characteristics

**Permeability:** Rheomac SF 100 silica fume admixture is a micro-filling material that physically fills the voids between cement particles. Rheomac SF 100 silica fume admixture dramatically lowers permeability and reduces the size and number of capillaries that allow contaminants to enter the matrix.

#### Rapid Chloride Permeability



#### Test Typical Compressive Strengths



**Compressive Strength:** As a pozzolan, Rheomac SF 100 silica fume admixture reacts chemically within a cementitious matrix to increase the amount of calcium silicate hydrate (CSH gel) that is formed. The CSH gel is the bonding agent that holds the matrix of a cementitious mixture together in the hardened state. The additional CSH gel increases strength and decreases permeability.

**Specific Gravity:** The specific gravity of Rheomac SF 100 silica fume admixture is 2.2.

## DESCRIPTION

**RHEOMAC SF 100** is a dry, compacted, silica fume mineral admixture formulated to produce concrete with special performance qualities. It improves the hardened characteristics of concrete in two ways.

Firstly, **RHEOMAC SF 100** is a pozzolan which reacts chemically within the concrete to increase the amount of calcium silicate hydrate gel formed, thus improving the strength and impermeability of the concrete. Secondly, **RHEOMAC SF 100** is an ultra-fine material that, when added to concrete, physically fills the voids between cement particles resulting in an extremely dense and impermeable concrete.

**RHEOMAC SF 100** meets ASTM C 1240 requirements.

## FIELDS OF APPLICATION

The reduced permeability of concrete produced with **RHEOMAC SF 100** greatly limits the ingress of water, chlorides, sulphates, and aggressive chemicals known for promoting reinforcing steel corrosion and other distressed in the concrete. This makes **RHEOMAC SF 100** an ideal product for use in basement structures, parking deck, bridge decks, marine structures, and any construction that requires the protection provided by impermeable concrete.

Because of its pozzolanic and void-filling properties, the addition of **RHEOMAC SF 100** to conventional concrete also provides ultra high compressive strengths. This allows for design flexibility, resulting in reduced member size, increased span lengths, and improves overall structural economics.

As a result of the preceding advantages, **RHEOMAC SF 100** will improve performance in prestressed, precast, and ready-mixed concrete application.

**RHEOMAC SF 100** can be used with portland cements approved under ASTM AASHTO or CRD specification. When air entrainment is desired, an air-entraining admixture is recommended. Please consult BASF Construction Chemicals representative. It is also recommended that **RHEOMAC SF 100** be used in conjunction with high range, water-reducing admixture, such as RHEOBUILD admixtures.

## FEATURES AND BENEFITS

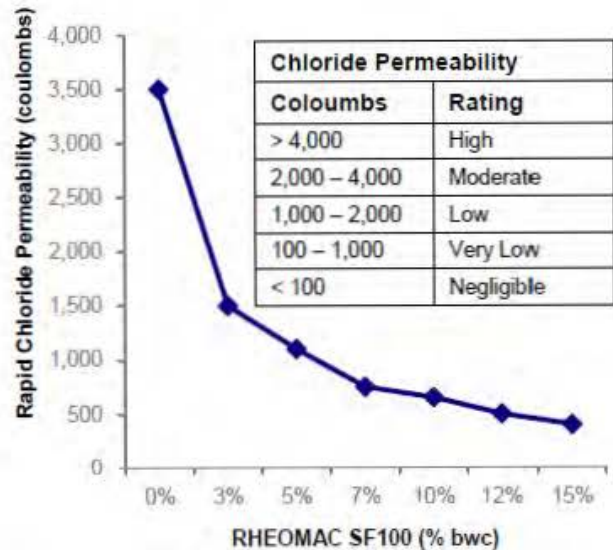
**RHEOMAC SF 100** aids in the production of concrete with the following special qualities :

- Dramatically improved durability
- Uniformly high compressive strength
- Abrasion and erosion protection
- Better flexural strengths at all ages
- Low permeability

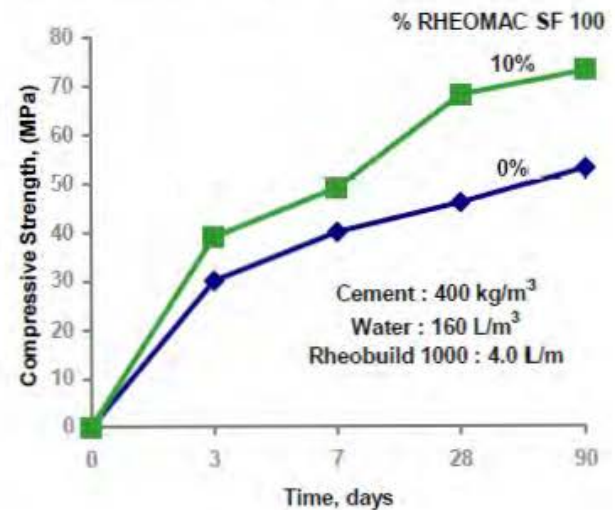
- Excellent freeze/thaw resistance

## TYPICAL PERFORMANCE DATA

Example of the influence of **RHEOMAC SF 100** on rapid chloride permeability



## Compressive Strength (MPa)



How it works

**E4. ASTM C 618 (Class N) calcined natural pozzolan – metakaolin**

**Resource Materials Testing, Inc.**

*"Specialists in Fly Ash Testing"*

**REPORT OF NATURAL POZZOLAN ANALYSIS**

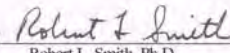
TO: Grace Davison  
 Attn: Mr. Mark Burkhardt  
 213 Kaolin Road  
 Aiken, SC 29801

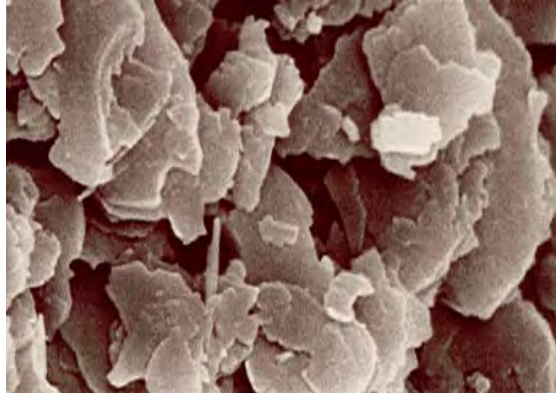
PROJECT NO. RMT-462  
 SAMPLE NO.: 16663  
 DATE REC.: 10-24-08  
 DATE REP.: 11-05-08

PROJECT NAME: Grace Davison Standard Metakaolin  
 SAMPLE ID: Oct 2008 IL DOT PRO Sample

<b>CHEMICAL ANALYSIS:</b>	<b>RESULTS:</b>	<b>AASHTO M 295 - SPEC</b>
Silicon Dioxide, SiO <sub>2</sub> , %	51.68	----
Aluminum Oxide, Al <sub>2</sub> O <sub>3</sub> , %	42.45	----
Iron Oxide, Fe <sub>2</sub> O <sub>3</sub> , %	2.31	----
Sum of SiO <sub>2</sub> , Al <sub>2</sub> O <sub>3</sub> & Fe <sub>2</sub> O <sub>3</sub> , %	96.44	75 Min
Calcium Oxide, CaO, %	0.36	----
Magnesium Oxide, MgO, %	0.28	----
Sodium Oxide, Na <sub>2</sub> O, %	0.08	----
Potassium Oxide, K <sub>2</sub> O, %	0.32	----
Sulfur Trioxide, SO <sub>3</sub> , %	0.06	5.0 Max
Moisture Content, %	0.64	3.0 Max
Loss on Ignition, %	0.50	6.0 Max
<b>PHYSICAL ANALYSIS:</b>	<b>RESULTS:</b>	<b>AASHTO M 295- SPEC</b>
Amount Retained on No. 325 Sieve, %	3.5	10 Max
Sieve Uniformity, % Points from Ave	----	5 Max
Blaine Fineness, cm <sup>2</sup> /g	28,115	----
Accelerated Strength Activity Index ASTM C1240		
Portland Cement @ 7 days, % of Control	121	85 Min
Autoclave Expansion, %	-0.06	----
Density	2.79	----
Density Uniformity, % from Ave	----	----
Increase of Drying Shrinkage, %*	----	----
Reactivity with Cement Alkalis, %*		
Reduction of Mortar Expansion, %	----	----
Mortar Expansion, % of LA Cement Control	----	----
Air Entrainment of Mortar, %	----	----

\*Optional Requirements applicable only when requested by purchaser. This material meets the requirements of AASHTO M 295, AASHTO M 321, and ASTM C 618 for the parameters tested.

By   
 Robert L. Smith, Ph.D.



### **SEM Photo of the Metakaolin Particles**

*Advanced Cement Technologies' PowerPozz™ HRM is a manufactured pozzolanic mineral admixture which significantly enhances many performance characteristics of cement-based mortars, concretes, and related products.*

*PowerPozz™, derived from purified kaolin clay, is a white, amorphous, alumino-silicate which reacts aggressively with calcium hydroxide to form compounds with cementitious value.*

*Produced under ISO 9002, PowerPozz™ is subjected to strict process quality controls to assure product uniformity and consistent performance.*

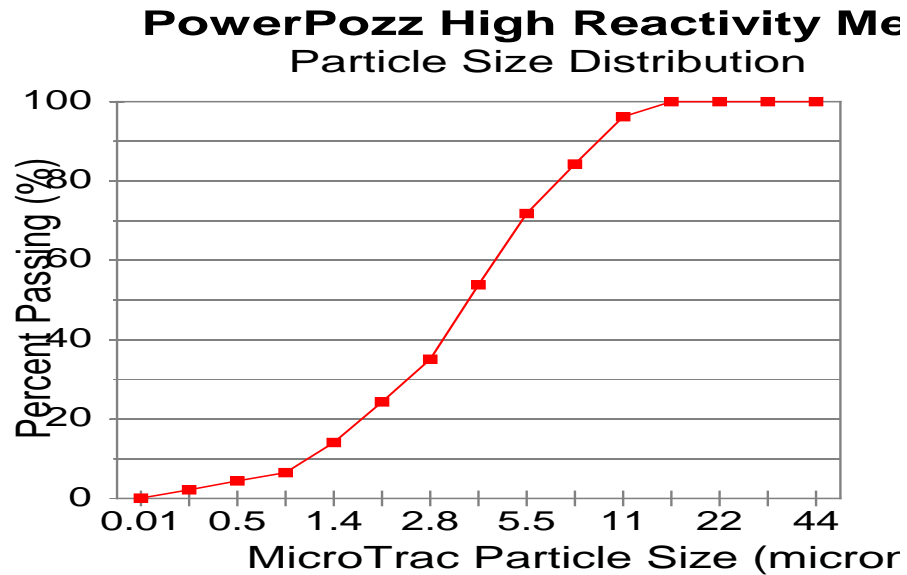
*Used at 5-15% replacement of cement by weight, PowerPozz™ will contribute to: increased strength; reduced permeability; greater durability; and effective control of efflorescence and degradations caused by alkali-silica reaction (ASR) in concrete.*

**PowerPozz™ is milled and classified to exacting particle size distribution specifications.**

**In optimizing the PSD for PowerPozz™, a number of factors were considered to be important:**

- Pozzolanic reactivity and rate of reaction
- Micropacking characteristics when used with Ordinary Portland Cement (OPC)
- Effect on water demand and /or water-reducing admixture demand
- Dispersion efficiency in batching and mixing processes
- Dry product handling and storage characteristics
- Effect on fresh product rheological characteristics
- Color, brightness, reflectivity

The PowerPozz™ Particle Size Distribution (PSD) is illustrated below:



The material is 99.9% finer than 16 $\mu$ m, and has a mean particle size of 3 $\mu$ m (as measured by MicroTrac laser diffraction granulometer method). The PSD of PowerPozz™ has been engineered with a range of OPC - based applications in mind. ACT has the ability to custom grind and classify to meet unique customer requirements.

*All information, while provided in good faith, with every effort made to assure accuracy, is provided by Advanced Cement Technologies at no charge, and without warranty—express or implied. Data given, unless otherwise stated, are based on standard testing procedures which are available on request. Variations do occur in individual tests and the results stated herein cannot be taken as minima or maxima for specification purposes.*

*As we cannot anticipate all possible applications of our products, nor variations in manufacturing equipment, formulae, methods, or practices, we guarantee only that the products will meet the specifications of Advanced Cement Technologies at the time of sale. Advanced Cement Technologies reserves the right to change specifications should it become necessary to do so. The products are sold without express or implied warranty, with all warranties of fitness of purpose being disclaimed, and on the condition that the purchaser is responsible for the determination of the product's suitability for a particular purpose.*

*Statements concerning the possible use of our products are not intended as recommendations for use. No liability is accepted for any infringements of any existing or future patents.*

*All products sold, unless otherwise stated, will be subject to the general sales conditions of Advanced Cement Technologies.*

**E5. Ultra-fine fly ash (UFFA)**

Boral  
Material  
Technologies



BORAL MATERIAL TECHNOLOGIES INC.  
45 Northeast Loop 410, Suite 700  
San Antonio, TX 78216  
Phone (210) 349-4069  
Fax (210) 349-8512

**SUPPLIER'S CERTIFICATION**

**MICRON<sup>3</sup>**

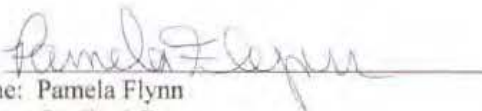
This is to certify that Boral Micron<sup>3</sup> shipped from Plant Rockdale, located near Rockdale, TX, meets or exceeds the following specifications according to "Fly Ash and Raw or Calcined Natural Pozzolan for Use as a Mineral Admixture in Portland Cement Concrete":

American Society for Testing & Materials....ASTM C-618, Class "F"

American Association of State Highway and  
Transportation Officials.....AASHTO M-295, Class "F"

American Association of State Highway and  
Transportation Officials.....AASHTO M-321, Class "F"

**BORAL MATERIAL TECHNOLOGIES INC.**

By:   
Name: Pamela Flynn  
Title: Quality Manager

### Ingredients of UFFA (from Material Safety Data Sheet)

Hazardous Component (Specific Chemical Identity, Common Name(s))	OSHA PEL	ACGIH TLV	Other Limits Recommended
Silica, Amorphous (SiO <sub>2</sub> ) CAS# 7631-86-9.	80 mg/m <sup>3</sup> / %SiO <sub>2</sub> (total dust)	10 mg/m <sup>3</sup> (total dust)	NIOSH: 6 mg/m <sup>3</sup>
Silica, Crystalline (SiO <sub>2</sub> ) CAS# 148-086-97.	30 mg/m <sup>3</sup> / (%SiO <sub>2</sub> )+2(total dust) 10 mg/m <sup>3</sup> / (%SiO <sub>2</sub> )+2(resp. dust)	0.1 mg/m <sup>3</sup> (resp. dust)	0.05 mg/m <sup>3</sup>
Alumina, Respirable (Al <sub>2</sub> O <sub>3</sub> ) CAS#1344-28-1.	15 mg/m <sup>3</sup> (total dust)	10 mg/m <sup>3</sup> (total dust)	NA
Calcium Oxide (CaO) CAS# 1305-78-8.	5 mg/m <sup>3</sup>	2 mg/m <sup>3</sup>	NA
Titanium Dioxide, Respirable (TiO <sub>2</sub> ) CAS# 13463-67-7.	15 mg/m <sup>3</sup> (total dust)	10 mg/m <sup>3</sup> (total dust)	NA
Ferric Oxide (Fe <sub>2</sub> O <sub>3</sub> ) CAS# 1309-37-1.	10 mg/m <sup>3</sup> (total dust)	5 mg/m <sup>3</sup> (total dust)	NA
Magnesium Oxide (MgO) CAS# 1309-48-4.	15 mg/m <sup>3</sup>	10 mg/m <sup>3</sup>	NA

1. Composition is variable depending on coal source and power plant characteristics. 2. This product does not have a significant respirable particle size distribution. However, various material handling operations may produce dust with respirable particles. 3. Materials present at >0.5% and <12% and not listed in OSHA or ACGIH include Potassium Oxide and Carbon.  
 \* Also subject to alternative TLV for respirable particulates not otherwise classified (NOC) = 3mg/m<sup>3</sup>.

# ASTM C 618 TEST REPORT

Sample Number: S-081126002  
 Sample Date: from Rockdale TX November 2008

Report Date: 1/7/2009  
 Sample Source: Micron 3  
 Tested By: jx

TESTS	RESULTS	ASTM C 618 CLASS F/C	AASHTO M 295 CLASS F/C
<b>CHEMICAL TESTS</b>			
Silicon Dioxide (SiO <sub>2</sub> ), %	52.42		
Aluminum Oxide (Al <sub>2</sub> O <sub>3</sub> ), %	27.12		
Iron Oxide (Fe <sub>2</sub> O <sub>3</sub> ), %	4.51		
Sum of SiO <sub>2</sub> , Al <sub>2</sub> O <sub>3</sub> , Fe <sub>2</sub> O <sub>3</sub> , %	84.05	70.0/50.0 min.	70.0/50.0 min.
Calcium Oxide (CaO), %	9.40		
Magnesium Oxide (MgO), %	1.74		
Sulfur Trioxide (SO <sub>3</sub> ), %	0.95	5.0 max.	5.0 max.
Sodium Oxide (Na <sub>2</sub> O), %	0.41		
Potassium (K <sub>2</sub> O), %	1.11		
Total Alkalies (as Na <sub>2</sub> O), %	1.14		
<b>PHYSICAL TESTS</b>			
Moisture Content, %	0.07	3.0 max.	3.0 max.
Loss on Ignition, %	0.39	6.0 max.	5.0 max.
Amount Retained on No. 325 Sieve, %	0.05	34 max.	34 max.
Specific Gravity	2.50		
Autoclave Soundness, %	-0.06	0.8 max.	0.8 max.
SAI, with Portland Cement at 7 Days, % of Control	114.2	75 min.*	75 min.*
SAI, with Portland Cement at 28 Days, % of Control	115.4	75 min.*	75 min.*
Water Required, % of Control	89.3	105 max.	105 max.

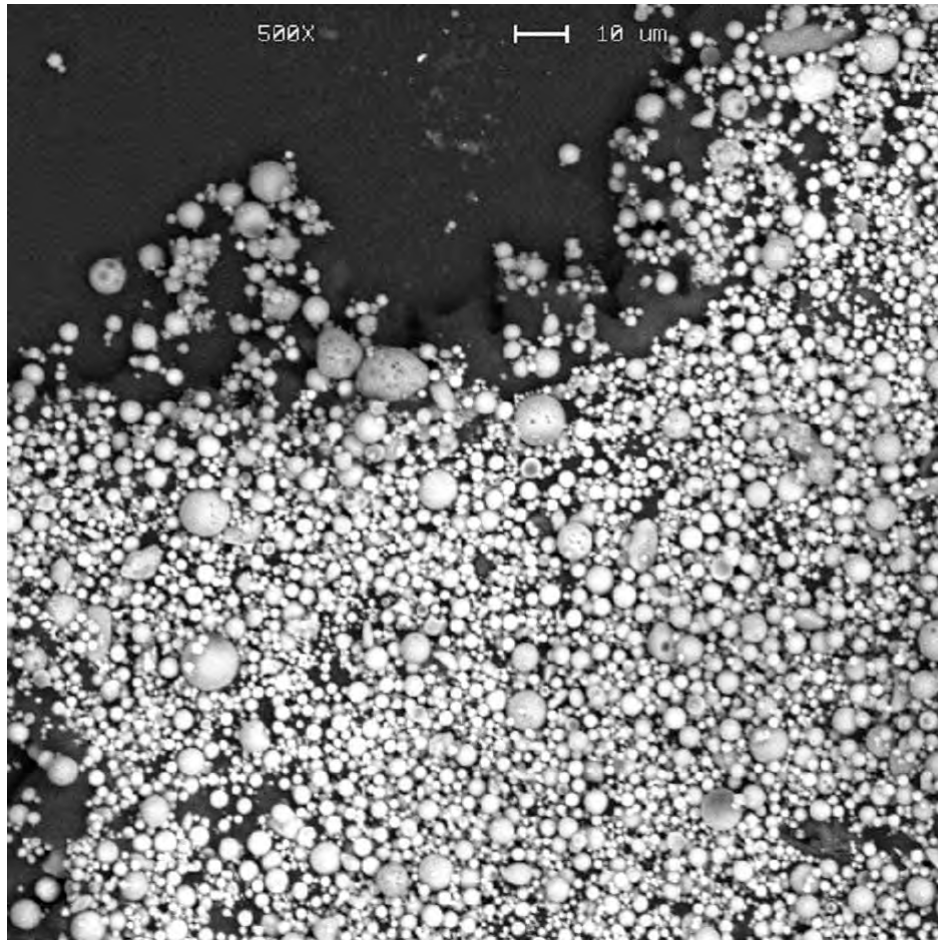
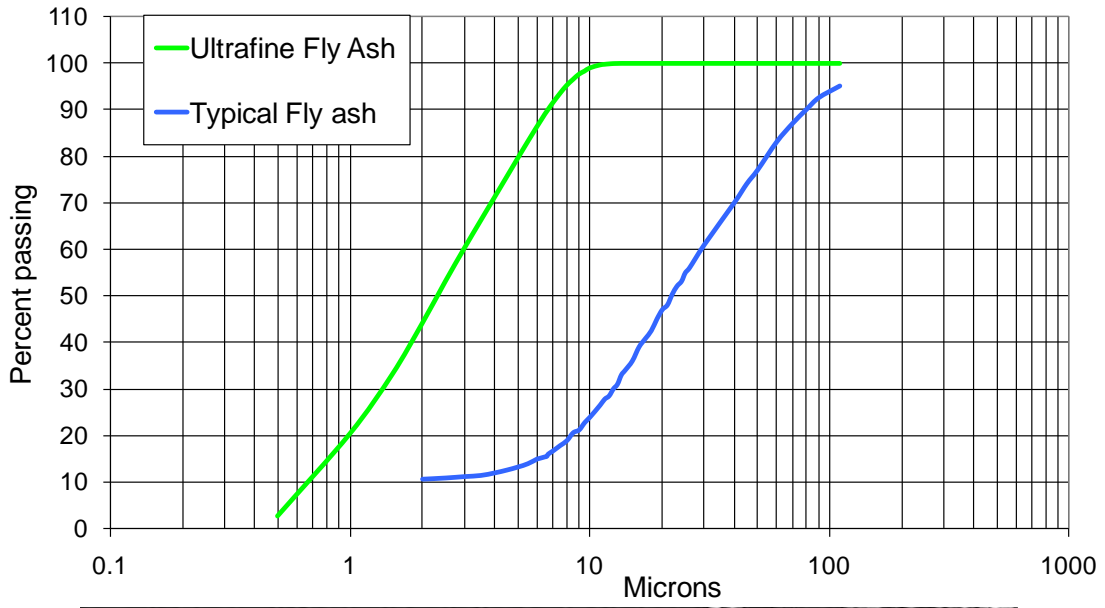
Meets: ASTM C 618 and AASHTO M 295, FDOT Section 929, TxDOT DMS 4610, SCDHPT and MDOT specifications for Class F Fly Ash

\* Meeting the 7 day or 28 day Strength Activity Index will indicate specification compliance.

Approved By:   
 Diana Benfield  
 QC Specialist

Approved By:   
 Brian Shaw  
 Materials Testing Manager

### Particle Size of Ultrafine Fly ash



SEM Photo of the UFFA Particles

**E6. ASTM C 989 GGBFS - Ground granulated blast-furnace slag**

# **LEHIGH**

## **HEIDELBERGCEMENT Group**

**TECHNICAL SERVICES**  
**SALES & MARKETING**  
 2300 Clayton Rd., Suite 300  
 Concord, CA 94520  
 Telephone (925) 521-3601

**PLANT LOCATION**  
 Lehigh Hanson West

LIN 08-06-0743

(M/V: 19 JUN. 2008 New Ambition)

<b>ALLCEM GGBFS (SLAG CEMENT) TEST REPORT</b>			
<b>Specification: ASTM C 989-05 Grades 100 &amp; 120</b>	<b>Report Date: 9-Sep-08</b>		
STANDARD CHEMICAL AND PHYSICAL REQUIREMENTS	TEST RESULTS	ASTM C 989 SPECIFICATIONS	
		Grade 100	Grade 120
Sulfur Trioxide (SO <sub>3</sub> ), %	1.50	4.0 Max	4.0 Max
Sulfur Sulfide (S), %	0.800	2.5 Max	2.5 Max
Chloride (Cl), %	0.002	---	---
(ASTM C 204) Blaine Fineness, m <sup>2</sup> /km	532	---	---
(ASTM C 430) 325 Mesh, % Retained	99.7	20 Max	20 Max
Density	2.92	---	---
(ASTM C 185) Air Content, %	4.4	12 Max	12 Max
<b>SLAG ACTIVITY INDEX, %</b>			
7 Day Individual	135	70 Min	90 Min
7 Day Average of last 5	---	75 Min	95 Min
28 Day Individual	153	90 Min	110 Min
28 Day Average of last 5	---	95 Min	115 Min
<b>REFERENCE CEMENT</b>			
Total Alkali, %	0.715	0.60 - 0.90	0.60 - 0.90
(ASTM C 204) Blaine Fineness, m <sup>2</sup> /km	385	---	---
C <sub>3</sub> S, %	62.08	---	---
C <sub>2</sub> S, %	12.43	---	---
C <sub>3</sub> A, %	8.46	---	---
C <sub>4</sub> A, %	7.17	---	---
<b>COMPRESSIVE STRENGTH, psi</b>			
7 Day Reference Cement	4940	---	---
28 Day Reference Cement	5910	5000 psi Min	5000 psi Min
7 Day Slag and Cement Reference	6680	---	---
28 Day Slag and Cement Reference	9050	---	---

This GGBFS meets the requirements of ASTM C 989-05 (Grade 100 and Grade 120)



Heidelberg Technology Center - Research and Support

## E7. Type I/II low-alkali Portland cement

Item	Test method	Spec. limit	Test result
Air content of mortar %	C185	12.0 max	7.9
Blaine fineness m <sup>2</sup> /kg air permeability test	C204	280 min 420 max	397
Autoclave expansion %	C151	0.80 max	0.03
Normal consistency %	C187	N/A	26.6
Compressive strengths, psi (MPa)	C109		
1-Day		N/A	1998 (13.8)
3-Day		1740 (12.0) min	3472 (23.9)
7-Day		2760 (19.0) min	4600 (31.7)
Setting times min	C191		
Vicat initial		45 min	111
Vicat final		375 max	240
Pass 325 mesh %		72 min	98.7
Heat of hydration (cal/g)-7 days		N/A	70.7
False set %	C451	50 min	85